



UNIVERSITY of the
WESTERN CAPE

Pharmacological Characterization and Chemo-informatics Analysis of Compounds from *Leonotis leonurus*

Chioma O N Oghenetega
3758537

A thesis submitted in fulfilment of the requirements for the degree of Doctor of Pharmacy
in the School of Pharmacy, University of the Western Cape.

Supervisor: Dr. Kenechukwu Obikeze

Co-Supervisor: Dr. Samuel Egieyeh

November 2021

<http://etd.uwc.ac.za/>

DECLARATION

I declare that the thesis, *Pharmacological Characterization and Chemo-informatics Analysis of Compounds from Leonotis leonurus* is my work and has not been submitted for any degree or examination in any other university, and that all the sources used or quoted have been indicated and acknowledged by complete references.

Chioma O N Oghenetega

Signature: 

UWC, Bellville.

November 2021.



Abstract

The central nervous system (CNS), consisting of the brain and the spinal cord, is responsible for integrating sensory information and influencing most bodily functions. The CNS is protected from toxic and pathogenic agents in the blood by permeability barrier mechanisms. These barrier mechanisms, specifically the blood brain barrier (BBB) presents a challenge for the discovery of CNS active drugs as it is requirement for these drugs to permeate the BBB to reach their target site in the CNS. The conventional processes of drug design and discovery from natural products are time consuming, tedious, expensive and have a high failure rate. It has been reported from various studies that the use of computational modelling and simulations in drug design and discovery is less costly and less time-consuming with a greater chance of success than the conventional processes. The process of drug discovery and design can, therefore, be easily carried out using proven computer models, software, and web-based tools. As a result of the above stated facts, this study aims to utilize *in silico* as well as *in vitro* methods in identifying and characterizing promising drug-like bioactive compounds from *Leonotis leonurus* with Central Nervous System (CNS) activity, more specifically in treating Alzheimer's disease (AD).

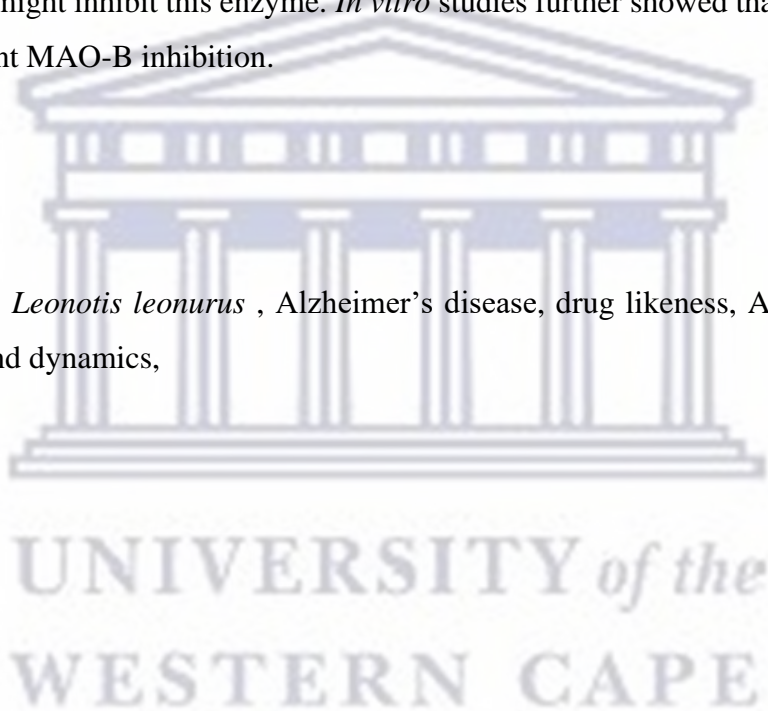
Literature search on isolated compounds from *Leonotis leonurus* was carried out using the terms '*Leonotis leonurus*' AND 'Ethnobotanical uses' AND 'Bioactive Compounds'. The structures and simplified molecular-input line-entry system (SMILES) of known compounds were obtained from PubChem. The identified isolated compounds whose structures were not found on PubChem were drawn in 2D and 3D using ChemDraw Pro16.0 and ChemDraw 3D 16.0 respectively. The canonical SMILES were then compiled into a spreadsheet and imputed into the online ADME prediction site www.swissadme.ch to predict the chemo-informatics properties and drug likeness of the compounds. Data Warrior, a visualization software was used to analyse and visualize the data. It was also used to generate the toxicity profile of each compound from their structure. A scoring function matrix on the requirements of an ideal CNS drug was developed in this study using the chemo-informatics properties obtained from these two toolkits.

Target prediction studies was conducted by inputting the SMILES unto www.swisstargetprediction.ch. Compounds which were predicted to target monoamine oxidase B (MAO-B) and Microtubule Associated Protein Tau (MAPT) (known protein targets for AD) were then docked on MAO-B (PDB ID: 2vrl) in the Molecular Operating Environment (MOE). This was

done to further validate the predictions seen from swiss targets website. *In vitro* studies were then carried out using a fluorometric method which was based on the hydrolysis of the substrate p-tyramine by MAO-B to produce H₂O₂. The assay was carried out using and following the methods of the MAO-B inhibition assay kit from Sigma Aldrich Chemicals (Sigma-Aldrich Corp., St. Louis, MO, USA) or Merck Chemicals (Merck KGaA, Darmstadt, Germany). Compounds predicted to have MAO-B activity were purchased from Sigma Aldrich and tested in this assay.

Based on the scoring function matrix, 7 of the 36 compounds identified from *Leonotis leonurus* were predicted to be ideal CNS drug candidates. and so can be further studied for their possible targets in the CNS. Molecular docking studies on MAO-B showed that three compounds (apigenin, luteolin and vitexin) might inhibit this enzyme. *In vitro* studies further showed that one compound, vitexin, had significant MAO-B inhibition.

Key words: MAO-B *Leonotis leonurus* , Alzheimer's disease, drug likeness, ADMET, vitexin , Molecular docking and dynamics,



DEDICATION

I dedicate this work to my Lord and Saviour, Jesus Christ, because of His sacrifice, I have a reason to face each new day. I also dedicate this to my loving husband, Joshua O Oghenetega. You have been a great support to me through this journey and I highly appreciate, celebrate and love you. This work is also dedicated to my son, David E K Oghenetega. You joined me on this journey, watching me each day and trying to do what I do. May you also achieve so much more than I have. You are so loved.



ACKNOWLEDGEMENT

I would like to firstly thank my Lord and Saviour, Jesus Christ, who paid the price for me to have the life I live today and who also gave me all that I need for life and godliness. To him be all the glory and praise.

I would like to sincerely thank and appreciate my supervisor, Dr. Kenechukwu C Obikeze for his guidance, support, and patience through this journey. It was truly a long journey, but I am sincerely grateful for his words of encouragement and for his willingness to share his expertise throughout this journey. In the same vein, I would like to like to express my sincerest gratitude to my co-supervisor, Dr. Samuel A Egieyeh for critically scrutinizing my work, pinpointing areas for improvement and pushing for excellence. I am deeply grateful that I was opportune to be supervised by two great academics.

My thanks go to my late father, Engr Ndukwe M Uduma and my mother, Mrs Nnena M Uduma for providing all I needed to be who I am today. Your love and sacrifices are not forgotten. I am so glad to have you as parents. And to my big brothers, Chika M Uduma and Chima M Uduma thank you for your love, prayers, and encouragement. You now have a Dr for a sister. Lol.

I would also like to truly appreciate the love and support of my father in law, Rev. George O Daniel-Oghenetega, my mother in law, Dr. (Mrs) Benedicta O Daniel-Oghenetega, my ‘siblings by the law’ Barrister Caleb E Oghenetega, Esther U Oghenetega and Timothy O Oghenetega. I could not have asked for a better family to be married to. Thank you so much for your support, I deeply appreciate you all.

To my son, David E K Oghenetega, thank you for beautifying this journey with your presence. You came right on time. You would do so much more than I have done in life. Your journey would be even more beautiful than mine.

And finally, to my Love, my very own ‘personal person’, Joshua O Oghenetega. Thank you for being a strong support system. You encouraged, prayed for, stayed by, and stood with me through this journey. I am deeply grateful to God for placing you in my life. May God richly bless you. I love you deeply.

Table of Contents

DECLARATION	i
Abstract	ii
DEDICATION	iv
ACKNOWLEDGEMENT	v
Table of Contents	vi
List of Figures	ix
List of Tables	xii
List of Appendices	xiii
Abbreviations	xiv
Chapter 1	1
1. INTRODUCTION	1
1.1 Drug discovery for Central Nervous Diseases	1
1.1.1 Epidemiology and Pharmacology of CNS conditions	1
1.1.2 Drug Kinetics as a challenge to drug discovery	2
1.2 Drug design and discovery	3
1.2.1 Computational Modelling as a drug discovery tool	4
1.3 Medicinal Plants	6
1.3.1 Medicinal plants as sources of drug compounds	6
1.4 Problem Statement	6
1.5 Aim	7
1.6 Objectives	7
1.7 Thesis Layout	7
Chapter 2	9
2. LITERATURE REVIEW	9
2.1 The Central Nervous System	9
2.1.1 The Blood-Brain Barrier (BBB)	9
2.1.2 Alzheimer's disease	11
2.1.2.1 MAO-B enzyme as a drug target	13
2.2 Drug Discovery and Design	15
2.2.1 Pharmacokinetics- ADME	15
	vi

2.2.2	Drug likeness	18
2.2.2.1	Rules of Drug Likeness	18
2.2.3	Computer-Aided Drug Discovery and Design (CADD)	20
2.2.3.1	Chemo-informatics	21
2.2.3.2	Molecular Docking as a CADD tool	24
2.3	<i>Leonotis leonurus</i>	27
2.3.1	Taxonomy of <i>Leonotis leonurus</i>	27
2.3.2	Traditional Uses:	28
2.3.3	Studies on the effect of <i>L. leonurus</i> :	28
2.3.4	Compounds isolated from <i>L. leonurus</i>	31
2.3.5	Bioactivity of isolated compounds	34
Chapter 3		39
3.	CHEMO-INFORMATICS CHARACTERIZATION AND DRUG-LIKENESS OF <i>LEONOTIS LEONURUS</i> COMPOUNDS	39
3.1	Introduction	39
3.2	Research question addressed.....	40
3.3	Methodology	41
3.3.1	Data collection and preparation of the dataset	41
3.3.2	Data Analysis and Visualization	42
3.3.3	Scoring Function Matrix for oral administration with CNS activity	42
3.4	Results	44
3.4.1	Description of the dataset	44
3.4.2	Physicochemical Properties of <i>L. leonurus</i> Compounds	46
3.4.3	Pharmacokinetic profiling and drug-likeness	49
3.4.3.1	Oral Bioavailability models	50
3.4.3.1.1	Lipinski's Rule of Five	50
3.4.3.1.2	Egan Model	53
3.4.3.1.3	Veber's model	55
3.4.4	Absorption and Distribution	57
3.4.4.1	Human Intestinal Absorption and Blood-Brain Barrier Permeation	57
3.4.5	Metabolism: Biotransformation	62
3.4.6	Interaction with Cytochrome P450 enzyme	64

3.4.7	Toxicity Profile of Compounds	69
3.4.8	Summary of ADMET properties	70
Chapter 4		79
4.	<i>IN SILICO</i> TARGET PREDICTION FOR COMPOUNDS ISOLATED FROM L. LEONURUS AND PREDICTION OF POSSIBLE MAO-B INHIBITORS	79
4.1	Introduction.....	79
4.2	Research Question:.....	80
4.3	Methods.....	80
4.4	Results.....	81
4.4.1	Protein target predictions by swisstargetprediction.ch	81
4.4.2	Compounds predicted to target proteins indicative of an ethnobotanical use	101
4.4.3	Compounds predicted to target AD	105
4.4.4	Molecular docking studies	106
Chapter 5		113
5.	<i>IN VITRO</i> ASSAY OF MAO-B INHIBITION	113
5.1	Introduction.....	113
5.2	Research Question:.....	113
5.3	Materials and Method.....	113
5.3.1	Preparation of test compounds	113
5.3.2	Fluorometric MAO-B inhibition assay	114
5.3.3	Data analysis	115
5.4	Results.....	116
Chapter 6		126
6.	DISCUSSION AND CONCLUSION	126
6.1	Discussion.....	126
6.2	Conclusion.....	130
6.3	Limitation of this study.....	130
6.4	Recommendations.....	130
REFERENCES		131
APPENDIX		143

List of Figures

Figure 1.1: Phases of Drug Discovery.....	5
Figure 2.1: 3D structure of human MAO-B (PDB ID: 2vrl); visualized by Chimera (Pettersen et al., 2004).....	14
Figure 3.1: Scatter plots showing the physicochemical properties of the 36 compounds isolated from <i>Leonotis leonurus</i> as well as compounds which passed the individual limits. The red lines represent the desired ideal values for each physicochemical property. All the labdane diterpenes had values within the set limits of the physicochemical properties. The phenyl ethanoid had values above the desired values of five of the six physicochemical properties (molecular weight (MW), rotatable bonds, hydrogen bonds acceptors, hydrogen bond donors and total polar surface area (TPSA)). The diterpene ester was above the ideal value of three desired values: MW, rotatable bonds and MLogP. Most of the flavonoids had TPSA that exceeded the ideal value of 140 Å (as stipulated by Egan et al., 2000) probably due to the preponderance of hydroxyl group on the compounds.....	47
Figure 3.2: Visualization of results of Lipinski's rule. Graphs showing the breakdown of physicochemical properties under Lipinski's rule (top right and left). All the compounds assessed (lower left 3D plot).....	51
Figure 3.3: 3-D visualization showing compounds that passed Lipinski's rule.....	52
Figure 3.4: Optimization of vitexin to pass the various models and improve on its activity.....	53
Figure 3.5: Graphs showing the breakdown of physicochemical properties under Egan's rule (top right and left). All the compounds assessed (lower left).....	54
Figure 3.6: Graphs showing compounds that passed Egan's rule.....	55
Figure 3.7: Graphs showing breakdown of physicochemical properties under Veber's rule (top right and left). The red lines represent the desired ideal values for TPSA and rotatable bonds. All the compounds assessed (lower left) compounds which passed Veber's rule (lower right).....	56
Figure 3.8: Graphs showing compounds which passed Veber's rule.....	57
Figure 3.9: BOILED EGG illustration of the 36 compounds adsorption across the BBB and the gastrointestinal tract, and the probability of being a P-gp substrate.	58
Figure 3.10: Illustration showing the possibility of the 36 compounds from <i>L. leonurus</i> being P-gp substrates.	59
Figure 3.11: Plot showing the extent of gastrointestinal absorption as well as the probability of the 36 compounds crossing the BBB.	61
Figure 3.12: Graph showing the predicted number of metabolic reactions each compound would generate as generated by Qikprop.	63
Figure 3.13: C-map showing the interaction between compounds that inhibit CYP450 and drugs metabolized by CYP450.....	69
Figure 3.14: Graph showing the mutagenic and tumorigenic predictions for the <i>L. leonurus</i> compounds.....	70

Figure 4.1: C-map network showing the target prediction suggesting that EDD and leoleirin C may be responsible for the ethnobotanical use for Cancer whilst geniposidic acid and vitexin may be responsible for the ethnobotanical use of partial paralysis.....	102
Figure 4.2: C-map network showing the target prediction suggesting that compound X may be responsible for the ethnobotanical use for cancer, diabetes, and pain, whilst acteoside and dihydroxyphytyl palmitate may be responsible for the ethnobotanical use of cancer and pain....	102
Figure 4.3: C-map network showing the target prediction suggesting that cynaroside and luteolin 7-O- β -glucoside-3-methyl ether may be responsible for ethnobotanical use for cancer.	103
Figure 4.4: C-map network showing the target prediction suggesting that comosiin may be responsible for ethnobotanical use for cancer.	103
Figure 4.5: C-map network showing the target prediction suggesting that chryseriol may be responsible for ethnobotanical use for jaundice and cancer.....	103
Figure 4.6: C-map network showing the target prediction suggesting that luteolin may be responsible for ethnobotanical use for cancer, depression, diabetes, and arthritis.....	104
Figure 4.7: C-map network showing the target prediction suggesting that 6-Methoxyluteolin-4-methyl ether may be responsible for ethnobotanical use for cancer.	104
Figure 4.8: C-map network showing the target prediction suggesting that apigenin may be responsible for ethnobotanical use for cancer and depression.	104
Figure 4.9: C-map network showing the target prediction suggesting that apigenin may be responsible for ethnobotanical use for cancer, partial paralysis, and pain.	105
Figure 4.10: C-map network showing targets found in AD pathway and possible compounds with such activities	106
Figure 4.11: Ligand Interaction diagrams of the lowest S-cores of the test compounds	110
Figure 4.12: Ligand Interaction diagrams of the lowest score of known MAO-B inhibitors	111
Figure 5.1: Fluorescence produced by MAO-B - catalysed cleavage of tyramine	116
Figure 5.2: Inhibition of fluorescence produced by MAO-B - catalysed cleavage of tyramine, by selegiline (5 μ M, 10 μ M, 20 μ M).....	117
Figure 5.3: Percentage relative inhibition of MAO-B activity by selegiline (5 μ M, 10 μ M, 20 μ M).	117
Figure 5.4: Inhibition of fluorescence produced by MAO-B - catalysed cleavage of tyramine, by apigenin (5 μ M, 10 μ M, 20 μ M, 30 μ M and 40 μ M).	118
Figure 5.5: Percentage relative inhibition of MAO-B activity by apigenin (5 μ M, 10 μ M, 20 μ M, 30 μ M and 40 μ M).	119
Figure 5.6: Inhibition of fluorescence produced by MAO-B - catalysed cleavage of tyramine, by vitexin (5 μ M, 10 μ M, 20 μ M, 30 μ M and 40 μ M).....	120
Figure 5.7: Percentage relative inhibition of MAO-B activity by vitexin (5 μ M, 10 μ M, 20 μ M, 30 μ M and 40 μ M).	121
Figure 5.8: Inhibition of fluorescence produced by MAO-B - catalysed cleavage of tyramine, by luteolin (5 μ M, 10 μ M, 20 μ M, 30 μ M and 40 μ M).....	122
Figure 5.9: Percentage relative inhibition of MAO-B activity by luteolin (5 μ M, 10 μ M, 20 μ M, 30 μ M and 40 μ M).	123

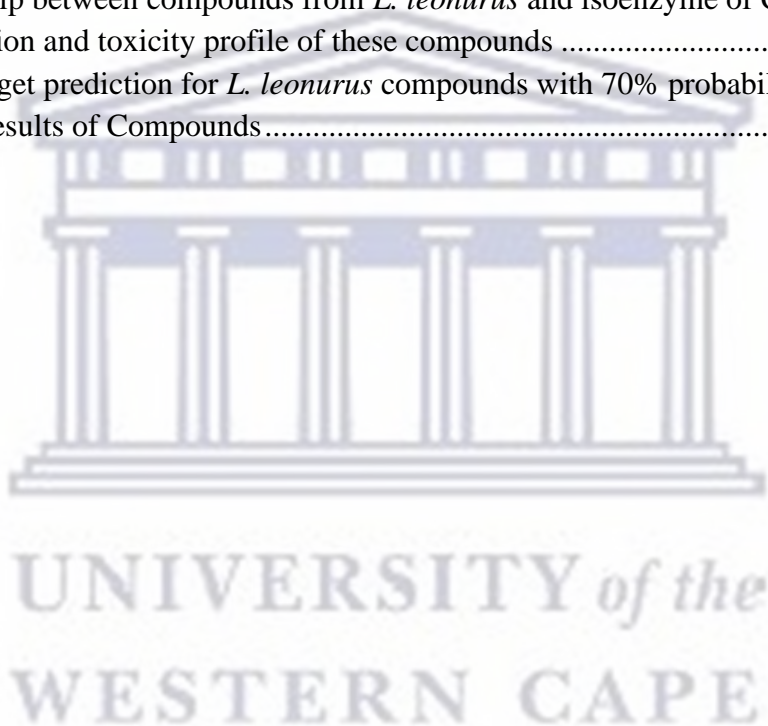
Figure 5.10: Inhibition of fluorescence produced by MAO-B - catalysed cleavage of tyramine, by geniposidic acid (5 μ M, 10 μ M, 20 μ M, 30 μ M and 40 μ M)..... 124

Figure 5.11: Percentage relative inhibition of MAO-B activity by geniposidic acid (5 μ M, 10 μ M, 20 μ M, 30 μ M and 40 μ M)..... 125



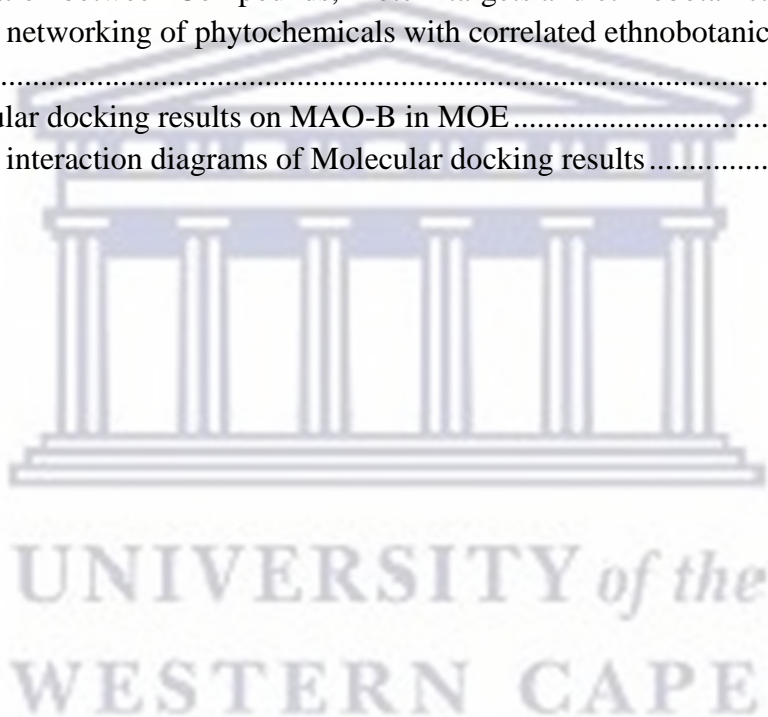
List of Tables

Table 2.1: Active Sites of Human MAO-B.....	14
Table 2.2: Tools used for molecular docking studies (Attique et al., 2019).	26
Table 2.3: List of Compounds isolated from <i>L. leonurus</i>	31
Table 3.1: Scoring function matrix for drug-likeness for orally administered, CNS active compound (hypothetical example).	43
Table 3.2: Compounds isolated from <i>L. leonurus</i> and their phytochemical class.....	44
Table 3.3: Compounds which did not pass the various physicochemical limits.	48
Table 3.4: Metabolic reactions and the number of metabolites for <i>L. leonurus</i> compounds as predicted by Qikprop and biotransformer.ca.....	64
Table 3.5: Interactions between compounds from <i>L. leonurus</i> and isoenzyme of CYP450.	65
Table 3.6: Relationship between compounds from <i>L. leonurus</i> and isoenzyme of CYP450 including the absorption and toxicity profile of these compounds	72
Table 4.1: Protein target prediction for <i>L. leonurus</i> compounds with 70% probability and above	82
Table 4.2: Docking results of Compounds	107



List of Appendices

Appendix 1: Predicted physicochemical properties of Phytochemicals from <i>L. leonurus</i>	143
Appendix 2: Lipophilicity prediction of phytochemicals from <i>L. leonurus</i>	152
Appendix 3: Water solubility prediction of Phyto-compounds from <i>L. leonurus</i>	161
Appendix 4: Pharmacokinetics predictions of Phyto-compounds in <i>L. leonurus</i>	166
Appendix 5: Drug likeness prediction of Phytochemicals from <i>L. leonurus</i>	169
Appendix 6: Medicinal Chemistry prediction of Phytochemicals from <i>L. leonurus</i>	172
Appendix 7: Metabolic reactions and the number of metabolites for <i>L. leonurus</i> compounds as predicted on biotransformer.ca and Qikprop.....	175
Appendix 8: Pictorial results of the target predictions from swisstargetspredictions.ch	181
Appendix 9: Target prediction of Compounds using swistargetprediction.ch.....	199
Appendix 10: Correlation between Compounds, Protein targets and ethnobotanical uses.....	248
Appendix 11: C-Map networking of phytochemicals with correlated ethnobotanical uses and point of actions	279
Appendix 12: Molecular docking results on MAO-B in MOE.....	291
Appendix 13: Ligand interaction diagrams of Molecular docking results.....	298



Abbreviations

ABC: ATP-binding cassette

ACE: Acetylcholinesterase

AChEIs: Acetylcholinesterase inhibitors

AD: Alzheimer's disease

ADORA2A: Adenosine A2A receptors

ADMET: Absorption, Distribution, Metabolism, Excretion, Toxicity

AEXS: Aromatase excess syndrome

AKR1B1: Aldose reductase

AROD: Aromatase deficiency

ATP: Adenosine triphosphate

BBB: Blood brain barrier

BChE: Butyrylcholinesterase

BEC: Brain endothelial cells

BHT: Butylated hydroxytoluene

BOILED: Brain Or IntestinaL Estimated permeation method model

CADDD: Computer Aided Drug Discovery and Design

CNS: Central nervous system

COX-1: Cyclooxygenase 1

CSF: Cerebrospinal fluid

CYP: Cytochrome

DPPH: 1,1-Diphenyl-2-picrylhydrazyl

DMSO: Dimethyl sulfoxide

DYRK1A: Dual specificity tyrosine-phosphorylation-regulated kinase 1A

EDD: (13S)-9 α , 13 α -epoxylabda-6 β (19),15(14) diol dilactone

FAD: Flavin adenine dinucleotide

FITTED: Flexibility Induced Through Targeted Evolutionary Description

FRAP: Ferrous reducing antioxidant

FTD: Frontotemporal dementia

GABA_A: Gamma Aminobutyric acid type A

GI: Gastro intestine

GLIDE: Grid-based Ligand Docking with Energetics

GOLD: Genetic Optimization for Ligand Docking

GSTs: Glutathione S transferases

HSA: Human serum albumin

HTS: High throughput screening

ICM: Internal Coordinate Modelling

MAPT: Microtubule-associated protein Tau

MAO-A: Monoamine oxidase A

MAO-B: Monoamine oxidase B

MCT1: Monocarboxylic acid transporter 1

MDDR: MDL Drug Data Report Database

MDR1: Multidrug resistance gene 1

MOE: Molecular operating environment

NATs: N-acetyltransferases

NMDLA: N-methyl-DL-aspartic acid

NO: Nitric oxide

NPs: Natural products

OATPs: Organic anion transporting polypeptides

P-gp: P-glycoprotein

PIA: Passive intestinal absorption

PRKCG: Protein kinase C gamma type PSA: Polar surface area

PTAFR: Platelet-activating factor receptors

PTZ: Pentylentetrazole

QSAR: Quantitative structure-activity relationships

QSPR: Quantitative structure-property relationships

RFU: Relative fluorescence unit

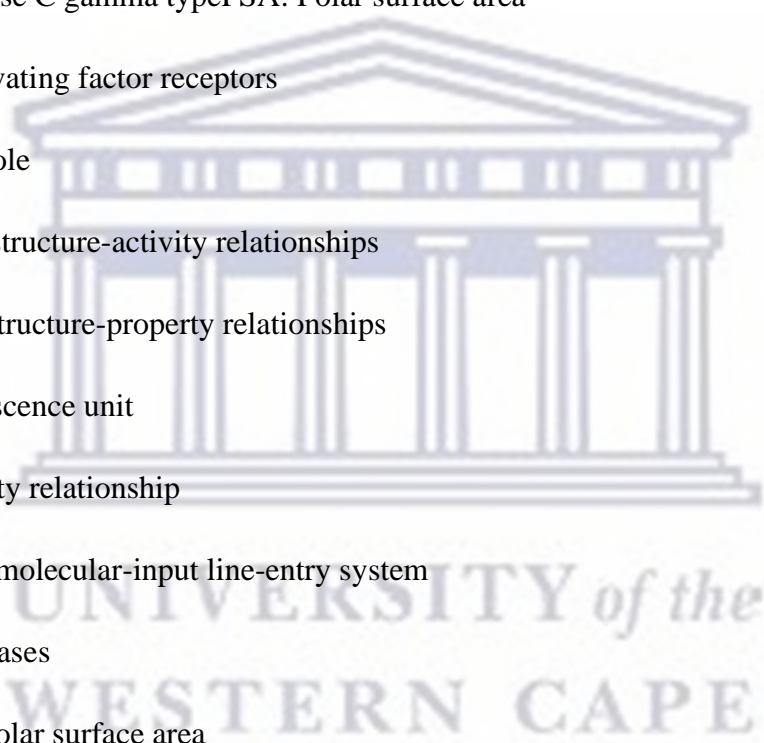
SAR: Structure activity relationship

SMILES: Simplified molecular-input line-entry system

SULTs: Sulfotransferases

TPSA: Topological polar surface area

UGTs: UDP-glucuronosyltransferases



Chapter 1

1. INTRODUCTION

1.1 Drug discovery for Central Nervous Diseases

1.1.1 *Epidemiology and Pharmacology of CNS conditions*

The central nervous system (CNS) is one of two parts of the nervous system consisting of the brain and the spinal cord. It is responsible for integrating sensory information and influencing most bodily functions including awareness, movements, sensations, thoughts, speech, memory, and reflex actions. Both the brain and spinal cord are enclosed in the meninges and further housed in the skull (for the brain) and spinal canal (for the spinal cord) (Queensland Brain Institute, 2017). The CNS is protected from toxic and pathogenic agents in the blood by three permeability barrier mechanisms: i.) The blood-brain barrier (BBB) ii.) The blood-spinal cord barrier and iii.) The blood-cerebrospinal fluid (CSF) barrier (Palmer, 2010a).

CNS diseases or disorders are a group of health conditions that disrupt either the structure or function of the CNS. CNS disorders account for about a third of the global disease and disability burden and are expected to increase exponentially in the years to come, mainly due to an increase in the number of people in the 65 and above age group which has the greatest incidence of the disease (Alavijeh et al., 2005; Palmer, 2010a). CNS disorders can be broadly classified as neurodegenerative or non-neurodegenerative disorders (Palmer, 2010a). Neurodegenerative disorders occur when there is a loss of cells from the brain or spinal cord or both due to injury or illness or a combination of both. This is usually gradual and progressive and would present as loss of memory (dementia and its forms), disorders of movement (e.g., Parkinson's disease) and demyelinating disorders (e.g., multiple sclerosis) (Palmer, 2010a). Disruption of the permeability barrier mechanisms mentioned above, specifically the BBB, plays a role in the development and progression of many CNS disorders particularly neurodegenerative disorders like Alzheimer's and Parkinson's disease (Palmer, 2010a, 2010b). The BBB which is made up of tight junctions formed by endothelial cells of the brain capillaries between the brain and the blood does not only act as a protective barrier against toxins and infectious agents but can also become a barrier to the influx of medicines and potential medicines, red blood cells, leukocytes, proteins, and peptides into the brain. This impermeable characteristic of the BBB means that it acts as a

functional interface which maintains homeostasis by regulating the movement of chemicals and cells between the circulatory system and the CNS, therefore providing the environment for neuronal activity to be efficient (Palmer, 2011, 2010b). Since the disruption of BBB functionality plays a role in the development and progression of CNS disorders, it has become an important target of drug design and discovery (Palmer, 2010b).

Although the role of the BBB in disease aetiology has been a focus for drug discovery, there are some gaps and challenges in the current treatment of neurodegenerative diseases. These gaps and challenges are seen because most of the disorders within the CNS are still poorly understood in terms of the underlying pathophysiology, and so understanding the exact mode of action of current CNS drugs is still limited (Pardridge, 2002; Caban et al., 2017). This is also the reason why despite the high prevalence of CNS disorders in the overall population, the discovery and development of drugs for CNS diseases has one of the lowest success rates, as well as a longer delay in regulatory approval times and drug availability (Pardridge, 2002; Molinoff, 2011; Caban et al., 2017). For example, in the management of Alzheimer's disease (AD) there has not been an effective treatment that is potent enough to slow down the progression of the disease, possibly due to the many differing hypotheses for the pathogenesis of the disease (Folch et al., 2016; Weller and Budson, 2018).

1.1.2 *Drug Kinetics as a challenge to drug discovery*

Drug kinetics also known as pharmacokinetics is the study of the movement of drugs around the body after administration. It looks at how the body absorbs, distributes, metabolizes, and excretes drugs, mainly based on the physicochemical properties of drug compounds. In conventional drug discovery methods, this study is carried out towards the end of the drug discovery process after *in vivo* studies have ascertained the pharmacological effects of a promising drug candidate (Fan and de Lannoy, 2014). However, the challenge with going through the stepwise method is that promising drugs which have shown strong potency and efficacy at target sites may fail to reach those therapeutic sites in optimal concentrations and time to produce the same effect when *in vivo* studies are carried out, leading to a waste of resources (Fan and de Lannoy, 2014). Drugs that have their therapeutic target in the brain or CNS have an even greater challenge as they need to have physicochemical properties which enable them to cross the BBB. Successful drug

candidates for the treatment of CNS diseases would have to satisfy the criteria of potency, therapeutic efficacy, oral bioavailability, target selectivity as well as an acceptable side effect profile which is mainly dependent on the therapeutic targets. These drug candidates face a variety of challenges in becoming successful including the complexity of the brain, the tendency of CNS drugs to cause unwanted CNS effects and the BBB as a permeation barrier (Alavijeh et al., 2005). As mentioned earlier, it is pertinent that when designing promising CNS drugs, in addition to having good potency and selectivity, they should also be able to cross the BBB be it via passive diffusion or aided transport mechanisms (Alavijeh et al., 2005; Palmer, 2010a). Drugs that cross the BBB via passive diffusion have to be small in size (molecular weight less than 500Da) and highly lipophilic (Pardridge, 2002). However, beyond the size and solubility characteristics of drug compounds, penetration into the CNS can be influenced by membrane glycoprotein efflux transporters in the BBB that expel molecules out of the brain across the endothelial cell membranes (Alavijeh et al., 2005). The most prominent of these is a phosphorylated glycoprotein called P-glycoprotein (P-gp), a member of the ATP-binding cassette (ABC) superfamily of membrane transporters, which is encoded by multidrug resistance gene 1 (MDR1) in humans. P-gp contributes to the poor BBB penetration of many highly lipophilic drugs, therefore, a successful CNS drug candidate needs to be a poor substrate to all efflux transporters in addition to being smaller than 500Da in size and lipophilic (Alavijeh et al., 2005). One way of achieving the development of a successful CNS candidate is the use of computational techniques to design drugs that have the attributes of a successful CNS drug candidate (Pajouhesh and Lenz, 2005).

1.2 Drug design and discovery

Drug discovery is the process of identifying compounds that have the potential of becoming new therapeutic agents (Balunas and Kinghorn, 2005). In the early years of drug discovery, the discovery of a new drug molecule was based on the biological activity seen when natural products (that is compounds that are derived from natural sources such as plants, animals, and microorganisms) were administered in traditional medicine. This led to the discovery of quinine from *Cinchona ledgeriana* (cinchona bark), artemisinin from *Artemisia annua L.*, and galantamine from *Galanthus woronowii* Losinsk. just to name a few (Balunas and Kinghorn, 2005; Ji et al., 2009). Natural products, especially those from medicinal plants, have been a great source of both new drugs and drug ‘leads’ aimed at various pharmacological targets (Balunas

and Kinghorn, 2005). The process of identifying these compounds have involved the use of a series of experimental models that are time-consuming, tedious, expensive and have a high failure rate (Macalino et al., 2015). Drug design on the other hand is the process of using the information of a biological target to find a new therapeutic agent. This relies mainly but not solely on computational modelling techniques, simulations, and bioinformatics approaches. In modern times, the use of computational modelling and simulations in drug design and discovery has been reported to be less costly and less time-consuming, while having a greater chance of success than traditional methods of drug discovery (Zhou and Zhong, 2017). The process of drug discovery and design can, therefore, be easily carried out using proven computer models, software, and web-based tools (Gfeller et al., 2014; Daina et al., 2017).

1.2.1 *Computational Modelling as a drug discovery tool*

Computational modelling in drug discovery and design is the science of using computers to simulate the various steps of drug discovery and design (Balunas and Kinghorn, 2005). Its role in drug discovery is to increase predictions of drugs and drug ‘leads’ based on existing knowledge of the quantitative relationship between the structure and biological activity of known targets and small compounds. The role of computational modelling in drug design is, generally, to develop new drug molecules based on the existing knowledge of targets and lead compounds. The development of new drug molecules can be done by optimizing drug ‘leads’ which have already been identified from natural products and stored in compound libraries (Balunas and Kinghorn, 2005). In addition to discovering and designing drugs, computational modelling, as well as other computer-aided methods, can be used in generating data that is stored in virtual chemical libraries (Xu and Hagler, 2002; Begam and Kumar, 2012). Informatics, which is the study of the structure, behaviour and interactions of natural and computational systems plays a role in data generation and mining (University of Edinburgh, 2015). In drug design and discovery, chemo-informatics and bioinformatics are the areas of informatics that play this role (Romano and Tatonetti, 2019). Chemo-informatics is the application of computer science to understand and characterize the molecular attributes and chemical activity of compounds, whilst bioinformatics techniques are used to discover how drug candidates produce therapeutic activity within the human body. This can include predicting interactions between drugs and proteins,

analysis of the impact on biological pathways and functions, and elucidation of genomic variants that can alter drug response (Romano and Tatonetti, 2019).

Figure 1.1 shows the different phases of conventional drug discovery for a single drug as well as the timeline required to achieve these phases. Computational modelling and simulations reduce the development years of the drug discovery process from approximately 10-16 years to about 6-8 years and the total cost of the process to about a third (Baldi, 2010). In addition to reducing the cost and time of the drug discovery process, computational modelling has several benefits over the conventional drug discovery process. These benefits include a more logical process of identifying lead compounds, as the basis of the drug discovery is specific and target-based and not blind screening. The process is more transparent and is easy to manage, and finally, the coordination amongst disciplines is uncomplicated and more transparent (Baldi, 2010).

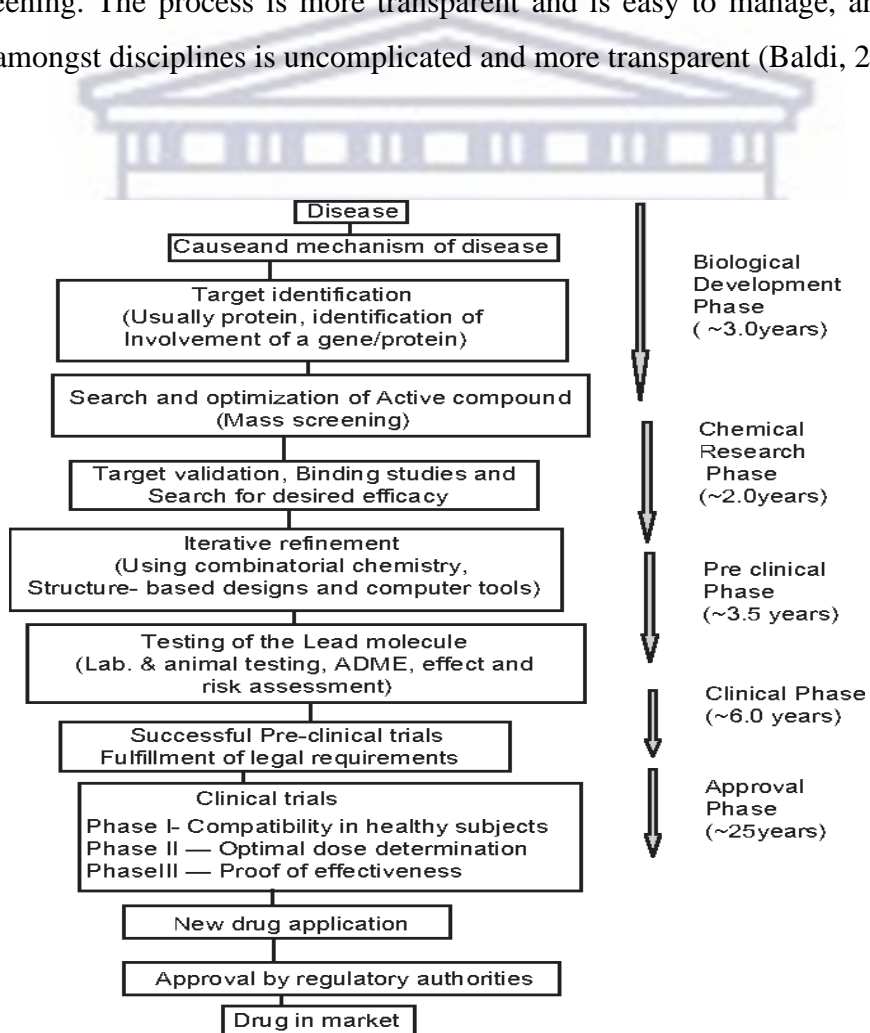


Figure 1.1: Phases of Drug Discovery

1.3 Medicinal Plants

1.3.1 Medicinal plants as sources of drug compounds

Medicinal plants have been used in the treatment of diseases for centuries all over the world, with the knowledge of their usage passed on from one generation (Balunas and Kinghorn, 2005; Rafieian-Kopaei, 2012). Initial use was in the form of crude drugs formulated as poultices, teas, powders, and alcohol distillation amongst others. Investigation into the active compounds (also known as phytochemicals) responsible for the outcomes seen with medicinal plants started in the early 20th century and this led to the discovery of many novel compounds which have been formulated into drugs for various therapeutic uses including morphine isolated from *Papaver somniferum* (opium plant), quinine from *Cinchona ledgeriana* (cinchona bark), artemisinin from *Artemisia annua L.*, and galantamine from *Galanthus woronowii* Losinsk (Balunas and Kinghorn, 2005; Ji et al., 2009). *Leonotis leonurus* is one of such plants used in traditional medicines in South Africa to treat pain, depression, hypertension, epilepsy, headaches, chest infections, and skin rashes (Mazimba, 2015; Nsuala et al., 2015). It has been claimed in traditional medicine to have hallucinogenic and psychoactive properties when the leaves or buds are dried and smoked, suggesting that the plant compounds penetrate the CNS. Several studies have been carried out on various extracts from this plant to confirm the traditional uses, and the plant has been reported to produce antiepileptic and antidepressant activity (Bienvenu et al., 2002; Nielsen et al., 2004; Muhizi et al., 2005). These reported effects indicate that the plant contains bioactive compounds with CNS activity and so compounds that have been isolated from the plant are ideal candidates for evaluation for CNS activity.

1.4 Problem Statement

The development of successful CNS drugs using traditional assay methods is resource-intensive and has a high attrition rate due to the many challenges including the presence of the BBB. Plants and their products as good sources of drug candidates, provide a wealth of small compounds that can be extracted and tested for a needed biological activity. Since the development of successful CNS active drugs can be resource-intensive, computer-aided drug discovery is used to cut down on the resources used and the attrition rate of drug development from natural products. *Leonotis leonurus*, being one of the plants used in the treatment of CNS conditions such as depression and AD, has the potential of producing successful CNS drug candidates. Several phytochemicals

have been identified from the plant and assessing their potential CNS activity as well as their pharmacokinetic properties is the next logical step in the preclinical drug development process. This study set out to answer the following questions:

- Does any of the compounds isolated from *L. leonurus* have the desired drug-like and pharmacokinetic properties to be developed into potential drug candidates for the CNS?
- Are any of the compounds isolated from *L. leonurus* effective against any of the identified targets for AD such as the monoamine oxidase B (MAO-B) enzyme?

1.5 Aim

This study aimed to utilize *in silico* and *in vitro* methods in identifying and characterizing promising drug-like bioactive compounds from *Leonotis leonurus* with potential CNS activity as MAO-B inhibitors, for the treatment of AD.

1.6 Objectives

The objectives of this study included the following:

- To identify compounds isolated from *Leonotis leonurus*.
- To conduct a chemo-informatics characterization of the identified compounds.
- To predict the pharmacological effects of the identified compounds via target prediction and molecular docking.
- To conduct *in vitro* MAOB inhibitory assays of the compounds with predicted CNS activity.

1.7 Thesis Layout

The first chapter of the study introduces the reader to the epidemiology of CNS diseases as well as the barriers to the treatment of such conditions. It also introduces the reader to the concept of computer-aided methods in drug discovery, design, and development of CNS drugs, with a focus on natural products. Chapter two presents the review of literature underpinning the barriers to developing CNS drugs, the use of computational methods in drug discovery and studies reporting the biological effects of *Leonotis leonurus*. Chapter three presents the investigation of the chemo-informatics profile of the compounds isolated from *Leonotis leonurus*, the methods used to

determine the chemo-informatics profile of the compounds, and the results of the experiments. Chapter four presents the investigation of the pharmacological characteristics of the compounds isolated from *Leonotis leonurus* using *in silico* methods, narrowing down to MAO-B inhibition, and the results of the experiments. In Chapter Five, the *in vitro* method used to confirm the predicted inhibition of MAO-B by some of the compounds, and the results of the experiments are presented. Chapter six is a general discussion of the significant findings of the study, the implications of the research, recommendations, and the conclusions for future research.



Chapter 2

2. LITERATURE REVIEW

2.1 The Central Nervous System

The central nervous system synchronizes the activities of bodily functions, as well as the collection of signals from the environment, the integration of such signals, the memory of such information, and the generation of adaptive patterns of behaviour (Schneider, 2013; Queensland Brain Institute, 2017). Both the brain and spinal cord are enclosed in the meninges and further housed in the skull (for the brain) and spinal canal (for the spinal cord). The nervous tissue of the brain and spinal cord is protected by the cerebrospinal fluid and then by an impermeable membrane of capillaries called the blood-brain barrier (Schneider, 2013; Queensland Brain Institute, 2017). This system can be affected negatively by many factors such as degenerative disorders or infections or even hormonal imbalances, to cause CNS-related diseases like AD and Parkinson's disease. Drugs that are to be used in the treatment of these disease conditions need to be able to cross the BBB, which acts as a protective barrier between the brain tissue and the brain capillaries. It is also important to understand the rate and extent to which any drug molecule can cross this barrier, this is to mitigate any related side-effects in the central nervous system (Schneider, 2013).

2.1.1 *The Blood-Brain Barrier (BBB)*

The BBB was identified first by Paul Ehrlich, when he observed that basic dyes, when injected into the circulatory system, stained other organs apart from the brain. To further confirm this observation, one of his students did a reverse of the experiment and observed that the dye stained the brain but not the other organs within the periphery. These observations led to the belief that there was a barrier between the central and peripheral nervous systems preventing the movement of molecules between the blood and brain (Carvey et al., 2009). The structure of the BBB is made up of specialised brain endothelial cells (BEC). These cells differ from those of the rest of the body as they have extensively tight junctions, no fenestration, and a sparse pinocytotic vesicular transport (Fan and de Lannoy, 2014). It has also been demonstrated that within the BEC, there is the presence of enzymes that metabolize lipid-soluble small molecules once they

penetrate the BEC forming another aspect of the brain barrier. Examples of these enzymes include different isoenzymes of Cytochrome (CYP) P450 (CYP3A4, CYP1B1, CYP2B and CYP2D6) and monoamine oxidase (MAO) (McFadyen et al., 1997; Carvey et al., 2009; Ferguson and Tyndale, 2011). Although CYP enzymes are found in the brain, their level is approximately 0.5-2% of that in the liver, which makes it unlikely that they influence the overall systematic pharmacokinetics of drugs. CYPs, however, appear to play an important role in regulating the levels of endogenous GABA_A receptor agonists that maintain brain cholesterol homeostasis and eliminate retinoid (Hedlund et al., 2001).

Subsequent studies on the CNS demonstrated the presence of numerous transport systems within the BBB surface which account for the movement of molecules across the barrier (Carvey et al., 2009). One of these transport mechanisms identified as part of the barrier integrity of the BBB is P-glycoprotein (P-gp), a member of the ATP-binding cassette (ABC) superfamily of membrane transporters. P-gp acts as an efflux transporter that expels molecules out of the brain across the endothelial cell membrane; therefore, protecting the brain from potentially harmful substances (Alavijeh et al., 2005; Ebinger and Uhr, 2006). The knowledge of the presence of P-gp in the BBB has been used in the development of small lipophilic drugs which are desired to act in the peripheral system and not in the central nervous system. These drugs are designed to be P-gp substrates and so produce an effect in the periphery without affecting the brain. An example of such a drug is loperamide, a mild opioid that is used as an antidiarrheal (Carvey et al., 2009). Apart from efflux transporters, there are influx transporters such as organic anion transporting polypeptides (OATPs) and monocarboxylic acid transporter 1 (MCT1), which move much-needed large or water-soluble molecules like glucose, and amino acids into the brain for proper brain function. Both the efflux and influx transporters are said to act jointly at the luminal membrane of the BBB thereby intensifying the selective expulsion of drugs from the brain (Carvey et al., 2009; Fan and de Lannoy, 2014). In addition to these forms of barrier mechanisms, the BEC also acts as a signal interface stimulating the release of prostaglandins and nitric oxide to initiate anorexia in the event of systemic infections (Langhans, 2007). The BBB can therefore be described as a physical and metabolic barrier with transport systems that maintains homeostasis of the brain and its environment (Carvey et al., 2009; Palmer, 2010a).

Interference with the BBB and its function plays a critical role in the development and progression of several brain disorders and diseases. In some cases, increased BBB permeability

results from an underlying pathology such as a traumatic brain injury, while in other cases, such as in multiple sclerosis and AD, disruption to the BBB may be the precipitating event (Palmer, 2010a). When the BBB is compromised, elements from the blood such as toxins and metals which are normally excluded from the brain gain access and potentially contribute to the progression of brain diseases (Carvey et al., 2009). Apart from having a compromised permeation system, other aspects of the BBB like the transport systems and the enzymatic barrier are also altered. In drug therapy, dysfunction of the BBB and its function can lead to an increase in the entry of drugs that are normally excluded from the brain. This knowledge can be used positively as it would mean that drugs that can be helpful in the treatment of CNS diseases but do not cross the intact BBB may have the potential of crossing the disease-compromised BBB (Carvey et al., 2009).

2.1.2 *Alzheimer's disease*

As stated earlier, the BBB plays an important role in maintaining the homeostasis of the brain and its environment, and interference with the functioning of the BBB is increasingly recognized as a potential contributor to the pathogenesis of several neurological diseases including late-onset AD (Yamazaki and Kanekiyo, 2017). AD is a progressive neurodegenerative disorder that is the main cause of dementia in the elderly, and it is projected to affect 131.5 million people worldwide by 2050 (Alzheimer's disease International, 2015). Dementia because of AD is represented by a significant loss of cognitive function involving memory loss and impairment, language disturbance, difficulties with reasoning and organization as well as visuospatial dysgnosia, which is a loss of the sense of awareness in the relation of oneself to one's surroundings (Borroni et al., 2017). Pathologically, AD is categorized by the accumulation of extracellular senile plaques containing amyloid- β ($A\beta$) peptides in the brain parenchyma and cerebral amyloid angiopathy, which is the accumulation of $A\beta$ in the vessel. AD is also characterized by the accumulation of phosphorylated tau-forming neurofibrillary tangles in the neurons, which are usually accompanied by neuronal cell death and cerebral atrophy (Borroni et al., 2017; Yamazaki and Kanekiyo, 2017). It has become increasingly evident that factors including ageing, cerebral and vascular damage, as well as the accumulation of $A\beta$, can affect multiple components of the BBB and thereby instigate the impairment of the BBB. When the BBB homeostasis is disturbed

the clearance of A β is weakened, which results in a vicious cycle between A β accumulation and BBB dysfunction as AD progresses (Yamazaki and Kanekiyo, 2017).

In addition to this, in early-stage AD, the brain activates several signalling pathways as a response to the disorder. These pathways produce inflammatory signals such as cytokines and reactive oxygen species (ROS), which lead to oxidative stress (Borroni et al., 2017). Oxidative stress is also mediated by hydrogen peroxide which is produced when monoamine oxidase (MAO), an enzyme located in the outer mitochondrial membrane, metabolises monoamine neurotransmitters such as dopamine, norepinephrine, and serotonin via oxidative deamination (Borroni et al., 2017). There are two isoforms of MAO (MAO-A and MAO-B), with different substrate selectivity and tissue distribution patterns. The predominant form of MAO found in the brain is MAO-B (Borroni et al., 2017). In AD, the expression of MAO-B is increased, resulting in the excessive metabolism of monoamine neurotransmitters, leading to the increased production of hydrogen peroxide and ROS, which in turn promote the degeneration of neurons. This process occurs in early-stage AD and has been observed to persist as the disease progresses (Borroni et al., 2017). Considering the role MAO-B plays in the progression of AD, inhibiting its activity may delay the progression of the disease (Borroni et al., 2017).

The treatment of AD is currently targeted towards symptomatic therapy, and so the focus has been on cholinergic deficiency, oxidative stress, the amyloid cascade, inflammation, and excitotoxicity (Shah et al., 2008; Weller and Budson, 2018). Clinical trials underway are investigating various classes of drugs including inhibitors and modulators of γ -secretase and β -secretase enzymes which are catalysts for the generation of A β , inhibitors of A β aggregation, inhibitors of Tau hyper phosphorylation, inhibitors of Tau aggregation, and 5-HT6 inhibitors, while the amyloid beta-directed antibody Aducanumab was recently approved by the FDA (Noscira SA, 2012; TauRx Therapeutics Ltd, 2014; Eisai Inc., 2016 ; Folch et al., 2016; Merck Sharp & Dohme Corp., 2018; Eli Lilly and Company, 2019; Dunn et al., 2021). Acetylcholinesterase inhibitors (AChEIs) are currently the main class of drugs used in treating cognitive dysfunction in AD. AChEIs, however, do not prevent the progressive loss of neurons, which is characteristic of AD (Thomas, 2000; Folch et al., 2016). The second class of drugs approved for the treatment of AD are the N-Methyl-D-aspartate (NMDA) receptor antagonists, specifically memantine which is used in the advanced stages of AD (Shah et al., 2008; Folch et al., 2016). As a result, several

studies have veered towards the use of other known drug classes such as anti-inflammatory agents, antioxidants, and statins for the treatment of AD (Thomas, 2000; Shah et al., 2008).

MAO-B inhibitors are a class of drugs that are used in treating Parkinson's disease but have been observed to be effective in the treatment of AD. L-deprenyl (Selegiline), an MAO-B inhibitor has been observed to enhance the central monoaminergic system via several mechanisms separate from its inhibition of MAO-B. These mechanisms include blocking the response of NMDA-receptors to elevated levels of N-acetylated polyamines, inducing antioxidant enzymes such as superoxide dismutase and catalase, anti-apoptotic activity and enhancing the neurovascular stimulatory effect of nitric oxide (NO) (Thomas, 2000). Nitric oxide plays an important role in cerebral circulation as a vasodilator, increasing cerebral blood flow and alleviating the restriction of blood to the surrounding neurons. In AD, it has been observed that there is a decrease in NO production. The stimulation of NO production by MAO-B inhibitors implies that the NO synthase, a catalyst of NO, is activated. This reaction ensures adequate tissue perfusion thereby alleviating oxidative stress and preventing the progression of neurodegeneration (Thomas, 2000).

2.1.2.1 MAO-B enzyme as a drug target

MAO-B is a well-known target for antidepressant and neuroprotective drugs. It is a dimeric enzyme that consists of 520 amino acids that fold into a compact structure. The active site of MAO-B consists of a 420 Å³-hydrophobic substrate cavity interconnected with an entrance cavity of 290 Å³ (which means that it is a bipartite active site). This substrate binding site is lined by several aromatic and aliphatic amino acids which provides a highly hydrophobic environment (Binda et al., 2002). Two of these amino acids, Tyr 398, and Tyr 435, are responsible for stabilizing the substrate binding site by forming an aromatic sandwich at the site (Binda et al., 2002). Between the two cavities, the entrance, and the substrate cavity, four amino acid residues, Tyr 326, Ile 199, Leu 171 and Phe 198 form a boundary (Binda et al., 2002). When small inhibitors are bound within the substrate cavity, Ile 199 rotates into a closed conformation to create the bipartite active site (which is characteristic of MAO-B), whereas, when large inhibitors are bound to the substrate cavity, Ile 199 forms an open conformation. This suggests that Ile 199 is a structural determinant for substrates and inhibitors of MAO-B, and therefore it is called a

gating residue. Tyr 326 also exhibits conformational changes when an inhibitor binds to the substrate cavity, but these changes are modest. The observations seen with these two amino acid residues suggest that they serve as structural determinants of substrates and inhibitors of MAO-B (Milczek et al., 2011). In addition to this active site, MAO-B is covalently linked by a cysteine residue (Cys 397) to flavin adenine dinucleotide (FAD), a redox-active cofactor involved in several catalytic reactions and a major site of alkylation. MAO-B is also non-covalently bonded to FAD by Lys 296 and Trp 388 (Geha et al., 2002). Figure 2.1 shows the 3-D structure of the human MAO-B as performed with UCSF Chimera, developed by the Resource for Biocomputing, Visualization, and Informatics at the University of California, San Francisco, with support from NIH P41-GM103311. Table 2.1 gives a summary of the active sites of the human MAO-B.

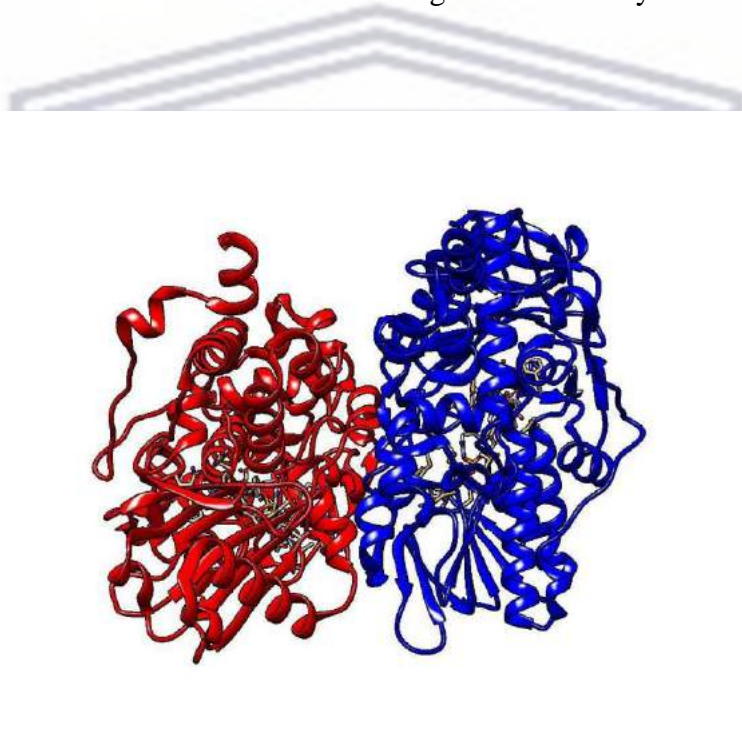


Figure 2.1: 3D structure of human MAO-B (PDB ID: 2vrl); visualized by Chimera (Pettersen et al., 2004).

Table 2.1: Active Sites of Human MAO-B.

Amino Acid	Leucine	Phenylalanine	Isoleucine	Lysine	Tyrosine	Tryptophan
Position	171	198	199	296	326	388

2.2 Drug Discovery and Design

The process of drug discovery is cumbersome, expensive, and time-consuming. Traditionally, this process consists of seven steps: 1.) Disease selection (target identification), 2.) Target hypothesis (target validation), 3.) Lead compound identification (screening), 4.) Lead optimization, 5.) Pre-clinical trial, 6.) clinical trial and 7.) Pharmacogenomics optimization. These are followed sequentially and so a delay in one of the steps hinders the progress of the drug discovery process (Xu and Hagler, 2002; Macalino et al., 2015). Assays carried out to evaluate the efficacy of potential therapeutic agents obtained from either plant sources or chemically synthesized in the lab requires a lot of resources, with no guarantees of successful drug development. A test compound could show favourable pharmacological activity at the initial pharmacodynamics stages of drug discovery, and fail the next stage of testing (i.e., absorption, distribution, metabolism, excretion, and toxicity - ADMET profiling), thereby wasting the resources spent in the process (Xu and Hagler, 2002; Macalino et al., 2015). To avoid the possible waste of time, money, and other resources in drug discovery, *in silico* methods are used to predict the pharmacokinetic properties of small molecules even before they are tested for various pharmacological activities. This cuts down drastically on the chances of spending resources on determining the efficacy of a drug with unfavourable pharmacokinetic properties (Xu and Hagler, 2002; Macalino et al., 2015).

2.2.1 Pharmacokinetics- ADME

Pharmacokinetics can simply be described as what the body does to drugs. It describes the rate and extent to which drugs gain access into systemic circulation (absorption), the transportation of drugs around the body and partitioning into various organs/tissues including their intended target site (distribution), the biotransformation of drugs by hepatic microsomal enzymes (metabolism) and the elimination of drugs from the system after achieving the desired activity in the body (excretion). These properties are part of the parameters used in determining the oral bioavailability profile of a drug and hence its drug-likeness (Schneider, 2013; Ntie-Kang et al., 2018; Faccenda et al., 2019; Le, 2020). It also looks at the possibility of a drug causing adverse effects to the body either because of bioaccumulation or as a result of drug-drug interactions with an enzyme-inducing or inhibiting drug (Schneider, 2013).

Absorption can take place via any of the following transport mechanisms: i.) passive diffusion, ii.) filtration, iii.) bulk flow, iv.) active transport, v.) facilitated transport, vi.) ion-pair transport, vii.) endocytosis or viii.) exocytosis. Absorption depends mostly on a drug's lipophilicity and solubility amongst other physicochemical properties (Alavijeh et al., 2005). These properties are considered when a drug is given orally and would need to move through the phospholipid bilayer of the gastrointestinal epithelial cell membrane. A simple measurement of absorption of a drug is its bioavailability, which in lay terms is the percentage of the drug that gets into systemic circulation (blood) following administration (Alavijeh et al., 2005). The ability of a drug molecule to cross the gastrointestinal membrane into circulation is dependent on intestinal membrane permeability, the surface area of the membrane available for permeation and the concentration of the drug molecule in the gastrointestinal fluid. This ability is further dependent on the molecule's size, charge, and lipophilicity (Fan and de Lannoy, 2014). The lipophilicity of a drug also affects its level of distribution, in that, the more lipophilic a drug is, the more it binds to plasma proteins, which in turn leads to an increase in its distribution (Alavijeh et al., 2005). In addition to its effect on absorption and distribution, the lipophilicity of a drug affects the rate at which it is metabolized by hepatic microsomal enzymes as drugs with high lipophilicity have a higher affinity for these enzymes (Riley et al., 2001).

Passive intestinal absorption looks at the ability of a drug molecule to go through the phospholipid bilayer of the cell membrane. This process requires the drug molecule to be lipophilic or hydrophobic enough to pass the membrane and it is measured using the log of the partition coefficient between n-octanol and water ($\log P$). However, the degree of the passage of the drug molecule drops when the value of $\log P$ is either too high or too low (Xu and Hagler, 2002). Drug molecules that act in the CNS need to cross the BBB to exert their effect. This property is measured using $\log BB$ (the logarithm of the ratio of steady-state concentration of drug in the brain to that in the blood) and $\log P$ in relation to total polar surface area (TPSA) (Xu and Hagler, 2002; Schneider, 2013). The polarity of CNS acting drugs is very critical to whether they can cross the BBB, and a compound must have a TPSA value less than 90\AA^2 to be able to permeate the BBB. Polar compounds are unable to cross the BBB and therefore, they only act in the circulatory system (Durojaye et al., 2019). Although the preceding statement is correct, there are exceptions to this rule. Some extremely polar compounds such as L-Dopa, though unable to

cross the BBB by passive diffusion, are recognized by an amino acid transporter and so actively transported across the membrane into the brain (Klebe, 2013). It is also observed that compounds that cross the BBB also have a high ability to be passively absorbed into the human intestine (Klebe, 2013).

Metabolic reactions of drugs or other xenobiotics occur via oxidation, reduction, hydrolysis, or conjugation reactions mainly by hepatic microsomal enzymes. The primary metabolic reaction for drugs is oxidative reaction mainly by Cytochrome P 450 enzymes (Alavijeh et al., 2005). Drug metabolism and clearance occurs in a series of reactions which can be categorized into two phases. Phase I involves the catalysis of chemical compounds through various reactions which include oxidation, reduction, opening or closing of a ring and hydrolysis. This phase is mostly done by Cytochrome P450 enzymes. Amongst the CYP family, CYP3A is the most predominant subfamily in the liver and with CYP3A4 being the predominant subgroup in human tissue, and responsible for the metabolism of more than 50% of prescribed drugs (Christians et al., 2005). If a phytochemical, therefore, inhibits this enzyme, other drugs which are metabolised by this enzyme will experience an increase in load potentially leading to toxicity. It has been established that CYP enzymes are present in extrahepatic tissues like the brain where they are responsible for the metabolism of centrally acting drugs (Ferguson and Tyndale, 2011). Phytochemicals that are predicted to be inhibitors of CYP enzymes and can cross the BBB can cause a reduction in the metabolism of other CNS drugs which are metabolized by these enzymes and hence increase the toxicity of these drugs in the CNS. However, it has also been observed that the CYP enzymes are not present in the brain in levels sufficient to affect the overall pharmacokinetics of drugs in the body (Hedlund et al., 2001). Phase II metabolic reactions involve the biotransformation of chemical compounds or their metabolites by conjugating them with highly polar endogenous molecules making them more hydrophilic, less toxic, and readily eliminated. The enzymes responsible for this phase are mostly transferases which include glutathione S transferases (GSTs), UDP-glucuronosyltransferases (UGTs), sulfotransferases (SULTs) and N-acetyltransferases (NATs) (Murray, 2013; Di, 2014; Kar and Leszczynski, 2018). The purpose of this phase is to conjugate small molecules with highly polar endogenous molecules, making the resulting molecule more hydrophilic than the parent molecule, thereby deactivating the parent molecule, and enhancing its excretion from the body. Examples of conjugation reactions include glucuronidation, sulfation, methylation, acetylation, glutathione, and amino acid conjugation

(Jancova et al., 2010; Murray, 2013). It can then be summarised that the greater the lipophilicity of a drug, the greater its bioavailability and hence its chance of being drug-like.

2.2.2 *Drug likeness*

The drug-likeness of a small molecule assesses the probability of good bioavailability when given orally. This allows for the identification of molecules with properties consistent with known drugs with good oral bioavailability and hence the possibility of being ‘lead’ compounds. Determination of the drug-likeness of a compound, therefore, provides an opportunity for the optimization of these compounds by altering individual properties (Terstappen and Reggiani, 2001; Seifert et al., 2003; Gangrade et al., 2016). The properties involved in the determination of drug-likeness include the molecular weight, the number of rotatable bonds, the number of hydrogen-bond acceptors, the number of hydrogen-bond donors, polarity (TPSA) and lipophilicity (MlogP). The molecular weight of a compound affects its bioavailability in that a compound with a molecular weight higher than 500Da is captured by the liver on the sole ground of its size and excreted quickly in bile (Klebe, 2013). The lipophilicity of a compound (measured using TPSA and Log P) plays a huge role in its adsorption. It also affects the compound’s binding capacity to proteins for distribution, in that, the higher the lipophilicity the greater its ability to bind to proteins, resulting in greater distribution (Alavijeh et al., 2005). In addition to its effect on absorption and distribution, the lipophilicity of a drug affects the rate at which the compound is metabolized by hepatic microsomal enzymes as drugs with high lipophilicity have a higher affinity for these enzymes (Riley et al., 2001).

2.2.2.1 *Rules of Drug Likeness*

The concept of drug-likeness covers the possibility of a small bioactive molecule being able to meet certain quantitative properties assigned because of research carried out by experts in the pharmaceutical industry. These properties were determined by comparing the similarity in physicochemical properties of already known drugs in the market, which ultimately determine favourable pharmacokinetic properties of small molecules. This has led to several models being created to enable other researchers to eliminate undesirable compounds or optimize desired ‘lead’ compounds in the process of drug design and discovery (Ursu et al., 2011; Schneider,

2013). One common and highly utilized model for determining drug-likeness is that of Lipinski and his colleagues at Pfizer. This model states that the absorption of a compound or small molecule is likely to be impaired if it has any of the following properties:

- More than 5 hydrogen bond donors or more than 10 hydrogen bond acceptors
- A molecular weight more than 500
- A LogP greater than 5 or MoruguchiLogP (MLogP) greater than 4.15 (Lipinski, 2000).

Compounds that are substrates of biological transporters are however exempted from this rule (Ghose et al., 1999). Another model utilised is Ghose's rule of drug-likeness, which considers both physicochemical and structural properties of compounds, like the presence of functional groups and workable substructures. This rule states that for a compound to be considered a drug it should possess the following properties:

- Physicochemical properties consisting of a calculated log *P* (ALOGP) between -0.4 and 5.6, a molar refractivity between 40 and 130, a molecular weight between 160 and 480, and the total number of atoms between 20 and 70.
- Its structure should have a combination of some of the following groups: a benzene ring, a heterocyclic ring (both aliphatic and aromatic), an aliphatic amine (preferably tertiary), a carboxamide group, an alcoholic hydroxyl group, a carboxy ester, and a keto group.
- It should be chemically stable in the physiological buffer, which can be seen clearly in the absence of a reactive functional group or structural moiety (Ghose et al., 1999).

The Egan rule, another drug-likeness model, looks at the lipophilicity and hydrophilicity of a molecule as these properties are responsible for the absorption of a compound (except for outliers where the molecule is a substrate of an active transporter). Instead of the calculated Log P being used, AlogP98 is used to determine lipophilicity and polar surface area (PSA) is used to determine hydrophilicity. Values of $<131.6\text{\AA}^2$ for polarity and <5.88 for WLog P are used as the cut off for a molecule to be drug-like. Both properties are seen to be inversely proportional, with the LogP increasing as the PSA decreases (Egan et al., 2000). According to Veber et al (2002), a molecule is seen to have good oral bioavailability when it has reduced molecular flexibility as seen in the number of rotatable bonds it has as well as its polarity, this being independent of its molecular weight. They, therefore, suggested that molecules with ≤ 10 rotatable bonds and a polar surface area $\leq 140\text{\AA}^2$ will have a high probability of having good bioavailability (Veber et

al., 2002). There have been studies that utilize a modification or combination of the above models to create new models to determine the drug-likeness of a 'lead' molecule, an example is the use of Lipinski's rule of five together with a modification of Ghose's rule to determine the drug-likeness of compounds from MDL Drug Data Report Database (MDDR) (Ajay et al., 1998).

2.2.3 Computer-Aided Drug Discovery and Design (CADD)

As mentioned earlier, the process of drug discovery and design can be cumbersome, and time and resource consuming. This has led to the need to utilize computer-aided or *in silico* methods referred to as computer-aided drug discovery and design (CADD). CADD methods increase the knowledge output of the required physicochemical properties of small molecules based on already existing knowledge (Kapetanovic, 2008). They have been used to streamline the process of drug discovery, design, development, and optimization in a significantly cost-effective manner. They accelerate the process of hit identification (active drug candidates), hit to 'lead' selection (candidates for further evaluation) and 'lead' optimization i.e., to improve the pharmacokinetic and physicochemical properties of 'lead' compounds to enable them to be suitable drugs (Kapetanovic, 2008). Commonly used CADD processes utilize either the knowledge of the structure of the ligand or target (small compounds, receptors, amino acids, etc.) - structure-based design, or the knowledge of the bioactivity of the ligand-ligand-based design (Macalino et al., 2015). Quantitative structure-activity relationships (QSAR) and quantitative structure-property relationships (QSPR) are also used to predict the activity and toxicity of a compound based on its structure, and these relationships are also part of the processes utilized under CADD (Kapetanovic, 2008). These various processes under CADD can either be used alone or preferably complementary to each other. They can also be integrated into other experimental non-*in silico* processes which have a greater influence on rational drug design (Macalino et al., 2015). *In silico* methods are, therefore, used in predicting the potential drug-likeness and pharmaceutical properties of small molecules, as well as in modelling and predicting the multiple pharmacological properties of a test compound. These methods reduce the time spent in drug discovery and give the scientist a vast array of information within a short time as opposed to the singular results obtained from conventional assay methods (Terstappen and Reggiani, 2001; Ekins et al., 2007). In addition to predicting the drug-likeness and pharmacological properties of drug molecules, *in silico* methods are used in generating large data

repositories of candidate compounds to be used in drug discovery (also called data-driven drug discovery) (Jorgensen, 2004; Butte and Ito, 2012; Romano and Tatonetti, 2019). By using data mining on these repositories in addition to the knowledge of the disease, novel therapeutic hypotheses are systematically generated. This avoids systematic biases which are usually present in hypothesis-driven models and improves the return rate on subsequent conventional drug discovery methods, eventually lowering cost and increasing productivity. This form of drug discovery relies heavily on computers and informatics techniques such as bioinformatics and chemo-informatics (Jorgensen, 2004; Butte and Ito, 2012; Romano and Tatonetti, 2019).

2.2.3.1 Chemo-informatics

Chemo-informatics is the application of computer technologies to predict the molecular attributes and chemical behaviour of compounds (Xu and Hagler, 2002; Romano and Tatonetti, 2019). Generally, Chemo-informatics methods are used to exploit either the direct measures of chemical activity of compounds (reactive groups and ADMET profile) or the indirect measures of chemical activity (compound classes and structural motifs) for drug design and discovery. Exploiting these measurements can be done in either a prospective or retrospective manner (Romano and Tatonetti, 2019). Prospectively, the activity of a test compound is predicted by comparing its structure to that of a compound with known chemical activity. Retrospectively, a compound of interest is first identified (also known as ‘hits’) and then chemo-informatics methods are used to generate libraries of compounds with similar structure and activity as the first compound. Chemo-informatics methods have been used mainly in drug discovery and design and especially in relation to natural products (NPs) (Romano and Tatonetti, 2019). These methods are used to discover ‘lead’ compounds (this can be based on the structure of the target or the ligand itself), optimize the lead compounds and model the ADMET properties of these compounds (Gasteiger, 2016). Unlike the step-wise conventional methods of drug discovery and design, chemo-informatics enables the researcher to carry out ADMET profiling predictions earlier in the process together with the screening and synthesis of lead compounds. This approach, called the multi-parametric optimization strategy, eliminates drug candidates which would fail the development process due to poor ADMET properties as early as possible, thereby avoiding expenses that would have been spent and wasted on the development and design of these candidates (Xu and Hagler, 2002; Segall, 2012; Bhalerao et al., 2013). Another benefit of

chemo-informatics is the use of high-throughput and virtual screening technologies to identify lead compounds from compound libraries and to filter out unwanted chemical entities. This filter can be based on desired drug-like properties and ADMET profiles or on the chemical interactions with an identified target. The use of chemo-informatics is not limited by the lack of information about a target or ligand structure (Gasteiger, 2016). In fact, chemo-informatics uses known data analytic approaches to derive the structure-activity relationship (SAR) of a test compound. Information obtained from the high throughput and virtual screening can then be uploaded to virtual compound libraries for knowledge sharing (Xu and Hagler, 2002). One disadvantage of chemo-informatics is that it relies critically on data to develop models and the quality of the dataset influences the quality of the models developed. It has been discovered that some datasets are either full of errors or have incomplete chemical reactions which ultimately affects the quality of models developed (Gasteiger, 2016). As mentioned earlier, chemo-informatics techniques are used in predicting ADMET properties of potential leads and this process can be conducted at the earlier stages of drug development. These techniques involve the use of models which have been developed based on the information on the structural target and desirable physicochemical and structural features of compounds (Xu and Hagler, 2002; Yamashita and Hashida, 2004). Examples of models and desired ligand properties for each of the pharmacokinetic properties are discussed below:

Absorption:

Knowledge of the structure of the cell membrane has led to the use of passive intestinal absorption (PIA) models in chemo-informatics. These models use the interrupted phospholipid bilayer of the cell membrane which acts as a barrier system for the movement of compounds in or out of the cell (Xu and Hagler, 2002). These models also consider the knowledge that passive diffusion through the cell membrane is the predominant pathway for lipophilic compounds, whilst hydrophilic compounds with low molecular weight (i.e., less than 200) must go through the water-filled channels of the tight junctions between the membrane (Xu and Hagler, 2002). The lipophilicity of a compound is measured as log P (which is the log of the partition coefficient between n-octanol and water), and this value determines the permeability of the compound across the cell membrane. However, it has been observed that both low and high log P values correspond to a reduction in the permeability of the compound as weak lipophilic compounds cannot penetrate the cell membrane whilst strong lipophilic compounds are excessively partitioned into

the lipid portion of the cell membrane (Xu and Hagler, 2002). Apart from the lipophilicity of a compound, absorption models have also taken into consideration the polar surface area (PSA) or topological polar surface area (TPSA) of a compound, as it has been observed in several studies that there is a strong relationship between PIA and PSA (Xu and Hagler, 2002; Yamashita and Hashida, 2004). Other physicochemical and structural features considered in these models include molecular weight, hydrogen-bond descriptors (donors and acceptors), polarizability and free energy (Xu and Hagler, 2002; Yamashita and Hashida, 2004).

Distribution:

QSAR models have been used to predict the ability of a drug to bind to human serum albumin (HSA) protein, a major transporter of drugs and metabolites across the body system (Bhalerao et al., 2013). These models measure the binding energy of compounds to attach to HSA thereby measuring the availability of compounds to move from the circulatory system to target tissues (Xu and Hagler, 2002; Yamashita and Hashida, 2004; Bhalerao et al., 2013). The binding energy of a compound is also determined by its hydrophobicity as measured by clogP. However, CNS drugs need to cross the BBB to cause physiological or biochemical changes. These models then take into consideration the log of the brain-blood partition ratio (log BB), the molecular weight of the compound, excess molar refraction, polarizability of the compounds, hydrogen bond acidity or basicity and molecular volume (Xu and Hagler, 2002; Yamashita and Hashida, 2004).

Metabolism:

Based on the knowledge obtained from *in vitro* and *in vivo* studies on the metabolism of compounds in the cell, high throughput screening (HTS) has been used to predict the metabolic stability of compounds. It has also been used to predict substrates and inhibitors of specific CYP isoenzymes and to identify major metabolites (Xu and Hagler, 2002; Bhalerao et al., 2013). The models used to predict the metabolism of compounds include QSAR and pharmacophore (i.e., the atoms and functional groups required for a specific pharmacological activity) models, protein models and expert systems (Braga and Andrade, 2012). The QSAR models are used to predict the substrates and inhibitors of CYP isoenzyme whilst the protein models are used to identify possible substrates and their metabolites through molecular docking (Xu and Hagler, 2002; Braga and Andrade, 2012). Expert systems are virtual libraries that are screened to identify

potential metabolites of a compound based on prior structure-based knowledge (Xu and Hagler, 2002).

Excretion:

The prediction of the half-life of a compound gives the probability of the length of time it would take for half the concentration of a compound to be eliminated from the body. QSPR models are used to predict this property. These models utilize multivariate descriptors of compounds in their analysis, such as the polarity, molecular weight, hydrogen bonding properties, polar surface area and polarizability amongst others (Kidron et al., 2012).

Toxicity:

Apart from the effect of metabolism and excretion on drug toxicity, toxicity can be related to the chemical structure of the compound. Therefore, mathematical models have been developed to predict the toxicity profile of compounds based on the structure-activity relationship, taking into consideration the molecular properties of the compound and existing biological data (Xu and Hagler, 2002; Gasteiger, 2016).

2.2.3.2 Molecular Docking as a CADD tool

Molecular docking is a key tool in structure-based molecular biology and computer-based drug design (Morris and Lim-Wilby, 2008). This method aims to predict the predominant binding mode of the ligand-receptor complex structure through two interrelated steps: Predicting the conformations of the ligand in the active site of the receptor (also known as the pose); and then assessing the binding affinity of each conformation in a rank system via a scoring function (Morris and Lim-Wilby, 2008). This methodology can be used to illustrate the interaction between a small molecule and a protein at the nano scale, hence enabling the researcher to describe the behaviour of small molecules at the active site of its target protein, as well as the fundamental biochemical processes behind these interactions (Morris and Lim-Wilby, 2008; Meng et al., 2011; Attique et al., 2019). Docking can also be used to perform high throughput screening on the virtual library of compounds, ranking the conformations of each compound and proposing hypotheses of the structural interaction of these compounds with a protein target

(Morris and Lim-Wilby, 2008). Therefore, molecular docking can be used to analyse all factors involved in drug design and discovery (Attique et al., 2019).

Molecular docking methodology is made up of two methods: Structure-based and Ligand-based methods (Attique et al., 2019). The structure-based method is the approach where the structural information of the protein receptor is exploited for the development of its ligand. The structure of the protein receptor is a prerequisite for this method as it relies on the knowledge of the 3-D structure of the receptor to sample the conformations of the tested ligands. And so, it is generally preferred where the high-resolution structure of the protein is available. When the active site of a protein receptor is characterized based on its structure, it sheds light on the binding features of the receptor, and this makes it possible to design ligands that would bind specifically to that receptor target (Aparoy et al., 2012; Attique et al., 2019). On the other hand, the ligand-based method is used in the absence of the 3-D structure information of the protein receptor, and it relies on knowledge of ligands that bind to the biological target of interest. It is the method of choice when there is a lot of information about the ligands. It exploits the knowledge of compounds through chemical similarity searches (Aparoy et al., 2012; Attique et al., 2019). The docking process can be carried out in three ways: rigid ligand and rigid protein; flexible ligand and rigid protein; flexible ligand and flexible protein (Meng et al., 2011). These processes are done to find the best fit that elucidates the desired activity. Rigid ligand and rigid protein docking are the process in which both the ligand and protein are treated as rigid bodies with a fixed conformation and so they cannot change their spatial shape during docking (Sauton et al., 2008). Amongst the three ways, rigid ligand and rigid protein is the quickest docking process to carry out but does not give an accurate result of the possible best fit. This means that this process requires that pre-generated multiple conformers for the ligand or protein be employed for the accuracy of results (Sauton et al., 2008). In the flexible ligand and rigid protein docking process, the ligand takes on as many shape conformations as possible while the receptor protein remains in a fixed rigid conformation. This is the most common approach used as it trades off the accuracy of results for computational time and cost (Meng et al., 2011). Flexible ligand and flexible protein docking is the process in which both the ligand and protein take on as many shape conformations as possible during the docking process. Although the flexible ligand and flexible protein approach is ideal, as it supports the theory that the protein also changes conformation in the binding process, it is expensive to perform (Meng et al., 2011).

Several computational tools have been developed to be used in molecular docking, particularly in drug discovery. Some of these tools include Glide, Gold, Auto dock, PyRx, Surflex, ICM, FITTED, and MOE (Molecular Operating Environment). Table 2.2 lists the description and advantages of each of these tools.

Table 2.2: Tools used for molecular docking studies (Attique et al., 2019).

Software/Tool	Algorithm	Scoring Term	Advantages
Molecular Operating Environment (MOE)	High-Speed _ shapes algorithms	London dG, FlexX, DrugScore, Mcdock	Customizable, available source-code, gives binding affinity score, shows interacting amino acids with position, and is user-friendly.
Glide (Grid-based Ligand Docking with Energetics)	Monte Carlo	Glide score	Lead discovery and lead optimization
GOLD (Genetic Optimization for Ligand Docking)	Genetic algorithm	GoldScore, ChemScore, ASP (Astex Statistical Potential), CHEMPLP (Piecewise Linear Potential), User-defined	Allows atomic overlapping between protein and ligand
AutoDock	Lamarckian genetic algorithm	Empirical free-energy function	Adaptability to user-defined input
PyRx	Lamarckian genetic algorithm	Binding energy, Internal energy, Internal energy, Unbound energy	Temperature Resistance. Pyrex's excellent thermal properties at both high and low temperatures are one of its key features.
Surflex	Surflex-Dock search Algorithm	Bohm's scoring function	High accuracy level by extending force fields
ICM (Internal Coordinate Modelling)	Monte Carlo minimization	Virtual library screening scoring function	Allows side chain flexibility to find a parallel arrangement of two rigid helices

FITTED (Flexibility Induced Through Targeted Evolutionary Description)	Genetic algorithm	Potential of Mean Force (PMF), Drug Score	Analyses the effect of water molecules on protein–ligand complexes
--	----------------------	---	--

The advantages of MOE over the other docking tools include a user-friendly graphical interface that displays a good graphical view of docking results, showing the ligand-receptor binding residues, their positions, and interactions. It also helps to visualize, characterize, and evaluate the interactions between proteins and ligands. MOE also identifies hydrogen bonds, hydrophobic interactions, salt bridges, and solvent exposure. The scoring function used in MOE is known as the S-score. The S-score is also used to predict the binding affinity of inhibitors with receptor proteins. The lower the S-core of an inhibitor the stronger its affinity with the binding site of the receptor (Attique et al., 2019). Knowledge of the binding site of the receptor before the docking process significantly increases the efficiency of the process. This knowledge is sometimes already known, while in some other cases, a comparison between the target protein and a family of proteins helps to provide this information (Meng et al., 2011).

2.3 *Leonotis leonurus*

Leonotis leonurus R. Br. (Lamiaceae), is also known as Wild dagga or Lion’s ear (Leon- Lion, Otis- Ear) because of the resemblance of its flowers to a Lion’s ear. It is a perennial shrub and a member of the mint family. It is widespread throughout South Africa and favours warm dry climates. It grows to a height of 2-3m and 1.5m in width. It is used as an ornamental plant due to its aerial parts (Agnihotri et al., 2009; Narukawa et al., 2015; Turner, 2015).

2.3.1 Taxonomy of *Leonotis leonurus*

Family: Lamiaceae

Genus: Leonotis

Species: Leonurus

Common Names: Lion’s Ear, Wild dagga, leonotis (Turner, 2015).

2.3.2 *Traditional Uses:*

L. leonurus is claimed to have mild hallucinogenic and psychoactive effects when the leaves or buds are dried and smoked. As such the plant is used for recreational purposes amongst some tribes in Africa and as a substitute for cannabis in Mexico. Apart from its recreational use, smoked leaves are used in the southern part of Africa to alleviate epileptic fits and as a cure for partial paralysis (Narukawa et al., 2015; Nsuala et al., 2015). Various parts of the plant are made into different formulations and used traditionally in the treatment of disease. The leaves and stem of the plant are formulated into decoctions and used as a topical treatment for muscular cramps, boils, eczema, and other skin diseases. This decoction is also used to treat respiratory diseases like asthma, chest infections, coughs, colds, tuberculosis, feverish headaches, hypertension, irregular or painful menstruation and viral hepatitis (Van Wyk and Gericke, 2000; Van Wyk et al., 2000; Wu et al., 2013; Narukawa et al., 2015). Being a part of the minty family, the leaves of *L. leonurus* are drunk as a minty tea. The whole plant is also made into tea which is used to treat obesity, cancer, arthritis, and bladder and kidney disorder. The fresh juice of the stem is used as a blood cleanser, while the leaves, root and bark of the plant are used as an emetic and to alleviate the symptoms of snake bites, scorpion, and bee stings. In ethno veterinary medicine, infusion of the roots and leaves is used in poultry against anaplasmosis and eye inflammation (Wu et al., 2013; Mazimba, 2015; Nsuala et al., 2015).

2.3.3 *Studies on the effect of Leonotis leonurus:*

As mentioned in the preceding section, *L. leonurus* is used in the treatment of various ailments and for recreational purposes, this knowledge has led to research on the plant to validate the traditional medicinal claims of the plant. Bienvenu et al. (2002) tested the aqueous leaf extract against seizures induced by pentylenetetrazole (PTZ), picrotoxin, bicuculline and N-methyl-DL-aspartic acid (NMDLA) to determine the mechanism for its ethnobotanical use in the treatment of epileptic seizures. It was observed that there was a dose-dependent anticonvulsant activity on seizures induced by PTZ and NMDLA with an increased effect on seizure latency but no anticonvulsant effect on bicuculline-induced seizures and picrotoxin (except in increasing seizure latency) (Bienvenu et al., 2002). Another study conducted on the methanolic leaf extract of the plant reported a significant delay in the onset of seizures and a significant reduction in the convulsant effect induced by PTZ in male albino mice (Muhizi et al., 2005). In yet another study

on the anticonvulsant effect of *L. leonurus*, it was reported that the highest concentrations of ethanolic leaf extract of the plant had a weak GABA_A receptor activity but none of the concentrations of the aqueous leaf extract of *L. leonurus* showed any activity on the GABA_A receptor (Risa et al., 2004). These observations suggest that *L. leonurus* may contain bioactive compounds (which are soluble in both water and methanol) that elicit anticonvulsant activity by enhancing GABAergic activity. In a bid to determine the mode of action of *L. leonurus* in alleviating depression, the ethanolic leaf extract of *L. leonurus* was tested for its affinity for the serotonin reuptake transport protein. It was, however, observed to have a low affinity for the protein at the highest dose administered and therefore a low inhibition of serotonin reuptake (Nielsen et al., 2004).

With respect to the cardiovascular effect of the plant, Ojewole (2003), observed that the aqueous leaf extract caused a significant dose-related decrease in arterial blood pressures and heart rate for normal and spontaneously hypertensive rats (Ojewole, 2003). This was, however, not the case in another study conducted by Obikeze (2004), where it was reported that the organic leaf extracts of *L. leonurus* caused an increase in systolic, diastolic, and mean arterial blood pressure at higher doses but a reduction at lower doses of the extract (Obikeze, 2004). Similar observations to Obikeze (2004) were made in another study by Mugabo et al (2012) who observed that the aqueous leaf extracts of *L. leonurus* in the isolated perfused rat heart caused a positive inotropic and a negative chronotropic effect at lower doses, with toxicity seen with doses greater than 2.0mg/ml (Mugabo et al., 2012). Another study reported the dose-dependent decreases in the heart rate, systolic and diastolic pressure of male rats when the aqueous leaf extract was administered (Tshambuluka et al., 2011). Yet another study by Obikeze et al (2013) reported a dose-dependent increase in mean arterial pressure and heart rate in both *in vitro* and *in vivo* assays with one of five fractions of the methanolic leaf extract of the plant called fraction C (Obikeze et al., 2013). The cardio protective effect of organic extracts of *L. leonurus* in reducing clotting time as well as inhibiting fibrin formation in obese rats was also observed in a study conducted by Mnonopi et al (2011).

The antidiabetic and anticholesteremic effects of *L. leonurus* were studied by Ojewole (2005) and Oyedemi et al. (2011). The aqueous leaf extract of *L. leonurus* was reported to have a significant hypoglycaemic effect when it was administered to streptozotocin-induced diabetic

mice and rats (Ojewole, 2005). This result was corroborated by a study done by Oyedemi et al (2011), where similar results were obtained with the aqueous leaf extract of *L. leonurus* in streptozotocin-induced diabetic male Wistar rats. Furthermore, the plant extracts significantly reduced cholesterol, high density lipoproteins (HDL), and triacylglycerol levels whilst significantly increasing low density lipoprotein levels (Oyedemi et al., 2011). In another study, it was observed that the organic leaf extract of *L. leonurus* stimulated the production of insulin in hyperglycaemic obese rats and did not induce the production of insulin in normoglycemic lean rats (Mnonopi et al., 2012).

The aqueous leaf extract of *L. leonurus* was reported to exhibit antibacterial activity against *Staphylococcus aureus*, *Bacillus subtilis* and *Klebsiella pneumoniae* (Stafford et al., 2005). However, the aqueous leaf extract showed no activity against *Bacillus cereus*, *Staphylococcus epidermis*, *Staphylococcus aureus*, *Micrococcus kristinae*, *Streptococcus pyrogens*, *Escherichia coli*, *Salmonella pooni*, *Serratia marcescens*, *Pseudomonas aeruginosa* and *Klebsiella pneumoniae*, while the methanolic and acetone extracts were observed to have an antimicrobial effect against all these organisms except *Klebsiella pneumoniae* (and *Staph. Epidermis* for the acetone extract) (Jimoh et al., 2010). The organic extract of the leaves of *L. leonurus* showed greater than 99% growth inhibition against *Mycobacterium tuberculosis* when compared with the control, rifampicin (Naidoo et al., 2011).

The aqueous, methanolic and acetone extracts of *L. leonurus* exhibited high antioxidant activity in the ferrous reducing antioxidant (FRAP) and 1,1-Diphenyl-2-picrylhydrazyl (DPPH) radical scavenging assay when compared to the control, butylated hydroxytoluene (BHT) (Jimoh et al., 2010). This observation was corroborated in another study which found a concentration-dependent antioxidant activity with the plant's extracts (Oyedemi et al., 2011).

In a study done by Ojewole, (2005) to test the effect of the aqueous leaf extract of *L. leonurus* on 'hot plate' and 'acetic acid' induced pain and fresh-egg albumin induced paw oedema in rats, it was observed that the plant extract reduced the pain perception and inflammation of the paw significantly (Ojewole, 2005). In another study done by El-Ansari et al. (2009), 70% methanol and chloroform extracts of the plant's flowers were tested against carrageenan-induced hind rat paw oedema and seen to produce a 20% and 41% reduction, respectively, in paw size (El-Ansari

et al., 2009). Furthermore, Prostaglandin synthesis was seen to be totally inhibited by the ethanolic extract of *L. leonurus* through cyclooxygenase 1 (COX-1) inhibition (Stafford et al., 2005).

El-Ansari et al (2009) tested the toxicity of the flowering aerial part of the plant on male albino rats using 70% methanol and chloroform extracts. They discovered that these extracts were non-toxic to the rats but rather protected the liver of the rats from Paracetamol-induced hepatotoxicity (El-Ansari et al., 2009).

2.3.4 Compounds isolated from *L. leonurus*

Preliminary studies have reported on the presence of alkaloids, terpenoids (mono-, di-, and sesquiterpenoids), iridoid glycoside, phenolic compounds, quinines, saponins, tannins, and sterols in aqueous and organic extracts of the plant (El-Ansari et al., 2009). In addition, the flowers of the plant have also been reported to contain flavonoids and acyclic diterpene esters (El-Ansari et al., 2009; Mazimba, 2015; Nsuala et al., 2015). Table 2.3 shows the breakdown of the phytochemicals and the part of the plant from which they were isolated.

Table 2.3: List of Compounds isolated from *L. leonurus*

S/No	Bioactive Compound	Type of Extract	Part of the Plant	Reference
1	6-Methoxyluteolin-4'-methylether	Methanol	Flowering aerial part	(El-Ansari et al., 2009)
2	13R-premarrubin	Acetone	Leaves	(Laonigro et al., 1979)
3	13S-premarrubin	Acetone	Leaves	(Laonigro et al., 1979)
4	13 ξ -hydroxylabd-5(6), 8(9)-dien-7-on-16 15-olide	Acetone	Aerial Part	(Narukawa et al., 2015)

S/No	Bioactive Compound	Type of Extract	Part of the Plant	Reference
5	14 α -hydroxy-9 α , 13 α -epoxylabd-5(6)-en-7-on-16, 15-olide	Acetone	Aerial Part	(Narukawa et al., 2015)
6	16 ϵ pi-Leoleorin F	Acetone	Leaves	(Wu et al., 2013)
7	Acteoside	Ethanol	Flowering tops	(Agnihotri et al., 2009)
8	Apigenin	Methanol	Flowering aerial part	(El-Ansari et al., 2009)
9	Apigenin-6-C- α -arabinoside-8-C- β -glucoside	Methanol	Flowering aerial part	(El-Ansari et al., 2009)
10	Apigenin-7-O-(6"-O-p-coumaryl)- β -glucoside	Methanol	Flowering aerial part	(El-Ansari et al., 2009)
11	Chrysoeriol (Luteolin 3'-methyl ether)	Methanol	Flowering aerial part	(El-Ansari et al., 2009)
12	Compound X	Acetone	Leaves	(Cragg and Little, 1962; Narukawa et al., 2015)
13	Compound Y / Leoleorin A	Acetone	Leaves	(Cragg and Little, 1962; Wu et al., 2013)
14	Comosiin (Apigenin-7-O- β -glucoside)	Methanol	Flowering aerial part	(El-Ansari et al., 2009)
15	Cynaroside (Luteolin-7-O-glucoside)	Methanol	Flowering aerial part; Leaves	(Agnihotri et al., 2009; El-Ansari et al., 2009; He et al., 2012)
16	Dihydroxylphytyl palmitate	Ethanol	Flowering tops	(Agnihotri et al., 2009)

S/No	Bioactive Compound	Type of Extract	Part of the Plant	Reference
17	(13S)-9 α , 13 α -epoxylabda-6 β (19),15(14)diol dilactone (EDD)	Methanol	Stems and Leaves	(Obikeze et al., 2008; Narukawa et al., 2015)
18	Geniposidic acid	Ethanol	Flowering tops	(Agnihotri et al., 2009)
19	Leoleorin B	Acetone	Leaves; Aerial part	(Wu et al., 2013; Narukawa et al., 2015)
20	Leoleorin C	Water and Methane	Leaves	(Naidoo et al., 2011; Wu et al., 2013)
21	Leoleorin D	Acetone	Leaves	(Wu et al., 2013)
22	Leoleorin E	Acetone	Leaves	(Wu et al., 2013)
23	Leoleorin F	Acetone	Leaves	(Naidoo et al., 2011; He et al., 2012; Wu et al., 2013)
24	Leoleorin G	Water and Acetone	Leaves; Aerial part	(He et al., 2012; Wu et al., 2013; Narukawa et al., 2015)
25	Leoleorin H	Water and Acetone	Leaves	(He et al., 2012; Wu et al., 2013)
26	Leoleorin I	Water and Acetone	Leaves	(He et al., 2012; Wu et al., 2013)
27	Leoleorin J	Acetone	Leaves	(Wu et al., 2013)
28	Leonurun	Acetone	Leaves	(Muhizi et al., 2005; McKenzie et al., 2006)

S/No	Bioactive Compound	Type of Extract	Part of the Plant	Reference
29	Luteolin	Methanol	Flowering aerial part; Leaves	(El-Ansari et al., 2009; He et al., 2012)
30	Luteolin 7-O- β -glucoside-3'-methyl ether	Methanol	Flowering aerial part	(El-Ansari et al., 2009)
31	Marrubiin	Acetone	Leaves; Aerial part	(Rivett, 1964; Narukawa et al., 2015)
32	Nepetaefolin	Water and Acetone	Leaves	(He et al., 2012)
33	Stachydrine	Water	Flowering Aerial part	(Kuchta et al., 2013)
34	Succinic Acid	Ethanol	Flowering tops	(Agnihotri et al., 2009)
35	Uracil	Ethanol	Flowering tops	(Agnihotri et al., 2009)
36	Vitexin (Apigenin-8-C- β -glucoside)	Methanol	Flowering aerial part	(El-Ansari et al., 2009)

2.3.5 Bioactivity of isolated compounds

Acteoside:

Acteoside is a phenyl ethanoid isolated from the flowering tops of the plant, also known as verbascoside. Acteoside is used as an antioxidant, anti-infective, immunosuppressant, chelating and antineoplastic/ phyto-genic agent (National Center for Biotechnology Information, 2018). Acteoside also has hepatoprotective properties (Yim et al., 1997), it inhibits the oxidation of lipids in the tissue especially polyunsaturated fatty acid by reactive oxygen species (a process

which could result ultimately in tissue damage) (Pan and Hori, 1994; Mylonas and Kouretas, 1999) as well as inhibiting tyrosine kinase and tumour growth (Kunvári et al., 1999).

Cynaroside (Luteolin 7-O-glucoside):

Cynaroside is a flavonoid isolated from the flowering aerial part and leaves of the plant. It was reported to have antimalarial activity comparable to chloroquine and artemisinin against the D6 and W2 malaria clone (Agnihotri et al., 2009). In another study, cynaroside was reported to have significant microbicidal activity against chloroquine- and pyrimethamine resistant *P. falciparum* and inhibitory activity against plasmodium Fab I enzyme, that is, the enoyl-ACP reductase enzyme of *P. falciparum*. In this same study, cynaroside was seen to have microbicidal activity against *Leishmania donovani*, an intracellular compound that causes the disease leishmaniasis (Kırmızıbekmez et al., 2004). Cynaroside was also reported to have antioxidant activity against superoxide radical, hydroxyl radical and hydrogen peroxide (Park et al., 2000).

EDD:

EDD is a labdane diterpene isolated from the stems and leaves of the plant. In the novel study done to extract and identify this compound, it was tested to determine its cardiovascular activity. The results showed that at lower doses this compound reduced hypertensive parameters but caused an increase of these parameters when higher doses were administered (Obikeze et al., 2008).

Geniposidic Acid:

Geniposidic acid is an iridoid glycoside isolated from the flowering tops of the plant. It was observed to promote collagen synthesis in false aged model rats (Li et al., 1998). It also has hypotensive and purgative effects (Inouye et al., 1974; Wu et al., 2007).

Leoleorin A – J and 16-epi-leoleorin F:

Leoleorin A-J and 16-epi-leoleorin F, labdane diterpenes isolated from the leaves and aerial parts of the plants were tested for their effect on CNS receptors. More specifically, opioid sigma 1, acetylcholine M₃, histamine H₁, dopamine D₁, and serotonin 5HT_{1A} and 5HT₃ receptors. All eleven compounds showed inhibition of the CNS but via different pathways (Wu et al., 2013).

Serotonin 5HT_{1A} was inhibited by leoleorin A, D, H, and I whilst 5HT₃ was inhibited by leoleorin J only. Dopamine D₁ receptor was inhibited by leoleorin D, E, G and H. Histamine H₁ was inhibited by leoleorin B, C, E and F. Acetylcholine M₃ receptor was inhibited by 16-epi-leoleorin F only, and opioid sigma 1 receptor was inhibited by leoleorin C (Wu et al., 2013). According to another study on the CNS focused on the gamma aminergic pathway, Leoleorin G and I showed no activity at the GABA_A site (He et al., 2012). Leoleorin A and B showed mild to moderate inhibitory effects against oestrogen sulfotransferase, an enzyme that plays a key role in the maintenance of cellular oestrogen levels, when compared to meclofenamic acid (Narukawa et al., 2014, 2015).

Leonurun:

Leonurun is a labdane diterpene isolated from the leaves of the plant. In an anticonvulsant study carried out by Muhizi et al., (2005) it was discovered that compound I, characterized to be 20-acetoxy-9 α ,13 α -epoxylabda-14-en-6 β (19)-lactone and named leonurun had a therapeutic and preventive anticonvulsant effect against PTZ-induced seizures in mice (Muhizi et al., 2005). In another study by McKenzie et al., (2006) identifying this compound as a novel compound, it was observed that leonurun had a positive inotropic effect on the isolated perfused rat heart (McKenzie et al., 2006).

Apigenin and Luteolin:

Apigenin and luteolin are flavonoids extracted from the flowering aerial parts and leaves of the plant. It was observed in an *in silico* study conducted by Chimenti et al., (2010), that apigenin and luteolin had inhibitory activity against MAO-B, this was also confirmed by an *in vitro* study conducted by Chaurasiya et al., (2014). In another study into the antidepressant activity of luteolin, it was observed that luteolin showed antidepressant-like effects in a dose-dependent manner by acting as a positive modulator of the GABA_A Receptor-Cl⁻ ion channel complex (de la Peña et al., 2014).

Marrubin:

Marrubin is a labdane diterpene isolated from leaves and aerial parts of the plant. In a study to ascertain the presence of marrubin in the organic extract of *L. leonurus*, marrubin as well as the organic extract of *L. leonurus* were tested against the conventional treatments for coagulation,

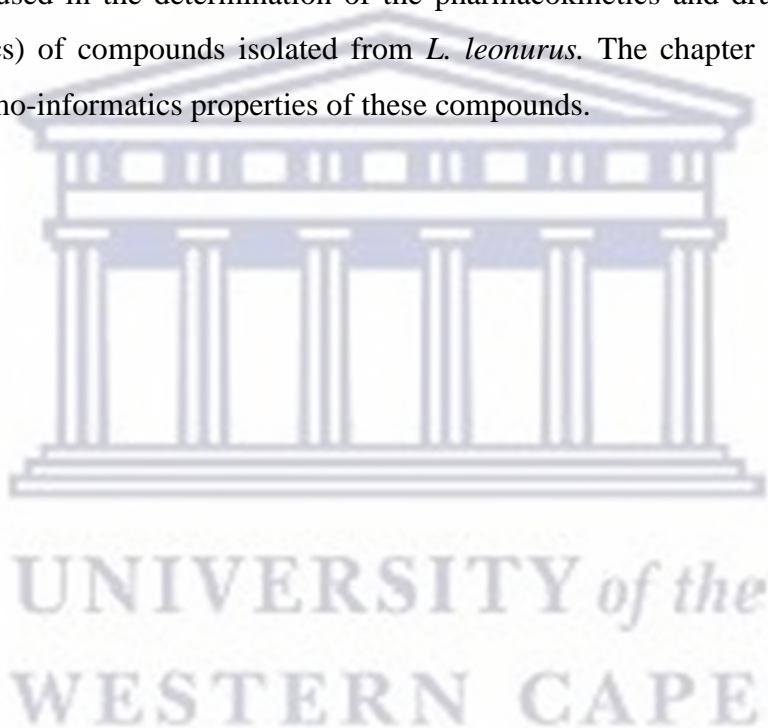
platelet aggregation and inflammation in obese and normal-weight rats. It was observed that marrubini and the organic extract of *L. leonurus* exhibited similar cardio protective effects in prolonging clotting time, inhibiting fibrin formation and inhibiting cyclooxygenase (COX) enzyme (Mnonopi et al., 2011). In another study conducted by Mnonopi et al., (2012), marrubiin was reported to stimulate the production of insulin in hyperglycaemic obese rats. This study also compared the antidiabetic effect of the organic extract of *L. leonurus* with that of marrubiin and the effect was observed to be similar (Mnonopi et al., 2012). Marrubiin was also reported to have a weak to moderate oestrogen sulphur transferase inhibitory effect when compared to meclofenamic acid (Narukawa et al., 2015).

Vitexin:

Vitexin is a flavonoid isolated from the flowering aerial parts of the plant. It was observed in a study to determine the antidiabetic, anti-AD, and anti-inflammatory properties of vitexin that it inhibited protein tyrosine phosphatase 1B, a negative regulator of insulin signalling pathways. It was also observed to have weak inhibitory activity on butyrylcholinesterase (BChE) and β -site amyloid precursor (BACE1), both enzymes involved in the pathogenesis of AD. It, however, did not inhibit nitric oxide production responsible for inflammation in this study (Choi et al., 2014). In another study on the activity of vitexin on AD, it was observed that this compound inhibited the amyloid β peptide-induced NO generation in the ganglion neurons of rats, thereby protecting these cells from degeneration (Guimarães et al., 2015). Vitexin was also reported to have an antidepressant activity which was thought to be mediated through an increase in catecholamine levels in the synaptic cleft as well as through interactions with the serotonergic 5-HT_{1A}, noradrenergic α_2 , and dopaminergic D₁, D₂, and D₃ receptors (Can et al., 2013). Other bioactive properties of vitexin studied include anticancer, neuroprotection and hepatoprotection (Peng et al., 2021; Wu et al., 2021).

The development of successful CNS drugs using traditional drug discovery and development approaches are resource-intensive and have a high attrition rate due to the many challenges including the assurance of efficacy, low toxicity, and a desired pharmacokinetic profile (e.g., adequate permeation through the BBB) for the hit compounds. The use of computer-aided strategies in drug discovery and development allows for the prediction of the efficacy, toxicity, and pharmacokinetic profiles of hit compounds before the expensive process of synthesis,

bioactivity assay and *in vivo* preclinical studies. Plants and their products provide a wealth of small compounds that can be extracted and tested for a needed biological activity. *Leonotis leonurus*, being one of the plants used in the treatment of CNS conditions such as depression and seizures, has the potential of providing successful CNS drug candidates for the treatment of AD. The identification of these candidates, however, is still being carried out. Therefore, identifying compounds isolated from *L. leonurus* with CNS activity, as well as the characterisation of their pharmacokinetic properties using *in silico* methods is desirable. In this study, the identification of potential CNS drug candidates from *L. leonurus* compounds based on their chemo-informatics properties and activity as inhibitors of MAO-B activity was carried out. The next chapter presents the methodology used in the determination of the pharmacokinetics and drug-like properties (chemo-informatics) of compounds isolated from *L. leonurus*. The chapter also presents the results on the chemo-informatics properties of these compounds.



Chapter 3

3. CHEMO-INFORMATICS CHARACTERIZATION AND DRUG-LIKENESS OF *LEONOTIS LEONURUS* COMPOUNDS

3.1 Introduction

Chemo-informatics is the process of data mining from raw data of chemical compounds, utilizing computer programmes, to extract usable data or information (Xu and Hagler, 2002; Lo et al., 2018). It involves, amongst others, the use of chemical structure descriptors to determine the diversity analysis and chemical profile of compounds. Data mining aims to recognize trends or patterns in the raw bioactivity data of chemical compounds which provide knowledge into the relationship between bioactivity related features of these compounds and specific activities or properties (Xu and Hagler, 2002; Begam and Kumar, 2012). Data mined using computer programmes would include information on the descriptors of compounds with specified bioactivity, chemical interactions between compounds and proteins, the pharmacokinetic properties of potential lead compounds, and the potential targets of lead compounds (Xu and Hagler, 2002; Gasteiger, 2016). In the early days of drug discovery, the process of analysing pharmacokinetic properties was performed after the identification of lead compounds via *in vitro* screening. This process does not guarantee the discovery of ‘drug-like’ compounds but might result in lead compounds with poor pharmacokinetic profiles that may not proceed to the clinical phases of drug discovery. The implication is that money, time, and human resources will be wasted in the process (Xu and Hagler, 2002; Begam and Kumar, 2012). As a result of the emergence of the chemo-informatics process, the prediction of the pharmacokinetic properties of potential lead compounds can be done at the earlier stage of drug discovery saving both time and money (Xu and Hagler, 2002; Begam and Kumar, 2012).

This study utilized *in silico* methods to predict the absorption, distribution, metabolism, excretion, and toxicity profile (ADMET) of small bioactive molecules isolated from *Leonotis leonurus* R. Br. (Lamiaceae), a traditional medicinal plant indigenous to Southern Africa, and used for both recreational purposes and the treatment of various ailments (Nsuala et al., 2015). Currently, 36 small molecules have been isolated from this plant and evaluated for a variety of pharmacological activities (Cragg and Little, 1962; Rivett, 1964; Laonigro et al., 1979; Muhizi

et al., 2005; McKenzie et al., 2006; Obikeze et al., 2008; Agnihotri et al., 2009; El-Ansari et al., 2009; Naidoo et al., 2011; He et al., 2012; Kuchta et al., 2013; Wu et al., 2013; Narukawa et al., 2015). With the utilization of *in silico* methods, this study assessed the pharmacokinetic properties of these compounds in a bid to evaluate the possible drug-likeness and ADMET of these compounds as well as other properties that are relevant to their development into potential drug candidates. The *in silico* method used in predicting the ADMET profile, drug-likeness, and cytochrome P450 interaction properties of these molecules was an online web tool, SwissADME (www.swissadme.ch) (Daina and Zoete, 2016). Although there are several online tools for predicting ADMET, swissadme.ch was chosen for this study as it incorporates several free open-access and fast predictive models which are adapted from renowned publications as well as SwissADME's in-house original deep learning methods (Daina et al., 2017). It is a freely available online toolkit that provides a 'one-stop shop' for predicting the various components of the ADMET profile of small molecules (Daina et al., 2017). It also gives the user the option of making multiple inputs of canonical Simplified Molecular-Input Line-Entry System (SMILES) at a time as against the single input allowed in other online tools thereby making it more time-efficient. It provides the user with results that are easy to interpret thus enabling efficient conversion of these results to medicinal chemistry for drug design purposes (Daina et al., 2017). It also gives the user an 'at a glance' display of the results which can be saved and shared (Daina et al., 2017).

This chapter presents the methodology used in the determination of the pharmacokinetic and drug-like properties (chemo-informatics) of compounds found in *L. leonurus*, as well as the results of the chemo-informatics characterization of these compounds.

3.2 Research question addressed

1. What are the pharmacokinetic properties, drug-likeness, and other chemo-informatics properties of compounds isolated from *L. leonurus*?

3.3 Methodology

3.3.1 Data collection and preparation of the dataset

A thorough search of ScienceDirect[®], PubMed[®] and Google Scholar[®] for literature on compounds isolated from *Leonotis leonurus* was carried out using the terms '*Leonotis leonurus*' AND/OR 'Ethnobotanical uses' AND/OR 'Bioactive Compounds' AND/OR 'Compounds'. Articles identified from the search were read and the names of compounds reported to be isolated from *L. leonurus* were noted. The structures and SMILES of compounds identified from the literature search were obtained from PubChem[®], and structures of identified isolated compounds not found on PubChem[®] were drawn in 2D and 3D using ChemDraw Pro 16.0 and ChemDraw 3D 16.0 (both Perkin Elmer, United States) respectively.

The SMILES were imputed into the online ADME prediction site www.swissadme.ch to predict the physicochemical properties, lipophilicity, water-solubility, pharmacokinetics, drug-likeness, and medicinal chemistry properties of the compounds. The SwissADME online toolkit was also used to determine if a compound was a substrate of the P-gp transporter or an inhibitor of various isoenzymes of the cytochrome (CYP) P450 enzyme system using the support vector machine algorithm (SVM) which compared each compound to a dataset of known substrates of P-gp and inhibitors of CYP. In addition to swissadme.ch, the online web tool pkCSM (Pires et al., 2015) was used to predict the interaction of the compounds with the various isoforms of CYP to assess the likelihood of them being substrates or inhibitors. The BOILED Egg (Brain Or Intestinal Estimated permeation method model) which visually shows the absorption of molecules through the human gastrointestinal tract (white portion) and across the blood-brain barrier (yolk) (Daina and Zoete, 2016) was also created on www.swissadme.ch using a modified method of the Egan model. To do this lipophilicity was calculated using WlogP (calculation of Log P as carried out by Wildeman and Crippen) (Daina and Zoete, 2016; Daina et al., 2017). The software QikProp[®] (Schrödinger, New York) was also used to generate data on the predicted metabolic reactions of the compounds using their SMILES. The SMILES of the identified compounds were also imputed into the online platform biotransformer (www.biotransformer.ca) (Djombou-Feunang et al., 2019) to predict the number of metabolic reactions, metabolites produced and type of metabolic transformation for each compound. For compound optimization for vitexin, the online web tool, swissbioisostere.ch (Wirth et al., 2013), was used to predict the possible molecular replacements to enable the compound to pass Lipinski's rule.

3.3.2 *Data Analysis and Visualization*

The visualization software Data Warrior® (Sander et al., 2015) was used to generate graphs from the values obtained from [www. swissadme.ch](http://www.swissadme.ch) and QikProp® to visually identify compounds conforming to the limits for bioavailability (as delineated by the rules of Lipinski, Egan and Veber) and the predicted metabolic reactions of the compounds (Egan et al., 2000; Lipinski, 2000; Veber et al., 2002). For Lipinski's rule, a 3D graph of molecular weight against hydrogen bond acceptors and donors with a colour scheme showing WlogP was generated to determine molecules with good bioavailability while a graph of TPSA vs rotatable bond was drawn to determine molecules with good oral bioavailability according to Veber's model. To identify compounds with good GIT absorption and penetration of the BBB, a modification of the Egan egg model (using WlogP instead of AlogP98) was employed. A plot of lipophilicity (WLOGP) versus polarity of the compounds (TPSA) was generated using Data warrior® to allow for visualization of compounds with favourable permeation of the gut and BBB (Egan et al., 2000; Daina and Zoete, 2016). Data Warrior® was also used to generate the toxicity profile of each compound from its structure. Visualization graphs were then plotted to show the tumorigenic and mutagenic abilities of each compound.

3.3.3 *Scoring Function Matrix for oral administration with CNS activity*

Using the properties seen to be important for an orally administered, CNS-active drug candidate, a scoring function matrix for drug-likeness was created with all the information generated. Table 3.1 presents a breakdown of the scoring function using a hypothetical toxic compound as an example. From an aggregate weighting of 10, BBB permeation was considered the most important property of a CNS drug and so was assigned the greatest weighting (4) in the matrix. This property was also given the greatest weighting as it has been observed that compounds that penetrate the BBB possess the physicochemical properties ideal for absorption via the GIT (Xu and Hagler, 2002; Schneider, 2013). Toxicity was assigned the next highest weighting of 3, as toxicity is one of the leading causes of attrition in drug discovery (Kramer et al., 2007). GI absorption was assigned a weighting of 2 because although oral administration is ideal for most drugs, a drug candidate can be formulated for other routes of administration if required (Xu and Hagler, 2002; Schneider, 2013). Finally, CYP inhibitors were given a total weighting of 1 as this

relates to the inhibition of CYP enzymes by compounds, which could result in the toxicity of drugs that are substrates of CYP. A weighting of 1 was given since these pharmacokinetic interactions could easily be prevented by avoiding the concomitant administration of possible CYP inhibitors with these drugs. Under CYP inhibitors, inhibition of CYP3A4 and CYP2D6 was given a higher weighting than the inhibition of other CYP isoenzymes as these are the two main isoenzymes responsible for the metabolism of most drugs (Christians et al., 2005; Sridhar et al., 2012). Each compound was evaluated, with a scored value of 1, 0 or -1 given for each of the properties where a value of 1 represented the presence of a desirable property, 0 represented the absence of a desirable property and -1 represented the presence of a non-desirable property. The score assigned to each compound with relation to each property is the multiplication of the value given and the weighting of each property. The total score of each compound is the sum of the individual score for each property per compound.

Table 3.1: Scoring function matrix for drug-likeness for orally administered, CNS active compound (hypothetical example).

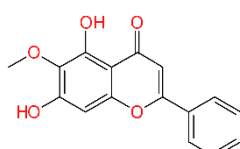
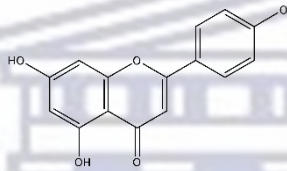
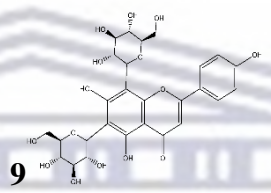
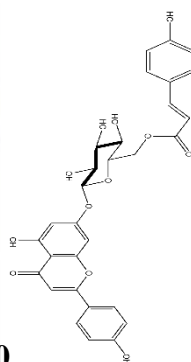
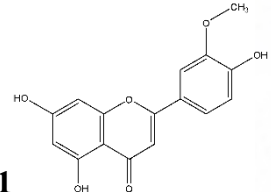
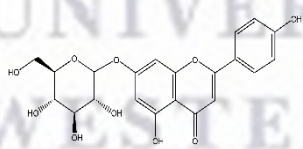
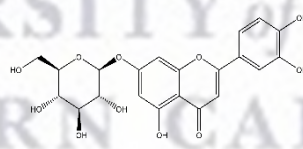
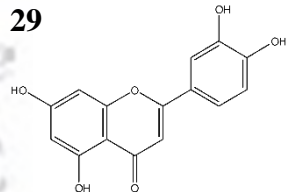
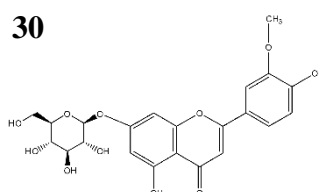
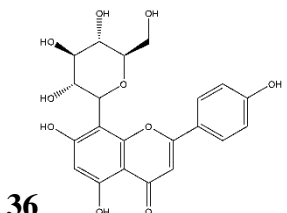
Property	value (1, 0, -1)	Weighting	Score
CYP inhibition			
• CYP3A4	1	0.25	0.25
• CYP2D6	1	0.25	0.25
• CYP2C19	1	0.17	0.17
• CYP2C9	1	0.17	0.17
• CYP1A2	1	0.17	0.17
GI absorption	1	2	2
BBB permeability	1	4	4
Toxicity	-1	3	-3
Total			4.0

3.4 Results

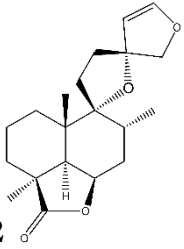
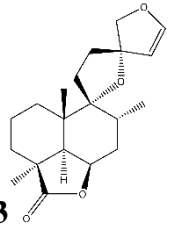
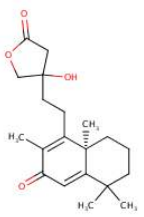
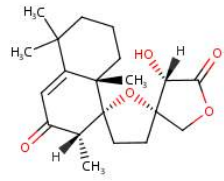
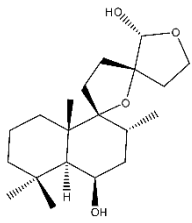
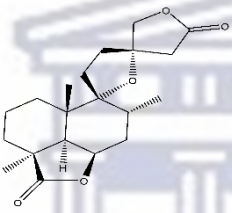
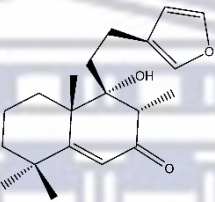
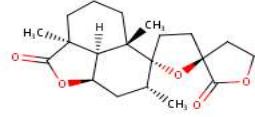
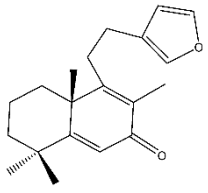
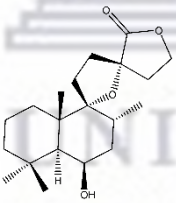
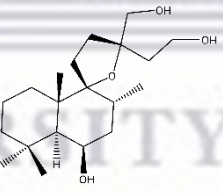
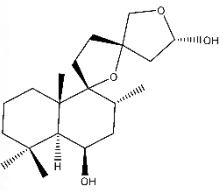
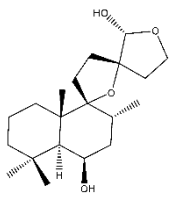
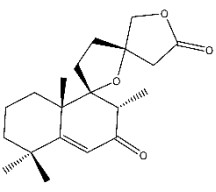
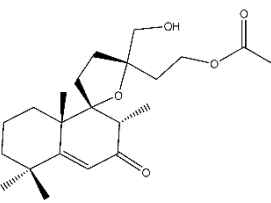
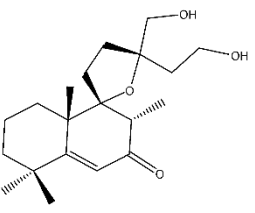
3.4.1 Description of the dataset

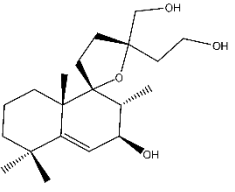
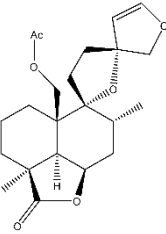
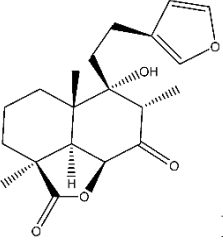
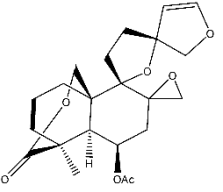
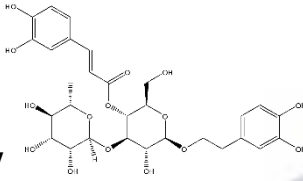
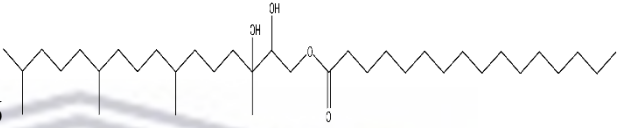
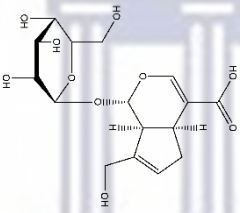
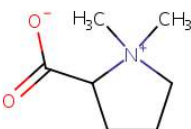
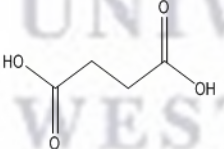
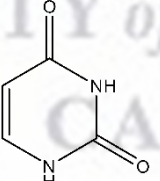
A literature search of articles for compounds isolated from *Leonotis leonurus* yielded 36 compounds from various phytochemical classes including 10 flavonoids, 20 labdane diterpenes, 1 phenyl ethanoid, 1 diterpene ester, 1 iridoid glycoside, 1 betaine, 1 dicarboxylic acid and 1 nucleic acid (Table 3.2).

Table 3.2: Compounds isolated from *L. leonurus* and their phytochemical class.

Flavonoids			
<p>1</p>  <p>6-Methoxyluteolin-4-methyl ether</p>	<p>8</p>  <p>Apigenin</p>	<p>9</p>  <p>Apigenin-6-C-α-arabinoside-8-C-β-glucoside</p>	<p>10</p>  <p>Apigenin-7-O-6-O-p-coumaryl-β-glucoside</p>
<p>11</p>  <p>Chrysoeriol</p>	<p>14</p>  <p>Comosiin</p>	<p>15</p>  <p>Cynaroside</p>	<p>29</p>  <p>Luteolin</p>
<p>30</p>  <p>Luteolin 7-O-β-glucoside-3-methyl ether</p>	<p>36</p>  <p>Vitexin</p>		

Labdane Diterpenes

<p>2</p>  <p>13R-premarrubin</p>	<p>3</p>  <p>13S-premarrubin</p>	<p>4</p>  <p>13ξ-hydroxy-8(9)-dien-7-on-16 15-olide</p>	<p>5</p>  <p>14α-hydroxy-9α 13α-epoxy-16 15-olide</p>
<p>6</p>  <p>16epi-Leoleorin F</p>	<p>12</p>  <p>Compound X</p>	<p>13</p>  <p>Leoleorin A</p>	<p>17</p>  <p>EDD</p>
<p>19</p>  <p>Leoleorin B</p>	<p>20</p>  <p>Leoleorin C</p>	<p>21</p>  <p>Leoleorin D</p>	<p>22</p>  <p>Leoleorin E</p>
<p>23</p>  <p>Leoleorin F</p>	<p>24</p>  <p>Leoleorin G</p>	<p>25</p>  <p>Leoleorin H</p>	<p>26</p>  <p>Leoleorin I</p>

<p>27</p>  <p>Leoleorin J</p>	<p>28</p>  <p>Leonurun</p>	<p>31</p>  <p>Marrubin</p>	<p>32</p>  <p>Nepetaefolin</p>
<p>Phenyl Ethanoid</p>		<p>Diterpene Ester</p>	
<p>7</p>  <p>Acteoside</p>	<p>16</p>  <p>Dihydroxyphytylpalmitate</p>		
<p>Iridoid Glycoside</p>		<p>Betaine</p>	
<p>18</p> <p>Geniposidic acid</p> 	<p>33</p> <p>Stachydrine</p> 		
<p>Dicarboxylic Acid</p>		<p>Nucleic Acid</p>	
<p>34</p> <p>Succinic Acid</p> 	<p>35</p> <p>Uracil</p> 		

3.4.2 Physicochemical Properties of *L. leonurus* Compounds

Figure 3.1 represents the individual physicochemical properties of the various compounds isolated from *L. leonurus* with the x-axis representing the compound's serial numbers as given in Table 3.1. The properties represented are the molecular weight, number of rotatable bonds, number of hydrogen bond acceptors, number of hydrogen bond donors, TPSA and MLOGP. These properties were then used in predicting the bioavailability of compounds based on the various drug-likeness models.



Figure 3.1: Scatter plots showing the physicochemical properties of the 36 compounds isolated from *Leonotis leonurus* as well as compounds which passed the individual limits. The red lines represent the desired ideal values for each physicochemical property.

Various bioavailability models stipulate that a compound would have good oral bioavailability if it had: less than 5 hydrogen bond donors; less than 10 hydrogen bond acceptors; a molecular weight less than 500; LogP less than 5 or Moruguchi LogP (MLogP) less than 4.15; ≤ 10 rotatable bonds and $TPSA \leq 140 \text{ \AA}^2$ (Lipinski, 2000; Veber et al., 2002). This indicates that a compound with physicochemical properties outside the above ranges would have a poor oral bioavailability profile. Of the 36 *L. leonurus* compounds assessed, 9 compounds exceeded the limits of the various physicochemical properties indicative of good oral bioavailability. Of these 7 were flavonoids while the remaining two compounds (a phenylethanoid and a diterpene ester) were the only compounds from their phytochemical classes isolated from the plant. Table 3.3 shows the compounds which exceeded the set limits for the various physicochemical properties.

Table 3.3: Compounds which did not pass the various physicochemical limits.

Physicochemical property limit	Compounds exceeding set limits
≤ 10 rotatable bonds	<ul style="list-style-type: none"> ● acteoside (# 7) ● dihydroxyphytyl palmitate (#16)
a molecular weight less than 500	<ul style="list-style-type: none"> ● acteoside (#7) ● apigenin-6-C-α-arabinoside-8-C-β-glucoside (#9) ● apigenin-7-O-6-O-p-coumaroyl-β-glucoside (# 10) ● dihydroxyphytyl palmitate (# 16)
less than 10 hydrogen bond acceptors	<ul style="list-style-type: none"> ● acteoside (#7) ● apigenin-6-C-α-arabinoside-8-C-β-glucoside (#9) ● apigenin-7-O-6-O-p-coumaryl-β-glucoside (#10) ● cynaroside (#15) ● luteolin 7-O-β-glucoside-3'-methyl ether (#30)

less than 5 hydrogen bond donors	<ul style="list-style-type: none"> ● acteoside (#7) ● apigenin-6-C-α-arabinoside-8-C-β-glucoside (#9) ● apigenin-7-O-6-O-p-coumaryl-β-glucoside (#10) ● comosiin (#14) ● cynaroside (#15) ● geniposidic acid (#18) ● luteolin 7-O-β-glucoside-3'-methyl ether (#30) ● vitexin(#36)
TPSA $\leq 140\text{\AA}^2$	<ul style="list-style-type: none"> ● acteoside (#7) ● apigenin-6-C-α-arabinoside-8-C-β-glucoside (#9) ● apigenin-7-O-6-O-p-coumaryl-β-glucoside (#10) ● comosiin (#14) ● cynaroside (#15) ● geniposidic acid (#18) ● luteolin 7-O-β-glucoside-3'-methyl ether (#30) ● vitexin(#36)
LogP less than 5 or Moruguchi LogP (MLogP) less than 4.15	<ul style="list-style-type: none"> ● dihydroxyphytyl palmitate(#16)

All the labdane diterpenes had physicochemical properties that were within the limits for each of the physicochemical properties, thus satisfying the requirements of being drug-like even as natural products. It is important to note that the various drug-like limits were determined based on the evaluation of synthetically derived compounds, as such it is possible that naturally occurring compounds such as these would exceed these limits (Ntie-Kang et al., 2018). However, it has been reported that about 60% of natural products pass these limits and are therefore drug-like. It has also been reported that only about 10% of natural products fail the rule of five set by Lipinski (usually exceeding the limits of one or two of the properties) (Ntie-Kang et al., 2018).

3.4.3 Pharmacokinetic profiling and drug-likeness

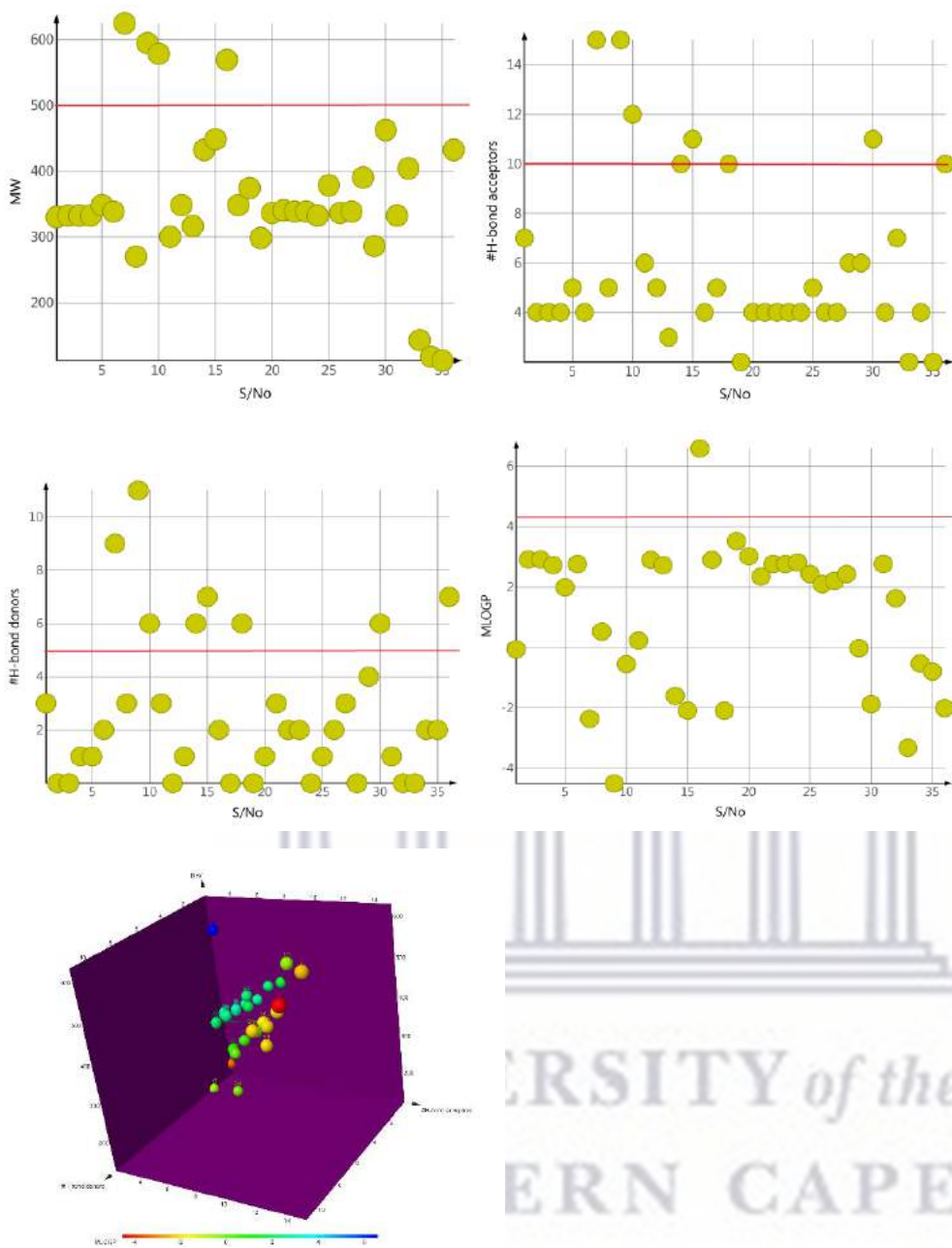
The results on the pharmacokinetic profile and drug-likeness of the compounds as evaluated *in silico* using the models described in Section 2.2.2.1 are presented below.

3.4.3.1 Oral Bioavailability models

3.4.3.1.1 Lipinski's Rule of Five

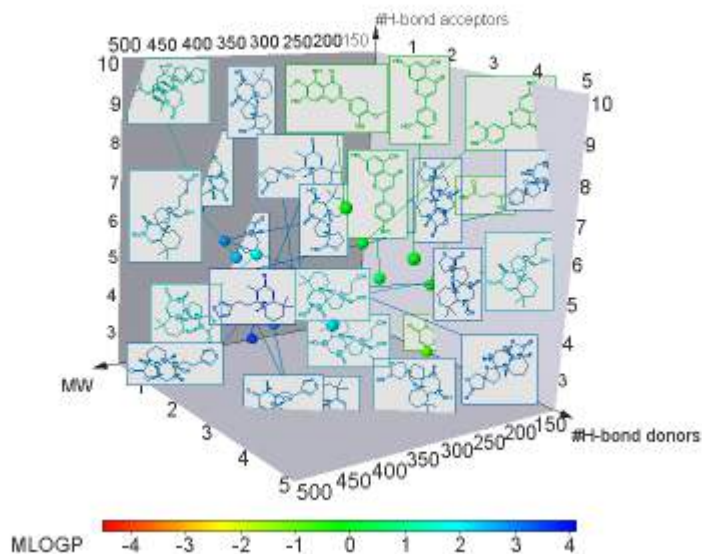
Lipinski's rule of five states that a compound is more likely to have poor oral bioavailability when it has more than 5 hydrogen bond donors, more than 10 hydrogen bond acceptors, a molecular weight more than 500, LogP greater than 5 or Moruguchi LogP (MLogP) greater than 4.15 (Lipinski, 2000). However, compounds that are substrates of biological transporters are exempted from this rule (Ghose et al., 1999). If a compound passes this rule, it is considered as having good oral bioavailability and therefore is drug-like (Ntie-Kang et al., 2018). Out of the 36 compounds assessed using Lipinski's rule, 27 [2- 6-methoxyluteolin-4'-methylether (#1), 13R-premarrubin (#2), 13S-premarrubin (#3), 13 ξ -hydroxylabd-5(6) 8(9)-dien-7-on-16 15-olide (#4), 14 α -hydroxy-9 α , 13 α -epoxylabd-5(6)-en-7-on-16, 15-olide (#5), 16epi-leoleorin F (#6), apigenin (#8), chrysoeriol (#11), compound X (#12), leoleorin A (#13), EDD (#17), leoleorin B (#19), leoleorin C (#20), leoleorin D (#21), leoleorin E (#22), leoleorin F (#23), leoleorin G (#24), leoleorin H (#25), leoleorin I (#26), leoleorin J (#27), leonurun (#28), luteolin(#29), marrubin (#31) nepetaefolin (#32), stachydrine(#33), succinic acid (#34), and uracil (#35)] passed the rule (see Figures 3.2 and 3.3).





Breakdown of physicochemical properties of Lipinski's rule, showing MW, hydrogen bond acceptors/donors and MlogP

Figure 3.2: Visualization of results of Lipinski's rule. Graphs showing the breakdown of physicochemical properties under Lipinski's rule (top right and left). All the compounds assessed (lower left 3D plot).



Compounds which passed Lipinski's rule of five: <5 h-bond donors; <10 h-bond acceptors; MW<500; MlogP< 4.15

Figure 3.3: 3-D visualization showing compounds that passed Lipinski's rule

The compounds that failed Lipinski's rule did so because they exceeded the limits for one or more of the physicochemical properties. Acteoside (#7), apigenin-6-C- α -arabinoside-8-C- β -glucoside (# 9) and apigenin-7-O-6-O-p-coumaryl- β -glucoside (# 10) failed Lipinski's rule because they had molecular weights greater than 500 Dalton, and more hydrogen bond donors and acceptors than stipulated by Lipinski's rule. Dihydroxyphytyl palmitate (# 16) failed Lipinski's rule because it had a molecular weight greater than 500 and MLogP greater than 4.15. Comosiin (# 14), geniposidic acid (# 18) and vitexin (# 36) all failed because they had more hydrogen bond donors than desired. Cynaroside (# 15) and luteolin 7-O- β -glucoside-3-methyl ether (# 30) failed because they had more hydrogen bond donors and acceptors than required. Identifying the physicochemical property outside the stipulated limits allows for the optimisation for oral bioavailability, if the compound is found to possess a desirable pharmacological effect, by tweaking the offending physicochemical property. For example, vitexin (#36) failed Lipinski's rule because it had seven hydrogen bond donors (five or less is required for good bioavailability). Using swissbioisostere, an online web tool to predict possible molecular replacements in the desired compound for optimization, four possible replacements were predicted to improve the activity of vitexin and enable it to pass the various models of drug-likeness including Lipinski's. Figure 3.4 shows the various possibilities for the optimisation of vitexin based on the predictions of swissbioisostere.

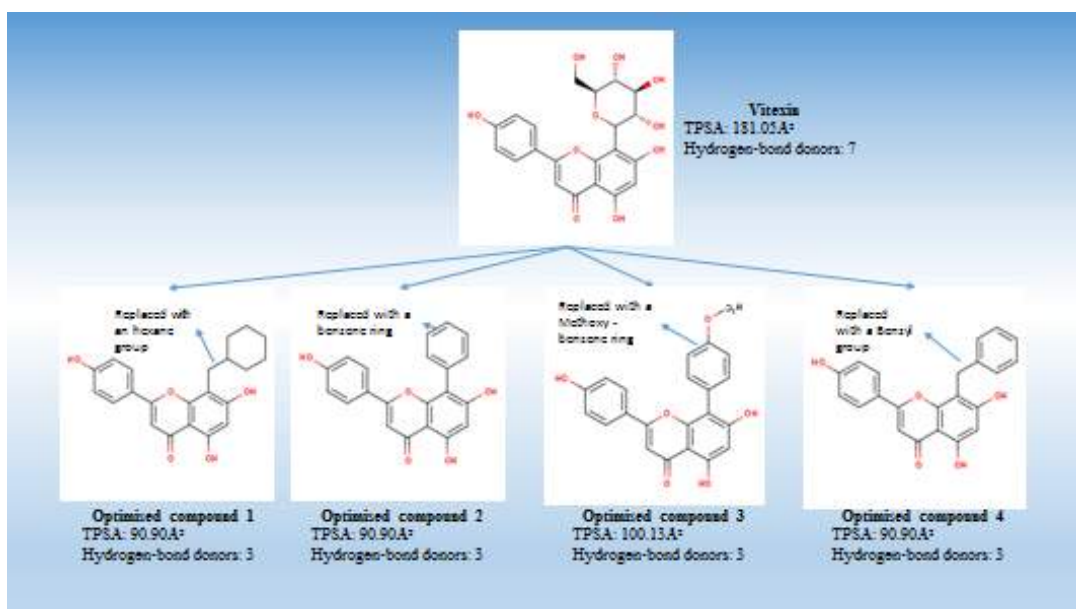
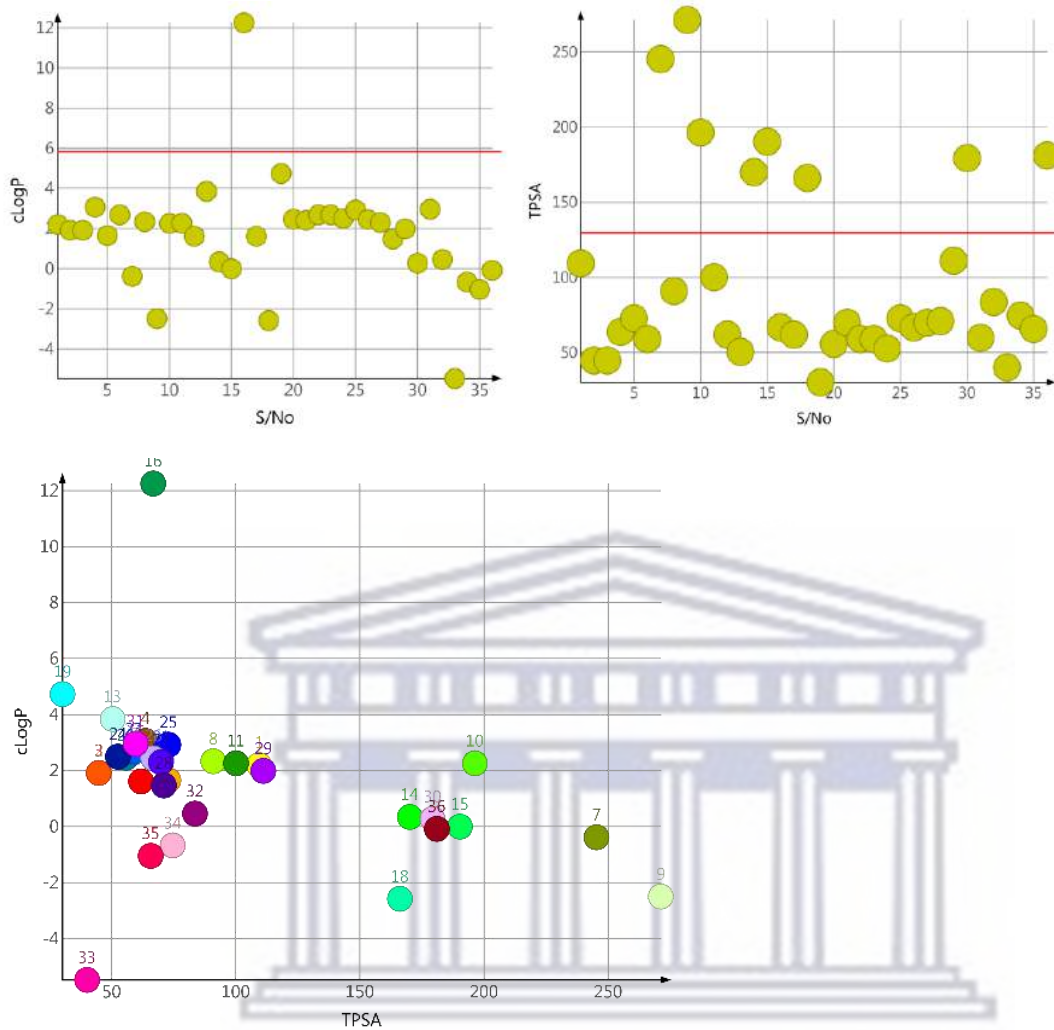


Figure 3.4: Optimization of vitexin to pass the various models and improve on its activity.

Compounds which failed Lipinski's rule because they had a molecular weight greater than 500 are unlikely to be successfully optimized, as the significant changes to the structure required to reduce molecular weight is likely to alter the pharmacological activity (Klebe, 2013).

3.4.3.1.2 Egan Model

The Egan rule evaluates the lipophilicity (measured as cLogP) and hydrophilicity (measured as TPSA) of a molecule, with these two properties exhibiting an inverse relationship (Egan et al., 2000). Compounds that are substrates of an active transporter form the outliers to this rule. The cut-off for drug-likeness is a value of less than 131.6Å² for polarity and less than 5.88 for cLogP (Egan et al., 2000). Like the results seen with Lipinski's rule, 27 compounds were predicted to have good oral bioavailability when evaluated using the Egan criteria and so can be described as drug-like (see Fig 3.5 and 3.6). The same compounds that passed Lipinski's rule passed Egan's law, while the compounds that failed Lipinski's rule also failed when Egan's rule was applied. Acteoside (#7), apigenin-6-C- α -arabinoside-8-C- β -glucoside (#9), apigenin-7-O-(6"-O-p-coumaryl)- β -glucoside (#10), comosiin (#14), cynaroside (#15), geniposidic acid (#18), luteolin 7-O- β -glucoside-3'-methyl ether (#30) and vitexin (#36) all failed the Egan rule because they had TPSA values higher than the cut-off values, while dihydroxylphytyl palmitate (#16) failed because it had a cLogP value greater than 5.88.



Breakdown of physicochemical properties of Egan rule, showing clogP and TPSA

Figure 3.5: Graphs showing the breakdown of physicochemical properties under Egan's rule (top right and left). All the compounds assessed (lower left).

UNIVERSITY of the
WESTERN CAPE

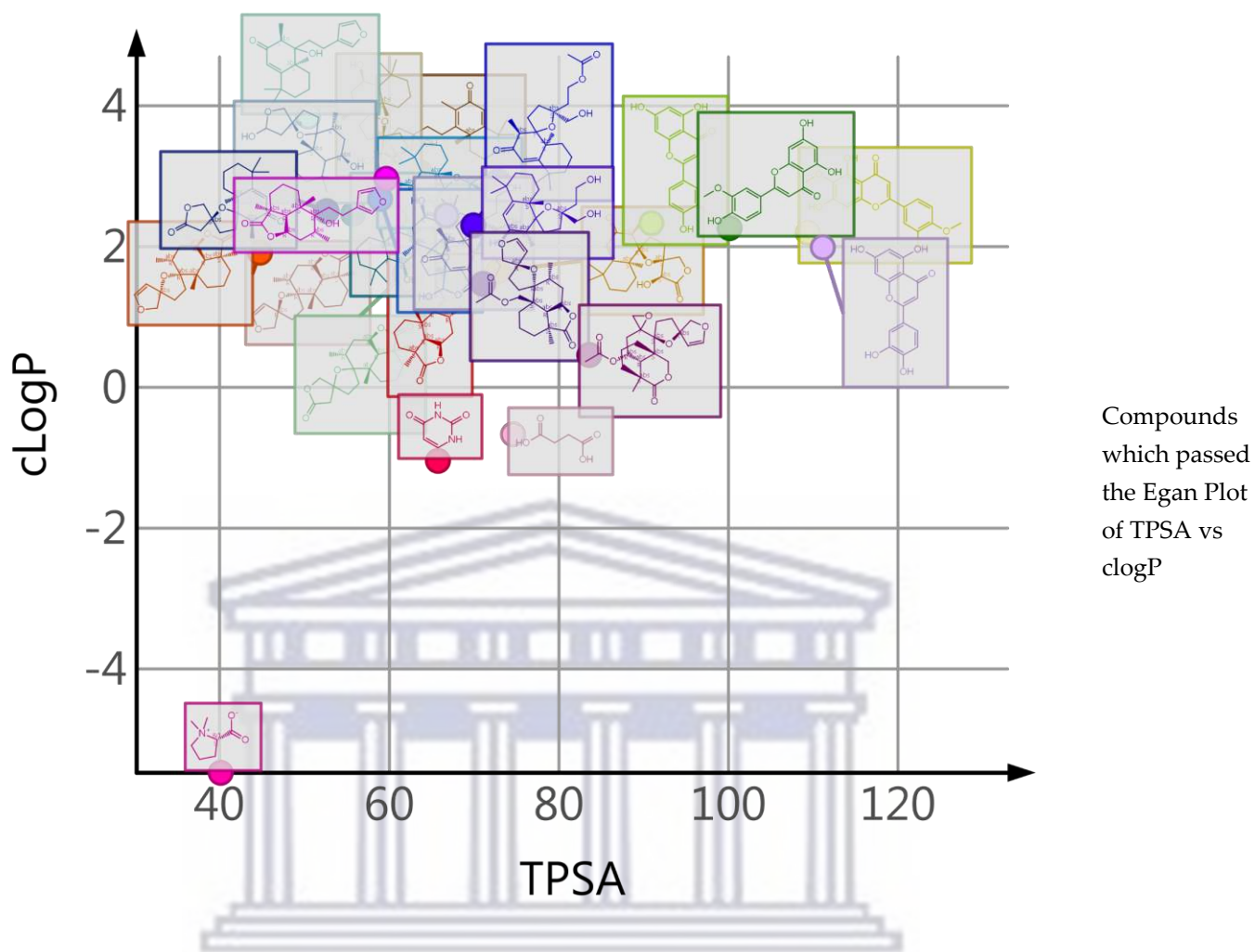


Figure 3.6: Graphs showing compounds that passed Egan's rule.

Compounds that failed the Egan rule but had desirable pharmacological effects can be optimized by bioisosterism. Following on the example given in section 3.4.3.1.1, optimizing vitexin for oral bioavailability under the Egan rule would require reducing the polarity to achieve a TPSA value less than 131.6\AA^2 , and figure 3.4 presents the pathways for optimizing the structure of vitexin to pass Egan's rule.

3.4.3.1.3 Veber's model

According to Veber *et al.*, (2002) a molecule is said to have good oral bioavailability when it has reduced molecular flexibility as seen in the number of rotatable bonds present and its polarity, independent of its molecular weight. They therefore suggested that molecules with 10 or less rotatable bonds and a polar surface area less than or equal to 140\AA^2 will have a high probability

of having good bioavailability (Veber et al., 2002). The results obtained were similar to those obtained with the Egan model and Lipinski's rule as the same molecules passed the criteria. Acteoside (# 7) failed Veber's law because it had more rotatable bonds and a higher TPSA than accepted. Apigenin-6-C- α -arabinoside-8-C- β -glucoside (#9), apigenin-7-O-(6''-O-p-coumaryl)- β -glucoside (# 10), comosiin (#14), cynaroside (#15), geniposidic acid (#18), luteolin 7-O- β -glucoside-3'-methyl ether (#30) and vitexin (#36) all failed because they had a polar surface area greater than 140\AA^2 . Acteoside (# 7) and dihydroxyphytyl palmitate (#16) failed because they had more than 10 rotatable bonds (see fig 3.7 and 3.8).

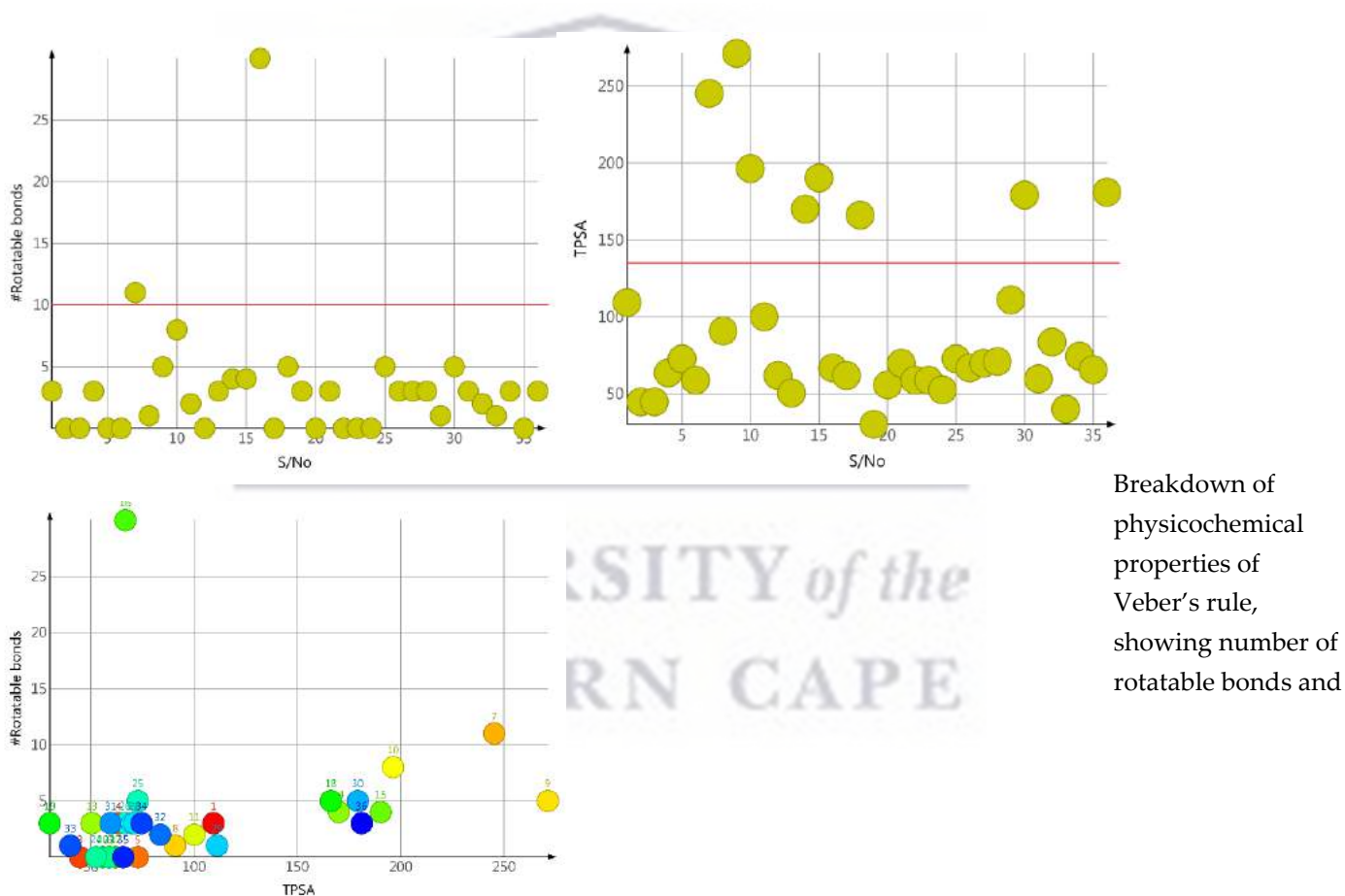


Figure 3.7: Graphs showing breakdown of physicochemical properties under Veber's rule (top right and left). The red lines represent the desired ideal values for TPSA and rotatable bonds. All the compounds assessed (lower left) compounds which passed Veber's rule (lower right).

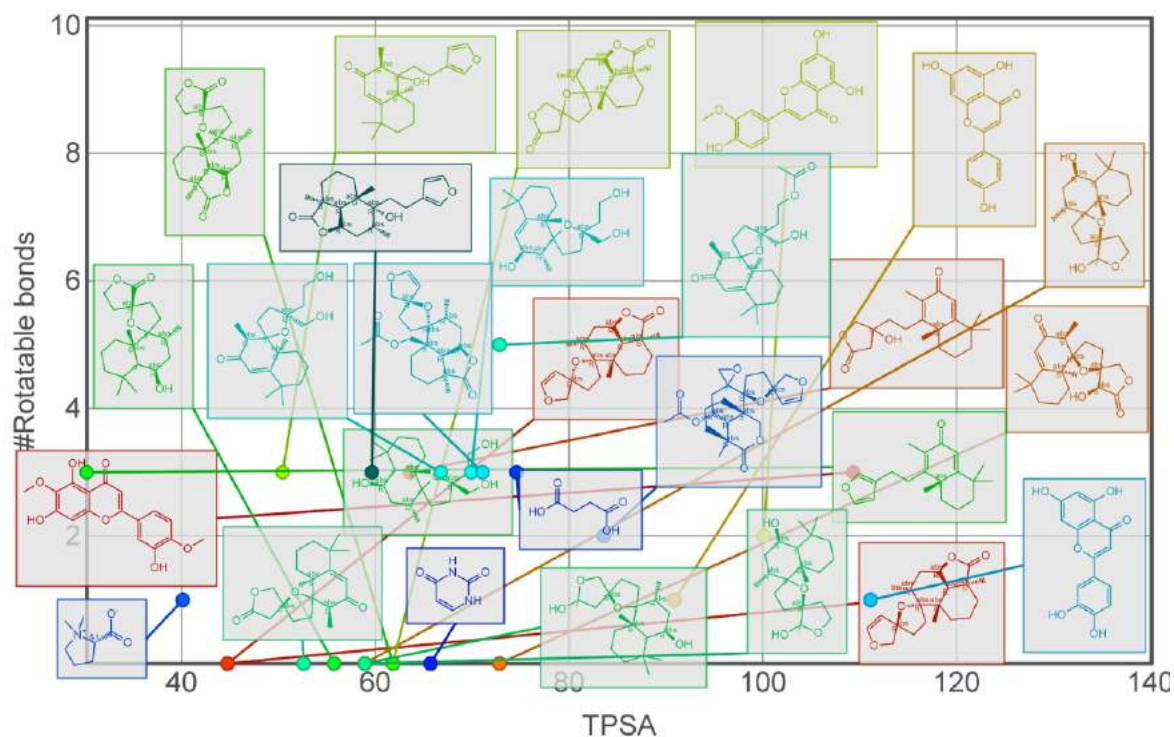


Figure 3.8: Graphs showing compounds which passed Veber's rule.

3.4.4 Absorption and Distribution

3.4.4.1 Human Intestinal Absorption and Blood-Brain Barrier Permeation

Absorption is the ability of the drug to pass through the intestinal wall into general blood circulation while distribution looks at the transportation of the drug around the body and to the intended target site (Schneider, 2013; Ntie-Kang et al., 2018). In the CNS, the BBB plays an important role in preventing compounds from being distributed into the CNS or to a target site in the CNS from systemic circulation (Xu and Hagler, 2002; Schneider, 2013). The BBB P-gp acts as an active efflux transporter of hydrophobic amphipathic drugs, and if absent or blocked could result in an increase in the presence of small BBB-permeant drug molecules in the CNS, that could in turn result in neurotoxicity or an altered pharmacological effect of the drug (Schinkel, 1999). The P-gp transporter is also responsible for transporting substrates back into the gastrointestinal lumen or extrahepatic tissue which could lead to poor absorption. Knowledge of the P-gp substrate status of a drug candidate is thus important in predicting both its oral bioavailability and distribution into the CNS (Mukkavilli et al., 2014).

The BOILED Egg model which visually presents the absorption of molecules in the human gastrointestinal system (represented as the egg white) and across the blood-brain barrier (represented as the yolk of the egg) was created on www.swissadme.ch using data from the modified Egan model and is presented in figure 3.9. Compounds in blue were predicted to be substrates of P-gp, while compounds in red were predicted as non-substrates of P-gp. Compounds located outside the egg structure were predicted to be poorly absorbed in the GIT and not BBB permeant.

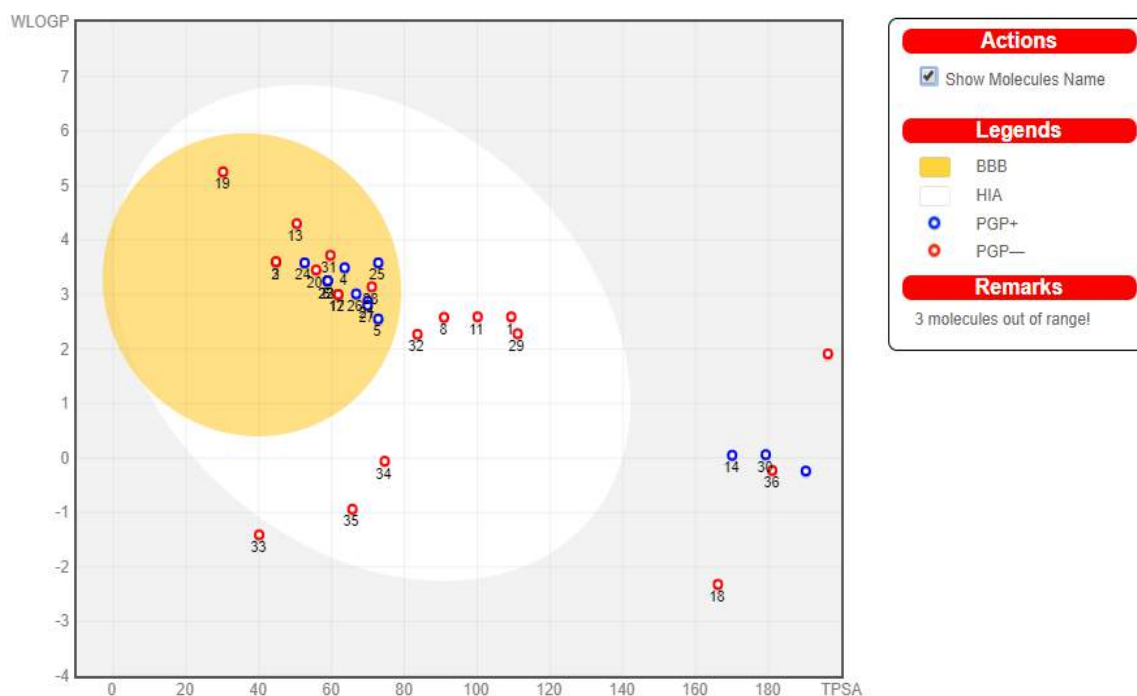


Figure 3.9: BOILED EGG illustration of the 36 compounds adsorption across the BBB and the gastrointestinal tract, and the probability of being a P-gp substrate.

13 ξ -hydroxylabd-5 (6), 8(9)-dien-7-on-16 15-olide (#4), 14 α -hydroxy-9 α , 13 α -epoxylabd-5(6)-en-7-on-16, 15-olide (#5), 16 ϵ pi-Leoleorin F (#6), acteoside (#7), apigenin-6-C- α -arabinoside-8-C- β -glucoside (#9), comosiin (#14), cynaroside (#15), dihydroxyphytyl palmitate (#16), leoleorin D (#21), leoleorin E (#22), leoleorin F (#23), leoleorin G (#24), leoleorin H (#25), leoleorin I (#26), leoleorin J (#27) and luteolin 7-O- β -glucoside-3'-methyl ether (#30) were predicted to be P-gp substrates (Figure 3.10).

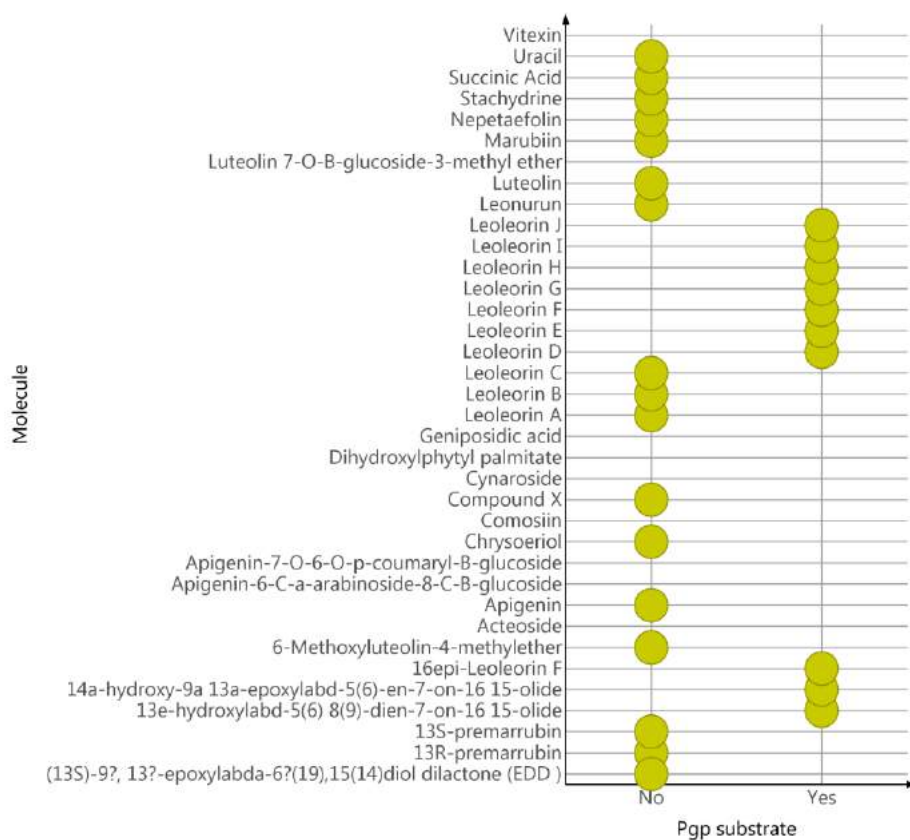
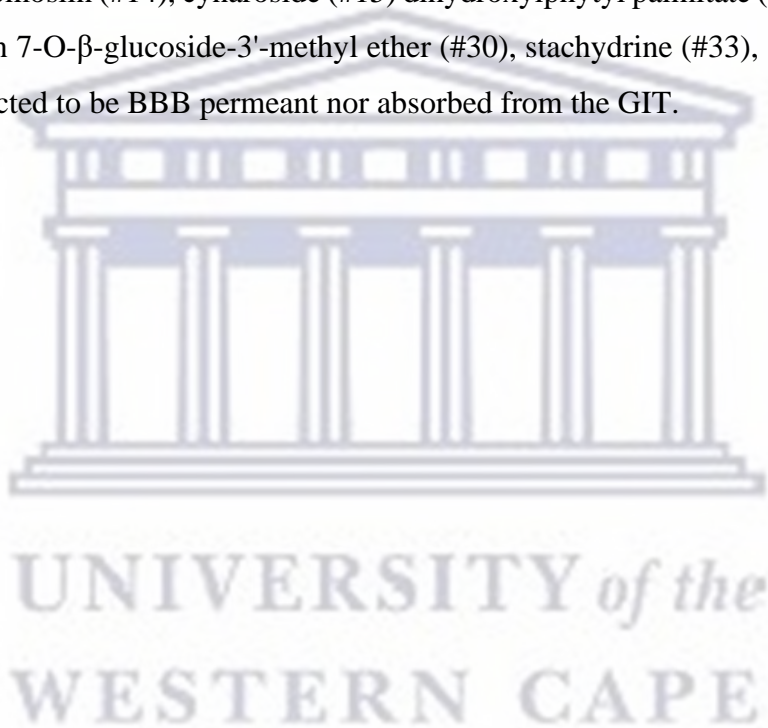


Figure 3.10: Illustration showing the possibility of the 36 compounds from *L. leonurus* being P-gp substrates.

On predictions for absorption in the human intestine (the egg white) and across the BBB (the yolk), 13R-premarrubin (#2), 13S-premarrubin (#3), 13 ξ -hydroxylabd-5(6), 8(9)-dien-7-on-16 15-olide (#4), 14 α -hydroxy-9 α , 13 α -epoxylabd-5(6)-en-7-on-16, 15-olide (#5), 16epi-Leoleorin F (#6), compound X (#12), leoleorin A (#13), EDD (#17), leoleorin B (#19), leoleorin C (#20), leoleorin D (#21), leoleorin E (#22), leoleorin F (#23), leoleorin G (#24), leoleorin H (#25), leoleorin I (#26), leoleorin J (#27), leonurun (#28) and marrubiin (#31) were predicted to be absorbed in the GIT and to be BBB permeant (Figures 3.11). For a small molecule to passively diffuse into the BBB or the GIT it should have a low molecular weight, a high degree of lipophilicity and be polar (Banks, 2009; Carpenter et al., 2014). This relationship was observed in this study as the compounds listed above as GIT and BBB permeant were also reported to be highly lipophilic, polar and have molecular weights less than 500 (as seen in their clogP and TPSA results in section 3.4.3.1.2). Therefore, these compounds are expected to have good absorption both in the GIT and BBB when administered *in vivo*, thus crossing one of the

important hurdles in the drug development pipeline. It was also observed that 6-methoxyluteolin-4'-methylether (#1), apigenin (#8), chrysoeriol (#11), luteolin (#29), nepetaefolin (#32), succinic acid (#34) and uracil (#35) were not predicted to be BBB permeant but had a high probability of being absorbed in the GIT. This observation can be attributed to the fact that compounds which permeate the BBB must have a TPSA value less than 90\AA^2 and these compounds had TPSA values above 90\AA^2 but below 140\AA^2 (Durojaye et al., 2019). These compounds have the benefit of being further studied as drugs for disease targets in the periphery, as these would have no expected CNS side effects due to non-penetration of the BBB (Carpenter et al., 2014). Acteoside (#7), apigenin-6-C- α -arabinoside-8-C- β -glucoside (#9), apigenin-7-O-(6"-O-p-coumaryl)- β -glucoside (#10), comosiin (#14), cynaroside (#15) dihydroxylphytyl palmitate (#16), geniposidic acid (#18), luteolin 7-O- β -glucoside-3'-methyl ether (#30), stachydrine (#33), and vitexin (#36) were neither predicted to be BBB permeant nor absorbed from the GIT.



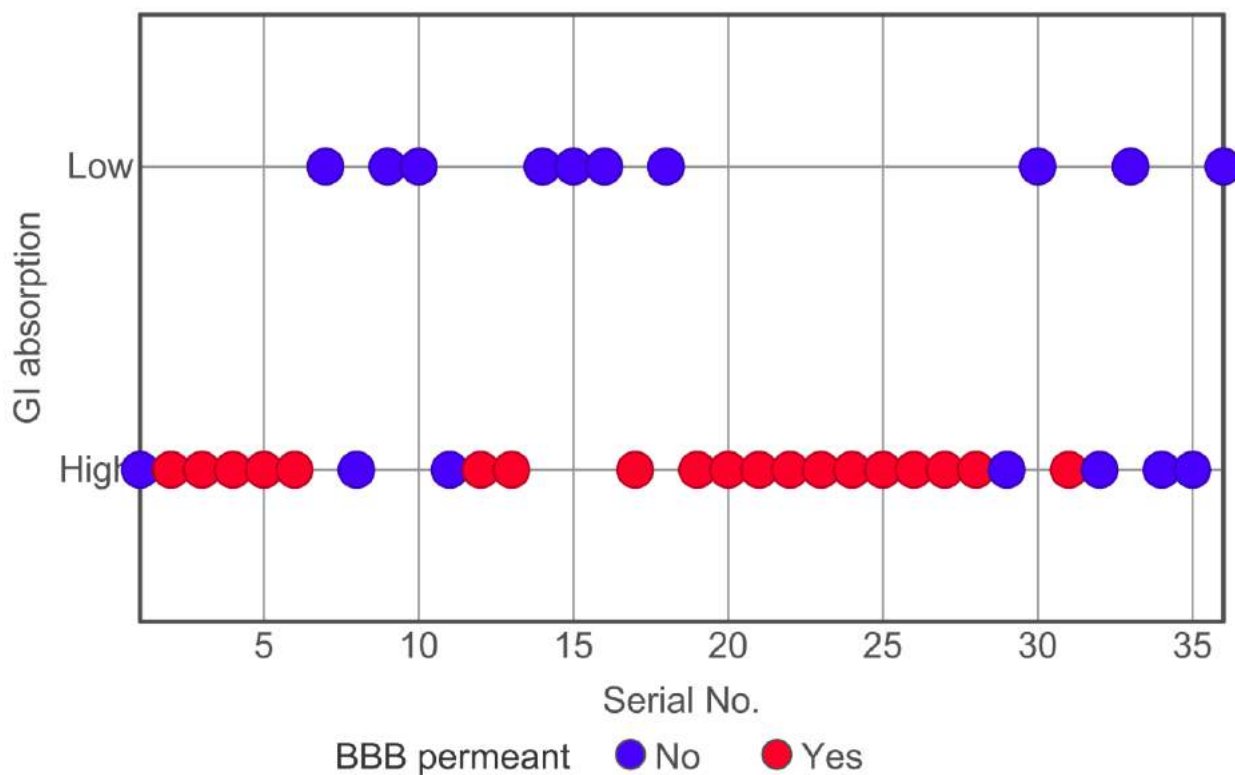


Figure 3.11: Plot showing the extent of gastrointestinal absorption as well as the probability of the 36 compounds crossing the BBB.

Of the 16 compounds predicted to be P-gp substrates, 10 of them [13 ξ -hydroxylabd-5(6), 8(9)-dien-7-on-16 15-olide (#4), 14 α -hydroxy-9 α , 13 α -epoxylabd-5(6)-en-7-on-16, 15-olide (#5), 16 ϵ pi-leoleorin F (#6), leoleorin D (#21), leoleorin E (#22), leoleorin F (#23), leoleorin G (#24), leoleorin H (#25), leoleorin I (#26), leoleorin J (#27)] were BBB permeant. The remaining 6 compounds [acteoside (# 7), apigenin-6-C- α -arabinoside-8-C- β -glucoside (# 9), comosiin (# 14), cynaroside (# 15), dihydroxyphytylpalmitate (# 16) and luteolin 7-O- β -glucoside-3-methyl ether (# 30)] predicted to be P-gp substrates were neither BBB permeant nor GI absorbed, making them poor candidates for CNS drug discovery as they are unlikely to be absorbed via the GIT nor penetrate the CNS. It is also noted that as P-gp substrates, they would likely be expelled from the CNS if they are introduced into the CNS.

6-Methoxyluteolin-4'-methylether (# 1), apigenin (# 8), chrysoeriol (# 11), luteolin (# 29), nepetaefolin (# 32), succinic acid (# 34), and uracil (# 35) were predicted to be GI absorbed and

non-P-gp substrates indicating the possibility of them being easily absorbed into systemic circulation from the gut and producing a biological effect without being expelled by P-glycoproteins. They were, however, not predicted to be BBB permeant thereby reducing their chances of being distributed into the CNS and producing CNS effects. Apigenin-7-O-(6''-O-p-coumaryl)- β -glucoside (#10), geniposidic Acid (#18), stachydrine (#33) and vitexin (#36) were predicted to be neither GI absorbed, BBB permeant nor substrates of P-glycoprotein, indicating that these compounds would be poorly absorbed in the GIT and may not cross the BBB. As mentioned earlier, polar compounds are unable to cross the BBB, and polar compounds with a desired CNS effect would require optimization by a stepwise removal or masking of polar groups to allow them to cross the BBB (Klebe, 2013).

Nineteen compounds were predicted to be BBB permeant, 10 of which were predicted to be P-gp substrates. This means that the remaining 9 compounds [13R-premarrubin (#2), 13S-premarrubin (#3), compound X (#12), leoleorin A (#13), EDD (#17), leoleorin B (#19), leoleorin C (#20), leonurun (#28) and marrubin (#31)] which were predicted to be BBB permeant and non-substrates of P-gp were the ideal candidates for an orally administered, CNS-active agent.

3.4.5 *Metabolism: Biotransformation*

Metabolism refers to the transformation of drug molecules by liver enzymes to make them more soluble for excretion (Schneider, 2013). This process is important as it influences the possibility of a drug causing toxic effects because of bioaccumulation (Schneider, 2013; Ntie-Kang et al., 2018). Biotransformation predictions indicate the likelihood of a molecule reaching the target site after entering the bloodstream in concentrations able to effect the desired change. If a compound undergoes too many metabolic reactions, the chances of it reaching its target site in sufficient amounts is tremendously reduced (Schneider, 2013; Ntie-Kang et al., 2018). Figure 3.12 is a graphical representation of the number of predicted metabolic reactions for each of the 36 compounds. Based on Qikprop, 31 compounds were predicted to undergo the ideal number of metabolic reactions, while 5 compounds fell outside the ideal range (4 of the compounds were predicted to undergo more than 8 reactions while one of the compounds did not undergo any metabolic reaction) (table 3.4 and Appendix 7.7). Uracil was predicted to undergo no reactions (thus implying that uracil would reach its target site unchanged and would be excreted

unchanged). Stachydrine and vitexin were predicted to undergo 9 metabolic reactions, acteoside was predicted to undergo 10 metabolic reactions and apigenin-6-C- α -arabinoside-8-C- β -glucoside was predicted to undergo 15 metabolic reactions indicating that these compounds were unlikely to reach a target site in sufficient quantities to produce the desired effect. However, the high number of metabolic reactions also implies the generation of many metabolites, some of which may be active.

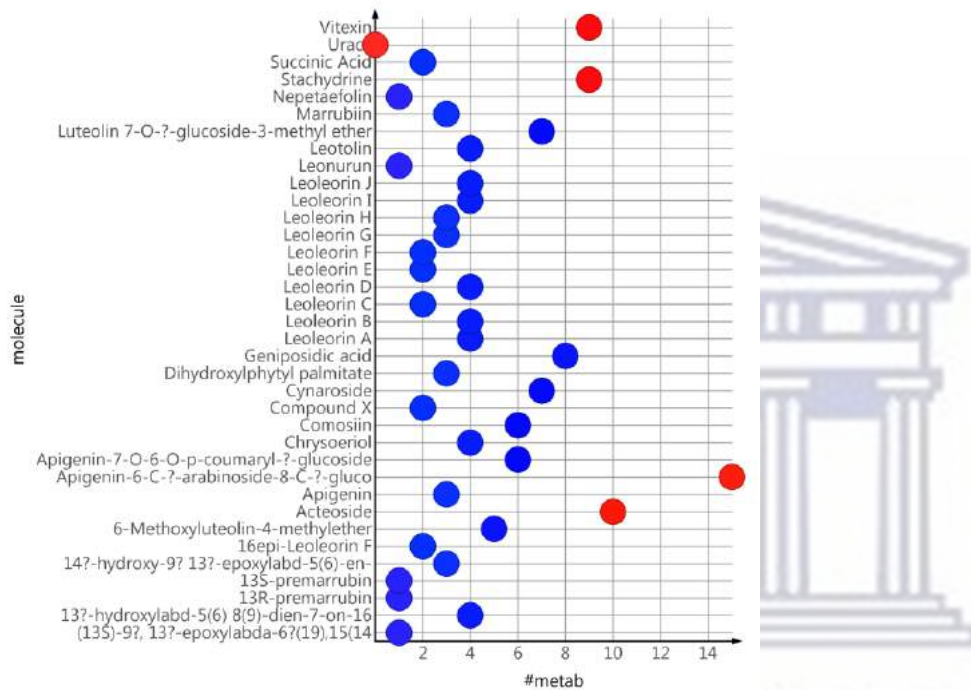


Figure 3.12: Graph showing the predicted number of metabolic reactions each compound would generate as generated by Qikprop.

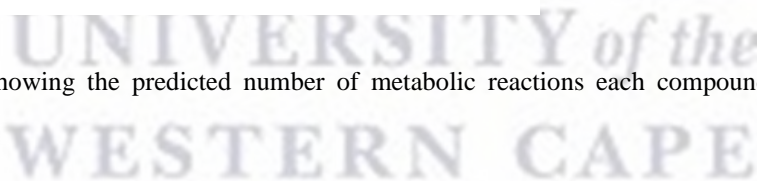


Table 3.4: Metabolic reactions and the number of metabolites for *L. leonurus* compounds as predicted by Qikprop and biotransformer.ca.

Compounds	No. of Metabolic Reactions (Qikprop)	No. of Metabolic Reactions(biotransformer.ca)	No. of Metabolites	Type of Metabolic Transformation
Stachydrine (#33)	9	0	0	Neither Phase I nor Phase II
Vitexin (#36)	9	6	7	Phase II
Acteoside (#7)	10	6	11	Phase II
Apigenin-6-C- α -arabinoside-8-C- β -glucoside (#9)	15	3	11	Phase II

Vitexin, acteoside and apigenin-6-C- α -arabinoside-8-C- β -glucoside were predicted to only undergo phase II metabolic reactions by biotransformer.ca, and although this was unusual, the prediction was supported by results from the online ADMET tool, pkCSM (section 3.4.6) which indicated that all three compounds were not substrates of the two main CYP enzymes responsible for Phase I drug metabolism.

3.4.6 Interaction with Cytochrome P450 enzyme

The cytochrome P450 (CYP) enzymes are involved in the metabolism of many exogenous molecules (natural products, drugs, and environmental carcinogens) and endogenous compounds such as hormones (Sridhar et al., 2012). An understanding of the interaction between drug

candidates and CYP enzymes aids the prediction of adverse drug-drug interactions. The predictions of the likelihood of each of the 36 compounds from *L. leonurus* as either substrates of, or inhibitors of the five major isoforms of cytochrome P450 enzymes is presented in table 3.5 below.

Table 3.5: Interactions between compounds from Leonotis leonurus and isoenzyme of CYP450.

Molecule Name	CYP2D6 substrate	CYP3A4 substrate	CYP1A2 inhibitor	CYP2C19 inhibitor	CYP2C9 inhibitor	CYP2D6 inhibitor	CYP3A4 inhibitor
6-Methoxyluteolin-4'-methylether	No	No	Yes	No	No	No	No
13R-premarrubin	No	Yes	No	No	No	No	No
13S-premarrubin	No	Yes	No	No	No	No	No
13 ξ -hydroxylabd-5(6), 8(9)-dien-7-on-16 15-olide	No	Yes	No	No	No	No	No
14 α -hydroxy-9 α , 13 α -epoxylabd-5(6)-en-7-on-16, 15-olide	No	Yes	No	No	No	No	No
16epi-Leoleorin F	No	Yes	No	No	No	No	No
Acteoside	No	No	No	No	No	No	No
Apigenin	No	No	Yes	Yes	Yes	No	Yes
Apigenin-6-C- α -arabinoside-8-C- β -glucoside	No	No	No	No	No	No	No

Molecule Name	CYP2D6 substrate	CYP3A4 substrate	CYP1A2 inhibitor	CYP2C19 inhibitor	CYP2C9 inhibitor	CYP2D6 inhibitor	CYP3A4 inhibitor
Apigenin-7-O-(6''-O-p-coumaryl)- β -glucoside	No	No	No	No	No	No	No
Chrysoeriol (Luteolin 3'-methyl ether)	No	No	Yes	No	Yes	No	Yes
Compound X	No	Yes	No	No	No	No	No
Compound Y / Leoleorin A	No	No	No	Yes	No	No	Yes
Comosiin (Apigenin-7-O- β -glucoside)	No	No	No	No	No	No	No
Cynaroside (Luteolin-7-O-glucoside)	No	No	No	No	No	No	No
Dihydroxylphytylpalmitate	No	Yes	No	No	No	No	No
EDD	No	Yes	No	No	No	No	No
Geniposidic acid	No	No	No	No	No	No	No
Leoleorin B	No	Yes	No	Yes	No	No	No
Leoleorin C	No	Yes	No	No	No	No	No
Leoleorin D	No	Yes	No	No	No	No	No
Leoleorin E	No	Yes	No	No	No	No	No
Leoleorin F	No	Yes	No	No	No	No	No
Leoleorin G	No	Yes	No	No	No	No	No

Molecule Name	CYP2D6 substrate	CYP3A4 substrate	CYP1A2 inhibitor	CYP2C19 inhibitor	CYP2C9 inhibitor	CYP2D6 inhibitor	CYP3A4 inhibitor
Leoleorin H	No	Yes	No	No	No	No	No
Leoleorin I	No	Yes	No	No	No	No	No
Leoleorin J	No	No	No	No	No	No	No
Leonurun	No	Yes	No	No	No	No	No
Luteolin	No	No	Yes	No	Yes	No	No
Luteolin 7-O- β -glucoside-3'-methyl ether	No	No	No	No	No	No	No
Marrubiin	No	No	No	Yes	Yes	No	Yes
Nepetaefolin	No	Yes	No	No	No	No	No
Stachydrine	No	No	No	No	No	No	No
Succinic Acid	Yes	No	No	No	No	No	No
Uracil	No	No	No	No	No	No	No
Vitexin (Apigenin-8-C- β -glucoside)	No	No	No	No	No	No	No

Out of the 36 compounds, 11 [acteoside (#7), apigenin-6-C- α -arabinoside-8-C- β -glucoside (#9), apigenin-7-O-(6"-O-p-coumaryl)- β -glucoside (#10), comosiin (#14), cynaroside (#15), geniposidic acid (#18), leoleorin J (#27), luteolin 7-O- β -glucoside-3'-methyl ether (#30), stachydrine (#33), uracil (#35) and vitexin (#36)] were identified as neither substrates nor inhibitors of the isoenzymes of CYP. This implies that these compounds do not go through Phase

I metabolism and are unlikely to produce pharmacokinetic drug-drug interactions via hepatic enzyme inhibition. There were 18 compounds [13R-premarrubin (#2), 13S-premarrubin (#3), 13 ξ -hydroxyabd-5(6), 8(9)-dien-7-on-16 15-olide (#4), 14 α -hydroxy-9 α , 13 α -epoxyabd-5(6)-en-7-on-16, 15-olide (#5), 16 β -leoleorin F (#6), compound X (#12), dihydroxyphytylpalmitate (#16), (13S)-9 α , 13 α -epoxyabd-6 β (19),15(14)diol dilactone (EDD) (#17), leoleorin B (#19), leoleorin C (#20), leoleorin D (#21), leoleorin E (#22), leoleorin F (#23), leoleorin G (#24), leoleorin H (#25), leoleorin I (#26), leonurun (#28) and nepetaefolin (#32)] predicted to undergo Phase I metabolism as substrates of CYP3A4, an isoenzyme significantly involved in drug metabolism (Christians et al., 2005; Sridhar et al., 2012). Apigenin (#8), chrysoeriol (#11), compound Y / leoleorin A (#13) and marrubiin (#31) were predicted to be inhibitors of CYP3A4 and not substrates of CYP3A4. Succinic acid (#34) was predicted to be a substrate of CYP2D6 and was neither a substrate nor an inhibitor of CYP3A4, 6-methoxyluteolin-4'-methylether (#1) was predicted to inhibit CYP1A2 and was neither a substrate nor inhibitor of CYP3A4, while luteolin (#29) was predicted to inhibit CYP1A2 and CYP2C9 but was not a substrate of CYP2D6 and CYP3A4.

Compounds that inhibit drug-metabolizing enzymes can lead to drug toxicity when taken concomitantly with conventional medicines. This is the mechanism for some unwanted adverse reactions which occur when conventional medicines are taken concomitantly with herbal preparations (figure 3.13) (Sridhar et al., 2012). For example, concomitant administration of warfarin, a drug with a narrow therapeutic index, with a plant product that has a bioactive compound like apigenin (which is predicted to inhibit CYP1A2, CYP2C9 and CYP3A4 the isoenzymes involved in the metabolism of warfarin), would lead to increased plasma concentrations of warfarin resulting in warfarin toxicity (Kaminsky and Zhang, 1997; Walker et al., 2014).

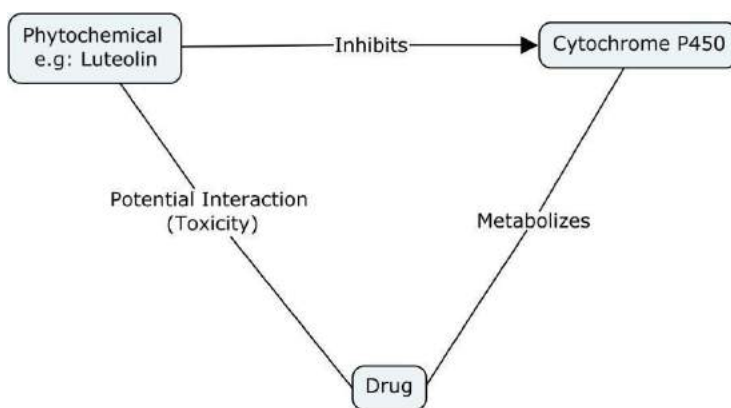


Figure 3.13: C-map showing the interaction between compounds that inhibit CYP450 and drugs metabolized by CYP450.

Apart from drug-drug interactions, CYP inhibition has been seen as a widely pursued area of research in the treatment and prevention of cancer. CYP enzymes are responsible for the metabolism of carcinogens, pro-carcinogens, and chemotherapeutics, giving them a part to play in cancer prevention and treatment strategies. They have also been implicated in tumour formation and development (Sridhar et al. 2012).

3.4.7 Toxicity Profile of Compounds

Toxicity represents the degree to which a compound is unsafe to the human body and the toxicity profile of a drug compound encompasses the ability of the compound to be mutagenic or tumorigenic (Schneider, 2013). It is a leading cause for the high attrition rates in drug discovery therefore it is key to determine the toxicity profile of a drug at the preclinical stage of drug development to reduce these rates (Kramer et al., 2007). This knowledge lowers toxicity related attrition reduces wastage of resources and identifies compounds with a better chance of becoming drugs (Kramer et al., 2007). DataWarrior software was used to generate the toxicity profile of the 36 compounds and predicted 3 compounds [6-methoxyluteolin-4-methylether (#1), nepetaefolin (#32) and uracil (#35)] to be both mutagenic and tumorigenic (figure 3.14). Apigenin (#8), apigenin-6-C- α -arabinoside-8-C- β -glucoside (#9), succinic acid (#34) and vitexin (#36) were predicted to be mutagenic but not tumorigenic, while the remaining 29 compounds were predicted to be neither mutagenic nor tumorigenic.

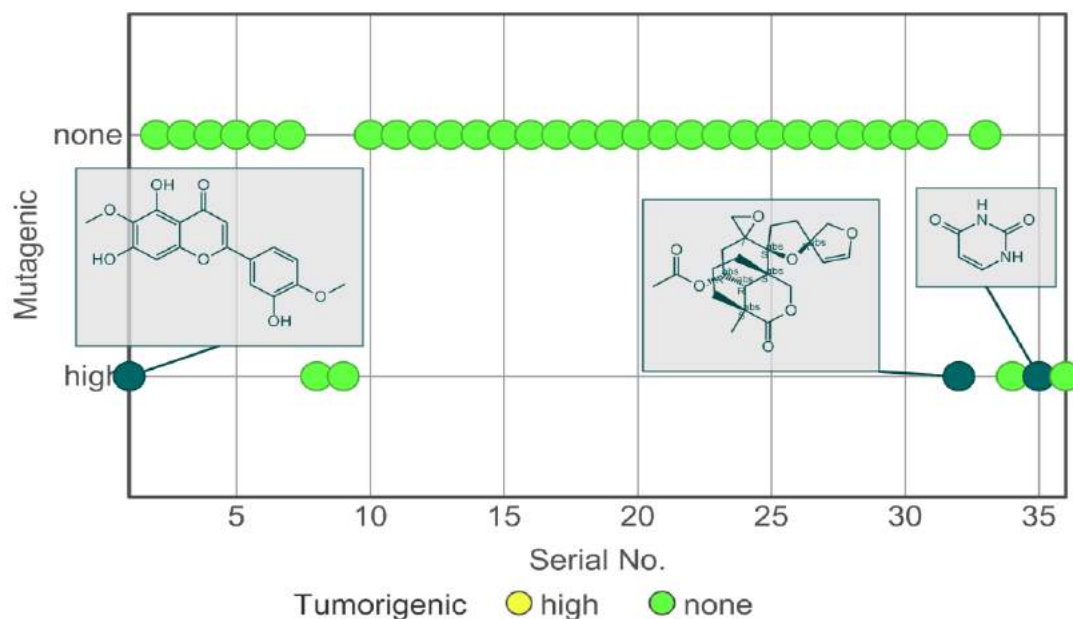


Figure 3.14: Graph showing the mutagenic and tumorigenic predictions for the *L. leonurus* compounds.

3.4.8 Summary of ADMET properties

From the results of the evaluation of the *L. leonurus* compounds for drug likeness (see Section 3.4.3.1 of Chapter 3), 27 of the 36 *L. leonurus* compounds were observed to pass the various limits set by Lipinski, Veber and Egan, making them drug like candidates. On the other hand, an ideal CNS drug faces the challenge of crossing the BBB. As such a compound may have good oral bioavailability but may be unable to cross the BBB to produce an effect in the CNS. Considering this, only 19 of the 27 compounds noted to have good oral bioavailability were predicted to cross the BBB (see Section 3.4.4.1 of Chapter 3). Further to this, the presence of P-glycoproteins in the CNS acts as another barrier to the absorption of compounds into the CNS. These efflux transporters are known to transport substrates out of the cell and so an ideal CNS drug should not be a P-gp substrate in addition to crossing the BBB (Alavijeh et al., 2005; Ebinger and Uhr, 2006). Based on this additional criterion, only 9 of the 19 compounds with good oral bioavailability and BBB permeability were predicted to be ideal CNS drug candidates (see Section 3.4.4.1 of Chapter 3). Metabolic enzymes are another component of the protective mechanisms in the CNS. These enzymes such as those of the CYP isoenzyme family break down lipid soluble molecules once they penetrate the BBB. CYP2D6 and CYP3A4 are the predominant isoenzymes responsible for the metabolism of more than 50% of drug molecules (Christians,

Schmitz, and Haschke, 2005). Inhibition of these enzymes can lead to increased concentration of compounds in the CNS, which could ultimately result in toxicity (Sridhar et al., 2012). To avoid drug-drug interactions linked to CYP isoenzyme inhibition, an ideal CNS drug should not inhibit the activity of these metabolic enzymes (McFadyen et al., 1997; Carvey et al., 2009; Ferguson and Tyndale, 2011). Based on this, 7 (13R-premarrubin, 13S-premarrubin, compound X, EDD, leoleorin B, leoleorin C and leonurun) of the 9 compounds that were predicted to cross the BBB and were not P-gp substrates did not inhibit the activity of CYP isoenzymes (see Section 3.4.6 of Chapter 3).

For a compound with desirable pharmacological effect, but less than ideal ADMET properties, optimization to improve the low scoring properties identified in the scoring matrix then becomes essential. To illustrate this, let us assume that chrysoeriol has been found to possess desirable CNS activity. From the scoring matrix (table 3.6) it can be seen that it is not BBB permeant and is an inhibitor of CYP enzymes. BBB permeation can then be increased via an aided transport mechanism across the BBB, and concomitant administration with drugs metabolised by CYP enzymes avoided. Another example, geniposidic acid has a total score of 4 which is rather poor, however, when looking at the individual properties it can also be seen that its inability to cross the BBB and be GI absorbed can be mitigated by an aided transport mechanism across these membranes.



Table 3.6: Relationship between compounds from *L. leonurus* and isoenzyme of CYP450 including the absorption and toxicity profile of these compounds.

Property value (1, 0, -1)	CYP inhibitors breakdown					P-gp Substrate	GI absorption	BBB permeability	Toxicity	Total Score
	CYP3A4	CYP2D6	CYP2C19	CYP2C9	CYP1A2					
Weighting	0.25	0.25	0.17	0.17	0.17	Yes/No	2	4	3	
'Ideal Compound' value	1	1	1	1	1	No	1	1	1	10.0
6- Methoxyluteolin -4'-methylether	0	0	1	0	0	No	1	0	-1	-0.8

13R-premarrubin	1	1	1	1	1	No	1	1	1	10.0
13S-premarrubin	1	1	1	1	1	No	1	1	1	10.0
13 ξ - hydroxylabd-5(6), 8(9)-dien-7-on-16 15-olide	1	0	0	1	1	Yes	1	1	1	9.6
14 α -hydroxy-9 α , 13 α -epoxylabd-5(6)-en-7-on-16, 15-olide	1	1	1	1	1	Yes	1	1	1	10.0
16epi-Leoleorin F	1	1	1	1	1	Yes	1	1	1	10.0

Acteoside	1	1	1	1	1	Yes	0	0	1	4.0
Apigenin	0	1	1	0	0	No	1	0	-1	-0.6
Apigenin-6-C- α - arabioside-8-C- β -glucoside	1	1	1	1	1	Yes	0	0	-1	-2.0
Apigenin-7-O- (6"-O-p- coumaryl)- β - glucoside	1	0	1	1	1	No	0	0	1	3.8
Chrysoeriol (Luteolin 3'- methyl ether)	0	0	1	0	0	No	1	0	1	5.2

Compound X	1	1	1	1	1	No	1	1	1	10.0
Compound Y / Leoleorin A	1	1	1	0	0	No	1	1	1	9.7
Comosiin (Apigenin-7-O- β -glucoside)	1	1	1	1	1	Yes	0	0	1	4.0
Cynaroside (Luteolin-7-O- glucoside)	1	1	1	1	1	Yes	0	0	1	4.0
Dihydroxylphytyl palmitate	1	1	1	1	1	Yes	0	0	1	4.0

EDD(13S)-9 α , 13 α -epoxylabda- 6 β (19),15(14)di oldilactone)	1	1	1	1	1	No	1	1	1	10.0
Geniposidic acid	1	1	1	1	1	No	0	0	1	4.0
Leoleorin B	1	0	0	1	0	No	1	1	1	9.4
Leoleorin C	1	1	1	1	1	No	1	1	1	10.0
Leoleorin D	1	1	1	1	1	Yes	1	1	1	10.0
Leoleorin E	1	1	1	1	1	Yes	1	1	1	10.0
Leoleorin F	1	1	1	1	1	Yes	1	1	1	10.0
Leoleorin G	1	1	1	1	1	Yes	1	1	1	10.0

Leoleorin H	1	1	1	1	1	Yes	1	1	1	10.0
Leoleorin I	1	1	1	1	1	Yes	1	1	1	10.0
Leoleorin J	1	1	1	1	1	Yes	1	1	1	10.0
Leonurun	1	1	1	1	1	No	1	1	1	10.0
Luteolin	0	1	1	0	0	No	1	0	1	5.4
Luteolin 7-O- β - glucoside-3'- methyl ether	1	1	1	1	0	Yes	0	0	1	3.8
Marrubiin	1	1	1	0	1	No	1	1	1	9.8
Nepetaefolin	1	1	1	1	1	No	1	0	-1	0.0

Stachydrine	1	1	1	1	1	No	0	0	1	4.0
Succinic Acid	1	1	1	1	1	No	1	0	-1	0.0
Uracil	1	1	1	1	1	No	1	0	-1	0.0
Vitexin (Apigenin-8-C- β -glucoside)	1	1	1	1	1	No	0	0	-1	-2.0

Non -Inhibitor

Inhibitor

The next chapter would present the results seen when CADD processes were utilized in predicting the pharmacological activity of the compounds found in *L. leonurus*.

Chapter 4

4. IN SILICO TARGET PREDICTION FOR COMPOUNDS ISOLATED FROM L. LEONURUS AND PREDICTION OF POSSIBLE MAO-B INHIBITORS

4.1 Introduction

Determining the site of action of small molecules in the human body also known as target identification and validation is an important step in drug discovery (Agamah et al., 2020). This step helps to provide a focus for the development of novel compounds as well as the better characterization of already known drugs (Byrne and Schneider, 2019). As mentioned in chapter two of this thesis, computer-aided (*in silico*) methods are used to support the drug discovery process, including target prediction, to reduce the inherent challenges with conventional approaches (Agamah et al., 2020). The *in silico* prediction of the activity of small molecules can be done using common CADD processes which utilize the knowledge of the structure of either the targets (small compounds, receptors, amino acids), known as structure-based design or the bioactivity of the ligand, known as ligand-based design. These approaches cover both quantitative structure-activity relationships (QSAR) and pharmacophore modelling of compounds to predict the site of action of these compounds (Kapetanovic, 2008; Macalino et al., 2015). The structure-based approach utilizes the 3D structure of the target of interest to screen potential ligands through molecular docking (Macalino et al., 2015). Molecular docking is one of the most successful and popular structure-based methods which can be used both in target identification and lead discovery and optimization. It aids in predicting the interaction between ligands and biological targets (Pinzi and Rastelli, 2019). Docking examines and models the molecular interactions between the 3D structure of a target macromolecule and a group of potential ligands to identify and optimize 'hit' compounds (Kapetanovic, 2008; Macalino et al., 2015). The concept of using molecular docking methods to identify targets is known as reverse docking. Reverse docking involves docking a small molecule in the potential binding site of a set of clinically relevant protein targets. Detailed analysis of the binding characteristics leads to ranking of the targets according to their interaction or binding energy (Kharkar et al., 2014; Huang et al., 2018). Generally, a protein target with a higher rank would have a greater probability of being a target of the query small molecule (Huang et al., 2018).

The ligand-based method on the other hand subjects a group of compounds with different structures but known activity through various computational models to develop theoretical predictive models which would be used in identifying and optimizing the structure of ‘lead’ compounds (Macalino et al., 2015). This approach is based on the similarity-property principle, which states that similar compounds should exhibit similar properties, in this case, should interact with similar targets (Ekins et al., 2007). Both the structure-based approach and the ligand-based approach can be used simultaneously in CADD. This chapter discusses the use of the ligand-based method to identify the possible targets of the 36 compounds found in *Leonotis leonurus*. The use of the structure-based docking method to validate the hypothesis that one of the targets would be related to CNS activity, specifically to MAO-B, is also presented.

4.2 Research Question:

- 1 What are the *in silico* predicted biological targets for bioactive compounds isolated from *L. leonurus*?
- 2 Are any of these compounds predicted to have potential CNS activity as MAO-B inhibitors, for the treatment of AD?

4.3 Methods

The SMILES of the 36 compounds were imputed one at a time into the website www.swisstargetprediction.ch to predict the possible target sites of the compounds in the human body. As a way of confirming the sensitivity of swisstargetprediction.ch, the structures of known ACE inhibitors (captopril, enalapril and lisinopril) were imputed into the web-based tool as a form of control. A probability of 0.7 (70%) was set as the cut off mark for probable targets. The information on disease conditions related to the resulting identified targets were obtained from the databases uniprot.org and genecards.org. Using Cmap tools, network maps were drawn to show the correlation between the resulting predicted targets, the disease conditions related to these targets and the ethnobotanical use of the plant to determine the compounds possibly responsible for specific ethnobotanical uses of the plant. The related disease conditions were identified from the online database, DisGeNET v.6.0 (Piñero et al., 2019).

Having established that MAO-B is one of the targets for some of the query compounds, molecular docking was used to validate this prediction by predicting the interaction of the compounds with

MAO-B. Molecular modelling and docking of the compounds which showed predicted activity on the MAO-B enzyme, a protein that plays a role in the pathophysiology of AD, was carried out using the MOE software package. The high-resolution crystal structure of MAO-B, complexed with benzyl hydrazine was obtained from the Protein Data Bank (PDB entry code 2VRL, 2.40Å resolution) (<http://www.rcsb.org>) and docked with these compounds. Since MAO-B is a dimer, one subunit of the enzyme was used in the study. The enzyme was prepared by adding hydrogen and using the default structure preparation tool (quickprep) of the MOE software package. Benzyl hydrazine was removed from the complex and the side chain in the active region of the enzyme was optimized by adding hydrogen and minimizing the energy (final energy gradient of 0.00001). The resulting structure was saved as an MOE file for the docking study. Energy minimization of the test molecules which were predicted to target MAO-B (targets for Alzheimer's activity) as well as three known MAO-B inhibitors (rasagiline, selegiline, clorgiline) was performed using the MMFF94x force field (solvation: R-field, thread: 4) at a gradient of 0.001 with an rmsd value less than 0.05; partial charges were calculated according to the standard parameters of the force field. The prepared ligands were saved as mol2 files and docked at the active site of the MAO-B subunit and the best fit (S-score) was recorded.

4.4 Results

4.4.1 *Protein target predictions by swisstargetprediction.ch*

From the swisstargetprediction web tool, 17 of the 36 compounds were predicted to interact with a protein target with a probability value greater than 70% (Table 4.1). The complete data on all the targets predicted for the 36 compounds is found in Appendix 7.9.

Table 4.1: Protein target prediction for *L. leonurus* compounds with 70% probability and above

Compound Name	Target	Gene code	Probability	Disease Condition
13 ξ -hydroxylabd-5(6) 8(9)-dien-7-on-16 15-olide	Cytochrome P450 19A1	CYP19A1	0.83	Aromatase excess syndrome (AEXS); Aromatase deficiency (AROD); Osteoporosis; Female infertility; polycystic ovarian syndrome; Endometriosis; Gynaecomastia; Mammary Neoplasms; Uterine fibroid; Borjeson-Forsman-Lehmann syndrome
Apigenin	Aldo-keto reductase family 1 member B10	AKR1B10	0.95	Lung Carcinoma; Liver Carcinoma; Diabetic Retinopathy; Neoplasms; Contact Dermatitis
	Oestrogen receptor	ESR1	0.95	Oestrogen resistance (ESTRR); Breast Neoplasm ;
	Cytochrome P450 1A2	CYP1A2	0.95	Adenocarcinoma; Anxiety disorder; Arteriosclerosis; Bladder Neoplasm
	Cyclin-dependent kinase 1	CDK1	0.95	Neoplasm; Cancer

Microtubule-associated protein tau	MAPT	0.95	AD; Frontotemporal dementia (FTD) ; Pick disease of the brain (PDB) ; Progressive supranuclear palsy 1 (PSNP1) ; Parkinson-dementia syndrome (PARDE) ; Palsy ; Niemann - Pick disease type C
Cytochrome P450 19A1	CYP19A1	0.95	Aromatase excess syndrome (AEXS); Aromatase deficiency (AROD); Infertility; Borjeson-Forssman-Lehmann syndrome
Cyclin-dependent kinase 4	CDK4	0.95	Melanoma, cutaneous malignant 3 (CMM3); Familial melanoma; Dedifferentiated liposarcoma; Well-differentiated liposarcoma
Estradiol 17-beta-dehydrogenase 1	HSD17B1	0.95	Spontaneous abortion; Adenoma; Malignant Neoplasm; Endometriosis; Polycystic Ovarian Syndrome
Aldose reductase	AKR1B1	0.95	Cataract; Complications with Diabetes Mellitus
Casein kinase II subunit alpha'	CSNK2A2	0.95	Malignant Neoplasm; Male infertility; Glioblastoma; Childhood leukaemia

	Amine oxidase [flavin-containing] A	MAOA	0.95	Brunner syndrome (BRNRS); Monoamine oxidase A deficiency; Unipolar depression; bipolar disorder; Hypertension
	Prostaglandin G/H synthase 1	PTGS1	0.95	Pain
	Cyclin-dependent kinase 2	CDK2	0.95	Cancer; Neoplasm
	Amine oxidase [flavin-containing] B	MAO-B	0.95	Parkinson's disease; bipolar disorder; Unipolar depression; Hypertension; Schizophrenia; Renal detachment
	Adenosine receptor A2a	ADORA2A	0.95	Huntington's disease; Parkinson's disease
6-Methoxyluteolin-4-methyl ether	Aldose reductase	AKR1B1	0.85	Cataract; Complications with Diabetes Mellitus
	Aldo-keto reductase family 1 member B15	AKR1B15	0.85	Longevity

Aldo-keto reductase family 1 member B10	AKR1B10	0.85	Lung Carcinoma; Liver Carcinoma; Diabetic Retinopathy; Neoplasms; Contact Dermatitis
Microtubule-associated protein tau	MAPT	0.8	AD; Frontotemporal dementia; Pick disease of the brain; Progressive supranuclear palsy 1; Parkinson's-dementia syndrome; Neurodegenerative disorders; Childhood disintegrative disorder
Xanthine dehydrogenase/oxidase	XDH	0.78	Xanthinuria; Reperfusion injury; cardiovascular disease; Hypertension; Heart failure; heart disease; Pyelonephritis; Hydronephrosis; Pulmonary Embolism; Nerve degeneration; Ischaemia; Gout; Diabetes Mellitus
Aldehyde oxidase	AOX1	0.78	Astrocytoma; Neoplasm; Crohn disease; Xanthinuria, type 1; Prostate carcinoma
FAD-linked sulfhydryl oxidase ALR	GFER	0.78	Myopathy, mitochondrial progressive, with congenital cataract, hearing loss and developmental delay (MPMCHD); Acute Kidney injury; Acute Liver failure;

	Adenosine receptor A1	ADORA1	0.73	Asthma; Anxiety disorder; Diabetes Mellitus; Epilepsy; Hypertensive disease
	Dual specificity tyrosine-phosphorylation-regulated kinase 1A	DYRK1A	0.73	Mental retardation, autosomal dominant 7 (MRD7); Intellectual disability; Autistic disorder; Febrile convulsions; Cerebral atrophy
Compound X	Protein kinase C gamma type	PRKCG	0.72	Spinocerebellar ataxia 14 (SCA14)
	Protein kinase C beta type	PRKCB	0.72	Lymphoid neoplasm
	Protein kinase C alpha type	PRKCA	0.72	AD; Arteriosclerosis; Rheumatoid arthritis; Asthma; Malignant neoplasm of breast; Colorectal carcinoma
Acteoside	Protein kinase C gamma type	PRKCG	0.97	Spinocerebellar ataxia 14
	Protein kinase C beta type	PRKCB	0.97	Insulin dependent Diabetes Mellitus; Lymphoid neoplasm; Diabetic Retinopathy

Protein kinase C alpha type	PRKCA	0.97	Cancer; Neoplasm; Schizophrenia
Protein kinase C theta type	PRKCQ	0.97	Rheumatoid Arthritis
Protein kinase C delta type regulatory subunit	PRKCD	0.97	Autoimmune lymphoproliferative syndrome 3 (ALPS3); Autosomal recessive systemic lupus erythematosus; Common variable immunodeficiency; Cancer
22 kDa interstitial collagenase	MMP1	0.95	Rosacea; Acne; Chronic Obstructive Airway disease; Inflammatory skin disease; Severe generalized recessive dystrophic epidermolysis bullosa
PEX	MMP2	0.95	Multicentric osteolysis, nodulosis, and arthropathy (MONA) Spectrum; Torg-Winchester syndrome
Stromelysin-1	MMP3	0.95	Coronary heart disease 6 (CHDS6)
67 kDa matrix metalloproteinase 9	MMP9	0.95	Intervertebral disc disease (IDD); Metaphyseal anadysplasia 2 (MANDP2); lumbar disc degeneration ; Neoplasm Metastasis

	Macrophage metalloelastase	MMP12	0.95	Adenocarcinoma; Arteriosclerosis; Asthma; Rheumatoid arthritis; Malignant neoplasms; cardiovascular diseases
	Collagenase 3	MMP13	0.95	Spondyloepimetaphyseal dysplasia Missouri type (SEMD-MO); Metaphyseal anadysplasia 1 (MANDP1); Metaphyseal chondrodysplasia, Spahr type (MDST) (Pyle disease); Rosacea
	Stromelysin-2	MMP10	0.95	Arteriosclerosis; Asthma; Bipolar disorder; Rheumatoid arthritis; Malignant neoplasms; Ulcerative colitis; Diabetes mellitus
	Matrix metalloproteinase-27	MMP27	0.95	Neoplasm metastasis; Neoplasms; Tumour cell invasion
Dihydroxyphytyl Palmitate	Protein kinase C gamma type	PRKCG	0.82	Spinocerebellar ataxia 14 (SCA14)
	Protein kinase C beta type	PRKCB	0.82	Lymphoid neoplasm; Diabetic Retinopathy

	Protein kinase C alpha type	PRKCA	0.82	Cancer; Neoplasm; Schizophrenia
	Protein kinase C theta type	PRKCQ	0.82	Rheumatoid arthritis; Autoimmune diseases; Diabetes mellitus, insulin resistance; Gastrointestinal stromal tumours
	Protein kinase C delta type regulatory subunit	PRKCD	0.82	Autoimmune lymphoproliferative syndrome 3 (ALPS3) ; Autosomal systemic lupus erythematosus ; Common variable immunodeficiency
Comosiin	Tyrosyl-DNA phosphodiesterase 1	TDP1	0.93	Spinocerebellar ataxia, autosomal recessive, with axonal neuropathy (SCAN1)
	Aldo-keto reductase family 1 member B10	AKR1B10	0.91	Lung Carcinoma; Liver Carcinoma; Diabetic Retinopathy; Neoplasms; Contact Dermatitis
	Aldose reductase	AKR1B1	0.91	Cataract; Complications with Diabetes Mellitus
	Aldo-keto reductase family 1 member B15	AKR1B15	0.91	Longevity
	Lysine-specific demethylase 4A	KDM4A	0.87	Malignant neoplasm of breast; Malignant neoplasm; non-small cell lung carcinoma; Neoplasm metastasis; Neoplasms; Malignant neoplasm of prostate; Carcinogenesis

	Lysine-specific demethylase 4B	KDM4B	0.87	Malignant neoplasm of breast; Colorectal carcinoma; Neoplasms; Carcinogenesis
	Lysine-specific demethylase 4C	KDM4C	0.87	Malignant neoplasm of breast; Carcinoma; Neoplasms; Childhood leukaemia
	Adenosine receptor A1	ADORA1	0.83	COPD, Asthma; Hypertension, Coronary Heart Disease; Pain; Bronchiectasis; Coronary Artery Disease; Migraine Disorder; Wolff-Parkinson-White Syndrome
	Muscle blind-like protein 1	MBNL1	0.71	Dystrophia myotonica 1 (DM1); Corneal dystrophy, Fuchs endothelial, 3 (FECD3);
	Muscle blind-like protein 2	MBNL2	0.71	Myotonic dystrophy
	Muscle blind-like protein 3	MBNL3	0.71	Nystagmus; Carcinogenesis; Liver carcinoma
Luteolin	22 kDa interstitial collagenase	MMP1	0.95	Severe generalized recessive dystrophic epidermolysis bullosa
	Cytochrome P450 1A2	CYP1A2	0.95	Adenocarcinoma; Anxiety disorder; Arteriosclerosis; Bladder Neoplasm

PEX	MMP2	0.95	Multicentric osteolysis, nodulosis, and arthropathy spectrum; Torg-Winchester syndrome; Nodulosis-arthropathy-osteolysis syndrome
Stromelysin-1	MMP3	0.95	Coronary heart disease 6 (CHDS6)
67 kDa matrix metalloproteinase 9	MMP9	0.95	Intervertebral disc disease (IDD); Metaphyseal anadysplasia 2 (MANDP2)
Aldose reductase	AKR1B1	0.95	Cataract; Complications with Diabetes Mellitus
Amine oxidase [flavin-containing] A	MAOA	0.95	Brunner syndrome (BRNRS); Monoamine oxidase A deficiency; Unipolar depression; bipolar disorder; Hypertension
Amine oxidase [flavin-containing] B	MAO-B	0.95	Parkinson's disease; Schizophrenia; Bipolar disorder; Hypertension; AD
ADP-ribosyl cyclase 1	CD38	0.95	AD; Sickle cell anaemia; Asthma; Arthritis; Autistic disorder; Autoimmune diseases; Burkitt lymphoma; Malignant neoplasms
Adenosine receptor A1	ADORA1	0.95	Hypertension, Coronary Heart disease; Pain; Asthma; Wolff- Parkinson- White Syndrome

	Macrophage metalloelastase	MMP12	0.95	Atherosclerosis; Malignant neoplasms; cardiovascular diseases; coronary heart disease; Diabetes mellitus
	Collagenase 3	MMP13	0.95	Spondyloepimetaphyseal dysplasia Missouri type (SEMD-MO); Metaphyseal anadysplasia 1 (MANDP1); Metaphyseal dysplasia, Spahr type (MDST)
	Xanthine dehydrogenase/oxidase	XDH	0.95	Xanthinuria 1 (XAN1), Gout
	Lactoylglutathione lyase	GLO1	0.95	Congenital adrenal hyperplasia; Alcohol use disorder; anxiety disorder; Autistic disorder; Arteriosclerosis; Malignant neoplasm; Depressive disorder; Diabetes
	Lysine--tRNA ligase	KARS	0.95	Charcot-Marie-Tooth disease, recessive, intermediate type, B (CMTRIB); Deafness, autosomal recessive, 89 (DFNB89); Intermediate osteopetrosis
Chryseriol	Cytochrome P450 1A2	CYP1A2	1	Colorectal Cancer; Cutaneous Melanoma; Schizophrenia and related disorders; Chronic Obstructive Airway Disease; Liver Diseases; Lung Neoplasm; Neural Tube Defect
	Multidrug resistance-associated protein 1	ABCC1	1	Hereditary Breast Cancer; Breast Cancer; Colorectal Cancer; Peripheral Neuropathy; Heart Disease; Hypertensive Disease; Malignant Neoplasm of Lung; Adverse Reaction to Drugs; Acute Leukaemia

Cytochrome P450 1B1	CYP1B1	1	Glaucoma; Anterior segment dysgenesis 6 (ASGD6); Glaucoma 3, primary congenital, A (GLC3A); Glaucoma, primary open angle (POAG); Glaucoma 1, open angle, A (GLC1A); Mammary Neoplasm; Cardiomegaly; Squamous cell Carcinoma
Cytochrome P450 1A1	CYP1A1	1	Mammary Neoplasm; Prostatic Neoplasm; Liver Carcinoma; Chronic Obstructive Airway Disease; Male Infertility; Hypertensive Disease; Spontaneous abortion; Kidney Neoplasm; Cutaneous Melanoma
Canalicular multispecific organic anion transporter 2	ABCC3	1	Carcinoma; Cholestasis; Rheumatoid Arthritis; Colorectal Neoplasm; Liver Carcinoma; Non-alcoholic Fatty Liver Disease; Diabetes Mellitus; Hyperprolactinemia; Malignant Neoplasm of the Lung; Liver Neoplasm
Canalicular multispecific organic anion transporter 1	ABCC2	1	Dubin-Johnson's Syndrome; Chronic Idiopathic Jaundice; Cholestasis; Conjugated Hyperbilirubinemia; Rheumatoid Arthritis; Seizures; Alopecia; Icterus (Jaundice)
Aldose reductase	AKR1B1	0.85	Cataract; Complications with Diabetes Mellitus
Aldo-keto reductase family 1 member B15	AKR1B15	0.85	Longevity

Aldo-keto reductase family 1 member B10	AKR1B10	0.85	Lung Carcinoma; Liver Carcinoma; Diabetic Retinopathy; Neoplasms; Contact Dermatitis
Plasmin light chain B	PLG	0.83	Plasminogen Deficiency; Ligneous Conjunctivitis; Hypoplasminogenemia; Hypertensive Disease; Coronary Heart Disease; Myocardial Infarction; Periodontitis; Gingival Disease; Schizophrenia; Skin Disease; Dermatological Disorders
Apolipoprotein(a)	LPA	0.83	Coronary Artery Disease; Coronary Heart Disease; Cardiovascular Disease; Atherosclerosis; Cerebrovascular Accident; Hypercholesterolemia; Myocardial Infarction; Thromboembolism;
Xanthine dehydrogenase/oxidase	XDH	0.82	Xanthinuria 1 (XAN1); Gout
Aldehyde oxidase	AOX1	0.82	Prostatic Neoplasm / Carcinoma; Hearing Loss / Impairment; Inflammatory Bowel Disease; Columnar Cell change of the Breast;
NADPH oxidase 4	NOX4	0.79	Heart Failure; Chronic Kidney Failure; Chemical and Drug Induced Liver Injury; Colonic Neoplasm; Renal Insufficiency; Hypertensive disease; Asthma; Glioma
Oestrogen receptor	ESR1	0.76	Oestrogen resistance; Breast Carcinoma; Mammary Neoplasms; Osteoporosis

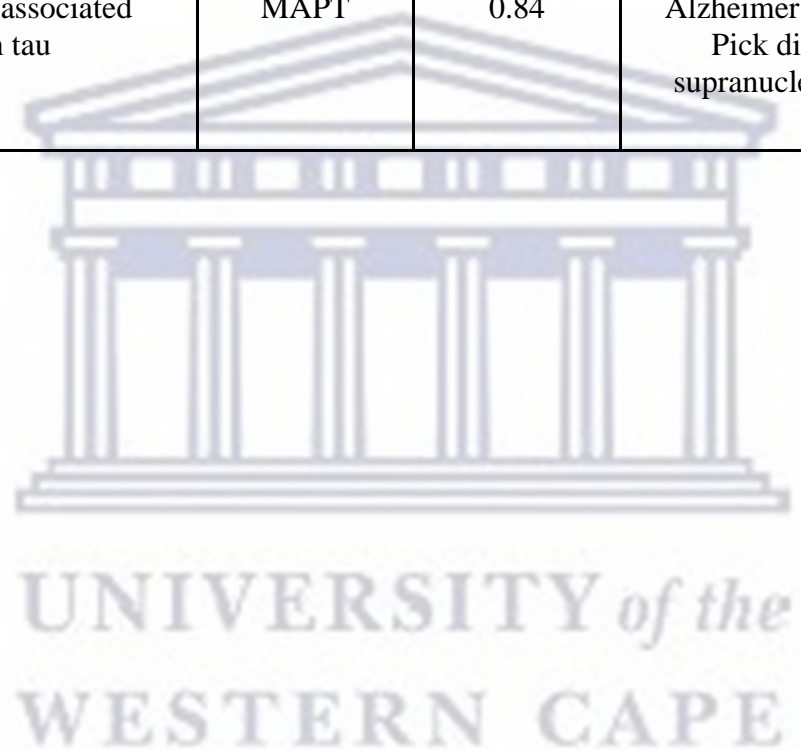
Apigenin-7-O-(6''-O-p-coumaroyl)- β -glucoside	Adenosine receptor A1	ADORA1	0.75	Hypertension; Coronary Heart disease; coronary artery disease; Pain; Asthma; Obstructive lung disease; Bronchiectasis; Wolff-Parkinson-White Syndrome
	Aldose reductase	AKR1B1	0.71	Cataract; Complications with Diabetes Mellitus
	Aldo-keto reductase family 1 member B15	AKR1B15	0.71	Longevity
	Aldo-keto reductase family 1 member B10	AKR1B10	0.71	Lung Carcinoma; Liver Carcinoma; Diabetic Retinopathy; Neoplasms; Contact Dermatitis
Succinic Acid	Egl nine homolog 1	EGLN1	1	Familial Erythrocytosis 3; Autosomal dominant secondary polycythaemia
	Egl nine homolog 2	EGLN2	1	Malignant neoplasms; non-small cell lung carcinoma; Colitis; Chronic obstructive airway disease; Fibrosis, Liver; Carcinogenesis
Cynaroside	Tyrosyl-DNA phosphodiesterase 1	TDP1	0.98	Spinocerebellar ataxia, autosomal recessive, with axonal neuropathy (SCAN1)
	Lysine-specific demethylase 4A	KDM4A	0.9	Malignant neoplasm of breast; Malignant neoplasm; non-small cell lung carcinoma; Neoplasm metastasis;

			Neoplasms; Malignant neoplasm of prostate; Carcinogenesis
Lysine-specific demethylase 4B	KDM4B	0.9	Malignant neoplasm of breast; Colorectal carcinoma; Neoplasms; Carcinogenesis
Lysine-specific demethylase 4C	KDM4C	0.9	Malignant neoplasm of breast; Carcinoma; Neoplasms; Childhood leukaemia
Aldo-keto reductase family 1 member B10	AKR1B10	0.88	Lung Carcinoma; Liver Carcinoma; Diabetic Retinopathy; Neoplasms; Contact Dermatitis
Aldose reductase	AKR1B1	0.88	Cataract; Complications with Diabetes Mellitus
Aldo-keto reductase family 1 member B15	AKR1B15	0.88	Longevity
Xanthine dehydrogenase/oxidase	XDH	0.82	Xanthinuria 1 (XAN1); Gout
Aldehyde oxidase	AOX1	0.82	Prostatic Neoplasm / Carcinoma; Hearing Loss / Impairment; Inflammatory Bowel Disease; Columnar Cell change of the Breast

	Adenosine receptor A1	ADORA1	0.79	COPD; Asthma; Hypertension; Coronary Heart Disease; Pain; Bronchiectasis; Coronary Artery Disease; Migraine Disorder; Wolff-Parkinson-White Syndrome
Luteolin 7-O- β -glucoside-3-methyl ether	Tyrosyl-DNA phosphodiesterase 1	TDP1	0.93	Spinocerebellar ataxia, autosomal recessive, with axonal neuropathy (SCAN1)
	Lysine-specific demethylase 4A	KDM4A	0.86	Malignant neoplasm of breast; Malignant neoplasm; non-small cell lung carcinoma; Neoplasm metastasis; Neoplasms; Malignant neoplasm of prostate; Carcinogenesis
	Lysine-specific demethylase 4B	KDM4B	0.86	Malignant neoplasm of breast; Colorectal carcinoma; Neoplasms; Carcinogenesis
	Lysine-specific demethylase 4C	KDM4C	0.86	Malignant neoplasm of breast; Carcinoma; Neoplasms; Childhood leukaemia
	Aldo-keto reductase family 1 member B10	AKR1B10	0.84	Lung Carcinoma; Liver Carcinoma; Diabetic Retinopathy; Neoplasms; Contact Dermatitis
	Aldose reductase	AKR1B1	0.84	Cataract; Complications with Diabetes
	Aldo-keto reductase family 1 member B15	AKR1B15	0.84	Longevity

	Adenosine receptor A1	ADORA1	0.8	COPD; Pain; Asthma; Coronary Heart Disease; Coronary Artery disease; Wolff-Parkinson-White syndrome
	Xanthine dehydrogenase/oxidase	XDH	0.77	Xanthinuria 1 (XAN1); Gout
	Aldehyde oxidase	AOX1	0.77	Prostatic Neoplasm / Carcinoma; Hearing Loss / Impairment; Inflammatory Bowel Disease; Columnar Cell change of the Breast
Leoleorin C	Platelet-activating factor receptor	PTAFR	0.85	Arteriosclerosis; Chronic obstructive airway disease; Neoplasms; Pneumococcal infections
	Microtubule-associated protein tau	MAPT	0.71	AD; Frontotemporal dementia; Pick disease of the brain; Progressive supranuclear palsy 1 (PSNP1); Parkinson-dementia syndrome (PARDE)
9,13-epoxyabda-6(19),15(14)diol dilactone (EDD)	Platelet-activating factor receptor	PTAFR	0.79	Arteriosclerosis; Chronic obstructive airway disease; Neoplasms; Pneumococcal infections
	Microtubule-associated protein tau	MAPT	0.74	Alzheimer disease, Frontotemporal dementia (FTD); Pick disease of the brain (PIDB); Progressive supranuclear palsy 1 (PSNP1); Parkinson-dementia syndrome (PARDE)

Geniposidic acid	Microtubule-associated protein tau	MAPT	0.74	Alzheimer disease, Frontotemporal dementia (FTD); Pick disease of the brain (PIDB); Progressive supranuclear palsy 1 (PSNP1); Parkinson-dementia syndrome (PARDE)
Vitexin	Microtubule-associated protein tau	MAPT	0.84	Alzheimer disease, Frontotemporal dementia (FTD); Pick disease of the brain (PIDB); Progressive supranuclear palsy 1 (PSNP1); Parkinson-dementia syndrome (PARDE)



It was observed that 13 ξ -hydroxylabd-5(6) 8(9)-dien-7-on-16 15-olide (#4) and apigenin (#8) had a probability of 0.83 in interacting with Cytochrome P450 19A1 (CYP19A1), an enzyme involved in the disease pathophysiology of aromatase excess syndrome (AEXS) and aromatase deficiency (AROD) as it is involved in the catalyses of androgens and testosterone (Corbin et al., 1988; Baravalle et al., 2017). There are currently no studies on the effect of the extracts of *L. leonurus* on these hormones.

6-Methoxyluteolin-4-methylether, apigenin, apigenin-7-O-(6''-O-p-coumaroyl)- β -glucoside, chryseriol, comosiin and luteolin had a probability of more than 0.7 of interacting with aldose reductase (AKR1B1). This enzyme is an important factor in the pathogenesis of diabetic complications as it causes an increase in reactive oxidative species production in various tissues of diabetic patients (Tang et al., 2012). There are studies done on the effect of *L. leonurus* plant extracts on diabetes (Ojewole, 2005; Oyedemi et al., 2011), and on its effect as an antioxidant (Jimoh et al., 2010; Oyedemi et al., 2011) but not on the oxidative stress caused by AKR1B1 in diabetic complications.

Leoleorin C and EDD were predicted to interact with platelet-activating factor receptors (PTAFR). This is the receptor for platelet activating factor, a phospholipid activator and mediator of platelet aggregation and dilation of blood vessels (Ashraf and Nookala, 2020). A study done by Mnonopi et al., (2011), showed that the organic extract of *L. leonurus* suppressed coagulation and platelet aggregation. This study identified marrubiin as the compound responsible for this activity (Mnonopi et al., 2011).

Apigenin, 6-methoxyluteolin-4-methylether, compound X, acteoside, dihydroxyphytyl palmitate, comosiin, luteolin, cynaroside, luteolin 7-O- β -glucoside-3-methyl ether, leoleorin C, EDD, geniposidic acid and vitexin all had targets located in the central nervous system (table 4.1). Apigenin, 6-methoxyluteolin-4-methylether, leoleorin C, EDD, geniposidic acid and vitexin have been previously predicted to target microtubule-associated protein tau (MAPT) which is a protein involved in the pathogenesis of AD and frontotemporal dementia (FTD) (Kobayashi et al., 2003; Behnam et al., 2015). Currently, there are no studies on the use of the extracts of this plant in the management of AD or any form of dementia.

Apigenin and luteolin were predicted to interact with the two forms of monoamine oxidases (A and B). These enzymes are responsible for metabolizing amine neurotransmitters (norepinephrine, epinephrine, serotonin, and dopamine) via oxidative deamination (Borroni et al., 2017). This

reaction produces inflammatory chemicals such as cytokines and reactive oxygen species (ROS), which lead to oxidative stress and is represented in various CNS conditions such as Parkinson's disease and AD (Borroni et al., 2017). There are no studies on the effect of *L. leonurus* on AD and Parkinson's disease, but studies have reported on the effect of the plant extracts as an anticonvulsant (Bienvenu et al., 2002; Muhizi et al., 2005). Apigenin was also predicted to interact with adenosine A2A receptors (ADORA2A). Adenosine A2A receptors are involved in the pathogenesis of Parkinson's disease and Huntington's disease (Pinna et al., 2017).

Acteoside, compound X and dihydroxyphytyl palmitate were predicted to interact with protein kinase C gamma type (PRKCG). The mutation or deletion of the PRKCG gene leads to the development of spinocerebellar ataxia 14, an autosomal dominant neurodegenerative disorder characterized by slow progressive cerebellar dysfunction (Shimobayashi and Kapfhammer, 2017). Cynaroside, comosiin and luteolin 7-O- β -glucoside-3-methyl ether were predicted to interact with tyrosyl-DNA phosphodiesterase 1, a DNA repair enzyme that can remove a variety of covalent adducts from DNA (Hirano et al., 2007). Mutation of this gene can lead to spinocerebellar ataxia, autosomal recessive, with axonal neuropathy 1 (SCAN1), a form of spinocerebellar ataxia (Takashima et al., 2002; Hirano et al., 2007). Finally, 6-methoxyluteolin-4-methyl ether was predicted to interact with dual specificity tyrosine-phosphorylation-regulated kinase 1A (DYRK1A). Overexpression of this enzyme leads to the development of cognitive deficits seen in Down's syndrome and AD (Nguyen et al., 2017). There are currently no studies on the use of *L. leonurus* or any of its isolated compounds in the treatment of cognitive deficits seen in Down's syndrome, AD, or spinocerebellar ataxia.

4.4.2 Compounds predicted to target proteins indicative of an ethnobotanical use

A search on uniprot.org and genecards.org of the 17 compounds with identified target proteins revealed correlations between the target and at least one ethnobotanical use for 14 compounds (apigenin, 6-methoxyluteolin-4-methylether, compound X, acteoside, luteolin, chryseriol, cynaroside, dihydroxyphytyl palmitate, luteolin 7-O- β -glucoside-3-methyl ether, comosiin, EDD, leoleorin C, geniposidic acid and vitexin) (Appendix 7.10 and 7.11). The network interaction

between these 14 compounds, their predicted protein targets and the related disease conditions of these targets is represented in Figures 4.1 to 4.9 below.

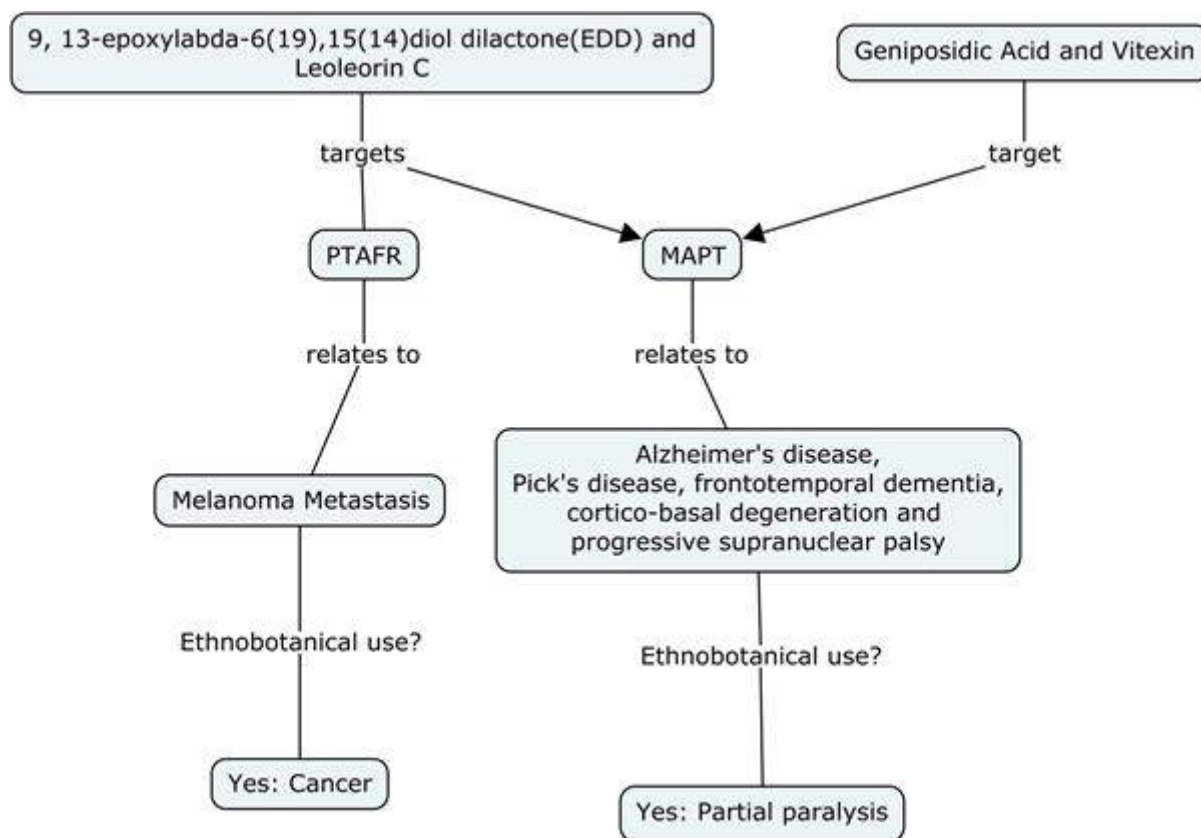


Figure 4.1: C-map network showing the target prediction suggesting that EDD and leoleorin C may be responsible for the ethnobotanical use for Cancer whilst geniposidic acid and vitexin may be responsible for the ethnobotanical use of partial paralysis.

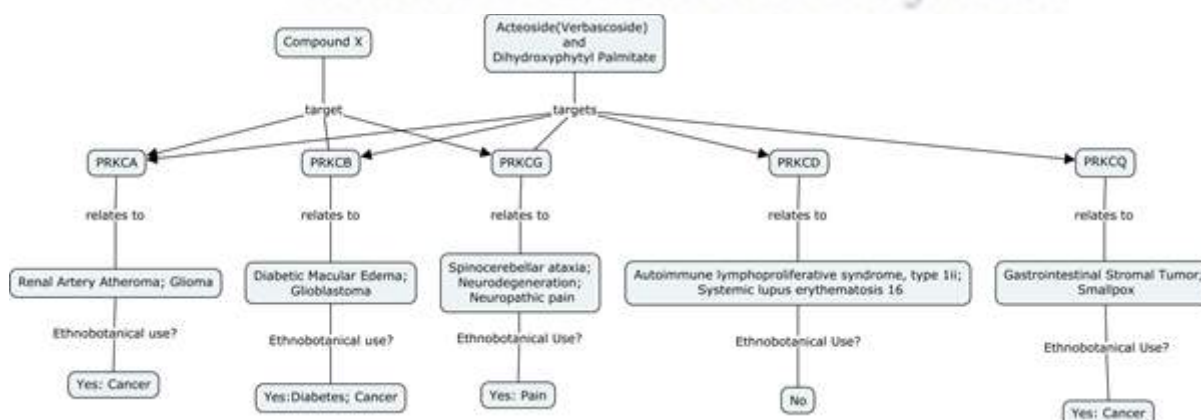


Figure 4.2: C-map network showing the target prediction suggesting that compound X may be responsible for the ethnobotanical use for cancer, diabetes, and pain, whilst acteoside and dihydroxyphytyl palmitate may be responsible for the ethnobotanical use of cancer and pain.

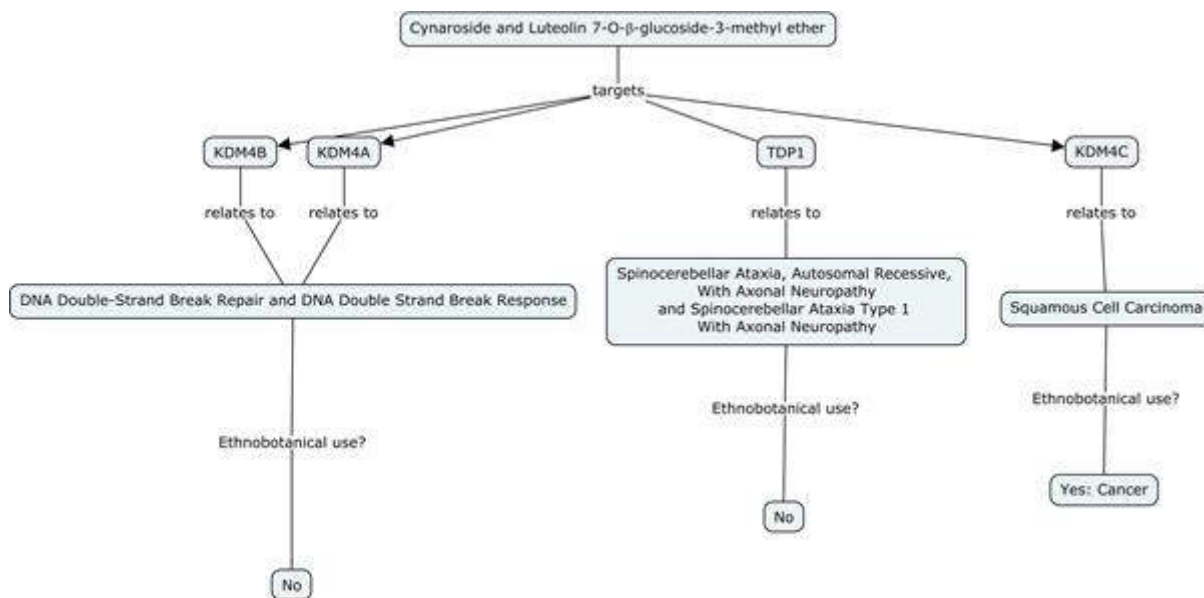


Figure 4.3: C-map network showing the target prediction suggesting that cynaroside and luteolin 7-O-β-glucoside-3-methyl ether may be responsible for ethnobotanical use for cancer.

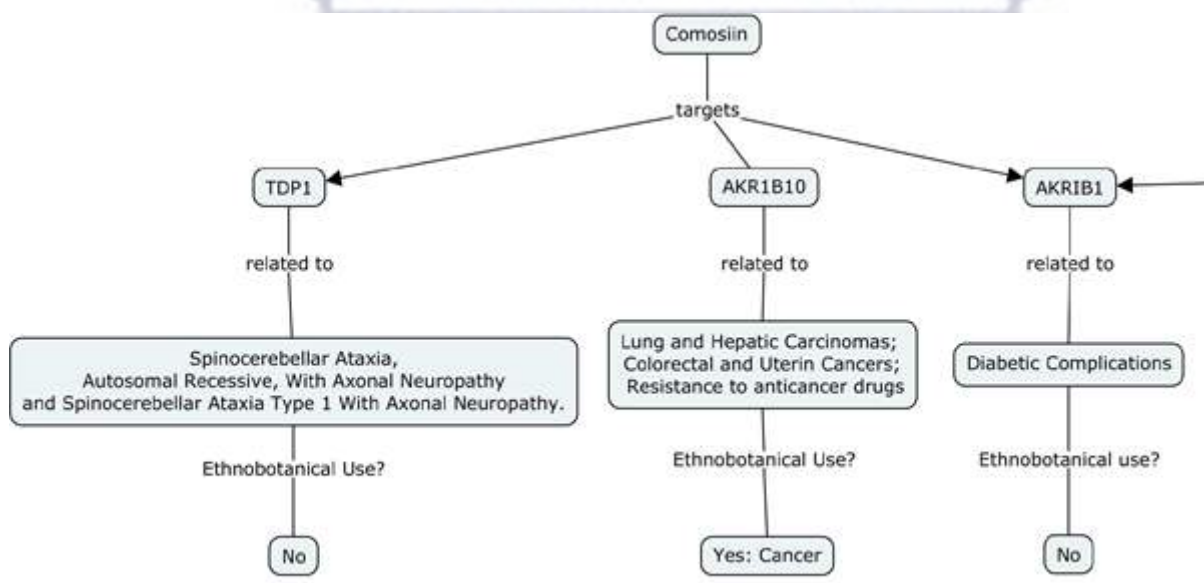


Figure 4.4: C-map network showing the target prediction suggesting that comosiin may be responsible for ethnobotanical use for cancer.

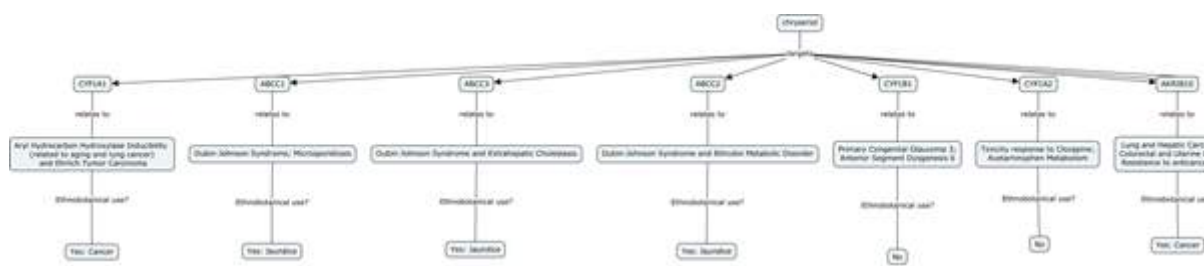


Figure 4.5: C-map network showing the target prediction suggesting that chryseriol may be responsible for ethnobotanical use for jaundice and cancer.

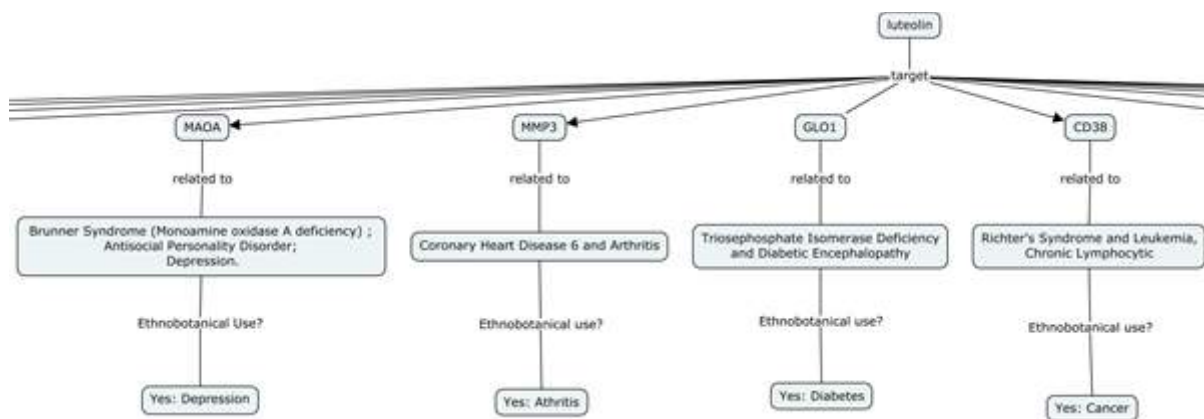


Figure 4.6: C-map network showing the target prediction suggesting that luteolin may be responsible for ethnobotanical use for cancer, depression, diabetes, and arthritis.

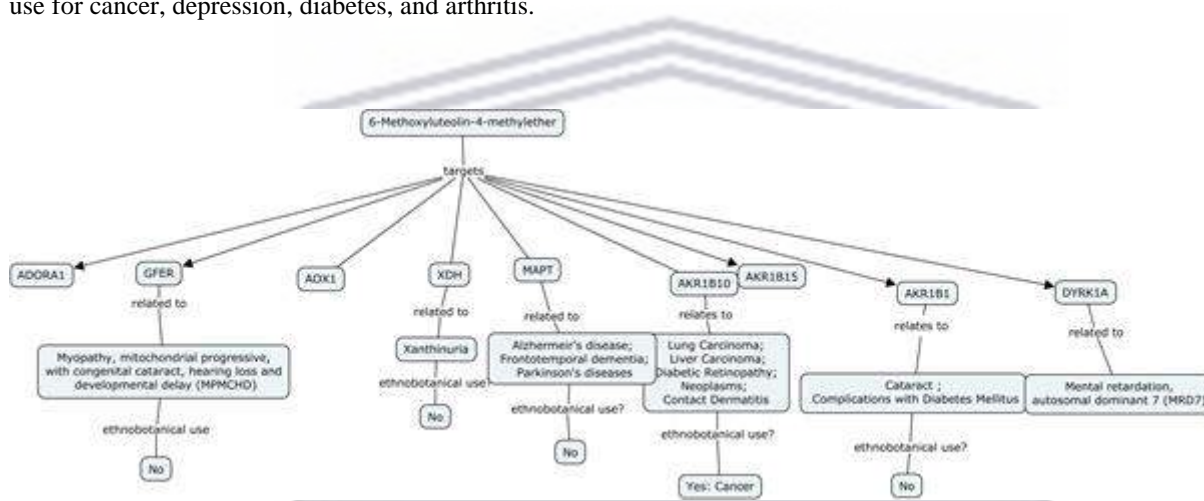


Figure 4.7: C-map network showing the target prediction suggesting that 6-Methoxyluteolin-4-methyl ether may be responsible for ethnobotanical use for cancer.

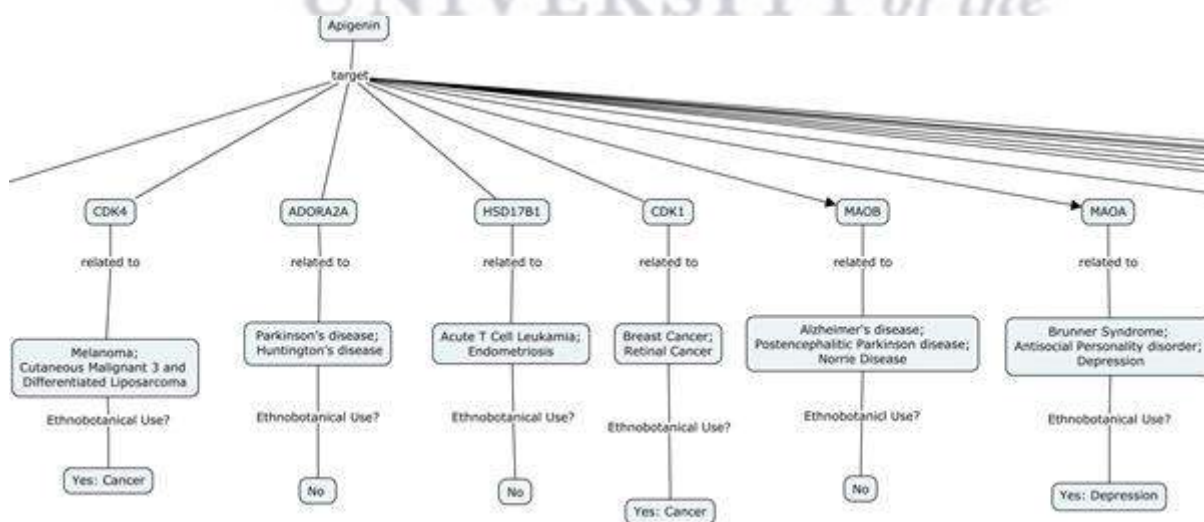


Figure 4.8: C-map network showing the target prediction suggesting that apigenin may be responsible for ethnobotanical use for cancer and depression.

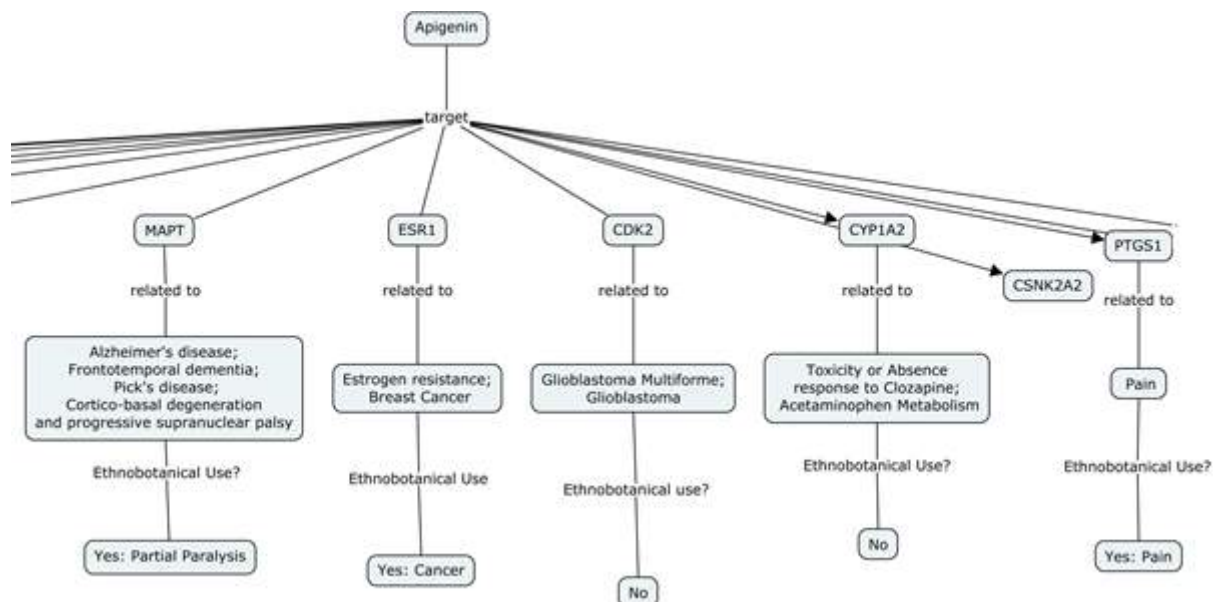


Figure 4.9: C-map network showing the target prediction suggesting that apigenin may be responsible for ethnobotanical use for cancer, partial paralysis, and pain.

4.4.3 Compounds predicted to target AD

It has been ascertained that apart from amyloid precursor protein which is the precursor for amyloid- β -peptide ($A\beta$) and AChE, two other protein targets are responsible for the progression of AD. These are microtubule-associated protein tau (MAPT) and monoamine oxidase B (MAO-B) (Cheng et al., 2015). From the C-map networking process, 6 compounds (apigenin, EDD, geniposidic acid, leoleorin C, vitexin and luteolin) were predicted to have a 70% probability of targeting either MAPT or MAO-B or both proteins. Figure 4.10 shows the network mapping of these compounds in relation to AD.

UNIVERSITY of the
WESTERN CAPE

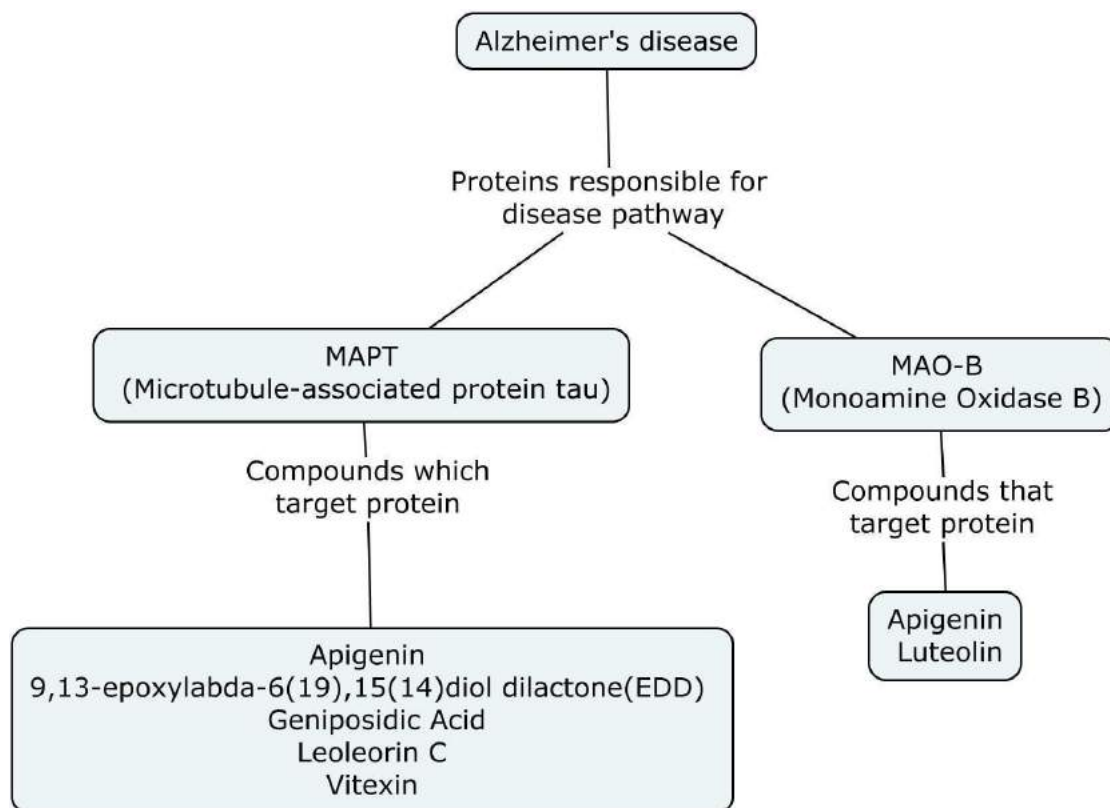


Figure 4.10: C-map network showing targets found in AD pathway and possible compounds with such activities

4.4.4 Molecular docking studies

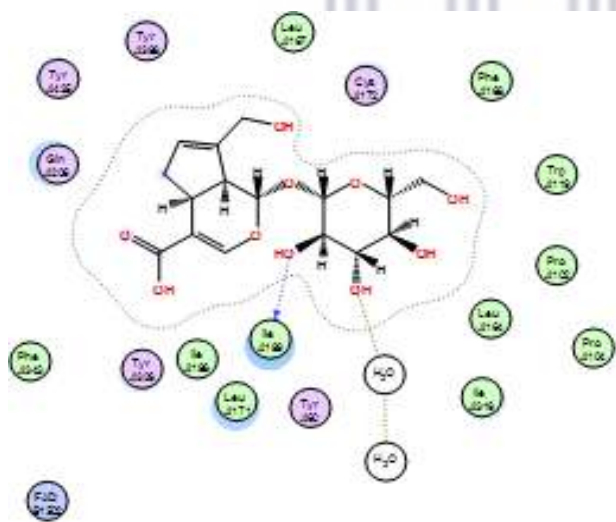
To validate the predictions of the ligand-based studies in the previous sections of this chapter, a structure-based analysis of the 6 compounds predicted to have CNS activity via the MAPT and MAO-B pathway was conducted using the MOE. The three lowest S-scores for each of the test compounds and for three known MAO-B inhibitors (rasagiline, selegiline, clorgiline), when docked with MAO-B, is presented in table 4.2 (full S-score results are presented in appendix 7.10). The lower the S-score the stronger the interaction between an inhibitor and the target site i.e., the stronger the binding affinity. It is also important to note that apart from the S-score and dissociation constant of an inhibitor, the identified active site of a protein needs to interact with the inhibitor for it to have its effect. It can be observed from these results that geniposidic acid, apigenin and luteolin had strong interactions with the MAO-B target site when compared to the S-score values of the known inhibitors. Another compound that showed some form of interaction, although less than that of the above-mentioned compounds is vitexin. EDD and leoleorin C had the lowest interaction with the MAO-B.

Table 4.2: Docking results of Compounds

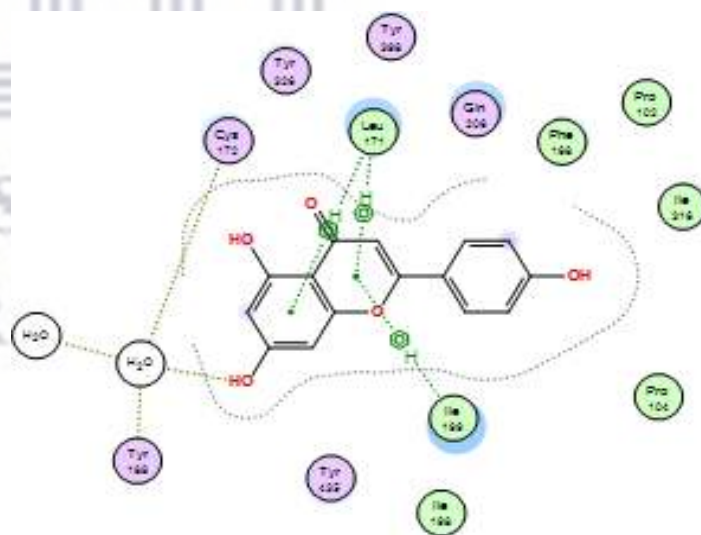
Compound Name	mol	rseq	mseq	S-score (kcal/mol)	Dissociation Constant (Kd)
Apigenin	<chem>O=C1c2c(O)cc(O)cc2OC(c2ccc(O)cc2)=C1</chem>	1	1	-7.58861	6.6932605548781764e+44
		1	1	-7.5119	2.3578415005227187e+44
		1	1	-7.10757	9.64167077980951e+41
EDD	<chem>O=C1[C@]2(C)[C@H]3[C@@](C)([C@@]4([C@H](C)C[C@H]3O1)O[C@@]1(C(=O)OCC1)CC4)CCC2</chem>	1	2	-2.02411	904362769681.2635
		1	2	-0.43019	347.6292967834247
		1	2	-0.2683	38.44484781115165
Geniposidic Acid	<chem>O=C(O)C=1[C@@H]2[C@H]([C@H](O[C@H]3[C@H](O)[C@@H](O)[C@H](O)[C@@H](CO)O3)OC=1)C(CO)=CC2</chem>	1	3	-7.88242	3.6405122867191176e+46
		1	3	-7.58534	6.402092767222514e+44
		1	3	-7.51417	2.4317751338199254e+44
Leoleorin C	<chem>O=C1[C@@]2(OC3([C@H](C)C[C@@H](O)C4C(C)(C)CCC[C@]34C)CC2)CCO1</chem>	1	4	-0.48063	690.3408589251535
		1	4	-0.45607	494.2976773229963
		1	4	-0.2075	16.81491985673691

Luteolin	<chem>O=C1c2c(O)cc(O)cc2OC(c2cc(O)c(O)cc2)=C1</chem>	1	5	-7.55454	4.211021953246489e+44
		1	5	-7.4638	1.2257155392670622e+44
		1	5	-7.46249	1.2040695417838972e+44
Vitexin	<chem>O=C1c2c(O)cc(O)c(C3[C@H](O)[C@@H](O)[C@H](O)[C@@H](CO)O3)c2OC(c2ccc(O)cc2)=C1</chem>	1	6	-3.08822	1745826038615668200
		1	6	-2.29836	37698776062643.24
		1	6	-1.84219	76163691366.04005
Selegiline	<chem>N(C(Cc1cccc1)C)(CC#C)C</chem>	1	7	-7.15518	1.842395235416646e+42
		1	7	-7.13217	1.347297753114662e+42
		1	7	-6.92645	8.208866214908303e+40
Rasagiline	<chem>N(CC#C)C1c2c(ccc2)CC1</chem>	1	8	-6.62888	1.433996950056769e+39
		1	8	-6.61132	1.1293328449257401e+39
		1	8	-6.5494	4.864775647229176e+38
Clorgiline	<chem>Clc1c(OCCCN(CC#C)C)ccc(Cl)c1</chem>	1	9	-8.23468	4.3847945800081924e+48
		1	9	-7.89565	4.358244796404204e+46
		1	9	-7.84382	2.1535439194118861e+46

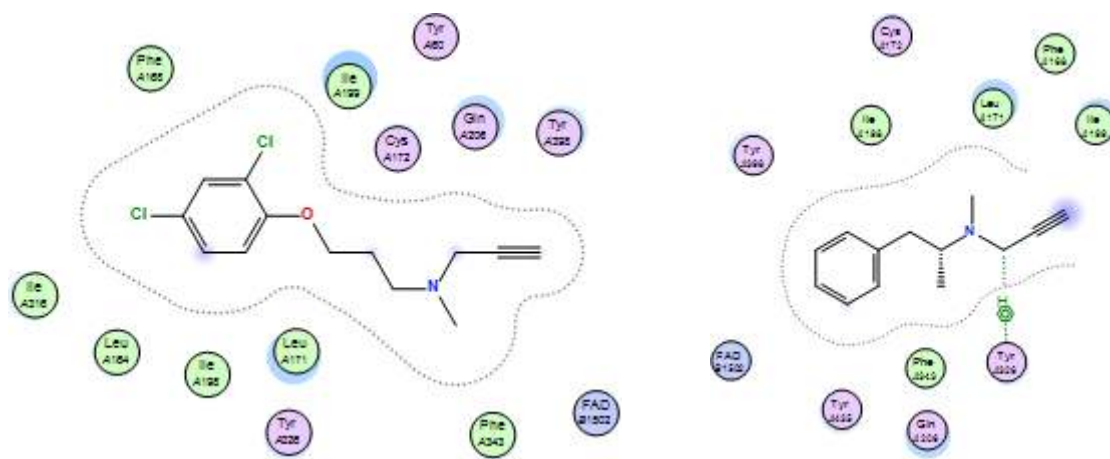
Figure 4.11 presents the ligand interaction diagrams of the lowest S-scores of each of the test compounds and identifies the site of interaction with MAO-B. It can be observed that geniposidic acid (S-value: -7.8824, dissociation constant: $3.6405122867191176 \times 10^{-46}$), apigenin (S-value: -7.5886, dissociation constant: $6.6932605548781764 \times 10^{-44}$), vitexin (S-value: -3.0882, dissociation constant: $1.7458260386156682 \times 10^{-200}$) and EDD (S-value: -2.0241, dissociation constant: $9.043627696812635 \times 10^{-2635}$) interacted with Ile 199, an amino acid known to be responsible for the activity of MAO-B. However, the type of interaction, as well as the S-value of these test compounds, differed. Apigenin showed an arene-hydrogen bond interaction with Ile 199 and Leu 171 with strong binding energy. Vitexin also showed similar interaction to apigenin but with lower binding energy, this could be as a result of its glucoside moiety which is highly hydrophilic and so prevents Van der Waal interaction with MAO-B. Luteolin was observed to sit within the pocket of the active site with proximity to FAD, a position like the known MAO-B inhibitors, clorgiline and rasagiline. Leoleorin C (S-value: -0.4806, dissociation constant: 690.3408589251535) was the only compound seen to have an arene-hydrogen bonding with FAD, but also had the lowest binding energy when compared to the other compounds. Geniposidic acid and EDD were observed to be backbone donors of Ile 199.



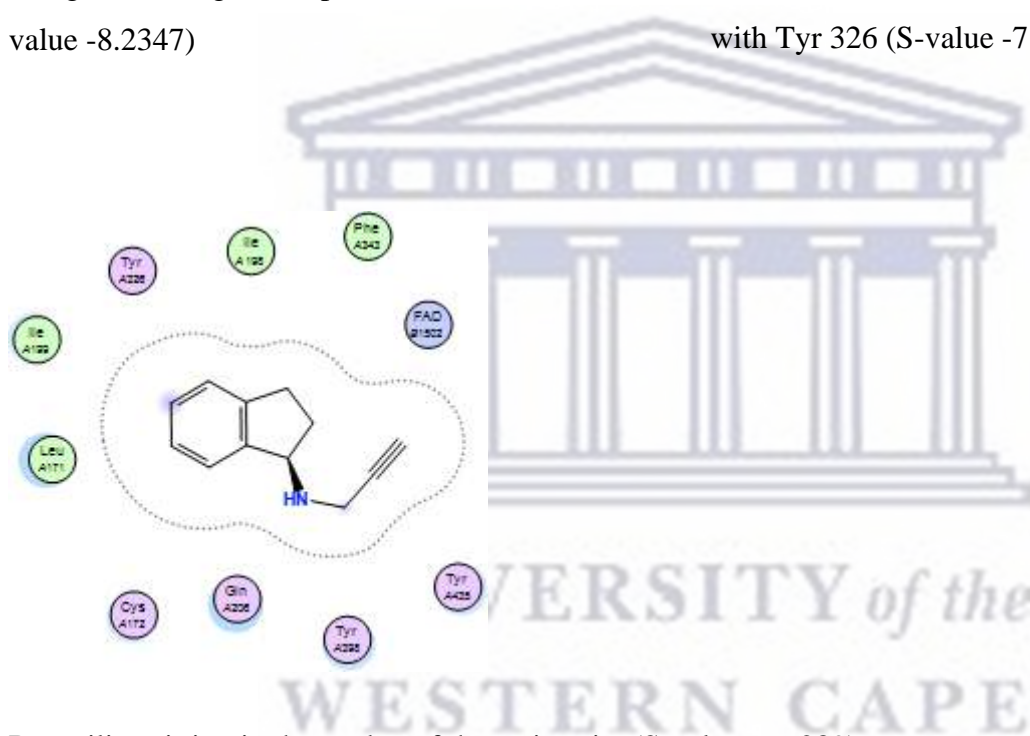
Geniposidic Acid being a backbone done to Ile 199 (S-value -7.8824)



Apigenin having an arene-hydrogen bond with Leu171 and Ile 199 (S-value -7.5886)



Clorgiline sitting in the pocket of the active site (S-value -8.2347) Selegiline having an arene-hydrogen bond with Tyr 326 (S-value -7.1552)



Rasagiline sitting in the pocket of the active site (S-value -6.6289)

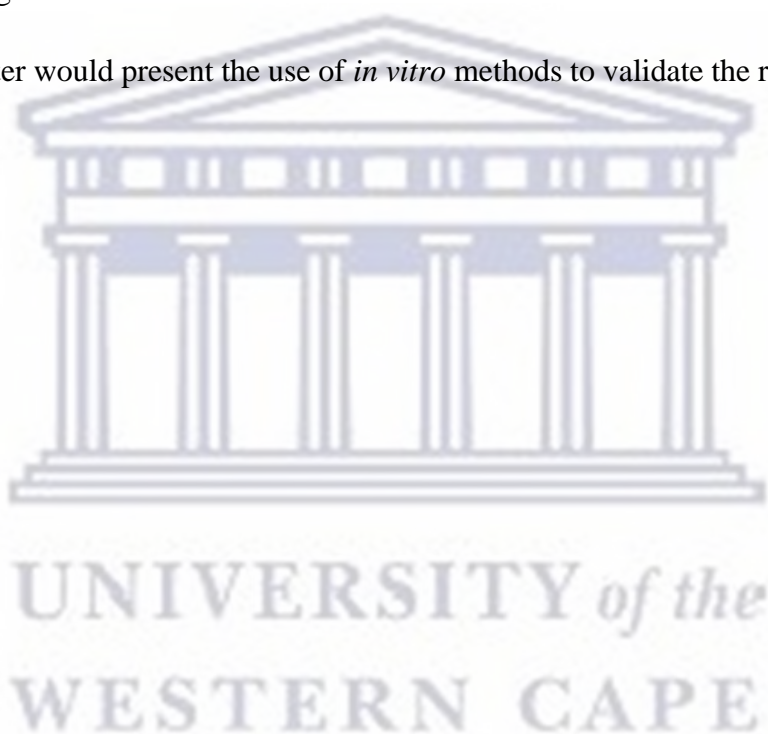
Figure 4.12: Ligand Interaction diagrams of the lowest score of known MAO-B inhibitors

In this chapter, 6 compounds were predicted to influence MAO-B and MAO-A enzyme activity following molecular docking of each of these compounds with the enzymes. However, these interactions or binding were to varying degrees, with apigenin identified as having the highest binding affinity (with 3 arene-hydrogen bonds to two active amino acids and high binding energy). This result was like those reported by Chimenti *et al.* (2010) and Chaurasiya *et al.* (2014) in which

studies it was observed that apigenin and luteolin both have an inhibitory effect on MAO-B (Chimenti et al., 2010; Chaurasiya et al., 2014). Vitexin is known for its neuroprotective activity which has been reported to be through various pathways such as inhibiting butyrylcholinesterase (BChE) and β -site amyloid precursor (BACE1) as well as the amyloid β peptide-induced NO generation in the ganglion neurons (Lima et al., 2018).

This chapter used ligand similarity to predict the targets for apigenin, 6-methoxyluteolin-4-methylether, compound X, acteoside, luteolin, chryseriol, cynaroside, dihydroxyphytyl palmitate, luteolin 7-O- β -glucoside-3-methyl ether, comosiin, EDD, leoleorin C, geniposidic acid and vitexin. Molecular docking results predicted that vitexin would inhibit MAO-B activity, with this protein involved in the pathogenesis of AD.

The succeeding chapter would present the use of *in vitro* methods to validate the results reported in Chapter 4.



Chapter 5

5. IN VITRO ASSAY OF MAO-B INHIBITION

5.1 Introduction

The inhibition of MAO-B has been identified as a way of delaying the progression of AD as the enzyme metabolizes monoamine neurotransmitters in the brain leading to the increased production of hydrogen peroxide and reactive oxygen species (ROS), which in turn, promotes the degeneration of neurons (Borroni et al., 2017). MAO-B inhibitors have also been reported to influence the progression of AD through other mechanisms apart from inhibiting the production of hydrogen peroxide and ROS including blocking the response of N-Methyl-D-aspartate (NMDA) receptors to elevated levels of N-acetylated polyamines; inducing antioxidant enzymes such as superoxide dismutase and catalase; anti-apoptotic activity; and enhancing the neurovascular stimulation of nitric oxide (NO) production and vasodilatation (Thomas, 2000).

The *in silico* studies on *L. leonurus* compounds (see chapter 4) predicted apigenin, EDD, geniposidic acid, leoleorin C, vitexin and luteolin as MAO-B inhibitors, and as such potential drug compounds for the treatment for AD. To confirm the predicted MAO-B inhibition, an *in vitro* MAO-B inhibition assay of vitexin, luteolin, apigenin and geniposidic acid was carried out. Due to the inability to obtain EDD and leoleorin, these compounds were not evaluated for MAO-B inhibition *in vitro*. This chapter presents the methods used in the *in vitro* evaluation of the compounds as well as the results and a discussion.

5.2 Research Question:

1. Do the *in silico* predictions for CNS activity for *L. leonurus* compounds correlate with *in vitro* inhibition of MAO-B?

5.3 Materials and Method

5.3.1 Preparation of test compounds

All chemicals were purchased from Sigma Aldrich Chemicals (Sigma-Aldrich Corp South Africa). Vitexin, luteolin, apigenin and geniposidic acid were dissolved in dimethyl sulfoxide (DMSO) to form 1.6% w/v, 1.5% w/v, 1.4% w/v, and 1% w/v stock concentrations respectively following the

directions of the manufacturers and stored at -20°C until they were ready to be used. Subsequent dilutions of each of the test compounds were made with the assay buffer to concentrations of $5\ \mu\text{M}$, $10\ \mu\text{M}$, $20\ \mu\text{M}$, $30\ \mu\text{M}$ and $40\ \mu\text{M}$. Selegiline (the reference compound, present in the assay kit) was reconstituted using the assay buffer to $5\ \mu\text{M}$, $10\ \mu\text{M}$ and $20\ \mu\text{M}$; $10\ \mu\text{M}$ concentrations as recommended by the manufacturer. Dilutions were freshly prepared on the day of the experiment.

5.3.2 Fluorometric MAO-B inhibition assay

The MAO-B inhibitory effect of the four compounds from *Leonotis leonurus* was determined using a fluorometric method as described by Can, (2018), using Sigma's MAO-B inhibitor screening kit according to the manufacturer's guidelines. The components of the kit included an MAO-B assay buffer, a high sensitivity probe in DMSO, the MAO-B enzyme, the MAO-B substrate (tyramine), a developer and an MAO-B inhibitor (selegiline). Measurements were carried out using a BioTek Synergy Mx Monochromator-based microplate reader with an inbuilt microplate data collection and analysis software (Gen5™) (BioTek Instruments, Inc., USA). The assay is based on the fluorometric detection of H_2O_2 , a by-product generated during the oxidative deamination of tyramine by MAO-B, by a fluorometric method (excitation at $535\ \text{nm}$, emission at $587\ \text{nm}$) over a 40 min period. Selegiline, a known MAO-B inhibitor, was used as a reference. The recombinant MAO-B enzyme was reconstituted with $22\ \mu\text{L}$ of MAO-B assay buffer while the developer was reconstituted with $220\ \mu\text{L}$ of MAO-B assay buffer diluted in the reaction buffer. The resulting solutions were stored at -20°C until they were ready to be used. The substrate (tyramine) was diluted in $110\ \mu\text{L}$ of distilled water and stored at -20°C until the time for use. To prepare an MAO-B working solution, $37\ \mu\text{L}$ assay buffer, $1\ \mu\text{L}$ developer solution, $1\ \mu\text{L}$ substrate solution and $1\ \mu\text{L}$ high sensitivity probe were mixed for each well. The solutions of test inhibitors ($10\ \mu\text{L}/\text{well}$ of $5\ \mu\text{M}$, $10\ \mu\text{M}$, $20\ \mu\text{M}$, $30\ \mu\text{M}$ and $40\ \mu\text{M}$), selegiline ($10\ \mu\text{L}/\text{well}$ of $5\ \mu\text{M}$, $10\ \mu\text{M}$ and $20\ \mu\text{M}$) and recombinant enzyme solution ($50\ \mu\text{L}/\text{well}$) were added to a black flat-bottom 96-well microplate and incubated at 37°C for 10 min. After the incubation period, the reaction was started by adding the MAO-B substrate solution ($40\ \mu\text{L}/\text{well}$), and fluorescence of the final solution was measured kinetically ($\lambda_{\text{ex}} = 535\ \text{nm}/\lambda_{\text{em}} = 587\ \text{nm}$) at 37°C for 40 minutes at 10 min. intervals. Enzyme control (EC) experiments were carried out simultaneously by replacing the inhibitor solution with the assay buffer solution ($10\ \mu\text{L}$). All experiments were done in duplicates.

5.3.3 Data analysis

Fluorescence values obtained from the kinetic enzyme assay measurements were plotted against time, and the slopes obtained using the equation

$$\text{Slope} = \frac{RFU2 - RFU1}{(T2 - T1)}$$

Where: RFU2 = Fluorescence measured at time T₂

RFU1= Fluorescence measured at time T₁

(RFU- relative fluorescence unit)

Percentage inhibition was then calculated using the equation:

$$\% \text{ relative inhibition} = \frac{(\text{Slope of EC}) - (\text{Slope of S})}{(\text{Slope of EC})} \times 100$$

Where: EC= Enzyme control

S= test inhibitors (including reference inhibitor)

Using GraphPad Prism software, a simple linear regression calculation of the recorded fluorescence was done to confirm the slope and the R-squared value of the results. Further to this, a dose-response curve of percentage inhibition versus inhibitor concentration was plotted using Microsoft Office Excel 2016 and the IC₅₀ was determined using the equation:

$$Y = mx + c$$

(Where: m=slope and c= intercept on the y axis) (Can, 2018).

The R-squared value was used to determine the strength of the linear relationship between the rate of fluorescence over time. A value larger than 0.7 indicated a strong relationship between the two variables (Mindrila et al., 2017).

5.4 Results

The enzyme kinetics of MAO-B in the presence of the substrate tyramine and the absence of an inhibitor (either selegiline or the test compounds) is presented in fig. 5.1. An increase in fluorescence readings was observed with time (from 47398 RFU at 0:00 time to 69245 RFU at 40:00 time), indicating an increase in the catalytic activity of MAO-B on tyramine with time.

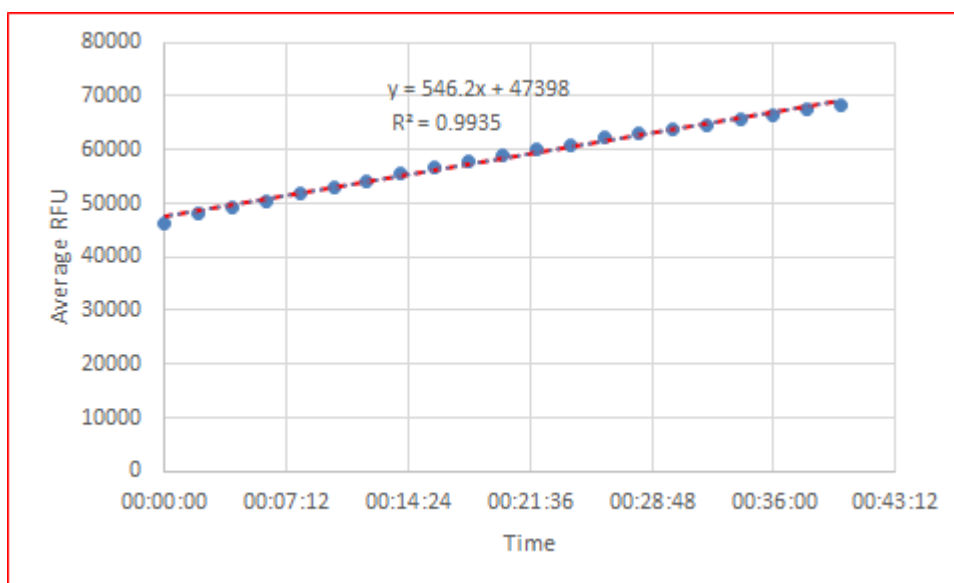


Figure 5.1: Fluorescence produced by MAO-B - catalysed cleavage of tyramine

Incubation of the enzyme and substrate with three different concentrations (5 μ M, 10 μ M, 20 μ M) of the known inhibitor, selegiline resulted in reductions in fluorescence produced when compared to the enzyme control. Reductions in fluorescence were however not concentration-dependent as the greatest reduction was observed with the 10 μ M selegiline concentration, while the least reduction in fluorescence was observed with the 5 μ M selegiline concentration (fig. 5.2). The rate of enzyme activity was however attenuated in a concentration-dependent manner by the inhibitor as the 20 μ M concentration of the inhibitor resulted in the slowest rate while the 5 μ M concentration resulted in the fastest rate of enzyme reaction.

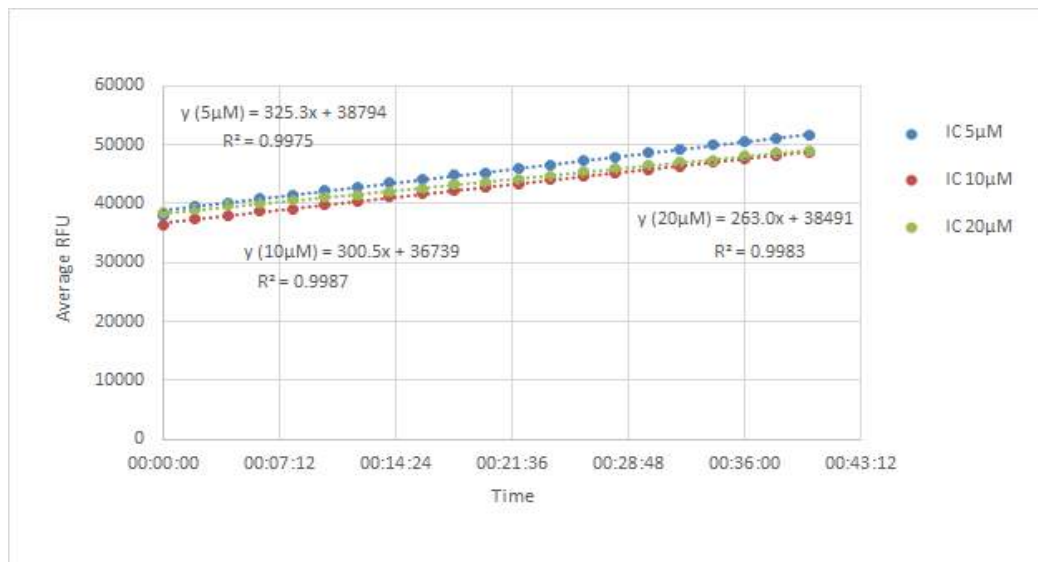


Figure 5.2: Inhibition of fluorescence produced by MAO-B - catalysed cleavage of tyramine, by selegiline (5µM, 10µM, 20µM).

To confirm the activity of selegiline as an inhibitor of MAO-B, a concentration-response curve of the percentage inhibition versus concentration was plotted for inhibitor concentrations 5 µM to 20 µM (figure 5.3). An increase in the % relative inhibition of MAO-B activity with increasing concentrations of selegiline was observed, thus confirming the inhibitory activity of the selegiline used in the study (Robinson, 1985).

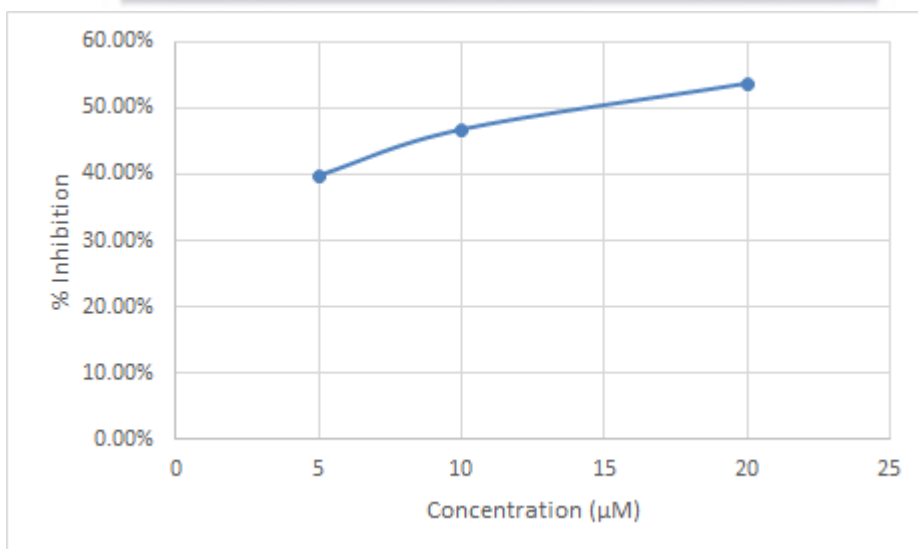


Figure 5.3: Percentage relative inhibition of MAO-B activity by selegiline (5µM, 10µM, 20µM).

Incubation of the enzyme and substrate with five different concentrations (5 μM - 40 μM) of the test compound apigenin resulted in reductions in the fluorescence produced when compared to the enzyme control (fig. 5.4). Reductions in fluorescence were however not concentration-dependent as the greatest reduction was observed with the 5 μM apigenin concentration, while the least reduction in fluorescence was observed with the 10 μM apigenin concentration (fig. 5.4). The rate of enzyme activity was not attenuated in a dose-dependent manner by the inhibitor as the 5 μM concentration of the inhibitor was the only concentration producing a reduction in the rate of enzyme activity ($R^2=0.9919$). None of the other concentrations produced a reduction in the rate of enzyme activity.

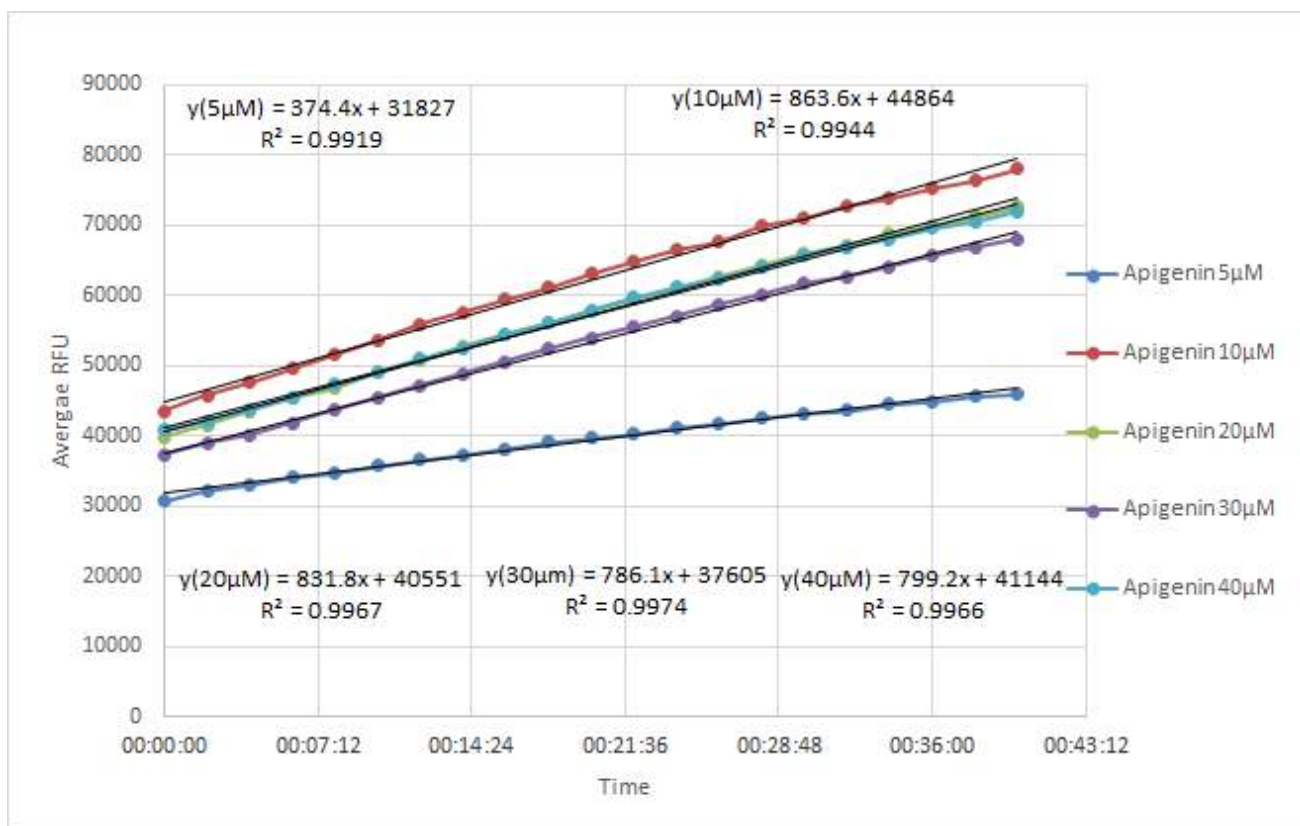


Figure 5.4: Inhibition of fluorescence produced by MAO-B - catalysed cleavage of tyramine, by apigenin (5 μM , 10 μM , 20 μM , 30 μM and 40 μM).

The 5 μM dose of apigenin produced the maximum inhibition of MAO-B enzyme activity with a 30% relative inhibition of enzyme activity (Fig 5.5). None of the other concentrations of apigenin produced a relative inhibition of enzyme activity, with both the 10 μM and 40 μM concentrations producing relative increases (56% and 31% respectively) in enzyme activity.

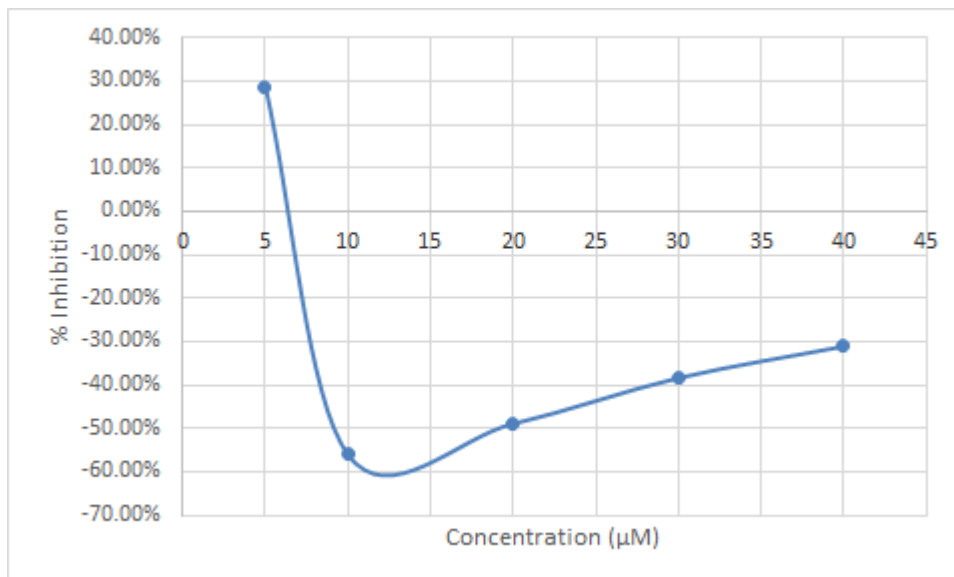


Figure 5.5: Percentage relative inhibition of MAO-B activity by apigenin (5μM, 10μM, 20μM, 30μM and 40μM).

Incubation of the enzyme and substrate with five different concentrations (5 μM - 40 μM) of vitexin resulted in reductions in the fluorescence produced when compared to the enzyme control (fig. 5.6). Reductions in fluorescence were also not concentration-dependent as the greatest reduction was observed with the 30 μM vitexin concentration, while the least reduction in fluorescence was observed with the 5 μM vitexin concentration (fig. 5.6). The rate of enzyme activity was not attenuated in a concentration-dependent manner by the inhibitor as the 30 μM concentration of the inhibitor resulted in the smallest rate of enzyme reaction ($R^2= 0.7957$), indicating the greatest enzyme inhibition. The least inhibitory effect on enzyme activity was recorded with the 5 μM concentration, with the highest rate of enzyme activity ($R^2=0.9679$).

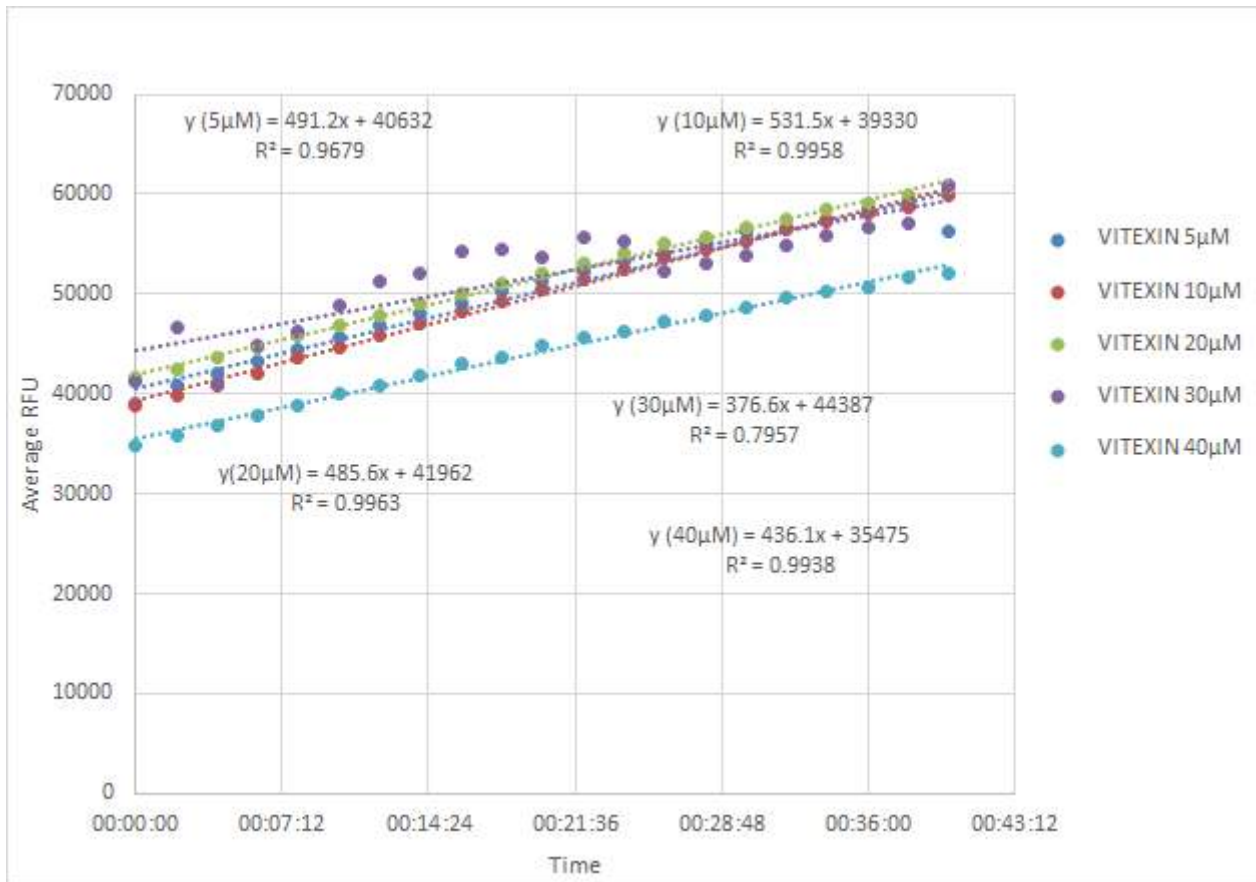


Figure 5.6: Inhibition of fluorescence produced by MAO-B - catalysed cleavage of tyramine, by vitexin (5μM, 10μM, 20μM, 30μM and 40μM).

The 30 μM concentration of vitexin produced the maximum inhibition of MAO-B enzyme activity with a 27% inhibition of enzyme activity relative to the control (Fig 5.7). This was followed by the 40 μM concentration of vitexin (22%), the 20 μM concentration of vitexin (14%), the 10 μM concentration of vitexin (6.4%) and then the 5 μM concentration of vitexin (2.7%).

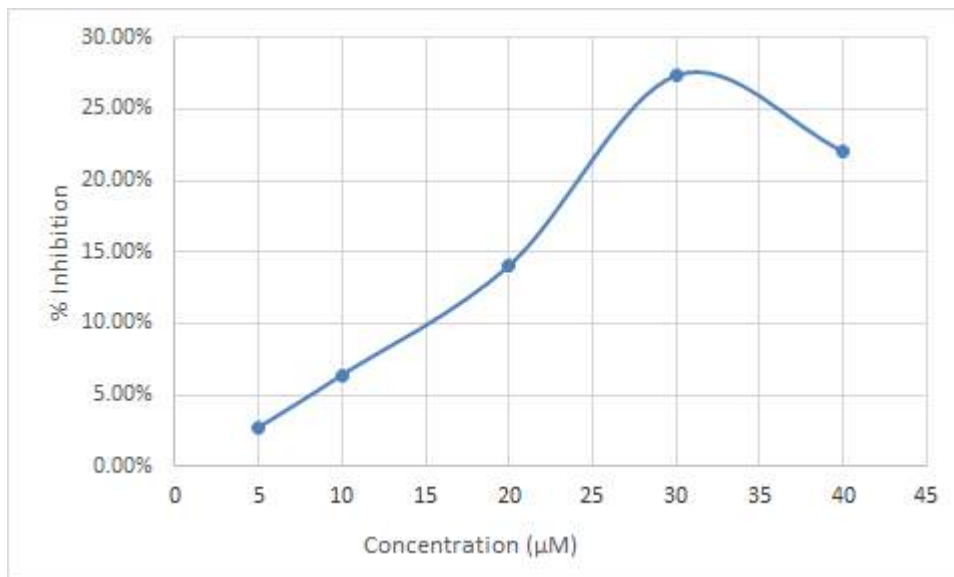


Figure 5.7: Percentage relative inhibition of MAO-B activity by vitexin (5μM, 10μM, 20μM, 30μM and 40μM).

Incubation of the enzyme and substrate with five different concentrations (5 μM - 40 μM) of the test compound luteolin resulted in reductions in the fluorescence produced when compared to the enzyme control (fig. 5.8). Reductions in fluorescence were however not concentration-dependent as the greatest reduction was observed with the 5 μM luteolin concentration, while the least reduction in fluorescence was observed with the 40 μM luteolin concentration (fig. 5.8). The rate of enzyme activity was not attenuated in a concentration-dependent manner by the inhibitor as the 5 μM concentration of the inhibitor resulted in the greatest reduction to enzyme activity ($R^2= 0.9848$), indicating the greatest enzyme inhibition. The least inhibitory effect on enzyme activity was recorded with the 10 μM concentration, with the highest rate of enzyme activity ($R^2= 0.9959$).

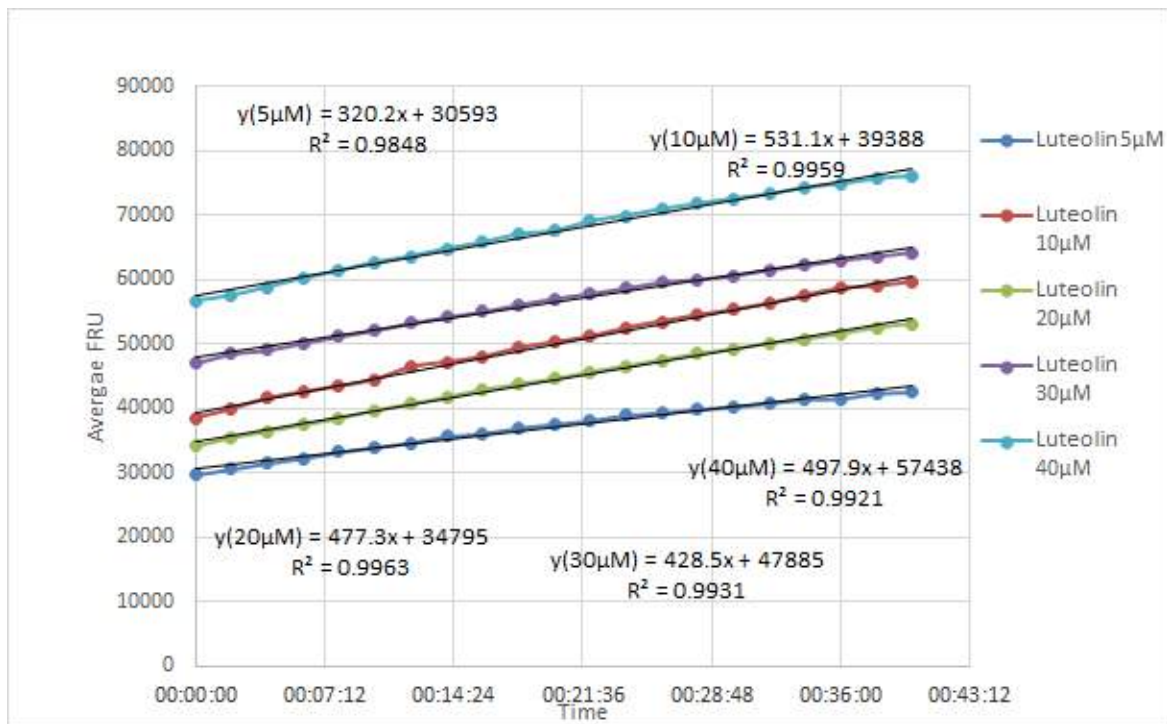


Figure 5.8: Inhibition of fluorescence produced by MAO-B - catalysed cleavage of tyramine, by luteolin (5µM, 10µM, 20µM, 30µM and 40µM).

The 5 µM dose of luteolin produced the maximum inhibition of MAO-B enzyme activity with a 40% relative inhibition of enzyme activity (Fig 5.9). This was followed by the 30 µM dose of luteolin (23%), the 20 µM dose of luteolin (14%), the 40 µM dose of luteolin (9.8%) and then the 10 µM dose of luteolin (4.7%).

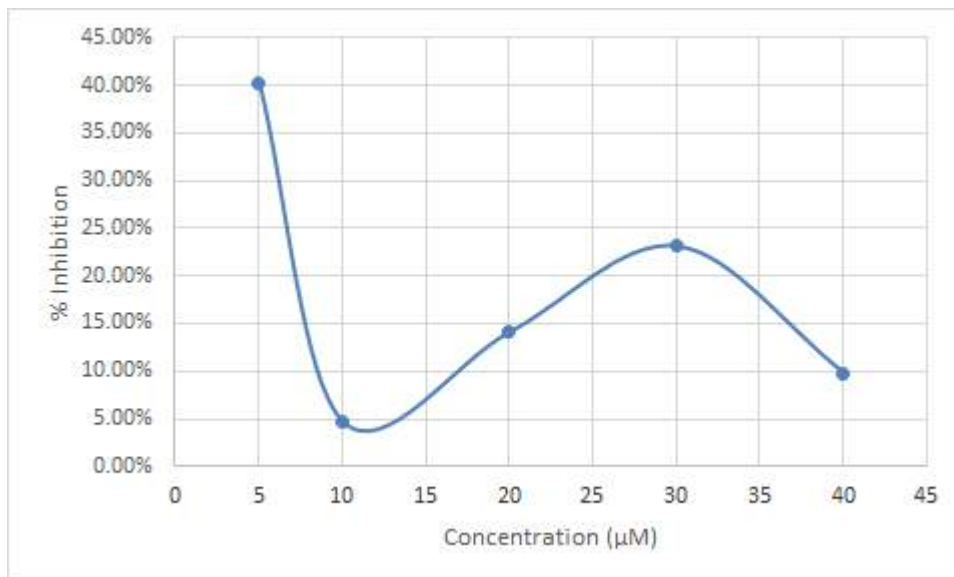


Figure 5.9: Percentage relative inhibition of MAO-B activity by luteolin (5μM, 10μM, 20μM, 30μM and 40μM).

Incubation of the enzyme and substrate with five different concentrations (5 μM - 40 μM) of the test compound geniposidic acid resulted in a slight reduction in the fluorescence produced when compared to the enzyme control (fig. 5.10). Reductions in fluorescence were however not concentration-dependent as the greatest reduction was observed with the 40 μM geniposidic acid concentration, while the least reduction in fluorescence was observed with the 5 μM geniposidic acid concentration (fig. 5.10). The rate of enzyme activity was not attenuated in a concentration-dependent manner by the inhibitor as the 20 μM concentration of the inhibitor resulted in the smallest rate of enzyme reaction ($R^2= 0.9943$), indicating the greatest enzyme inhibition. The least inhibitory effect on enzyme activity was recorded with the 5 μM concentration, with the highest rate of enzyme activity ($R^2= 0.99$).

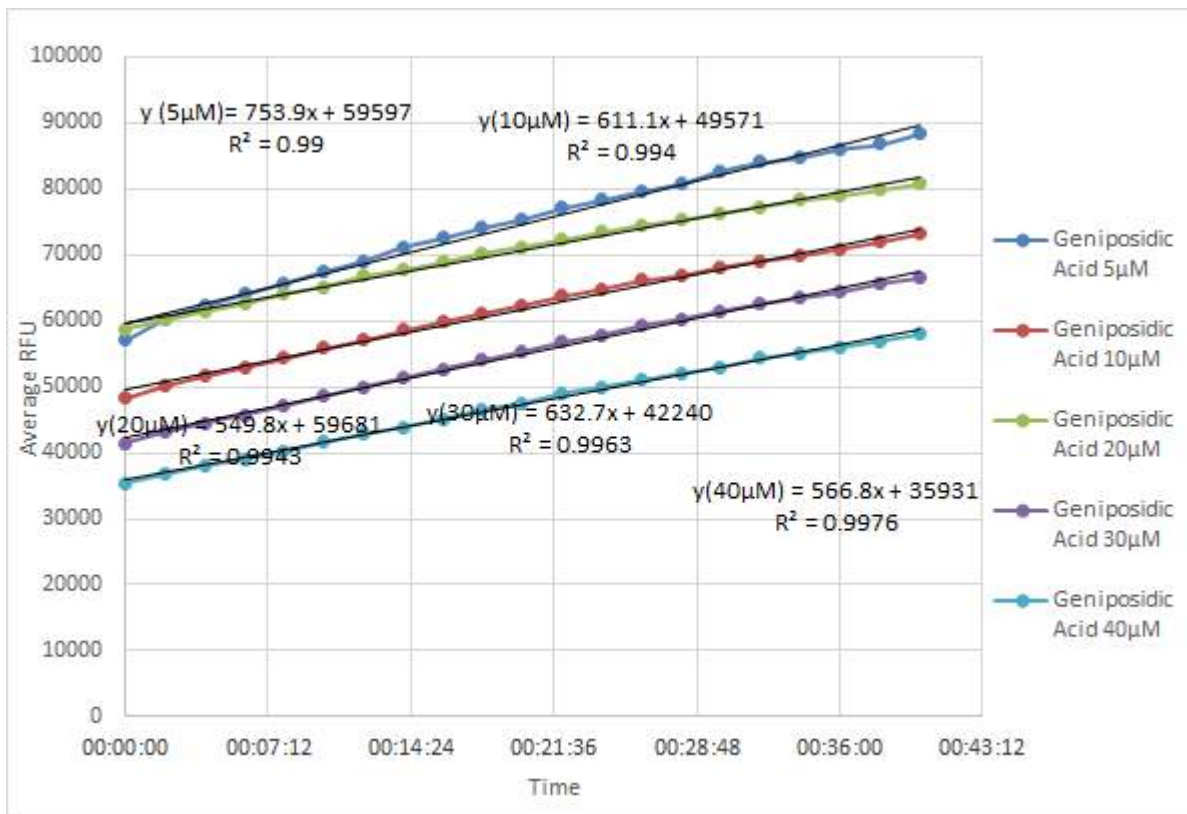


Figure 5.10: Inhibition of fluorescence produced by MAO-B - catalysed cleavage of tyramine, by geniposidic acid (5μM, 10μM, 20μM, 30μM and 40μM).

The 40 μM dose of geniposidic acid produced the maximum inhibition of MAO-B enzyme activity with a 0.7% relative inhibition of enzyme activity (Fig 5.11). This was followed by the 20 μM dose (0.5%). None of the other concentrations of geniposidic acid produced an inhibition of the enzyme activity, with the 5 μM dose producing the greatest (46.17%) increase, while the 10 μM and 30 μM produced smaller increases (12.84% and 14.23% respectively) in enzyme activity.

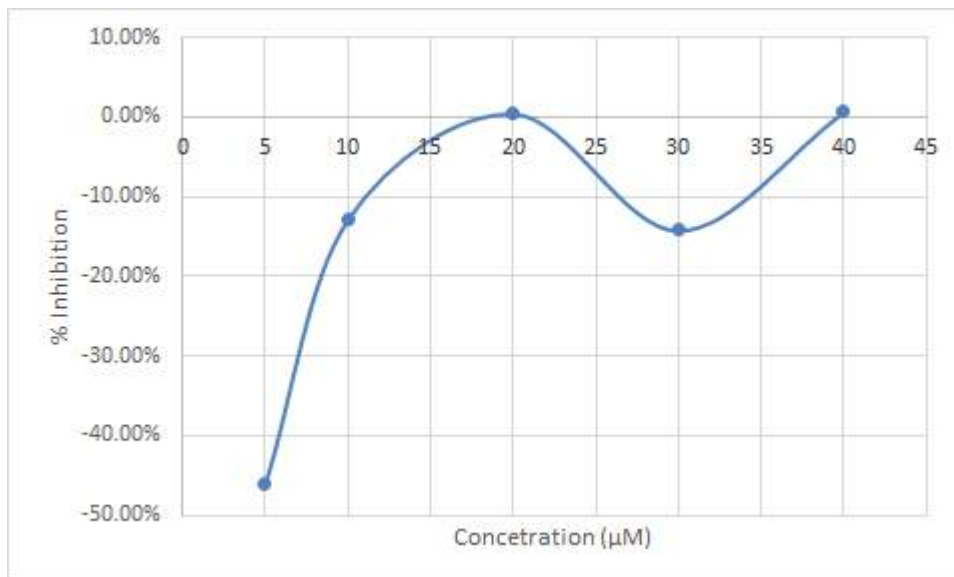


Figure 5.11: Percentage relative inhibition of MAO-B activity by geniposidic acid (5μM, 10μM, 20μM, 30μM and 40μM).

The results presented in this chapter show that luteolin, apigenin and vitexin inhibited MAO-B but in varying degrees. The % inhibition was not dependent on the increase in concentration for luteolin and apigenin. The highest percentage inhibition was observed with the lowest concentration of these two compounds. Vitexin, however, showed an increase in percentage inhibition as the concentrations increased up until 40μM at which point the percentage inhibition decreased. Geniposidic acid showed no inhibition of MAOB by any of the concentrations administered. These observations buttress those seen in the preceding chapter on molecular docking, where luteolin, apigenin and vitexin were observed to interact with the active site of MAO-B. The preceding chapter, however, indicated that apigenin and luteolin had a stronger binding affinity for MAO-B than vitexin (based on their binding energy) which were comparable with known MAO-B inhibitors. Geniposidic acid, on the other hand, was observed to interact with the active site of MAO-B with a binding energy score comparable to known inhibitors on the MOE but it did not inhibit MAO-B in *in vitro* studies.

The next chapter would discuss the findings of this study collectively and highlight the new knowledge obtained from this study.

Chapter 6

6. DISCUSSION AND CONCLUSION

6.1 Discussion

Natural products are a great source of hit/lead compounds in drug development research (Balunas and Kinghorn, 2005). This study identified and characterized CNS active compounds present in *Leonotis leonurus*, a traditional medicinal plant with a long history of ethnobotanical use for the treatment of epilepsy, partial paralysis, hypertension, and diabetes amongst others (Van Wyk and Gericke, 2000; Van Wyk et al., 2000; Wu et al., 2013; Narukawa et al., 2015; Nsuala et al., 2015). Based on the ethnobotanical use of *Leonotis leonurus* for CNS related diseases, this study utilized *in silico* and *in vitro* methods to identify and characterize promising drug-like bioactive compounds from the plant with potential CNS activity as MAO-B inhibitors, for the treatment of AD. The specific objectives pursued, the major findings, implications of such findings and related studies that validate the findings are presented in the following discussion.

The review of literature on compounds isolated from *Leonotis leonurus* identified 36 compounds from 8 phytochemical classes, supporting the previously reported findings that *Leonotis leonurus* contains a wide variety of phytochemicals (Mazimba, 2015; Nsuala et al., 2015). The presence of these phytochemicals, which interact with various macromolecules in the human proteome, would account for the wide range of bioactivity reported with the extracts of this plant. For example, vitexin reported to be present in the methanol extract of the flowering aerial parts of the plant, exhibits a wide variety of biological activity including antioxidation, anti-inflammation, anti-cancer, neuro-protection, antidiabetic, cardio-protection, and hepatoprotection (Peng et al., 2021; Wu et al., 2021).

The treatment of CNS-related diseases comes with the challenge of discovering drugs that are not just effective against an identified disease target, but which also have the pharmacokinetic properties favourable to crossing the BBB to reach the identified disease target. These compounds need to have certain physicochemical characteristics to be ideal CNS drug candidates as the presence of favourable interactions between a drug and an identified protein target does not guarantee its suitability as a drug (Xu and Hagler, 2002; Macalino et al., 2015). For this reason, ADMET profiling of drug candidates is a necessary part of the drug development process (Attique

et al., 2019). It informs the drug-likeness profile of these candidates and helps to identify those with good drug-likeness profile, a necessity for an ideal drug (Schneider, 2013; Ntie-Kang et al., 2018; Faccenda et al., 2019; Le, 2020). This study created a scoring matrix to easily identify phytochemicals that are ideal CNS drug candidates based on whether they had: Good oral bioavailability; crossed the BBB; were not effluxed by P-gp transporter; were not toxic and had limited chances of drug interactions via the inhibition of metabolic enzymes. Of the 36 compounds identified as having been isolated from *L. leonurus*, seven labdane diterpenes (13R-premarrubin, 13S-premarrubin, compound X, EDD, leoleorin B, leoleorin C and leonurun) were predicted as ideal compounds to target diseases in the CNS. The similarity principle states that structurally similar molecules tend to have similar properties and exert similar biological activities (Elango Ekaney et al., 2021). This would explain the observation that all seven compounds identified as ideal CNS drug candidates were structurally similar labdane diterpenes. Of these compounds, Leoleorin C has been reported with a moderate binding affinity for the sigma 1 receptor, a known receptor involved in the pathogenesis of addictions, pain, and amnesia. depression, schizophrenia, and AD (Maurice and Su 2009; H. Wu et al. 2013). As this study identified this compound to have favourable pharmacokinetic properties for the CNS, it is an ideal drug for further development for the treatment of these CNS conditions.

With the identification of *Leonotis leonurus* compounds with the physicochemical properties conducive to penetrating the CNS, it was important to determine which of the 36 compounds from the plant could alter the pathophysiology of AD, a neurodegenerative disease characterized by a significant loss of cognitive function. This was determined in this study by evaluating all compounds as inhibitors of monoamine oxidase B (MAO-B) enzyme, one of the known disease targets for AD (Borroni et al., 2017). The target prediction study indicated that 5 out of the 36 compounds had a high probability of targeting MAO-B, while 2 compounds were predicted to target MAO-A. Due to the difficulty in obtaining a standardized MAO-B protein for molecular docking purposes, all 6 compounds targeting either MAO-B or MAO-A or both were docked on the MAO-B (2vrl) protein which was readily available. Three of the compounds (geniposidic acid, apigenin and luteolin) had binding energies that were higher than those of the standard inhibitors, which could imply that these compounds would have greater MAO-B enzyme inhibitory effects than the standard inhibitors (Shrivaram and Shrikant, 2016). However, prior knowledge of the binding site of an enzyme is important in identifying inhibitors and their biological impact (Blat, 2010). It has been identified from previous studies that the active site of MAO-B is formed by a 420 Å³-hydrophobic

substrate cavity interconnected to an entrance cavity of 290 Å³. This cavity has amino acid residues which act as gatekeepers as well as interaction points including Tyr326, Ile199, Leu171 and Phe198. Tyr326 and Ile99 are known as structural determinant for substrates and inhibitors, when small inhibitors are bound within the substrate cavity, Ile 199 rotates into a closed conformation to create the bipartite active site (which is characteristic of MAO-B), whereas, when large inhibitors are bound to the substrate cavity, Ile 199 forms an open conformation (Milczek et al., 2011). This flexibility of Ile99 to conform to the structure and size of an inhibitor allows for the development of possible inhibitors to be more versatile. In addition to this cavity, MAO-B is also linked non-covalently to FAD (an active cofactor which is involved in several catalytic reactions) by two residues: Lys296 and Try388 (Binda et al., 2002; Geha et al., 2002; Milczek et al., 2011). It is therefore important for a substrate to interact with any of these amino acid residues in the active site or the cofactor FAD for the enzyme catalytic reaction to take place (Bugg, 2004). In this study geniposidic acid interacted with one of the amino acids (Ile199), apigenin interacted with two (Ile199, Leu171), while luteolin did not interact with any of the ‘gatekeeping’ amino acids, but it was observed to be in close proximity to the cofactor FAD. For a compound to exhibit activity like the known inhibitor compounds, it is expected to exhibit binding affinity like these compounds and interact with the identified important gatekeepers. Although geniposidic acid, apigenin and luteolin had greater binding affinity for the MAO-B enzyme than the standard inhibitors, none of them interacted with the gatekeeping amino acids in a way like the known inhibitors used in this study. It is however also interesting to note that the standard inhibitors rasagiline and clorgyline had no interactions with the gatekeeping amino acid residues at the active site and had lower binding affinity than the test compounds. This suggests that interactions with the gatekeeping amino acid residues were not necessary for enzyme inhibition as previously reported. This also makes it more difficult to predict enzyme inhibition from *in silico* studies using interactions with gatekeeping amino acids as it is obvious some inhibitors exert their effect without requiring these interactions. Based on interactions with amino acid residues geniposidic acid and apigenin were expected to exhibit MAO-B inhibition, while based on binding energy geniposidic acid, apigenin and luteolin were expected to exhibit MAO-B inhibition in the *in vitro* studies. In the *in vitro* studies however apigenin and luteolin showed weak inhibition of MAO-B, while geniposidic acid showed no form of inhibition of MAO-B. This is like other *in vitro* studies that have either reported no (Carradori et al. 2014; Chaurasiya et al. 2014), or weak (Y. N. Han, Noh, and Han 1987; X. H. Han et al. 2007; Chimenti et al. 2010) inhibition of MAO-B by apigenin and luteolin. This suggests that although these compounds exhibit a high binding affinity for the enzyme, the interactions were not

necessarily with the amino acid residues required for an inhibitory effect. As these compounds did not interact with the identified gatekeepers of the active pocket of the enzyme, it suggests that the gatekeepers are essential for inhibitory activity like selegiline, but that other interactions could also result in inhibition as observed with rasagiline and clorgyline. This would have to be interrogated in future studies.

Three compounds had some interactions with either the gatekeeper amino acids or FAD (EDD with Ile199, leoleorin C with FAD, and vitexin with Ile199 & Leu171), but all had binding affinities slightly lower than selegiline, rasagiline and clorgyline. This would suggest that these compounds could have some inhibitory activity although expected to be less than that of the standard inhibitors. Vitexin interacted with the same amino acids as apigenin but had a lower binding affinity for the active site. This could possibly be due to the presence of a glycoside moiety on the carbon-8 of vitexin, which is a C-glycoside of apigenin. It has been observed in other studies that the presence of glycoside moieties in flavonoids generates steric hindrance at the binding pockets of target proteins and increase the polarity of flavonoids which in effect reduces the ability of these compounds to penetrate to the target site, and ultimately weakens their binding affinity (Tronina et al., 2017). Interestingly, vitexin was the only compound to show significant inhibitory activity against MAO-B. This may suggest that the steric hindrance caused by the presence of the glycoside moiety in vitexin may have played a role in stabilizing the protein-ligand complex in such a way that the enzyme substrate could not displace vitexin from the active site (Iversen et al., 2001; Cornelius et al., 2013). EDD and leoleorin C could not be sourced for the *in vitro* study so it would be difficult to fully conclude that the binding affinity or pose of the compounds gives a definite prediction on the activity of the compounds. It is important to note that although molecular docking studies predict the possibility of 'hit' identification, various docking methods including the one used in this study have been simplified to make the docking process affordable (Ramírez and Caballero, 2016; Pantsar and Poso, 2018). These simplifications include handling the ligand as fully flexible but making the protein rigid (proteins are flexible and always in motion), neglecting the presence and effect of water molecules at the target site, and finally the lack of estimating detailed protein affinity and polarization effects of the ligand (Ramírez and Caballero, 2016; Pantsar and Poso, 2018). These simplifications may then fail to fully replicate actual protein - ligand interactions and may explain why some *in silico* predictions do not tally with the *in vitro* or *in vivo* observations.

6.2 Conclusion

The overall aim of this study was to utilize *in silico* and *in vitro* methods in identifying and characterizing promising drug-like bioactive compounds from *Leonotis leonurus* with potential CNS activity as MAO-B inhibitors, for the treatment of AD. This study has been able to achieve that aim by identifying seven ideal CNS drug candidates and one possible MAO-B inhibitor, vitexin. However, vitexin was identified as not having favourable CNS pharmacokinetics; this can be rectified via optimization of the compound. Quite recently, two highly soluble vitexin derivatives were synthesized via glycosylation (Wu et al., 2021). It would be interesting to see if these two compounds would have similar MAO-B inhibitory activities as vitexin thus presenting an opportunity for further studies.

6.3 Limitation of this study

The study could not evaluate the compounds for inhibition of MAPT as the crystalline protein structure could not be identified for molecular docking studies. Another limitation of this study was that EDD and leoleonin C were not evaluated for enzyme inhibition in the *in vitro* assay as these compounds could not be sourced.

6.4 Recommendations

To evaluate the activity of the compounds predicted to act on MAPT. Further studies should be carried out on optimizing the drug-likeness of vitexin without negatively impacting on its MAO-B inhibition. To evaluate the efficacy of vitexin in an *in vivo* model of AD.

REFERENCES

- Agamah, F.E., Mazandu, G.K., Hassan, R., Bope, C.D., Thomford, N.E., Ghansah, A., Chimusa, E.R., 2020. Computational/in silico methods in drug target and lead prediction. *Brief. Bioinform.* 21, 1663–1675. <https://doi.org/10.1093/bib/bbz103>
- Agnihotri, V.K., ElSohly, H.N., Smillie, T.J., Khan, I.A., Walker, L.A., 2009. Constituents of *Leonotis leonurus* flowering tops. *Phytochem. Lett.* 2, 103–105. <https://doi.org/10.1016/j.phytol.2009.02.001>
- Ajay, Walters, W.P., Murcko, M.A., 1998. Can We Learn to Distinguish between “Drug-like” and “Nondrug-like” Molecules? *J. Med. Chem.* 41, 3314–3324. <https://doi.org/10.1021/jm970666c>
- Alavijeh, M.S., Chishty, M., Qaiser, M.Z., Palmer, A.M., 2005. Drug metabolism and pharmacokinetics, the blood-brain barrier, and central nervous system drug discovery. *NeuroRX* 2, 554–571. <https://doi.org/10.1602/neurorx.2.4.554>
- Allen, M., Kachadorian, M., Quicksall, Z., Zou, F., Chai, H.S., Younkin, C., Crook, J.E., Pankratz, V.S., Carrasquillo, M.M., Krishnan, S., Nguyen, T., Ma, L., Malphrus, K., Lincoln, S., Bisceglia, G., Kolbert, C.P., Jen, J., Mukherjee, S., Kauwe, J.K., Crane, P.K., Haines, J.L., Mayeux, R., Pericak-Vance, M.A., Farrer, L.A., Schellenberg, G.D., Parisi, J.E., Petersen, R.C., Graff-Radford, N.R., Dickson, D.W., Younkin, S.G., Ertekin-Taner, N., Alzheimer’s disease Genetics Consortium (ADGC), 2014. Association of MAPT haplotypes with Alzheimer’s disease risk and MAPT brain gene expression levels. *Alzheimer’s Res. Ther.* 6, 39. <https://doi.org/10.1186/alzrt268>
- Alzheimer’s disease International, 2015. World Alzheimer Report - The Global Impact of Dementia. An analysis of Prevalence, Incidence, Cost and Trends.
- Aparoy, P., Kumar Reddy, K., Reddanna, P., 2012. Structure and Ligand Based Drug Design Strategies in the Development of Novel 5-LOX Inhibitors. *Curr. Med. Chem.* 19, 3763–3778. <https://doi.org/10.2174/092986712801661112>
- Ashraf, M.A., Nookala, V., 2020. Biochemistry, Platelet Activating Factor, StatPearls [Internet]. StatPearls Publishing.
- Attique, S.A., Hassan, M., Usman, M., Atif, R.M., Mahboob, S., Al-Ghanim, K.A., Bilal, M., Nawaz, M.Z., 2019. A Molecular Docking Approach to Evaluate the Pharmacological Properties of Natural and Synthetic Treatment Candidates for Use against Hypertension. *Int. J. Environ. Res. Public Health* 16. <https://doi.org/10.3390/ijerph16060923>
- Baldi, A., 2010. Computational approaches for drug design and discovery: An overview. *Syst. Rev. Pharm.* 1, 99. <https://doi.org/10.4103/0975-8453.59519>
- Balunas, M.J., Kinghorn, A.D., 2005. Drug discovery from medicinal plants. *Life Sci., Natureceuticals (Natural Products), Herbal Botanicals, and Psychoactive: Drug Discovery and Drug-Drug Interactions* 78, 431–441. <https://doi.org/10.1016/j.lfs.2005.09.012>
- Banks, W.A., 2009. Characteristics of compounds that cross the blood-brain barrier. *BMC Neurol.* 9, S3. <https://doi.org/10.1186/1471-2377-9-S1-S3>
- Baravalle, R., Di Nardo, G., Bandino, A., Barone, I., Catalano, S., Andò, S., Gilardi, G., 2017. Impact of R264C and R264H polymorphisms in human aromatase function. *J. Steroid Biochem. Mol. Biol.* 167, 23–32. <https://doi.org/10.1016/j.jsbmb.2016.09.022>
- Begam, B.F., Kumar, J.S., 2012. A Study on Cheminformatics and its Applications on Modern Drug Discovery. *Procedia Eng., International Conference on Modelling Optimization and Computing* 38, 1264–1275. <https://doi.org/10.1016/j.proeng.2012.06.156>

- Behnam, M., Ghorbani, F., Shin, J.-H., Kim, D.-S., Jang, H., Nouri, N., Sedghi, M., Salehi, M., Ansari, B., Basiri, K., 2015. Homozygous MAPT R406W mutation causing FTDP phenotype: A unique instance of a unique mutation. *Gene* 570, 150–152. <https://doi.org/10.1016/j.gene.2015.06.033>
- Bhalerao, S.A., Verma, D.R., D'souza, R.L., Teli, N.C., 2013. Chemoinformatics: The application of informatics methods to solve chemical problems. *Res. J. Pharm. Biol. Chem. Sci.* 4, 25.
- Bienvenu, E., Amabeoku, G.J., Eagles, P.K., Scott, G., Springfield, E.P., 2002. Anticonvulsant activity of aqueous extract of *Leonotis leonurus*. *Phytomedicine* 9, 217–223.
- Binda, C., Newton-Vinson, P., Hubálek, F., Edmondson, D.E., Mattevi, A., 2002. Structure of human monoamine oxidase B, a drug target for the treatment of neurological disorders. *Nat. Struct. Biol.* 9, 22–26. <https://doi.org/10.1038/nsb732>
- Blat, Y., 2010. Non-Competitive Inhibition by Active Site Binders. *Chemical Biology & Drug Design* 75, 535–540. <https://doi.org/10.1111/j.1747-0285.2010.00972.x>
- Borroni, E., Bohrmann, B., Grueninger, F., Prinssen, E., Nave, S., Loetscher, H., Chinta, S.J., Rajagopalan, S., Rane, A., Siddiqui, A., Ellenbroek, B., Messer, J., Pähler, A., Andersen, J.K., Wyler, R., Cesura, A.M., 2017. Sembragiline: A Novel, Selective Monoamine Oxidase Type B Inhibitor for the Treatment of Alzheimer's disease. *J. Pharmacol. Exp. Ther.* 362, 413–423. <https://doi.org/10.1124/jpet.117.241653>
- Braga, R.C., Andrade, C.H., 2012. QSAR and QM/MM Approaches Applied to Drug Metabolism Prediction. *Mini-Rev. Med. Chem.* 12, 573–582.
- Bugg, T., 2004. *Introduction to enzyme and coenzyme chemistry*, 2nd ed. ed. Blackwell Pub, Oxford, UK; Malden, MA, USA.
- Butte, A.J., Ito, S., 2012. Translational Bioinformatics: Data-driven Drug Discovery and Development. *Clin. Pharmacol. Ther.* 91, 949–952. <https://doi.org/10.1038/clpt.2012.55>
- Byrne, R., Schneider, G., 2019. In Silico Target Prediction for Small Molecules, in: Ziegler, S., Waldmann, H. (Eds.), *Systems Chemical Biology, Methods in Molecular Biology*. Springer New York, New York, NY, pp. 273–309. https://doi.org/10.1007/978-1-4939-8891-4_16
- Caban, A., Pisarczyk, K., Kopacz, K., Kapuśniak, A., Toumi, M., Rémuzat, C., Kornfeld, A., 2017. Filling the gap in CNS drug development: evaluation of the role of drug repurposing. *J. Mark. Access Health Policy* 5. <https://doi.org/10.1080/20016689.2017.1299833>
- Can, N.Ö., 2018. Investigation of monoamine oxidase inhibitory activities of new chalcone derivatives (Yeni şalkon türevlerinin monoamin oksidaz enzim inhibitör aktivitelerinin araştırılması). *Cukurova Med. J.* 43, 371–380. <https://doi.org/10.17826/cumj.341883>
- Can, Ö.D., Demir Özkay, Ü., Üçel, U.İ., 2013. Anti-depressant-like effect of vitexin in BALB/c mice and evidence for the involvement of monoaminergic mechanisms. *Eur. J. Pharmacol.* 699, 250–257. <https://doi.org/10.1016/j.ejphar.2012.10.017>
- Carpenter, T.S., Kirshner, D.A., Lau, E.Y., Wong, S.E., Nilmeier, J.P., Lightstone, F.C., 2014. A Method to Predict Blood-Brain Barrier Permeability of Drug-Like Compounds Using Molecular Dynamics Simulations. *Biophys. J.* 107, 630–641. <https://doi.org/10.1016/j.bpj.2014.06.024>
- Carradori, S., D'Ascenzio, M., Chimenti, P., Secci, D., Bolasco, A., 2014. Selective MAO-B inhibitors: a lesson from natural products. *Mol. Divers.* 18, 219–243. <https://doi.org/10.1007/s11030-013-9490-6>
- Carvey, P.M., Hendey, B., Monahan, A.J., 2009. The Blood Brain Barrier in Neurodegenerative Disease: A Rhetorical Perspective. *J. Neurochem.* 111, 291–314. <https://doi.org/10.1111/j.1471-4159.2009.06319.x>

- Chaurasiya, N.D., Ibrahim, M.A., Muhammad, I., Walker, L.A., Tekwani, B.L., 2014. Monoamine Oxidase Inhibitory Constituents of Propolis: Kinetics and Mechanism of Inhibition of Recombinant Human MAO-A and MAO-B. *Molecules* 19, 18936–18952. <https://doi.org/10.3390/molecules191118936>
- Cheng, X., Zhang, L., Lian, Y.-J., 2015. Molecular Targets in Alzheimer's disease : From Pathogenesis to Therapeutics [WWW Document]. *BioMed Res. Int.* <https://doi.org/10.1155/2015/760758>
- Chimenti, F., Fioravanti, R., Bolasco, A., Chimenti, P., Secci, D., Rossi, F., Yáñez, M., Orallo, F., Ortuso, F., Alcaro, S., Cirilli, R., Ferretti, R., Sanna, M.L., 2010. A new series of flavones, thioflavones, and flavanones as selective monoamine oxidase-B inhibitors. *Bioorg. Med. Chem.* 18, 1273–1279. <https://doi.org/10.1016/j.bmc.2009.12.029>
- Choi, J.S., Nurul Islam, Md., Yousof Ali, Md., Kim, E.J., Kim, Y.M., Jung, H.A., 2014. Effects of C-glycosylation on anti-diabetic, anti- Alzheimer's disease , and anti-inflammatory potential of apigenin. *Food Chem. Toxicol.* 64, 27–33. <https://doi.org/10.1016/j.fct.2013.11.020>
- Christians, U., Schmitz, V., Haschke, M., 2005. Functional interactions between P-glycoprotein and CYP3A in drug metabolism. *Expert Opin. Drug Metab. Toxicol.* 1, 641–654. <https://doi.org/10.1517/17425255.1.4.641>
- Corbin, C.J., Graham-Lorence, S., McPhaul, M., Mason, J.I., Mendelson, C.R., Simpson, E.R., 1988. Isolation of a full-length cDNA insert encoding human aromatase system cytochrome P-450 and its expression in non-steroidogenic cells. *Proc. Natl. Acad. Sci. U. S. A.* 85, 8948–8952. <https://doi.org/10.1073/pnas.85.23.8948>
- Cornelius, F., Kanai, R., Toyoshima, C., 2013. A Structural View on the Functional Importance of the Sugar Moiety and Steroid Hydroxyls of Cardiotonic Steroids in Binding to Na, K-ATPase*. *Journal of Biological Chemistry* 288, 6602–6616. <https://doi.org/10.1074/jbc.M112.442137>
- Cragg, G.E. and Little, G.M.L., 1962. The extractives of *Leonotis leonurus* R. *South Afr. J. Chem.* 15, 29–30.
- Daina, A., Michielin, O., Zoete, V., 2017. SwissADME: a free web tool to evaluate pharmacokinetics, drug-likeness, and medicinal chemistry friendliness of small molecules. *Sci. Rep.* 7, 42717. <https://doi.org/10.1038/srep42717>
- Daina, A., Zoete, V., 2016. A BOILED-Egg to Predict Gastrointestinal Absorption and Brain Penetration of Small Molecules. *ChemMedChem* 11, 1117–1121. <https://doi.org/10.1002/cmdc.201600182>
- de la Peña, J.B.I., Kim, C.A., Lee, H.L., Yoon, S.Y., Kim, H.J., Hong, E.Y., Kim, G.H., Ryu, J.H., Lee, Y.S., Kim, K.M., Cheong, J.H., 2014. Luteolin mediates the antidepressant-like effects of *Cirsium japonicum* in mice, possibly through modulation of the GABAA receptor. *Arch. Pharm. Res.* 37, 263–269. <https://doi.org/10.1007/s12272-013-0229-9>
- Di, L., 2014. The role of drug metabolizing enzymes in clearance. *Expert Opin. Drug Metab. Toxicol.* 10, 379–393. <https://doi.org/10.1517/17425255.2014.876006>
- Djoumbou-Feunang, Y., Fiamoncini, J., Gil-de-la-Fuente, A., Greiner, R., Manach, C., Wishart, D.S., 2019. BioTransformer: a comprehensive computational tool for small molecule metabolism prediction and metabolite identification. *J. Cheminformatics* 11. <https://doi.org/10.1186/s13321-018-0324-5>
- Du, X., Li, Y., Xia, Y.-L., Ai, S.-M., Liang, J., Sang, P., Ji, X.-L., Liu, S.-Q., 2016. Insights into Protein–Ligand Interactions: Mechanisms, Models, and Methods. *Int J Mol Sci* 17, 144. <https://doi.org/10.3390/ijms17020144>
- Dunn, B., Stein, P., Cavazzoni, P., 2021. Approval of Aducanumab for Alzheimer Disease—the FDA's Perspective. *JAMA Intern. Med.* <https://doi.org/10.1001/jamainternmed.2021.4607>

- Durojaye, O., Nwachukwu, J.N., Njoku, U.O., Tanze, M.M., Christian, N., Orum, T.G., Cosmas, S., 2019. Improving the Drug Bioavailability Property of Myricetin through a Structural Monosubstitution Modification Approach: An In-Silico Pharmacokinetics Study. *Afr. J. Biomed. Res.* 22, 347–352.
- Ebinger, M., Uhr, M., 2006. ABC drug transporter at the blood–brain barrier. *Eur. Arch. Psychiatry Clin. Neurosci.* 256, 294–298. <https://doi.org/10.1007/s00406-006-0664-4>
- Egan, W.J., Merz, K.M., Baldwin, J.J., 2000. Prediction of Drug Absorption Using Multivariate Statistics. *J. Med. Chem.* 43, 3867–3877. <https://doi.org/10.1021/jm000292e>
- Ekins, S., Mestres, J., Testa, B., 2007. In silico pharmacology for drug discovery: methods for virtual ligand screening and profiling. *Br. J. Pharmacol.* 152, 9–20. <https://doi.org/10.1038/sj.bjp.0707305>
- Elango Ekaney, L., Bekindaka Eni, D., Ntie-Kang, F., 2021. Chemical similarity methods for analyzing secondary metabolite structures. *Physical Sciences Reviews* 6. <https://doi.org/10.1515/psr-2018-0129>
- El-Ansari, M.A., Aboutabl, E.A., Farrag, A.R.H., Sharaf, M., Hawas, U.W., Soliman, G.M., El-Seed, G.S., 2009. Phytochemical and pharmacological studies on *Leonotis leonurus*. *Pharm. Biol.* 47, 894–902. <https://doi.org/10.1080/13880200902942428>
- Faccenda, E., Maxwell, S., Szarek, J.L., 2019. Clinical pharmacokinetics | Pharmacology Education Project [WWW Document]. URL <https://www.pharmacologyeducation.org/clinical-pharmacology/clinical-pharmacokinetics> (accessed 6.24.20).
- Fan, J., de Lannoy, I.A.M., 2014. Pharmacokinetics. *Biochem. Pharmacol.*, Special Issue: Pharmacology in 21st Century Biomedical Research 87, 93–120. <https://doi.org/10.1016/j.bcp.2013.09.007>
- Ferguson, C.S., Tyndale, R.F., 2011. Cytochromes P450 in the brain: Emerging evidence for biological significance. *Trends Pharmacol. Sci.* 32, 708–714. <https://doi.org/10.1016/j.tips.2011.08.005>
- Folch, J., Petrov, D., Ettcheto, M., Abad, S., Sánchez-López, E., García, M.L., Olloquequi, J., Beas-Zarate, C., Auladell, C., Camins, A., 2016. Current Research Therapeutic Strategies for Alzheimer’s disease Treatment [WWW Document]. *Neural Plast.* <https://doi.org/10.1155/2016/8501693>
- Fu, R., 2012. Analysis of Stachydrine in *Leonurus japonicus* Using an Agilent ZORBAX RRHD HILIC Plus Column with LC/ELSD and LC/MS/MS 6.
- Gangrade, D., Sawant, G., Mehta, A., 2016. Re-thinking drug discovery: In silico method 8.
- Gasteiger, J., 2016. Chemoinformatics: Achievements and Challenges, a Personal View. *Molecules* 21, 151. <https://doi.org/10.3390/molecules21020151>
- Geha, R.M., Chen, K., Wouters, J., Ooms, F., Shih, J.C., 2002. Analysis of Conserved Active Site Residues in Monoamine Oxidase A and B and Their Three-dimensional Molecular Modeling. *J. Biol. Chem.* 277, 17209–17216. <https://doi.org/10.1074/jbc.M110920200>
- Gfeller, D., Grosdidier, A., Wirth, M., Daina, A., Michielin, O., Zoete, V., 2014. SwissTargetPrediction: a web server for target prediction of bioactive small molecules. *Nucleic Acids Res.* 42, W32–W38. <https://doi.org/10.1093/nar/gku293>
- Ghose, A.K., Viswanadhan, V.N., Wendoloski, J.J., 1999. A Knowledge-Based Approach in Designing Combinatorial or Medicinal Chemistry Libraries for Drug Discovery. 1. A Qualitative and Quantitative Characterization of Known Drug Databases. *J. Comb. Chem.* 1, 55–68. <https://doi.org/10.1021/cc9800071>
- Glen, R.C., Galloway, W., Spring, D.R., Liwiki, G., 2016. Multiple-parameter optimization in drug discovery: example of the 5-HT1B GPCR. 605. <https://doi.org/10.1002/minf.201600056>

- Guimarães, C.C., Oliveira, D.D., Valdevite, M., Saltoratto, A.L.F., Pereira, S.I.V., França, S. de C., Pereira, A.M.S., Pereira, P.S., 2015. The glycosylated flavonoids vitexin, isovitexin, and quercetrin isolated from *Serjania erecta* Radlk (Sapindaceae) leaves protect PC12 cells against amyloid- β 25-35 peptide-induced toxicity. *Food Chem. Toxicol.* 86, 88–94. <https://doi.org/10.1016/j.fct.2015.09.002>
- Han, X.H., Hong, S.S., Hwang, J.S., Lee, M.K., Hwang, B.Y., Ro, J.S., 2007. Monoamine oxidase inhibitory components from *Cayratia japonica*. *Arch. Pharm. Res.* 30, 13. <https://doi.org/10.1007/BF02977772>
- Han, Y.N., Noh, D.B., Han, D.S., 1987. Studies on the monoamine oxidase inhibitors of medicinal plants I. Isolation of MAO-B inhibitors from *Chrysanthemum indicum*. *Arch. Pharm. Res.* 10, 142. <https://doi.org/10.1007/BF02857780>
- He, F., Lindqvist, C., Harding, W.W., 2012. Leonurenones A–C: Labdane diterpenes from *Leonotis leonurus*. *Phytochemistry* 83, 168–172. <https://doi.org/10.1016/j.phytochem.2012.07.014>
- Hedlund, E., Gustafsson, J.A., Warner, M., 2001. Cytochrome P450 in the brain; a review. *Curr. Drug Metab.* 2, 245–263. <https://doi.org/10.2174/1389200013338513>
- Hirano, R., Interthal, H., Huang, C., Nakamura, T., Deguchi, K., Choi, K., Bhattacharjee, M.B., Arimura, K., Umehara, F., Izumo, S., Northrop, J.L., Salih, M.A.M., Inoue, K., Armstrong, D.L., Champoux, J.J., Takashima, H., Boerkoel, C.F., 2007. Spinocerebellar ataxia with axonal neuropathy: consequence of a *Tdp1* recessive neomorphic mutation? *EMBO J.* 26, 4732–4743. <https://doi.org/10.1038/sj.emboj.7601885>
- Huang, H., Zhang, G., Zhou, Y., Lin, C., Chen, S., Lin, Y., Mai, S., Huang, Z., 2018. Reverse Screening Methods to Search for the Protein Targets of Chemo Preventive Compounds. *Front. Chem.* 6. <https://doi.org/10.3389/fchem.2018.00138>
- Inouye, H., Takeda, Y., Uobe, K., Yamauchi, K., Yabuuchi, N., Kuwano, S., 1974. Purgative activities of iridoid glucosides. *Planta Med.* 25, 285–288. <https://doi.org/10.1055/s-0028-1097945>
- Iversen, L.F., Andersen, H.S., Møller, K.B., Olsen, O.H., Peters, G.H., Branner, S., Mortensen, S.B., Hansen, T.K., Lau, J., Ge, Y., Holsworth, D.D., Newman, M.J., Hundahl Møller, N.P., 2001. Steric Hindrance as a Basis for Structure-Based Design of Selective Inhibitors of Protein-Tyrosine Phosphatases. *Biochemistry* 40, 14812–14820. <https://doi.org/10.1021/bi011389l>
- Jancova, P., Anzenbacher, P., Anzenbacherova, E., 2010. Phase II drug metabolizing enzymes. *Biomed. Pap. Med. Fac. Univ. Palacky Olomouc Czechoslov.* 154, 103–116. <https://doi.org/10.5507/bp.2010.017>
- Ji, H.-F., Li, X.-J., Zhang, H.-Y., 2009. Natural products and drug discovery. *EMBO Rep.* 10, 194–200. <https://doi.org/10.1038/embor.2009.12>
- Jimoh, F.O., Adedapo, A.A., Afolayan, A.J., 2010. Comparison of the nutritional value and biological activities of the acetone, methanol, and water extracts of the leaves of *Solanum nigrum* and *Leonotis leonorus*. *Food Chem. Toxicol. Int. J. Publ. Br. Ind. Biol. Res. Assoc.* 48, 964–971. <https://doi.org/10.1016/j.fct.2010.01.007>
- Jorgensen, W.L., 2004. The Many Roles of Computation in Drug Discovery. *Science* 303, 1813–1818. <https://doi.org/10.1126/science.1096361>
- Kaminsky, L.S., Zhang, Z.-Y., 1997. Human P450 metabolism of warfarin. *Pharmacol. Ther.* 73, 67–74. [https://doi.org/10.1016/S0163-7258\(96\)00140-4](https://doi.org/10.1016/S0163-7258(96)00140-4)
- Kapetanovic, I.M., 2008. Computer-aided drug discovery and development (CADD): In silico-chemico-biological approach. *Chem. Biol. Interact., Frontiers of Pharmacology and Toxicology* 171, 165–176. <https://doi.org/10.1016/j.cbi.2006.12.006>

- Kar, S., Leszczynski, J., 2018. Recent Advances of Computational Modeling for Predicting Drug Metabolism: A Perspective. *Curr. Drug Metab.* 18, 1106–1122.
<https://doi.org/10.2174/1389200218666170607102104>
- Kharkar, P.S., Warriar, S., Gaud, R.S., 2014. Reverse docking: a powerful tool for drug repositioning and drug rescue. *Future Med. Chem.* 6, 333–342.
<https://doi.org/10.4155/fmc.13.207>
- Kidron, H., del Amo, E.M., Vellonen, K.-S., Urtti, A., 2012. Prediction of the Vitreal Half-Life of Small Molecular Drug-Like Compounds. *Pharm. Res.* 29, 3302–3311.
<https://doi.org/10.1007/s11095-012-0822-5>
- Kırmızıbekmez, H., Çalış, I., Perozzo, R., Brun, R., Dönmez, A.A., Linden, A., Rüedi, P., Tasdemir, D., 2004. Inhibiting Activities of the Secondary Metabolites of *Phlomis brunneogaleata* against Parasitic Protozoa and Plasmodial Enoyl-ACP Reductase, a Crucial Enzyme in Fatty Acid Biosynthesis. *Planta Med.* 70, 711–717.
<https://doi.org/10.1055/s-2004-827200>
- Klebe, G., 2013. Optimization of Lead Structures, in: Klebe, G. (Ed.), *Drug Design: Methodology, Concepts, and Mode-of-Action*. Springer, Berlin, Heidelberg, pp. 153–172.
https://doi.org/10.1007/978-3-642-17907-5_8
- Kobayashi, T., Ota, S., Tanaka, K., Ito, Y., Hasegawa, M., Umeda, Y., Motoi, Y., Takanashi, M., Yasuhara, M., Anno, M., Mizuno, Y., Mori, H., 2003. A novel L266V mutation of the tau gene causes frontotemporal dementia with a unique tau pathology. *Ann. Neurol.* 53, 133–137. <https://doi.org/10.1002/ana.10447>
- Kramer, J.A., Sagartz, J.E., Morris, D.L., 2007. The application of discovery toxicology and pathology towards the design of safer pharmaceutical lead candidates. *Nat. Rev. Drug Discov.* 6, 636–649. <https://doi.org/10.1038/nrd2378>
- Kuchta, K., Volk, R.B., Rauwald, H.W., 2013. Stachydrine in *Leonurus cardiaca*, *Leonurus japonicus*, *Leonotis leonurus*: detection and quantification by instrumental HPTLC and ¹H-qNMR analyses. *Pharm.- Int. J. Pharm. Sci.* 68, 534–540.
- Kunvári, M., Páska, C., László, M., Orfi, L., Kövesdi, I., Eros, D., Bökönyi, G., Kéri, G., Gyurján, I., 1999. [Biological activity and structure of antitumor compounds from *Plantago media* L]. *Acta Pharm. Hung.* 69, 232–239.
- Langhans, W., 2007. Signals generating anorexia during acute illness: Symposium on ‘Eating, illness and the gut: is there disorder in the house?’ *Proc. Nutr. Soc.* 66, 321–330.
<https://doi.org/10.1017/S0029665107005587>
- Laonigro, G., Lanzetta, R., Parrilli, M., Adinolfi, M., Mangoni, L., 1979. The configuration of the diterpene spiroethers from *Marrubium vulgare* and from *Leonotis leonurus*. *Gazz Chim Ital* 109, 145–150.
- Le, J., 2020. Overview of Pharmacokinetics [WWW Document]. MSD Man. Prof. Ed. URL <https://www.msmanuals.com/professional/clinical-pharmacology/pharmacokinetics/overview-of-pharmacokinetics> (accessed 6.24.20).
- Li, Y., Sato, T., Metori, K., Koike, K., Che, Q.M., Takahashi, S., 1998. The promoting effects of geniposidic acid and aucubin in *Eucommia ulmoides* Oliver leaves on collagen synthesis. *Biol. Pharm. Bull.* 21, 1306–1310.
- Lima, L.K.F., Pereira, S.K.S., Junior, R. dos S.S., Santos, F.P. da S., Nascimento, A. de S., Feitosa, C.M., Figuerêdo, J. de S., Cavalcante, A. do N., Araújo, E.C. da C., Rai, M., 2018. A Brief Review on the Neuroprotective Mechanisms of Vitexin [WWW Document]. *BioMed Res. Int.* <https://doi.org/10.1155/2018/4785089>
- Lipinski, C.A., 2000. Drug-like properties and the causes of poor solubility and poor permeability. *J. Pharmacol. Toxicol. Methods* 44, 235–249

- Lo, B., Rensi, S., Tornig, W., Altman, R., 2018. Machine learning in chemoinformatics and drug discovery. *Drug Discov. Today* 23. <https://doi.org/10.1016/j.drudis.2018.05.010>
- Lukac, I., Wyatt, P.G., Gilbert, I.H., Zuccotto, F., 2021. Ligand binding: evaluating the contribution of the water molecules network using the Fragment Molecular Orbital method. *J Comput Aided Mol Des* 35, 1025–1036. <https://doi.org/10.1007/s10822-021-00416-3>
- Macalino, S.J.Y., Gosu, V., Hong, S., Choi, S., 2015. Role of computer-aided drug design in modern drug discovery. *Arch. Pharm. Res.* 38, 1686–1701. <https://doi.org/10.1007/s12272-015-0640-5>
- Maurice, T., Su, T.-P., 2009. The Pharmacology of Sigma-1 Receptors. *Pharmacol. Ther.* 124, 195–206. <https://doi.org/10.1016/j.pharmthera.2009.07.001>
- Mazimba, O., 2015. Leonotis leonurus: an herbal medicine review. *J. Pharmacogn. Phytochem.* 3.
- McFadyen, M.C., Melvin, W.T., Murray, G.I., 1997. Cytochrome P450 in normal human brain and brain tumours. *Biochem. Soc. Trans.* 25, S577. <https://doi.org/10.1042/bst025s577>
- McKenzie, J.M., Green, I.R., Mugabo, P., 2006. Leonurun, a Novel Labdane Diterpenoid from Leonotis leonurus. *South Afr. J. Chem.* 59, 114–116.
- Meng, X.-Y., Zhang, H.-X., Mezei, M., Cui, M., 2011. Molecular Docking: A powerful approach for structure-based drug discovery. *Curr. Comput. Aided Drug Des.* 7, 146–157.
- Milczek, E.M., Binda, C., Rovida, S., Mattevi, A., Edmondson, D.E., 2011. The ‘gating’ residues Ile199 and Tyr326 in human monoamine oxidase B function in substrate and inhibitor recognition. *FEBS J.* 278, 4860–4869. <https://doi.org/10.1111/j.1742-4658.2011.08386.x>
- Mindrila, D., Balentyne, P., Ed, M., 2017. Scatterplots and Correlation.
- Mnonopi, N., Levendal, R.-A., Davies-Coleman, M.T., Frost, C.L., 2011. The cardio protective effects of marrubiin, a diterpenoid found in Leonotis leonurus extracts. *J. Ethnopharmacol.* 138, 67–75. <https://doi.org/10.1016/j.jep.2011.08.041>
- Mnonopi, N., Levendal, R.-A., Mzilikazi, N., Frost, C.L., 2012. Marrubiin, a constituent of Leonotis leonurus, alleviates diabetic symptoms. *Phytomedicine* 19, 488–493. <https://doi.org/10.1016/j.phymed.2011.12.008>
- Molecular Operating Environment (MOE), 2019.01; Chemical Computing Group ULC, 1010 Sherbooke St. West, Suite #910, Montreal, QC, Canada, H3A 2R7, 2021.
- Molinoff, P.B., 2011. Neurotransmission and the Central Nervous System, in: Brunton, L.L., Chabner, B.A., Knollman, B.C. (Eds.), *Goodman and Gilman’s: The Pharmacological Basis of Therapeutics*. McGraw Hill Medical, pp. 363–395.
- Morris, G.M., Lim-Wilby, M., 2008. Molecular docking. *Methods Mol. Biol.* Clifton NJ 443, 365–382. https://doi.org/10.1007/978-1-59745-177-2_19
- Mugabo, P., Khan, F., Burger, A., 2012. Effects of Leonotis leonurus aqueous extract on the isolated perfused rat heart.
- Muhizi, T., Green, I.R., Amabeoku, G.J., Bienvenu, E., Bienvenu, E., 2005. An Anticonvulsant Diterpene Lactone Isolated from the Leaves of *Leonotis leonorus* (L) R. BR. *East Cent. Afr. J. Pharm. Sci.* 8, 54–61. <https://doi.org/10.4314/ecajps.v8i3.9727>
- Mukkavilli, R., Gundala, S.R., Yang, C., Donthamsetty, S., Cantuaria, G., Jadhav, G.R., Vangala, S., Reid, M.D., Aneja, R., 2014. Modulation of Cytochrome P450 Metabolism and Transport across Intestinal Epithelial Barrier by Ginger Biophenolics. *PLOS ONE* 9, e108386. <https://doi.org/10.1371/journal.pone.0108386>
- Murray, M., 2013. Chapter 6B. Phase II Drug-Metabolizing Enzymes, in: *Pharmacogenomics: An Introduction and Clinical Perspective*. McGraw-Hill Medical.
- Mylonas, C., Kouretas, D., 1999. Lipid peroxidation and tissue damage. *Vivo Athens Greece* 13, 295–309.

- Naidoo, D., Maharaj, V., Crouch, N.R., Ngwane, A., 2011. New labdane-type diterpenoids from *Leonotis leonurus* support circumscription of Lamiaceae s.l. *Biochem. Syst. Ecol.* 39, 216–219. <https://doi.org/10.1016/j.bse.2010.12.021>
- Narukawa, Y., Komori, M., Niimura, A., Noguchi, H., Kiuchi, F., 2015. Two new diterpenoids from *Leonotis leonurus* R. *Br. J. Nat. Med.* 69, 130–134. <https://doi.org/10.1007/s11418-014-0868-2>
- Narukawa, Y., Niimura, A., Noguchi, H., Tamura, H., Kiuchi, F., 2014. New diterpenoids with estrogen sulfotransferase inhibitory activity from *Leonurus sibiricus* L. *J. Nat. Med.* 68, 125–131. <https://doi.org/10.1007/s11418-013-0781-0>
- National Center for Biotechnology Information, 2018. Verbascoside [WWW Document]. URL <https://pubchem.ncbi.nlm.nih.gov/compound/5281800> (accessed 2.28.18).
- Nguyen, T.L., Fruit, C., Hérault, Y., Meijer, L., Besson, T., 2017. Dual-specificity tyrosine phosphorylation-regulated kinase 1A (DYRK1A) inhibitors: a survey of recent patent literature. *Expert Opin. Ther. Pat.* 27, 1183–1199. <https://doi.org/10.1080/13543776.2017.1360285>
- Nielsen, N.D., Sandager, M., Stafford, G.I., van Staden, J., Jäger, A.K., 2004. Screening of indigenous plants from South Africa for affinity to the serotonin reuptake transport protein. *J. Ethnopharmacol.* 94, 159–163. <https://doi.org/10.1016/j.jep.2004.05.013>
- Nsuala, B.N., Enslin, G., Viljoen, A., 2015. “Wild cannabis”: A review of the traditional use and phytochemistry of *Leonotis leonurus*. *J. Ethnopharmacol.* 174, 520–539. <https://doi.org/10.1016/j.jep.2015.08.013>
- Ntie-Kang, F., Nyongbela, K.D., Ayimele, G.A., Shekfeh, S., 2018. “Drug-Likeness” versus “Natural Product-Likeness” (preprint). <https://doi.org/10.20944/preprints201811.0561.v1>
- Obikeze, K., 2004. Cardiovascular effects of *Leonotis leonurus* extracts in normotensive rats and in isolated perfused rat heart (PhD Thesis). University of the Western Cape.
- Obikeze, K., Mugabo, P., Green, I., Dietrich, D., Burger, A., 2013. Effects of a Methanol Fraction of the Leaves of *Leonotis leonurus* on the Blood Pressure and Heart Rate of Normotensive Male Wistar Rats 7, 4.
- Obikeze, K.C., McKenzie, J.M., Green, I.R., Mugabo, P., 2008. Characterization and cardiovascular effects of (13S)-9 α ,13 α -epoxylabda-6 β (19),15(14) diol dilactone, a diterpenoid isolated from *Leonotis leonurus*. *South Afr. J. Chem.* 61, 119–122.
- Ojewole, J. a. O., 2005. Antinociceptive, anti-inflammatory and antidiabetic effects of *Leonotis leonurus* (L.) R. BR. [Lamiaceae] leaf aqueous extract in mice and rats. *Methods Find. Exp. Clin. Pharmacol.* 27, 257–264. <https://doi.org/10.1358/mf.2005.27.4.893583>
- Ojewole, J.A.O., 2003. P-2: Hypotensive effect of *Leonotis leonurus* aqueous leaf extract in rats. *Am. J. Hypertens.* 16, 40A-40A. [https://doi.org/10.1016/S0895-7061\(03\)00168-7](https://doi.org/10.1016/S0895-7061(03)00168-7)
- Oyedemi, S.O., Yakubu, M.T., Afolayan, A.J., 2011. Antidiabetic activities of aqueous leaves extract of *Leonotis leonurus* in streptozotocin induced diabetic rats. *J. Med. Plants Res.* 5, 119–125.
- Pajouhesh, H., Lenz, G.R., 2005. Medicinal chemical properties of successful central nervous system drugs. *NeuroRX* 2, 541–553. <https://doi.org/10.1602/neurorx.2.4.541>
- Palmer, A.M., 2011. The role of the blood brain barrier in neurodegenerative disorders and their treatment. *J. Alzheimer’s Dis. JAD* 24, 643–656. <https://doi.org/10.3233/JAD-2011-110368>
- Palmer, A.M., 2010a. The blood–brain barrier. *Neurobiol. Dis., Special Issue: Blood Brain Barrier* 37, 1–2. <https://doi.org/10.1016/j.nbd.2009.09.023>
- Palmer, A.M., 2010b. The role of the blood–CNS barrier in CNS disorders and their treatment. *Neurobiol. Dis., Special Issue: Blood Brain Barrier* 37, 3–12. <https://doi.org/10.1016/j.nbd.2009.07.029>

- Pan, N., Hori, H., 1994. The Interaction of Acteoside with Mitochondrial Lipid Peroxidation as an Ischemia/Reperfusion Injury Model, in: Hogan, M.C., Mathieu-Costello, O., Poole, D.C., Wagner, P.D. (Eds.), Oxygen Transport to Tissue XVI, Advances in Experimental Medicine and Biology. Springer US, Boston, MA, pp. 319–325.
https://doi.org/10.1007/978-1-4615-1875-4_51
- Pantsar, T., Poso, A., 2018. Binding Affinity via Docking: Fact and Fiction. *Molecules* 23, 1899.
<https://doi.org/10.3390/molecules23081899>
- Pardridge, W.M., 2002. Why is the global CNS pharmaceutical market so under-penetrated? *Drug Discov. Today* 7, 5–7. [https://doi.org/10.1016/S1359-6446\(01\)02082-7](https://doi.org/10.1016/S1359-6446(01)02082-7)
- Park, S.-W., Technology, S.-K.C.D. of F.S. and, University, K.N., Republic), T. 702-701 (Korea, 2000. Active Oxygen Scavenging Activity of Luteolin-7-O-beta-D-Glucoside Isolated from *Humulus japonicus*. *J Korean Soc Food Sci Nutr*.
- Peng, Y., Gan, R., Li, H., Yang, M., McClements, D.J., Gao, R., Sun, Q., 2021. Absorption, metabolism, and bioactivity of vitexin: recent advances in understanding the efficacy of an important nutraceutical. *Crit. Rev. Food Sci. Nutr.* 61, 1049–1064.
<https://doi.org/10.1080/10408398.2020.1753165>
- Petterson, E.F., Goddard, T.D., Huang, C.C., Couch, G.S., Greenblatt, D.M., Meng, E.C., Ferrin, T.E., 2004. UCSF Chimera—a visualization system for exploratory research and analysis. *J. Comput. Chem.* 25, 1605–1612. <https://doi.org/10.1002/jcc.20084>
- Piñero, J., Ramírez-Anguita, J.M., Saüch-Pitarch, J., Ronzano, F., Centeno, E., Sanz, F., Furlong, L.I., 2019. The DisGeNET knowledge platform for disease genomics: 2019 update. *Nucleic Acids Res.* gkz1021. <https://doi.org/10.1093/nar/gkz1021>
- Pinna, A., Wardas, J., Domenici, M.R., Popoli, P., Cossu, G., Morelli, M., 2017. Chapter 10 - Control of Motor Function by Adenosine A2A Receptors in Parkinson's and Huntington's Disease, in: Blum, D., Lopes, L.V. (Eds.), Adenosine Receptors in Neurodegenerative Diseases. Academic Press, San Diego, pp. 187–213. <https://doi.org/10.1016/B978-0-12-803724-9.00010-7>
- Pinzi, L., Rastelli, G., 2019. Molecular Docking: Shifting Paradigms in Drug Discovery. *Int. J. Mol. Sci.* 20. <https://doi.org/10.3390/ijms20184331>
- Pires, D.E.V., Blundell, T.L., Ascher, D.B., 2015. pkCSM: Predicting Small-Molecule Pharmacokinetic and Toxicity Properties Using Graph-Based Signatures. *J. Med. Chem.* 58, 4066–4072. <https://doi.org/10.1021/acs.jmedchem.5b00104>
- Prachayasittikul, Veda, Worachartcheewan, A., Shoombuatong, W., Prachayasittikul, Virapong, Nantasenamat, C., 2015. Classification of P-glycoprotein-interacting compounds using machine learning methods. *EXCLI J.* 14, 958–970. <https://doi.org/10.17179/excli2015-374>
- Prachayasittikul, Veda, Mandi, P., Prachayasittikul, S., Prachayasittikul, Virapong, Nantasenamat, C., 2017. Exploring the Chemical Space of P-Glycoprotein Interacting Compounds. *Mini Rev. Med. Chem.* 17, 1332–1345. <https://doi.org/10.2174/1389557516666160121120344>
- Queensland Brain Institute, 2017. Central Nervous System: brain and spinal cord [WWW Document]. URL <https://qbi.uq.edu.au/brain/brain-anatomy/central-nervous-system-brain-and-spinal-cord> (accessed 2.27.20).
- Rafieian-Kopaei, M., 2012. Medicinal plants and the human needs. *J HerbMed Pharmacol* 1, 1–2.
- Ramírez, D., Caballero, J., 2016. Is It Reliable to Use Common Molecular Docking Methods for Comparing the Binding Affinities of Enantiomer Pairs for Their Protein Target? *Int J Mol Sci* 17, 525. <https://doi.org/10.3390/ijms17040525>
- Riley, R.J., Parker, A.J., Trigg, S., Manners, C.N., 2001. Development of a Generalized, Quantitative Physicochemical Model of CYP3A4 Inhibition for Use in Early Drug Discovery. *Pharm. Res.* 18, 652–655. <https://doi.org/10.1023/A:1011085411050>

- Risa, J., Risa, A., Adersen, A., Gauguin, B., Stafford, G.I., van Staden, J., Jäger, A.K., 2004. Screening of plants used in southern Africa for epilepsy and convulsions in the GABAA-benzodiazepine receptor assay. *J. Ethnopharmacol.* 93, 177–182. <https://doi.org/10.1016/j.jep.2004.01.021>
- Rivett, D.E.A., 1964. The isolation of marrubiin from *Leonotis leonurus* R. *Isol. Marrubiin Leonotis Leonurus R* 1857–1858.
- Robinson, J.B., 1985. Stereo selectivity and isoenzyme selectivity of monoamine oxidase inhibitors. Enantiomers of amphetamine, N-methyl amphetamine and deprenyl. *Biochem. Pharmacol.* 34, 4105–4108. [https://doi.org/10.1016/0006-2952\(85\)90201-1](https://doi.org/10.1016/0006-2952(85)90201-1)
- Romano, J.D., Tatonetti, N.P., 2019. Informatics and Computational Methods in Natural Product Drug Discovery: A Review and Perspectives. *Front. Genet.* 10. <https://doi.org/10.3389/fgene.2019.00368>
- Sander, T., Freyss, J., von Korff, M., Rufener, C., 2015. DataWarrior: An Open-Source Program for Chemistry Aware Data Visualization and Analysis. *J. Chem. Inf. Model.* 55, 460–473. <https://doi.org/10.1021/ci500588j>
- Sauton, N., Lagorce, D., Villoutreix, B.O., Miteva, M.A., 2008. MS-DOCK: Accurate multiple conformation generator and rigid docking protocol for multi-step virtual ligand screening. *BMC Bioinformatics* 9, 184. <https://doi.org/10.1186/1471-2105-9-184>
- Schinkel, A.H., 1999. P-Glycoprotein, a gatekeeper in the blood–brain barrier. *Adv. Drug Deliv. Rev., Blood-brain Barrier as a Dynamic Interface for Drug Delivery to Brain* 36, 179–194. [https://doi.org/10.1016/S0169-409X\(98\)00085-4](https://doi.org/10.1016/S0169-409X(98)00085-4)
- Schneider, G., 2013. Prediction of Drug-Like Properties, Madame Curie Bioscience Database [Internet]. Landes Bioscience.
- Segall, M.D., 2012. Multi-Parameter Optimization: Identifying High Quality Compounds with a Balance of Properties. *Curr. Pharm. Des.* 18, 1292–1310
- Seifert, M.H.J., Wolf, K., Vitt, D., 2003. Virtual high-throughput in silico screening. *BIOSILICO* 1, 143–149. [https://doi.org/10.1016/S1478-5382\(03\)02359-X](https://doi.org/10.1016/S1478-5382(03)02359-X)
- Shah, R.S., Lee, H.-G., Xiongwei, Z., Perry, G., Smith, M.A., Castellani, R.J., 2008. Current approaches in the treatment of Alzheimer’s disease . *Biomed. Pharmacother.* 62, 199–207. <https://doi.org/10.1016/j.biopha.2008.02.005>
- Sivaraman, D., Srikanth, J., 2016. Discovery of Novel Monoamine Oxidase-B Inhibitors by Molecular Docking Approach for Alzheimer’s and Parkinson’s Disease Treatment. *Int. J. Pharm. Sci. Rev. Res.* 40(1), 245–250.
- Shimobayashi, E., Kapfhammer, J.P., 2017. Increased biological activity of protein Kinase C gamma is not required in Spinocerebellar ataxia 14. *Mol. Brain* 10, 34. <https://doi.org/10.1186/s13041-017-0313-z>
- Sridhar, J., Liu, J., Foroozesh, M., Stevens, C.L.K., 2012. Insights on Cytochrome P450 Enzymes and Inhibitors Obtained Through QSAR Studies. *Molecules* 17, 9283. <https://doi.org/10.3390/molecules17089283>
- Stafford, G.I., Jäger, A.K., van Staden, J., 2005. Effect of storage on the chemical composition and biological activity of several popular South African medicinal plants. *J. Ethnopharmacol.* 97, 107–115. <https://doi.org/10.1016/j.jep.2004.10.021>
- Takashima, H., Boerkoel, C.F., John, J., Saifi, G.M., Salih, M.A.M., Armstrong, D., Mao, Y., Quioco, F.A., Roa, B.B., Nakagawa, M., Stockton, D.W., Lupski, J.R., 2002. Mutation of TDP1, encoding a topoisomerase I-dependent DNA damage repair enzyme, in spinocerebellar ataxia with axonal neuropathy. *Nat. Genet.* 32, 267–272. <https://doi.org/10.1038/ng987>
- Tang, W.H., Martin, K.A., Hwa, J., 2012. Aldose Reductase, Oxidative Stress, and Diabetic Mellitus. *Front. Pharmacol.* 3. <https://doi.org/10.3389/fphar.2012.00087>

- Terstappen, G.C., Reggiani, A., 2001. In silico research in drug discovery. *Trends Pharmacol. Sci.* 22, 23–26.
- Thomas, T., 2000. Monoamine Oxidase-B inhibitors in the treatment of Alzheimer's disease. *Neurobiol. Aging* 21, 343–348. [https://doi.org/10.1016/s0197-4580\(00\)00100-7](https://doi.org/10.1016/s0197-4580(00)00100-7)
- Tronina, T., Strugała, P., Popłoński, J., Włoch, A., Sordon, S., Bartmańska, A., Huszcza, E., 2017. The Influence of Glycosylation of Natural and Synthetic Prenylated Flavonoids on Binding to Human Serum Albumin and Inhibition of Cyclooxygenases COX-1 and COX-2. *Mol. J. Synth. Chem. Nat. Prod. Chem.* 22, 1230. <https://doi.org/10.3390/molecules22071230>
- Tshambuluka, N.D., Mugabo, P., Green, I., 2011. Cardiovascular effects of aqueous leaf extract of *Leonotis leonurus* in anesthetized rats. LAP LAMBERT Academic Publishing.
- Turner, S., 2015. *Leonotis leonurus* [WWW Document]. URL <http://pza.sanbi.org/leonotis-leonurus> (accessed 2.23.18).
- University of Edinburgh, 2015. what is informatics.pdf.
- Ursu, O., Rayan, A., Goldblum, A., Oprea, T.I., 2011. Understanding drug-likeness. *WIREs Comput. Mol. Sci.* 1, 760–781. <https://doi.org/10.1002/wcms.52>
- Van Wyk, B., Gericke, N., 2000. *People's Plant: A guide to useful plants of South Africa*, 1st ed. Pretoria.
- Van Wyk, B., Van Oudtshoorn, B., Gericke, N., 2000. *Medicinal Plants of South Africa*, 2nd ed. Briza Publication, Pretoria.
- Veber, D.F., Johnson, S.R., Cheng, H.-Y., Smith, B.R., Ward, K.W., Kopple, K.D., 2002. Molecular Properties That Influence the Oral Bioavailability of Drug Candidates. *J. Med. Chem.* 45, 2615–2623. <https://doi.org/10.1021/jm020017n>
- Walker, L., Yip, V., Pirmohamed, M., 2014. Chapter 20 - Adverse Drug Reactions, in: Padmanabhan, S. (Ed.), *Handbook of Pharmacogenomics and Stratified Medicine*. Academic Press, San Diego, pp. 405–435. <https://doi.org/10.1016/B978-0-12-386882-4.00020-7>
- Waterhouse, R.N., 2003. Determination of lipophilicity and its use as a predictor of blood-brain barrier penetration of molecular imaging agents. *Mol. Imaging Biol.* 5, 376–389. <https://doi.org/10.1016/j.mibio.2003.09.014>
- Weller, J., Budson, A., 2018. Current understanding of Alzheimer's disease diagnosis and treatment. *F1000Research* 7. <https://doi.org/10.12688/f1000research.14506.1>
- Wirth, M., Zoete, V., Michielin, O., Sauer, W.H.B., 2013. SwissBioisostere: a database of molecular replacements for ligand design. *Nucleic Acids Res.* 41, D1137–D1143. <https://doi.org/10.1093/nar/gks1059>
- Wu, H., Li, J., Fronczek, F.R., Ferreira, D., Burandt, C.L., Setola, V., Roth, B.L., Zjawiony, J.K., 2013. Labdane Diterpenoids from *Leonotis leonurus*. *Phytochemistry* 91, 229–235. <https://doi.org/10.1016/j.phytochem.2012.02.021>
- Wu, S.D., Jiang, X.Y., Chen, Q.Y., Chen, X.Q., 2007. Comparison of techniques for the extraction of the hypotensive drugs geniposidic acid and geniposide from *Eucommia Ulmoides*. *J. Iran. Chem. Soc.* 4, 205–214.
- Wu, J.-Y., Wang, T.-Y., Ding, H.-Y., Zhang, Y.-R., Lin, S.-Y., Chang, T.-S., 2021. Enzymatic Synthesis of Novel Vitexin Glucosides. *Molecules* 26, 6274. <https://doi.org/10.3390/molecules26206274>
- Xu, J., Hagler, A., 2002. Chemoinformatics and Drug Discovery. *Molecules* 7, 566–600. <https://doi.org/10.3390/70800566>
- Yamashita, F., Hashida, M., 2004. In Silico Approaches for Predicting ADME Properties of Drugs. *Drug Metab. Pharmacokinet.* 19, 327–338. <https://doi.org/10.2133/dmpk.19.327>

- Yamazaki, Y., Kanekiyo, T., 2017. Blood-Brain Barrier Dysfunction and the Pathogenesis of Alzheimer's disease. *Int. J. Mol. Sci.* 18, 1965. <https://doi.org/10.3390/ijms18091965>
- Yim, D.-S., Yoo, S.-J., Lee, S.-Y., 1997. Biological Activities of Verbascoside from *Pedicularis resupinata* var. *oppositifolia*. *Korean J. Pharmacogn.* 28, 252–256.
- Young, T., Abel, R., Kim, B., Berne, B.J., Friesner, R.A., 2007. Motifs for molecular recognition exploiting hydrophobic enclosure in protein–ligand binding. *PNAS* 104, 808–813. <https://doi.org/10.1073/pnas.0610202104>
- Zhou, S.-F., Zhong, W.-Z., 2017. Drug Design and Discovery: Principles and Applications. *Mol. J. Synth. Chem. Nat. Prod. Chem.* 22. <https://doi.org/10.3390/molecules22020279>
- Zhou, Z., Hou, J., Mo, Y., Ren, M., Yang, G., Qu, Z., Hu, Y., 2020. Geniposidic acid ameliorates spatial learning and memory deficits and alleviates neuroinflammation via inhibiting HMGB-1 and downregulating TLR4/2 signalling pathway in APP/PS1 mice. *Eur. J. Pharmacol.* 869, 172857. <https://doi.org/10.1016/j.ejphar.2019.172857>



APPENDIX

Appendix 1: Predicted physicochemical properties of Phytochemicals from *L. leonurus*

Molecule	Canonical SMILES	Formula	MW	#Heavy atoms	#Aromatic heavy atoms	Fraction Csp3	#Rotatable bonds	#H-bond acceptors	#H-bond donors	MR	TPSA
6-Methoxyluteolin-4-methylether	<chem>COc1ccc(cc1O)c1cc(=O)c2c(o1)cc(c(c2O)OC)O</chem>	C ₁₇ H ₁₄ O ₇	330.29	24	16	0.12	3	7	3	86.97	109.36
13R-premarrubin	<chem>O=C1O[C@H]2[C@H]3[C@]1(C)CCC[C@]3(C)[C@]1([C@@H](C2)C)CC[C@]2(O1)COC=C2</chem>	C ₂₀ H ₂₈ O ₄	332.43	24	0	0.85	0	4	0	90.22	44.76
13S-premarrubin	<chem>O=C1O[C@H]2[C@H]3[C@]1(C)CCC[C@]3(C)[C@]1([C@@H](C2)C)CC[C@@]2(O1)COC=C2</chem>	C ₂₀ H ₂₈ O ₄	332.43	24	0	0.85	0	4	0	90.22	44.76

Molecule	Canonical SMILES	Formula	MW	#Heavy atoms	#Aromatic heavy atoms	Fraction Csp3	#Rotatable bonds	#H-bond acceptors	#H-bond donors	MR	TPSA
13e-hydroxyabd-5(6) 8(9)-dien-7-on-16 15-olide	<chem>O=C1OCC(C1)(O)CCC1=C(C)C(=O)C=C2[C@]1(C)CCCC2(C)C</chem>	C20H28O4	332.43	24	0	0.7	3	4	1	93.13	63.6
14a-hydroxy-9a 13a-epoxyabd-5(6)-en-7-on-16 15-olide	<chem>O=C1C=C2C(C)(C)CCC[C@@]2([C@]2([C@@H]1C)CC[C@]1(O2)COC(=O)[C@H]1O)C</chem>	C20H28O5	348.43	25	0	0.8	0	5	1	92.61	72.83
16epi-Leoleorin F	<chem>O[C@@H]1C[C@@H](C)C2([C@@]3(C1C(C)(C)CCC3)C)CC[C@]1(O2)CCOC1O</chem>	C20H34O4	338.48	24	0	1	0	4	2	93.85	58.92
Acteoside	<chem>OC[C@H]1O[C@@H](OCCc2cc(c(c2)O)O)[C@@H]([C@H]([C@@H]1OC(=O)/C=C/c1ccc(c(c1)O)O)O[C@@H]1O[C@@H](C)[C@@H]([C@H]([C@H]1O)O)O)O</chem>	C29H36O15	624.59	44	12	0.48	11	15	9	148.42	245.29

Molecule	Canonical SMILES	Formula	MW	#Heavy atoms	#Aromatic heavy atoms	Fraction Csp3	#Rotatable bonds	#H-bond acceptors	#H-bond donors	MR	TPSA
Apigenin	<chem>Oc1ccc(cc1)c1cc(=O)c2c(o1)cc(cc2O)O</chem>	C ₁₅ H ₁₀ O ₅	270.24	20	16	0	1	5	3	73.99	90.9
Apigenin-6-C-a-arabinoside-8-C-B-glucoside	<chem>OC[C@H]1OC([C@@H]([C@H]([C@@H]1O)O)O)c1c(O)c(C2O[C@H](CO)[C@H]([C@@H]([C@H]2O)O)O)c(c2c1oc(cc2=O)c1ccc(cc1)O)O</chem>	C ₂₇ H ₃₀ O ₁₅	594.52	42	16	0.44	5	15	11	139.23	271.2
Apigenin-7-O-6-O-p-coumaryl-B-glucoside	<chem>O=C(OC[C@H]1O[C@@H](Oc2cc(O)c3c(c2)oc(cc3=O)c2ccc(cc2)O)[C@@H]([C@H]([C@@H]1O)O)O)/C=C/c1ccc(cc1)O</chem>	C ₃₀ H ₂₆ O ₁₂	578.52	42	22	0.2	8	12	6	147.48	196.35
Chrysoeriol	<chem>COc1cc(ccc1O)c1cc(=O)c2c(o1)cc(cc2O)O</chem>	C ₁₆ H ₁₂ O ₆	300.26	22	16	0.06	2	6	3	80.48	100.13

Molecule	Canonical SMILES	Formula	MW	#Heavy atoms	#Aromatic heavy atoms	Fraction Csp3	#Rotatable bonds	#H-bond acceptors	#H-bond donors	MR	TPSA
Compound X	<chem>O=C1OCC2(C1)CCC1(O2)[C@H](C)C[C@@H]2[C@@H]3[C@]1(C)CCC[C@]3(C)C(=O)O2</chem>	C ₂₀ H ₂₈ O ₅	348.43	25	0	0.9	0	5	0	90.89	61.83
Leoleorin A	<chem>O=C1C=C2C(C)(C)CCC[C@@]2(C([C@@H]1C)(O)CCc1cocc1)C</chem>	C ₂₀ H ₂₈ O ₃	316.43	23	5	0.65	3	3	1	91.96	50.44
Comosiin	<chem>OC[C@H]1OC(O)c2cc(O)c3c(c2)oc(cc3=O)c2ccc(cc2)O[C@@H]([C@H]([C@@H]1O)O)O</chem>	C ₂₁ H ₂₀ O ₁₀	432.38	31	16	0.29	4	10	6	106.11	170.05
Cynaroside	<chem>OC[C@H]1O[C@@H](Oc2cc(O)c3c(c2)oc(cc3=O)c2ccc(c2)O)O[C@@H]([C@H]([C@@H]1O)O)O</chem>	C ₂₁ H ₂₀ O ₁₁	448.38	32	16	0.29	4	11	7	108.13	190.28

Molecule	Canonical SMILES	Formula	MW	#Heavy atoms	#Aromatic heavy atoms	Fraction Csp3	#Rotatable bonds	#H-bond acceptors	#H-bond donors	MR	TPSA
Dihydroxylph tyl palmitate	<chem>CCCCCCCCC CCCCC(=O)O CC(C(CCCC(CC CC(CCCC(C)C) C)C)(O)C)O</chem>	C36H72 O4	568.95	40	0	0.97	30	4	2	178. 81	66.76
EDD	<chem>O=C1OCC[C@]2 1CC[C@@]1(O2) [C@H](C)C[C@ @H]2[C@@H]3[C@]1(C)CCC[C @]3(C)C(=O)O2</chem>	C20H28 O5	348.43	25	0	0.9	0	5	0	90.8 9	61.83
Geniposidic acid	<chem>OC[C@H]1O[C @@H](O[C@@ H]2OC=C([C@ @H]3[C@H]2C(=CC3)CO)C(=O) O)[C@@H]([C@ H]([C@@H]1O) O)O</chem>	C16H22 O10	374.34	26	0	0.69	5	10	6	82.5 7	166.14
Leoleorin B	<chem>O=C1C=C2C(C)(C)CCC[C@@]2(C(=C1C)CCc1co cc1)C</chem>	C20H26 O2	298.42	22	5	0.55	3	2	0	90.2 8	30.21

Molecule	Canonical SMILES	Formula	MW	#Heavy atoms	#Aromatic heavy atoms	Fraction Csp3	#Rotatable bonds	#H-bond acceptors	#H-bond donors	MR	TPSA
Leoleorin C	<chem>O[C@@H]1C[C@@H](C)C2([C@@]3(C1C(C)(C)CCC3)C)CC[C@]1(O2)CCOC1=O</chem>	C ₂₀ H ₃₂ O ₄	336.47	24	0	0.95	0	4	1	92.89	55.76
Leoleorin D	<chem>OCC[C@]1(CO)CCC2(O1)[C@H](C)C[C@H](C1[C@]2(C)CCCC1(C)C)O</chem>	C ₂₀ H ₃₆ O ₄	340.5	24	0	1	3	4	3	96.04	69.92
Leoleorin E	<chem>OC1OC[C@@]2(C1)CCC1(O2)[C@H](C)C[C@H](C2[C@]1(C)CCC2(C)C)O</chem>	C ₂₀ H ₃₄ O ₄	338.48	24	0	1	0	4	2	93.85	58.92
Leoleorin F	<chem>O[C@@H]1C[C@@H](C)C2([C@@]3(C1C(C)(C)CCC3)C)CC[C@]1(O2)CCOC1O</chem>	C ₂₀ H ₃₄ O ₄	338.48	24	0	1	0	4	2	93.85	58.92

Molecule	Canonical SMILES	Formula	MW	#Heavy atoms	#Aromatic heavy atoms	Fraction Csp3	#Rotatable bonds	#H-bond acceptors	#H-bond donors	MR	TPSA
Leoleorin G	<chem>O=C1OC[C@@]2(C1)CCC1(O2)[C@H](C)C(=O)C=C2[C@]1(C)CC(C)C</chem>	C ₂₀ H ₂₈ O ₄	332.43	24	0	0.8	0	4	0	91.45	52.6
Leoleorin H	<chem>OC[C@@]1(CCOC(=O)C)CCC2(O1)[C@H](C)C(=O)C=C1[C@]2(C)CCCC1(C)C</chem>	C ₂₂ H ₃₄ O ₅	378.5	27	0	0.82	5	5	1	104.34	72.83
Leoleorin I	<chem>OCC[C@]1(CO)CCC2(O1)[C@H](C)C(=O)C=C1[C@]2(C)CCCC1(C)C</chem>	C ₂₀ H ₃₂ O ₄	336.47	24	0	0.85	3	4	2	94.6	66.76
Leoleorin J	<chem>OCC[C@]1(CO)CCC2(O1)[C@H](C)[C@@H](O)C=C1[C@]2(C)C(C)C</chem>	C ₂₀ H ₃₄ O ₄	338.48	24	0	0.9	3	4	3	95.56	69.92
Leonurun	<chem>CC(=O)OC[C@]12CCC[C@]3([C@@H]1[C@H](OC3=O)C[C@H]([C@@]12CC[C</chem>	C ₂₂ H ₃₀ O ₆	390.47	28	0	0.82	3	6	0	101.12	71.06

Molecule	Canonical SMILES	Formula	MW	#Heavy atoms	#Aromatic heavy atoms	Fraction Csp3	#Rotatable bonds	#H-bond acceptors	#H-bond donors	MR	TPSA
	<chem>@]2(O1)COC=C2)C)C</chem>										
Luteolin	<chem>Oc1cc(O)c2c(c1)oc(cc2=O)c1ccc(c(c1)O)O</chem>	C ₁₅ H ₁₀ O ₆	286.24	21	16	0	1	6	4	76.0 ₁	111.13
Luteolin 7-O-B-glucoside-3-methyl ether	<chem>OC[C@H]1O[C@@H](O)C2cc(O)c3c(c2)oc(cc3=O)c2ccc(c(c2)OC)O)[C@@H](C)[C@H]1O</chem>	C ₂₂ H ₂₂ O ₁₁	462.4	33	16	0.32	5	11	6	112.6 ₆	179.28
Marubiin	<chem>C[C@@H]1C[C@@H]2OC(=O)[C@@]3([C@H]2[C@]([C@@]1(O)CCc1ccc1)(C)CC3)C</chem>	C ₂₀ H ₂₈ O ₄	332.43	24	5	0.75	3	4	1	91.4	59.67
Nepetaefolin	<chem>CC(=O)O[C@@H]1CC2(CO2)[C@@]2([C@]34[C@@H]1[C@](C)(CCC3)C(=O)OC</chem>	C ₂₂ H ₂₈ O ₇	404.45	29	0	0.82	2	7	0	100.13	83.59

Molecule	Canonical SMILES	Formula	MW	#Heavy atoms	#Aromatic heavy atoms	Fraction Csp3	#Rotatable bonds	#H-bond acceptors	#H-bond donors	MR	TPSA
	<chem>4)CC[C@@]1(O)C=COC1</chem>										
Stachydrine	<chem>[O-]C(=O)C1CCC[N+](C)C</chem>	C7H13NO2	143.18	10	0	0.86	1	2	0	41.35	40.13
Succinic Acid	<chem>OC(=O)CCC(=O)O</chem>	C4H6O4	118.09	8	0	0.5	3	4	2	24.89	74.6
Uracil	<chem>O=c1cc[nH]c(=O)[nH]1</chem>	C4H4N2O2	112.09	8	6	0	0	2	2	27.68	65.72
Vitexin	<chem>OC[C@H]1OC([C@@H]([C@H]([C@@H]1O)O)O)c1c(O)cc(c2c1oc(cc2=O)c1ccc(cc1)O)O</chem>	C21H20O10	432.38	31	16	0.29	3	10	7	106.61	181.05

Appendix 2: Lipophilicity prediction of phytochemicals from *L. leonurus*

Molecule	Canonical SMILES	Formula	iLOGP	XLOGP3	WLOGP	MLOGP	Silicos-IT Log P	Consensus Log P
6-Methoxyluteolin-4-methylether	<chem>COc1ccc(cc1O)c1cc(=O)c2c(o1)cc(c(c2O)OC)O</chem>	C17H14O7	2.45	3.07	2.59	-0.07	2.59	2.13
13R-premarrubin	<chem>O=C1O[C@H]2[C@H]3[C@]1(C)CCC[C@]3(C)[C@]1([C@@H](C2)C)CC[C@]2(O1)COC=C2</chem>	C20H28O4	3.16	3.34	3.6	2.9	3.37	3.27
13S-premarrubin	<chem>O=C1O[C@H]2[C@H]3[C@]1(C)CCC[C@]3(C)[C@]1([C@@H](C2)C)CC[C@@]2(O1)COC=C2</chem>	C20H28O4	3.11	3.34	3.6	2.9	3.37	3.26
13e-hydroxylabd-5(6) 8(9)-dien-7-on-16 15-olide	<chem>O=C1OCC(C1)(O)CCC1=C(C)C(=O)C=C2[C@]1(C)CCCC2(C)C</chem>	C20H28O4	2.7	2.86	3.49	2.72	4.53	3.26

Molecule	Canonical SMILES	Formula	iLOGP	XLOGP3	WLOGP	MLOGP	Silicos-IT Log P	Consensus Log P
14a-hydroxy-9a 13a-epoxylabd-5(6)-en-7-on-16 15-olide	<chem>O=C1C=C2C(C)(C)CCC[C@@]2([C@]2([C@@H]1C)CC[C@@]1(O2)COC(=O)[C@H]1O)C</chem>	C20H28O5	2.32	2.5	2.55	1.98	3.21	2.51
16epi-Leoleorin F	<chem>O[C@@H]1C[C@@H](C)C2([C@@]3(C1C(C)(C)CCC3)C)CC[C@]1(O2)COC1O</chem>	C20H34O4	3.1	3.42	3.25	2.75	2.94	3.09
Acteoside	<chem>OC[C@H]1O[C@@H](OCCc2cc(c(c2)O)O)[C@@H]([C@H]([C@@H]1OC(=O)/C=C/c1ccc(c(c1)O)O)O)[C@@H]1O[C@@H](C)[C@@H]([C@H]([C@H]1O)O)O</chem>	C29H36O15	2.15	-0.5	-1.12	-2.37	-1.14	-0.6
Apigenin	<chem>Oc1ccc(cc1)c1cc(=O)c2c(o1)cc(cc2O)O</chem>	C15H10O5	1.89	3.02	2.58	0.52	2.52	2.11

Molecule	Canonical SMILES	Formula	iLOGP	XLOGP3	WLOGP	MLOGP	Silicos-IT Log P	Consensus Log P
Apigenin-6-C-a-arabinoside-8-C-B-glucoside	<chem>OC[C@H]1OC([C@@H]([C@H]([C@@H]1O)O)c1c(O)c(C2O[C@H](CO)[C@H]([C@@H]([C@H]2O)O)O)c(c2c1oc(cc2=O)c1ccc(cc1)O)O</chem>	C27H30O15	1.73	-2.26	-3.04	-4.51	-1.8	-1.98
Apigenin-7-O-6-O-p-coumaryl-B-glucoside	<chem>O=C(OC[C@H]1O[C@@H](Oc2cc(O)c3c(c2)oc(cc3=O)c2ccc(c2)O)[C@@H]([C@H]([C@@H]1O)O)O)/C=C/c1ccc(cc1)O</chem>	C30H26O12	2.7	3.57	1.91	-0.56	2.03	1.93
Chrysoeriol	<chem>COc1cc(ccc1O)c1cc(=O)c2c(o1)cc(cc2O)O</chem>	C16H12O6	2.44	3.1	2.59	0.22	2.55	2.18
Compound X	<chem>O=C1OCC2(C1)CCC1(O2)[C@H](C)C[C@@H]2[C@@H]3[C@]1(C)CCC[C@]3(C)C(=O)O2</chem>	C20H28O5	2.61	2.85	3	2.89	3.45	2.96

Molecule	Canonical SMILES	Formula	iLOGP	XLOGP3	WLOGP	MLOGP	Silicos-IT Log P	Consensus Log P
Leoleorin A	<chem>O=C1C=C2C(C)(C)CCC[C@@]2(C([C@@H]1C)(O)CCc1cocc1)C</chem>	C20H28O3	3.14	3.93	4.3	2.71	4.61	3.74
Comosiin	<chem>OC[C@H]1OC(Oc2cc(O)c3c(c2)oc(cc3=O)c2cc(c(cc2)O)[C@@H]([C@H]([C@H]1O)O)O</chem>	C21H20O10	1.98	1.81	0.05	-1.61	0.35	0.52
Cynaroside	<chem>OC[C@H]1O[C@@H](Oc2cc(O)c3c(c2)oc(cc3=O)c2ccc(c(c2)O)O)[C@@H]([C@H]([C@H]1O)O)O</chem>	C21H20O11	1.76	1.46	-0.24	-2.1	-0.12	0.15
Dihydroxylp hytyl palmitate	<chem>CCCCCCCCC CCCCC(=O)O CC(C(CCCC(C CCC(CCCC(C) C)C)C)(O)C)O</chem>	C36H72O4	7.82	13.82	10.56	6.58	12.06	10.17

Molecule	Canonical SMILES	Formula	iLOGP	XLOGP3	WLOGP	MLOGP	Silicos-IT Log P	Consensus Log P
EDD	<chem>O=C1OCC[C@]21CC[C@@]1(O)[C@H](C)C[C@@H]2[C@@H]3[C@]1(C)CCC[C@]3(C)C(=O)O2</chem>	C20H28O5	2.8	3.28	3	2.89	3.45	3.08
Geniposidic acid	<chem>OC[C@H]1O[C@@H](O[C@@H]2OC=C([C@@H]3[C@H]2C(=CC3)CO)C(=O)O)[C@@H]([C@H]([C@@H]1O)O)O</chem>	C16H22O10	2	-2.67	-2.32	-2.1	-2.45	-1.51
Leoleorin B	<chem>O=C1C=C2C(C)(C)CCC[C@@]2(C(=C1)CCc1cocc1)C</chem>	C20H26O2	3.4	4.73	5.25	3.51	5.5	4.48
Leoleorin C	<chem>O[C@@H]1C[C@@H](C)C2([C@@]3(C1C(C)(C)CCC3)C)CC[C@]1(O2)COC1=O</chem>	C20H32O4	3.13	3.98	3.45	3.01	3.53	3.42

Molecule	Canonical SMILES	Formula	iLOGP	XLOGP3	WLOGP	MLOGP	Silicos-IT Log P	Consensus Log P
Leoleorin D	<chem>OCC[C@]1(CO)CCC2(O1)[C@H](C)C[C@H](C1[C@]2(C)CC1(C)C)O</chem>	C20H36O4	3.03	2.94	2.88	2.34	3.27	2.89
Leoleorin E	<chem>OC1OC[C@@]2(C)CCC1(O2)[C@H](C)C[C@H](C2[C@]1(C)CCCC2(C)C)O</chem>	C20H34O4	2.89	3.42	3.25	2.75	2.94	3.05
Leoleorin F	<chem>O[C@@H]1C[C@@H](C)C2[C@@]3(C1C(C)C)CCC3)C)CC[C@]1(O2)COC1O</chem>	C20H34O4	3.1	3.42	3.25	2.75	2.94	3.09
Leoleorin G	<chem>O=C1OC[C@@]2(C1)CCC1(O2)[C@H](C)C(=O)C=C2[C@]1(C)CCCC2(C)C</chem>	C20H28O4	2.79	3.05	3.58	2.81	4.11	3.27

Molecule	Canonical SMILES	Formula	iLOGP	XLOGP3	WLOGP	MLOGP	Silicos-IT Log P	Consensus Log P
Leoleorin H	<chem>OC[C@@]1(C)COC(=O)C)CC2(O1)[C@H](C)C(=O)C=C1[C@]2(C)CCCC1(C)C</chem>	C22H34O5	3.26	3.02	3.58	2.42	4.35	3.33
Leoleorin I	<chem>OCC[C@]1(CO)CCC2(O1)[C@H](C)C(=O)C=C1[C@]2(C)CC1(C)C</chem>	C20H32O4	2.73	2.45	3.01	2.09	3.85	2.83
Leoleorin J	<chem>OCC[C@]1(CO)CCC2(O1)[C@H](C)[C@@H](O)C=C1[C@]2(C)CCCC1(C)C</chem>	C20H34O4	1.76	2.4	2.8	2.2	3.26	2.49
Leonurun	<chem>CC(=O)OC[C@]12CCC[C@]3([C@@H]1[C@H](OC3=O)C[C@H]([C@@]12)CC[C@]2(O1)COC=C2)C</chem>	C22H30O6	3.3	2.69	3.14	2.42	3.2	2.95

Molecule	Canonical SMILES	Formula	iLOGP	XLOGP3	WLOGP	MLOGP	Silicos-IT Log P	Consensus Log P
Luteolin	<chem>Oc1cc(O)c2c(c1)oc(cc2=O)c1cc(c(c1)O)O</chem>	C15H10O6	1.86	2.53	2.28	-0.03	2.03	1.73
Luteolin 7-O-B-glucoside-3-methyl ether	<chem>OC[C@H]1O[C@@H](Oc2cc(O)c3c(c2)oc(cc3=O)c2ccc(c(c2)OC)O)[C@@H]([C@H]([C@@H]1O)O)O</chem>	C22H22O11	1.66	1.79	0.06	-1.89	0.42	0.41
Marrubin	<chem>C[C@@H]1C[C@H]2OC(=O)[C@@]3([C@H]2[C@]([C@@]1(O)CCc1ccc1)(C)CCC3)C</chem>	C20H28O4	3.17	3.73	3.72	2.76	3.96	3.47
Nepetaefolin	<chem>CC(=O)O[C@@H]1CC2(CO2)[C@@]2([C@]34[C@@H]1[C@](C)(CCC3)C(=O)OC4)CC[C@@]1(O2)C=CO1</chem>	C22H28O7	3.12	1.41	2.27	1.62	3.02	2.29

Molecule	Canonical SMILES	Formula	iLOGP	XLOGP3	WLOGP	MLOGP	Silicos-IT Log P	Consensus Log P
Stachydrine	<chem>[O-]C(=O)C1CCC[N+](C)C1</chem>	C7H13NO2	-1.2	0.4	-1.41	-3.33	0.02	-1.1
Succinic Acid	<chem>OC(=O)CCC(=O)O</chem>	C4H6O4	0.32	-0.59	-0.06	-0.54	-0.63	-0.3
Uracil	<chem>O=c1cc[nH]c(=O)[nH]1</chem>	C4H4N2O2	0.52	-1.07	-0.94	-0.8	1.35	-0.19
Vitexin	<chem>OC[C@H]1OC([C@@H]([C@H]([C@@H]1O)O)c1c(O)cc(c2c1oc(cc2=O)c1ccc(cc1)O)O</chem>	C21H20O10	1.63	0.21	-0.23	-2.02	0.33	-0.02

UNIVERSITY of the
WESTERN CAPE

Appendix 3: Water solubility prediction of Phyto-compounds from *L. leonurus*

Molecule	ESOL Log S	ESOL Solubility (mg/ml)	ESOL Solubility (mol/l)	ESOL Class	Ali Log S	Ali Solubility (mg/ml)	Ali Solubility (mol/l)	Ali Class	Silicos-IT LogSw	Silicos-IT Solubility (mg/ml)	Silicos-IT Solubility (mol/l)	Silicos-IT class
6-Methoxyluteolin-4-methylether	-4.12	2.52E-02	7.63E-05	Moderately soluble	-5.03	3.06E-03	9.26E-06	Moderately soluble	-4.63	7.71E-03	2.33E-05	Moderately soluble
13R-premarrubin	-4.01	3.28E-02	9.88E-05	Moderately soluble	-3.96	3.67E-02	1.10E-04	Soluble	-3.63	7.85E-02	2.36E-04	Soluble
13S-premarrubin	-4.01	3.28E-02	9.88E-05	Moderately soluble	-3.96	3.67E-02	1.10E-04	Soluble	-3.63	7.85E-02	2.36E-04	Soluble
13e-hydroxyabd-5(6) 8(9)-dien-7-on-16 15-olide	-3.5	1.04E-01	3.13E-04	Soluble	-3.85	4.65E-02	1.40E-04	Soluble	-4.73	6.25E-03	1.88E-05	Moderately soluble

Molecule	ESOL Log S	ESOL Solubility (mg/ml)	ESOL Solubility (mol/l)	ESOL Class	Ali Log S	Ali Solubility (mg/ml)	Ali Solubility (mol/l)	Ali Class	Silicos-IT LogS w	Silicos-IT Solubility (mg/ml)	Silicos-IT Solubility (mol/l)	Silicos-IT class
14a-hydroxy-9a 13a-epoxylabd-5(6)-en-7-on-16 15-olide	-3.58	9.26E-02	2.66E-04	Soluble	-3.67	7.37E-02	2.11E-04	Soluble	-3.75	6.13E-02	1.76E-04	Soluble
16epi-Leoleorin F	-4.09	2.73E-02	8.07E-05	Moderately soluble	-4.34	1.56E-02	4.60E-05	Moderately soluble	-3.2	2.15E-01	6.35E-04	Soluble
Acteoside	-2.87	8.36E-01	1.34E-03	Soluble	-4.18	4.09E-02	6.55E-05	Moderately soluble	-0.22	3.77E+02	6.04E-01	Soluble
Apigenin	-3.94	3.07E-02	1.14E-04	Soluble	-4.59	6.88E-03	2.55E-05	Moderately soluble	-4.4	1.07E-02	3.94E-05	Moderately soluble
Apigenin-6-C-a-arabinoside-8-C-B-glucoside	-2.05	5.25E+00	8.83E-03	Soluble	-2.9	7.46E-01	1.26E-03	Soluble	-0.27	3.19E+02	5.36E-01	Soluble
Apigenin-7-O-6-O-p-coumaryl-B-glucoside	-5.54	1.69E-03	2.91E-06	Moderately soluble	-7.38	2.42E-05	4.18E-08	Poorly soluble	-4.82	8.72E-03	1.51E-05	Moderately soluble
Chrysoeriol	-4.06	2.61E-02	8.69E-05	Moderately soluble	-4.87	4.04E-03	1.35E-05	Moderately soluble	-4.52	9.07E-03	3.02E-05	Moderately soluble

Molecule	ESOL Log S	ESOL Solubility (mg/ml)	ESOL Solubility (mol/l)	ESOL Class	Ali Log S	Ali Solubility (mg/ml)	Ali Solubility (mol/l)	Ali Class	Silicos-IT LogS w	Silicos-IT Solubility (mg/ml)	Silicos-IT Solubility (mol/l)	Silicos-IT class
Compound X	-3.8	5.58E-02	1.60E-04	Soluble	-3.81	5.43E-02	1.56E-04	Soluble	-3.97	3.70E-02	1.06E-04	Soluble
Leoleorin A	-4.24	1.82E-02	5.75E-05	Moderately soluble	-4.69	6.48E-03	2.05E-05	Moderately soluble	-5.53	9.40E-04	2.97E-06	Moderately soluble
Comosiin	-3.78	7.19E-02	1.66E-04	Soluble	-5	4.32E-03	9.99E-06	Moderately soluble	-2.69	8.77E-01	2.03E-03	Soluble
Cynaroside	-3.65	1.01E-01	2.26E-04	Soluble	-5.06	3.89E-03	8.67E-06	Moderately soluble	-2.1	3.55E+00	7.91E-03	Soluble
Dihydroxylph tyl palmitate	- 10.09	4.58E-08	8.05E-11	Insoluble	- 15.29	2.89E-13	5.08E-16	Insoluble	-10.44	2.08E-08	3.65E-11	Insoluble
EDD	-4.07	2.99E-02	8.58E-05	Moderately soluble	-4.25	1.94E-02	5.58E-05	Moderately soluble	-3.97	3.70E-02	1.06E-04	Soluble
Geniposidic acid	-0.15	2.66E+02	7.10E-01	Very soluble	-0.27	2.01E+02	5.38E-01	Very soluble	2.38	9.02E+04	2.41E+02	Soluble
Leoleorin B	-4.64	6.83E-03	2.29E-05	Moderately soluble	-5.09	2.40E-03	8.06E-06	Moderately soluble	-6.32	1.42E-04	4.75E-07	Poorly soluble
Leoleorin C	-4.43	1.24E-02	3.69E-05	Moderately soluble	-4.85	4.73E-03	1.41E-05	Moderately soluble	-3.89	4.31E-02	1.28E-04	Soluble

Molecule	ESOL Log S	ESOL Solubility (mg/ml)	ESOL Solubility (mol/l)	ESOL Class	Ali Log S	Ali Solubility (mg/ml)	Ali Solubility (mol/l)	Ali Class	Silicos-IT LogS w	Silicos-IT Solubility (mg/ml)	Silicos-IT Solubility (mol/l)	Silicos-IT class
Leoleorin D	-3.61	8.45E-02	2.48E-04	Soluble	-4.07	2.90E-02	8.50E-05	Moderately soluble	-3.5	1.09E-01	3.20E-04	Soluble
Leoleorin E	-4.09	2.73E-02	8.07E-05	Moderately soluble	-4.34	1.56E-02	4.60E-05	Moderately soluble	-3.2	2.15E-01	6.35E-04	Soluble
Leoleorin F	-4.09	2.73E-02	8.07E-05	Moderately soluble	-4.34	1.56E-02	4.60E-05	Moderately soluble	-3.2	2.15E-01	6.35E-04	Soluble
Leoleorin G	-3.82	5.00E-02	1.50E-04	Soluble	-3.82	5.02E-02	1.51E-04	Soluble	-4.57	8.93E-03	2.69E-05	Moderately soluble
Leoleorin H	-3.76	6.59E-02	1.74E-04	Soluble	-4.21	2.31E-02	6.10E-05	Moderately soluble	-4.79	6.07E-03	1.60E-05	Moderately soluble
Leoleorin I	-3.27	1.80E-01	5.35E-04	Soluble	-3.5	1.08E-01	3.20E-04	Soluble	-4.17	2.26E-02	6.71E-05	Moderately soluble
Leoleorin J	-3.25	1.89E-01	5.59E-04	Soluble	-3.51	1.05E-01	3.09E-04	Soluble	-3.48	1.13E-01	3.33E-04	Soluble
Leonurun	-3.76	6.82E-02	1.75E-04	Soluble	-3.83	5.71E-02	1.46E-04	Soluble	-3.68	8.18E-02	2.09E-04	Soluble
Luteolin	-3.71	5.63E-02	1.97E-04	Soluble	-4.51	8.84E-03	3.09E-05	Moderately soluble	-3.82	4.29E-02	1.50E-04	Soluble

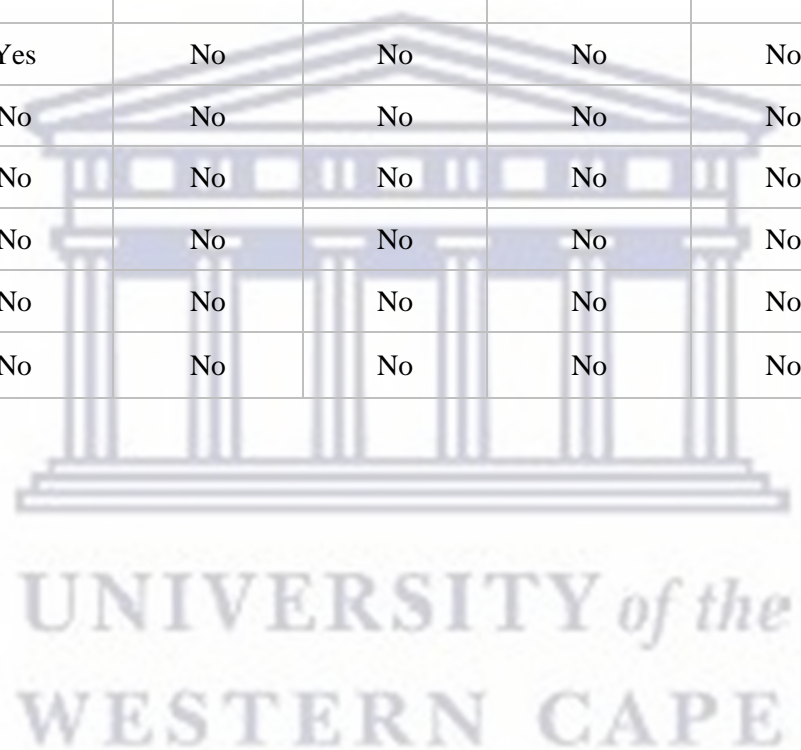
Molecule	ESOL Log S	ESOL Solubility (mg/ml)	ESOL Solubility (mol/l)	ESOL Class	Ali Log S	Ali Solubility (mg/ml)	Ali Solubility (mol/l)	Ali Class	Silicos-IT LogS w	Silicos-IT Solubility (mg/ml)	Silicos-IT Solubility (mol/l)	Silicos-IT class
Luteolin 7-O-B-glucoside-3-methyl ether	-3.86	6.33E-02	1.37E-04	Soluble	-5.17	3.10E-03	6.71E-06	Moderately soluble	-2.79	7.48E-01	1.62E-03	Soluble
Marrubin	-4.21	2.06E-02	6.21E-05	Moderately soluble	-4.67	7.03E-03	2.11E-05	Moderately soluble	-4.93	3.90E-03	1.17E-05	Moderately soluble
Nepetaefolin	-3.1	3.18E-01	7.87E-04	Soluble	-2.77	6.87E-01	1.70E-03	Soluble	-3.39	1.66E-01	4.11E-04	Soluble
Stachydrine	-0.91	1.75E+01	1.22E-01	Very soluble	-0.81	2.22E+01	1.55E-01	Very soluble	-0.94	1.65E+01	1.15E-01	Soluble
Succinic Acid	0	1.17E+02	9.94E-01	Very soluble	-0.51	3.69E+01	3.12E-01	Very soluble	0.61	4.86E+02	4.11E+00	Soluble
Uracil	-0.42	4.30E+01	3.84E-01	Very soluble	0.18	1.69E+02	1.51E+00	Highly soluble	-1.41	4.39E+00	3.92E-02	Soluble
Vitexin	-2.84	6.29E-01	1.46E-03	Soluble	-3.57	1.16E-01	2.68E-04	Soluble	-2.38	1.81E+00	4.20E-03	Soluble

Appendix 4: Pharmacokinetics predictions of Phyto-compounds in *L. leonurus*

Molecule	GI absorption	BBB permeant	P-gp substrate	CYP1A2 inhibitor	CYP2C19 inhibitor	CYP2C9 inhibitor	CYP2D6 inhibitor	CYP3A4 inhibitor	log Kp (cm/s)
6-Methoxyluteolin-4-methylether	High	No	No	Yes	No	Yes	Yes	Yes	-6.14
13R-premarrubin	High	Yes	No	No	No	No	No	No	-5.96
13S-premarrubin	High	Yes	No	No	No	No	No	No	-5.96
13e-hydroxyabd-5(6)8(9)-dien-7-on-16 15-olide	High	Yes	Yes	No	Yes	Yes	No	No	-6.3
14a-hydroxy-9a 13a-epoxyabd-5(6)-en-7-on-16 15-olide	High	Yes	Yes	No	No	No	No	No	-6.65
16epi-Leoleorin F	High	Yes	Yes	No	No	No	No	No	-5.94
Acteoside	Low	No	Yes	No	No	No	No	No	-10.46
Apigenin	High	No	No	Yes	No	No	Yes	Yes	-5.8
Apigenin-6-C-a-arabinoside-8-C-B-glucoside	Low	No	Yes	No	No	No	No	No	-11.53
Apigenin-7-O-6-O-p-coumaryl-B-glucoside	Low	No	No	No	No	Yes	No	No	-7.29

Molecule	GI absorption	BBB permeant	P-gp substrate	CYP1A2 inhibitor	CYP2C19 inhibitor	CYP2C9 inhibitor	CYP2D6 inhibitor	CYP3A4 inhibitor	log Kp (cm/s)
Chrysoeriol	High	No	No	Yes	No	Yes	Yes	Yes	-5.93
Compound X	High	Yes	No	No	No	No	No	No	-6.4
Leoleorin A	High	Yes	No	No	No	No	Yes	Yes	-5.44
Comosiin	Low	No	Yes	No	No	No	No	No	-7.65
Cynaroside	Low	No	Yes	No	No	No	No	No	-8
Dihydroxyphytyl palmitate	Low	No	Yes	No	No	No	No	No	0.04
EDD	High	Yes	No	No	No	No	No	No	-6.1
Geniposidic acid	Low	No	No	No	No	No	No	No	-10.48
Leoleorin B	High	Yes	No	No	Yes	Yes	No	Yes	-4.76
Leoleorin C	High	Yes	No	No	No	No	No	No	-5.53
Leoleorin D	High	Yes	Yes	No	No	No	No	No	-6.29
Leoleorin E	High	Yes	Yes	No	No	No	No	No	-5.94
Leoleorin F	High	Yes	Yes	No	No	No	No	No	-5.94
Leoleorin G	High	Yes	Yes	No	No	No	No	No	-6.16
Leoleorin H	High	Yes	Yes	No	No	No	No	No	-6.46
Leoleorin I	High	Yes	Yes	No	No	No	No	No	-6.61
Leoleorin J	High	Yes	Yes	No	No	No	No	No	-6.66
Leonurun	High	Yes	No	No	No	No	No	No	-6.77

Molecule	GI absorption	BBB permeant	P-gp substrate	CYP1A2 inhibitor	CYP2C19 inhibitor	CYP2C9 inhibitor	CYP2D6 inhibitor	CYP3A4 inhibitor	log Kp (cm/s)
Luteolin	High	No	No	Yes	No	No	Yes	Yes	-6.25
Luteolin 7-O-B-glucoside-3-methyl ether	Low	No	Yes	No	No	No	No	Yes	-7.85
Marrubin	High	Yes	No	No	No	No	Yes	No	-5.68
Nepetaefolin	High	No	No	No	No	No	No	No	-7.77
Stachydrine	Low	No	No	No	No	No	No	No	-6.89
Succinic Acid	High	No	No	No	No	No	No	No	-7.44
Uracil	High	No	No	No	No	No	No	No	-7.74
Vitexin	Low	No	No	No	No	No	No	No	-8.79



Appendix 5: Drug likeness prediction of Phytochemicals from *L. leonurus*

Molecule	Lipinski #violations	Ghose #violations	Veber #violations	Egan #violations	Muegge #violations	Bioavailability Score
6-Methoxyluteolin-4-methylether	0	0	0	0	0	0.55
13R-premarrubin	0	0	0	0	0	0.55
13S-premarrubin	0	0	0	0	0	0.55
13e-hydroxylabd-5(6)8(9)-dien-7-on-16 15-olide	0	0	0	0	0	0.55
14a-hydroxy-9a 13a-epoxylabd-5(6)-en-7-on-16 15-olide	0	0	0	0	0	0.55
16epi-Leoleorin F	0	0	0	0	0	0.55
Acteoside	3	4	2	1	4	0.17
Apigenin	0	0	0	0	0	0.55
Apigenin-6-C-a-arabinoside-8-C-B-glucoside	3	4	1	1	4	0.17
Apigenin-7-O-6-O-p-coumaryl-B-glucoside	3	2	1	1	3	0.17

Molecule	Lipinski #violations	Ghose #violations	Veber #violations	Egan #violations	Muegge #violations	Bioavailability Score
Chrysoeriol	0	0	0	0	0	0.55
Compound X	0	0	0	0	0	0.55
Leoleorin A	0	0	0	0	0	0.55
Comosiin	1	0	1	1	2	0.55
Cynaroside	2	0	1	1	3	0.17
Dihydroxyphytyl palmitate	2	4	1	1	2	0.17
EDD	0	0	0	0	0	0.55
Geniposidic acid	1	1	1	1	3	0.11
Leoleorin B	0	0	0	0	0	0.55
Leoleorin C	0	0	0	0	0	0.55
Leoleorin D	0	0	0	0	0	0.55
Leoleorin E	0	0	0	0	0	0.55
Leoleorin F	0	0	0	0	0	0.55
Leoleorin G	0	0	0	0	0	0.55
Leoleorin H	0	0	0	0	0	0.55
Leoleorin I	0	0	0	0	0	0.55

Molecule	Lipinski #violations	Ghose #violations	Veber #violations	Egan #violations	Muegge #violations	Bioavailability Score
Leoleorin J	0	0	0	0	0	0.55
Leonurun	0	0	0	0	0	0.55
Luteolin	0	0	0	0	0	0.55
Luteolin 7-O-B-glucoside-3-methyl ether	2	0	1	1	3	0.17
Marrubin	0	0	0	0	0	0.55
Nepetaefolin	0	0	0	0	0	0.55
Stachydrine	0	2	0	0	1	0.55
Succinic Acid	0	3	0	0	2	0.56
Uracil	0	4	0	0	2	0.55
Vitexin	1	0	1	1	2	0.55

UNIVERSITY of the
WESTERN CAPE

Appendix 6: Medicinal Chemistry prediction of Phytochemicals from L leonurus

Molecule	PAINS #alerts	Brenk #alerts	Leadlikeness #violations	Synthetic Accessibility
6-Methoxyluteolin-4-methylether	0	0	0	3.28
13R-premarrubin	0	0	0	5.85
13S-premarrubin	0	0	0	5.85
13e-hydroxylabd-5(6) 8(9)-dien-7-on-16 15-olide	0	0	0	4.44
14a-hydroxy-9a 13a-epoxylabd-5(6)-en-7-on-16 15-olide	0	0	0	5.72
16epi-Leoleorin F	0	0	0	6.23
Acteoside	1	2	2	6.37
Apigenin	0	0	0	2.96
Apigenin-6-C-a-arabinoside-8-C-B-glucoside	0	0	1	6.4
Apigenin-7-O-6-O-p-coumaryl-B-glucoside	0	1	3	5.81
Chrysoeriol	0	0	0	3.06
Compound X	0	1	0	5.59
Leoleorin A	0	0	1	4.63
Comosiin	0	0	1	5.12
Cynaroside	1	1	1	5.17
Dihydroxyphytyl palmitate	0	0	3	6.57

Molecule	PAINS #alerts	Brenk #alerts	Leadlikeness #violations	Synthetic Accessibility
EDD	0	1	0	5.52
Geniposidic acid	0	1	1	5.72
Leoleorin B	0	0	1	4.23
Leoleorin C	0	0	1	5.55
Leoleorin D	0	0	0	5.64
Leoleorin E	0	0	0	6.14
Leoleorin F	0	0	0	6.23
Leoleorin G	0	0	0	5.56
Leoleorin H	0	0	1	5.63
Leoleorin I	0	0	0	5.56
Leoleorin J	0	1	0	5.81
Leonurun	0	1	1	6.08
Luteolin	1	1	0	3.02
Luteolin 7-O-B-glucoside-3-methyl ether	0	0	1	5.28
Marrubin	0	0	1	4.86
Nepetaefolin	0	2	1	6.4
Stachydrine	0	1	1	1.72

Molecule	PAINS #alerts	Brenk #alerts	Leadlikeness #violations	Synthetic Accessibility
Succinic Acid	0	0	1	1.29
Uracil	0	0	1	1.35
Vitexin	0	0	1	5.12



Appendix 7: Metabolic reactions and the number of metabolites for *L. leonurus* compounds as predicted on biotransformer.ca and Qikprop

Compounds	No. of metabolic reactions (Qikprop)	No. of Metabolic Reactions (Biotransformer.ca)	No. of Metabolites (Biotransformer.ca)	Type of Metabolic Transformation (Biotransformer.ca)
6-Methoxyluteolin-4-methylether	5	3	3	Phase I
13R-premarrubin	1	0	0	0
13S-premarrubin	1	0	0	0
13e-hydroxyabd-5(6)8(9)-dien-7-on-16 15-olide	4	1	1	Phase II
14a-hydroxy-9a 13a-epoxyabd-5(6)-en-7-on-16 15-olide	3	2	2	Phase II

Compounds	No. of metabolic reactions (Qikprop)	No. of Metabolic Reactions (Biotransformer.ca)	No. of Metabolites (Biotransformer.ca)	Type of Metabolic Transformation (Biotransformer.ca)
16epi-Leoleorin F	2	2	2	Phase II
Acteoside	10	3	11	Phase II
Apigenin	3	2	2	Phase I
		2	3	Phase II
Apigenin-6-C-a-arabinoside-8-C-B-glucosid	15	6	11	Phase II
Apigenin-7-O-6-O-p-coumaryl-B-glucoside	6	1	3	Phase II
Chrysoeriol	4	3	2	Phase I

Compounds	No. of metabolic reactions (Qikprop)	No. of Metabolic Reactions (Biotransformer.ca)	No. of Metabolites (Biotransformer.ca)	Type of Metabolic Transformation (Biotransformer.ca)
		1	3	Phase II
Compound X	2	0	0	0
Leoleorin A	4	8	10	Phase I
		1	1	Phase II
Comosiin	6	2	3	Phase II
Cynaroside	7	5	6	Phase II
Dihydroxylphytyl palmitate	3	2	3	Phase II

Compounds	No. of metabolic reactions (Qikprop)	No. of Metabolic Reactions (Biotransformer.ca)	No. of Metabolites (Biotransformer.ca)	Type of Metabolic Transformation (Biotransformer.ca)
EDD	1	0	0	0
Geniposidic acid	8	3	8	Phase II
Leoleorin B	4	7	10	Phase I
Leoleorin C	2	2	2	Phase II
Leoleorin D	4	3	6	Phase II
Leoleorin E	2	2	2	Phase II
Leoleorin F	2	2	2	Phase II

Compounds	No. of metabolic reactions (Qikprop)	No. of Metabolic Reactions (Biotransformer.ca)	No. of Metabolites (Biotransformer.ca)	Type of Metabolic Transformation (Biotransformer.ca)
Leoleorin G	3	0	0	0
Leoleorin H	3	2	2	Phase II
Leoleorin I	4	2	4	Phase II
Leoleorin J	4	3	6	Phase II
Leonurun	1	0	0	0
Luteolin	4	1	1	Phase I
		4	6	Phase II






Compounds	No. of metabolic reactions (Qikprop)	No. of Metabolic Reactions (Biotransformer.ca)	No. of Metabolites (Biotransformer.ca)	Type of Metabolic Transformation (Biotransformer.ca)
Luteolin 7-O-?-glucoside-3-methyl ether	7	0	0	0
Marrubiin	3	1	1	Phase II
Nepetaefolin	1	1	1	Phase II
Stachydrine	9	0	0	0
Succinic Acid	2	0	0	0
Uracil	0	0	0	0
Vitexin	9	6	7	Phase II

Appendix 8: Pictorial results of the target predictions from swisstargetpredictions.ch

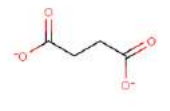
SwissTargetPrediction

Home | FAQ | Help | Download | Contact | Disclaimer

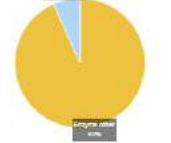
List of predicted targets
These targets have been predicted using the method described in:
Gteller D., Michielin O. & Zoete V. Shaping the interaction landscape of bioactive molecules. *Bioinformatics* (2013) 29:3073-3079.















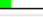
Retrieve data:     

Query Molecule



General Target Classes



Target	Common name	Uniprot ID	ChEMBL ID	Probability*	# sim. cmpds (3D / 2D)	Target Class
Epl nine homolog 1	EGU11	Q9GZT9	CHEMBL18007		2 / 2	Enzyme
Epl nine homolog 2 (by homology)	EGU12	Q9K930	CHEMBL3028		2 / 2	Enzyme
Tyrosyl-DNA phosphodiesterase 1	TDP1	Q8NUJ8	CHEMBL1075138		1 / 7	Enzyme
Histone deacetylase 3	HDAC3	O15379	CHEMBL1825		0 / 1	Enzyme
Histone deacetylase 1 (by homology)	HDAC1	Q13547	CHEMBL325		0 / 1	Enzyme
Histone deacetylase 2 (by homology)	HDAC2	Q82769	CHEMBL1937		0 / 1	Enzyme
Microtubule-associated protein tau	MAPT	P10030	CHEMBL1293224		0 / 4	Unclassified
Lysine-specific demethylase 9C	KDM9C	P41228	CHEMBL185176		0 / 3	Enzyme
Histone lysine demethylase PHF8	PHF8	Q9LUP1	CHEMBL1938212		0 / 4	Enzyme
Lysine-specific demethylase 2A	KDM2A	Q9Y2K7	CHEMBL1938210		0 / 4	Enzyme
Lysine-specific demethylase 5A (by homology)	KDM5A	P29376			0 / 3	Enzyme
Lysine-specific demethylase 5D (by homology)	KDM5D	Q8B100			0 / 3	Enzyme
Lysine-specific demethylase 5B (by homology)	KDM5B	Q9UGL1			0 / 3	Enzyme
Lysine-specific demethylase PHF2 (by homology)	PHF2	O75151			0 / 4	Enzyme
Lysine-specific demethylase 7 (by homology)	JHDM1D	Q82MT4	CHEMBL193177		0 / 4	Enzyme

* Probabilities have been computed based on a cross-validation. They may therefore not represent the actual probability of success for any new molecule (see FAQ).






Swiss Institute of Bioinformatics - © 2013

Succinic Acid

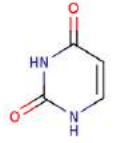
SwissTargetPrediction

Home | FAQ | Help | Download | Contact | Disclaimer

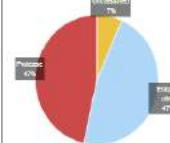
List of predicted targets
These targets have been predicted using the method described in:
Gteller D., Michielin O. & Zoete V. Shaping the interaction landscape of bioactive molecules. *Bioinformatics* (2013) 29:3073-3079.










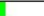





Retrieve data:     

Query Molecule



General Target Classes



Target	Common name	Uniprot ID	ChEMBL ID	Probability*	# sim. cmpds (3D / 2D)	Target Class
Microtubule-associated protein tau	MAPT	P10636	CHEMBL1293224		2 / 2	Unclassified
Thymidylate synthase (by homology)	TYMS	P04918	CHEMBL1932		1 / 1	Enzyme
Thymidine phosphorylase	TYMP	P18971	CHEMBL3106		1 / 5	Enzyme
Dihydropyrimidine dehydrogenase [NADPH]	DPYD	Q12882	CHEMBL5172		0 / 1	Enzyme
Tyrosyl-DNA phosphodiesterase 1	TDP1	Q8NUJ8	CHEMBL1075138		1 / 1	Enzyme
Poly [ADP-ribose] polymerase-1	PARP1	P09674	CHEMBL2106		0 / 10	Enzyme
Guanine deaminase	GDA	Q9Y2T3	CHEMBL3129		0 / 1	Enzyme
Autolysin on peptide fragment 1	F2	P00734	CHEMBL204		1 / 0	Serine Protease
Complex	CAP1(H)/CAP1(S)	P07884/P04052	CHEMBL2111357		1 / 0	Cysteine Protease
Caspase-3 subunit p12	CASP3	P42574	CHEMBL2324		1 / 0	Cysteine Protease
Caspase-2 subunit p18	CASP2	P42676	CHEMBL4894		1 / 0	Cysteine Protease
Caspase-7 subunit p20	CASP7	P55210	CHEMBL3408		1 / 0	Cysteine Protease
Caspase-6 subunit p18	CASP6	P55212	CHEMBL5006		1 / 0	Cysteine Protease
Caspase-8 subunit p18	CASP8	Q14790	CHEMBL3778		1 / 0	Cysteine Protease
Ribonuclease H1	RNASEH1	O00930	CHEMBL5593		0 / 1	Enzyme

* Probabilities have been computed based on a cross-validation. They may therefore not represent the actual probability of success for any new molecule (see FAQ).

Swiss Institute of Bioinformatics - © 2013

Uracil

SIB
Swiss Institute of Bioinformatics






SwissTargetPrediction

Home FAQ Help Download Contact Disclaimer

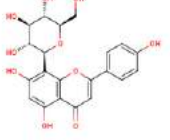
List of predicted targets

These targets have been predicted using the method described in:

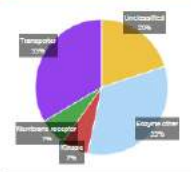
Gleliet D., Michelin O. & Zoete V. Shaping the interaction landscape of bioactive molecules. *Bioinformatics* (2013) 29:3673-3679.











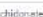




Retrieve data:     

Query Molecule



General Target Classes



Target	Common name	Uniprot ID	ChEMBL ID	Probability*	# sim. cmpds (3D / 2D)	Target Class
Microtubule-associated protein tau	MAPT	P10030	CHEMBL1283224		7 / 27	Unclassified
Tyrosyl-DNA phosphodiesterase 1	TDP1	Q9N3W8	CHEMBL1075138		14 / 11	Enzyme
Dual specificity tyrosine phosphorylation-regulated kinase 1A	DYRK1A	Q13027	CHEMBL2292		11 / 13	Ser_Thr_Tyr Kinase
Aldose reductase family 1 member B10 (by homology)	AKR1B10	Q60218	CHEMBL5983		12 / 50	Enzyme
Aldose reductase (by homology)	AKR1B1	P15121	CHEMBL1900		12 / 50	Enzyme
Aldose reductase family 1 member B16 (by homology)	AKR1B15	C5J8Z8			12 / 50	Enzyme
Adenosine receptor A1 (by homology)	ADORA1	P30642	CHEMBL226		204 / 12	Membrane receptor
Sodium/glucose cotransporter 1	SLC5A1	P13800	CHEMBL4979		90 / 4	Transporter
Sodium/glucose cotransporter 2	SLC5A2	P31639	CHEMBL3884		90 / 4	Transporter
Low affinity sodium/glucose cotransporter	SLC5A4	Q5N9Y1	CHEMBL1770047		90 / 4	Unclassified
Sodium/glucose cotransporter 6 (by homology)	SLC5A10	A0PJK1			90 / 4	Transporter
Sodium/myo-inositol cotransporter (by homology)	SLC5A3	P63794			90 / 4	Transporter
Sodium/glucose cotransporter 4 (by homology)	SLC5A9	Q2N3A0			90 / 4	Transporter
Sodium/myo-inositol cotransporter 2 (by homology)	SLC5A11	Q5WVX8	CHEMBL1744524		90 / 4	Unclassified
Alcohol dehydrogenase (NADP(+)) (by homology)	AKR1A1	P14550	CHEMBL2248		6 / 6	Enzyme

* Probabilities have been computed based on a cross-validation. They may therefore not represent the actual probability of success for any new molecule (see FAQ).

Swiss Institute of Bioinformatics - © 2013

Vitexin

SIB
Swiss Institute of Bioinformatics






SwissTargetPrediction

Home FAQ Help Download Contact Disclaimer

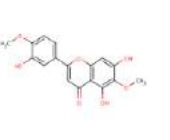
List of predicted targets

These targets have been predicted using the method described in:

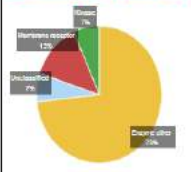
Gleliet D., Michelin O. & Zoete V. Shaping the interaction landscape of bioactive molecules. *Bioinformatics* (2013) 29:3673-3679.



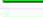












Retrieve data:     

Query Molecule



General Target Classes



Target	Common name	Uniprot ID	ChEMBL ID	Probability*	# sim. cmpds (3D / 2D)	Target Class
Aldose reductase (by homology)	AKR1B1	P15121	CHEMBL1900		8 / 50	Enzyme
Aldose reductase family 1 member B15 (by homology)	AKR1B15	C5J8Z8			8 / 50	Enzyme
Aldose reductase family 1 member B10 (by homology)	AKR1B10	Q60218	CHEMBL5983		8 / 50	Enzyme
Microtubule associated protein tau	MAPT	P10030	CHEMBL1283224		19 / 92	Unclassified
Xanthine dehydrogenase/oxidase	XDH	P47989	CHEMBL1928		1 / 15	Enzyme
Aldehyde oxidase (by homology)	AOX1	Q6R278	CHEMBL3257		1 / 15	Enzyme
FAD-linked xylitol oxidase ALR	OFER	P55789	CHEMBL1741189		2 / 4	Enzyme
Adenosine receptor A1 (by homology)	ADORA1	P30642	CHEMBL226		3 / 24	Membrane receptor
Dual specificity tyrosine-phosphorylation-regulated kinase 1A (by homology)	DYRK1A	Q13027	CHEMBL2292		2 / 20	Ser_Thr_Tyr Kinase
Adenosine receptor A2a (by homology)	ADORA2A	P28274	CHEMBL221		2 / 15	Membrane receptor
Arachidonate 5-lipoxygenase	ALOX5	P09917	CHEMBL215		3 / 55	Enzyme
Arachidonate 15-lipoxygenase (by homology)	ALOX15	P16050	CHEMBL2903		3 / 55	Enzyme
Arachidonate 12-lipoxygenase, 12S-type (by homology)	ALOX12	P18054	CHEMBL3897		3 / 55	Enzyme
Arachidonate 15-lipoxygenase B (by homology)	ALOX15B	Q15296	CHEMBL2457		3 / 55	Enzyme
Arachidonate 12-lipoxygenase, 12R-type (by homology)	ALOX12B	O75342			3 / 54	Enzyme

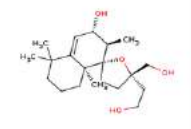
* Probabilities have been computed based on a cross-validation. They may therefore not represent the actual probability of success for any new molecule (see FAQ).

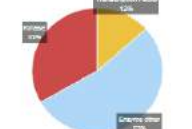
Swiss Institute of Bioinformatics - © 2013


6-Methoxyluteolin-4-methylether









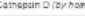


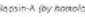



SwissTargetPrediction
 Swiss Institute of Bioinformatics
 Home FAQ Help Download Contact Disclaimer

List of predicted targets
 These targets have been predicted using the method described in:
 Gleiter D., Michielin O. & Zoete V. Shaping the interaction landscape of bioactive molecules, *Bioinformatics* (2013):29:3073-3079.

Query Molecule


General Target Classes


Retrieve data: 

Target	Common name	Uniprot ID	ChEMBL ID	Probability*	# sim. cmpds (30 / 20)	Target Class
Androgen receptor	AR	P10276	CHEMBL1871		61 / 35	Transcription Factor
Tyrosyl-DNA phosphodiesterase 1	TDP1	Q8NUW8	CHEMBL1070138		41 / 8	Enzyme
Protein kinase C gamma type (by homology)	PRKCG	P00129	CHEMBL2998		20 / 171	Ser_Thr Kinase
Protein kinase C beta type (by homology)	PRKCB	P06771	CHEMBL3045		28 / 171	Ser_Thr Kinase
Protein kinase C alpha type	PRKCA	P17252	CHEMBL299		28 / 171	Ser_Thr Kinase
Protein kinase C theta type (by homology)	PRKCQ	Q04759	CHEMBL3920		27 / 174	Ser_Thr Kinase
Protein kinase C delta type regulatory subunit	PRKCD	Q06855	CHEMBL2996		27 / 174	Ser_Thr Kinase
DNA polymerase alpha catalytic subunit	POLA1	P09894	CHEMBL1828		10 / 8	Enzyme
3-hydroxy-3-methylglutaryl-coenzyme A reductase	HMGCR	P04035	CHEMBL402		40 / 82	Enzyme
Quinone oxidoreductase (by homology)	GRYZ	Q08267	CHEMBL5116		7 / 21	Enzyme
Mineralocorticoid receptor	NR3C2	P08235	CHEMBL1994		52 / 5	Transcription Factor
cAMP-specific 3',5'-cyclic phosphodiesterase 1B	PDE1B	Q07343	CHEMBL276		5 / 3	Enzyme
cAMP-specific 3',5'-cyclic phosphodiesterase 4D	PDE4D	Q08499	CHEMBL298		5 / 3	Enzyme
cAMP-specific 3',5'-cyclic phosphodiesterase 4A (by homology)	PDE4A	P27815	CHEMBL254		5 / 3	Enzyme
cAMP-specific 3',5'-cyclic phosphodiesterase 4C (by homology)	PDE4C	Q08493	CHEMBL281		5 / 3	Enzyme

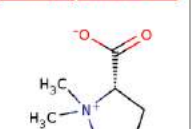
* Probabilities have been computed based on a cross-validation. They may therefore not represent the actual probability of success for any new molecule (see FAQ).

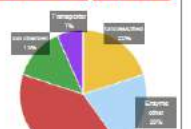
Swiss Institute of Bioinformatics - © 2013


Leoleorin J

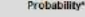

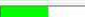












SwissTargetPrediction
 Swiss Institute of Bioinformatics
 Home FAQ Help Download Contact Disclaimer

List of predicted targets
 These targets have been predicted using the method described in:
 Gleiter D., Michielin O. & Zoete V. Shaping the interaction landscape of bioactive molecules, *Bioinformatics* (2013):29:3073-3079.

Query Molecule


General Target Classes


Retrieve data: 

Target	Common name	Uniprot ID	ChEMBL ID	Probability*	# sim. cmpds (30 / 20)	Target Class
Muscleblind-like protein 1	MBNL1	Q5NR56	CHEMBL1298317		1 / 2	Unclassified
Muscleblind-like protein 2 (by homology)	MBNL2	Q0V2F2			1 / 2	Unclassified
Muscleblind-like protein 3 (by homology)	MBNL3	Q8NUK0			1 / 2	Unclassified
Tyrosyl-DNA phosphodiesterase 1	TDP1	Q8NUW8	CHEMBL1070138		1 / 5	Enzyme
Cholinesterase (by homology)	BCHE	P00270	CHEMBL1914		1 / 8	Enzyme
Acetylcholinesterase	AChE	P22303	CHEMBL220		1 / 8	Enzyme
Renin	REN	P00797	CHEMBL280		0 / 19	Aspartic Protease
Cathepsin D (by homology)	CTSD	P07329	CHEMBL2681		0 / 19	Aspartic Protease
Angiotensin-converting enzyme	ACE	P12821	CHEMBL1908		0 / 80	Metallo Protease
Angiotensin-converting enzyme 2 (by homology)	ACE2	Q9BYF1	CHEMBL3726		0 / 80	Metallo Protease
Napsin-A (by homology)	NAPGA	Q98009			0 / 19	Aspartic Protease
Angiotensin-converting enzyme (by homology)	ACE	L7MLH0			0 / 80	Metallo Protease
Glutamate receptor ionotropic, kainate 1 (by homology)	GRK1	P39035	CHEMBL1918		0 / 13	Ion channel
Excitatory amino acid transporter 2	SLC1A2	P43004	CHEMBL4973		0 / 6	Transporter
Glutamate receptor ionotropic, kainate 2 (by homology)	GRK2	Q13002	CHEMBL2483		0 / 13	Ion channel

* Probabilities have been computed based on a cross-validation. They may therefore not represent the actual probability of success for any new molecule (see FAQ).

Swiss Institute of Bioinformatics - © 2013

Stachydrine

SwissTargetPrediction

Swiss Institute of Bioinformatics

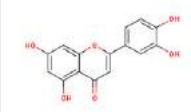
Home FAQ Help Download Contact Disclaimer

List of predicted targets


These targets have been predicted using the method described in:


Gleiter D, Michielin O, & Zoete V. Shaping the interaction landscape of bioactive molecules. *Bioinformatics* (2013) 29:3073-3079.
















Query Molecule



General Target Classes



Retrieve data: 

Target	Common name	Uniprot ID	ChEMBL ID	Probability*	# sim. empds (3D / 2D)	Target Class
22 kDa interstitial collagenase (by homology)	MMP1	P03980	CHEMBL332		4 / 2	Metallo Protease
Cytochrome P450 1A2 (by homology)	CYP1A2	P05177	CHEMBL3990		9 / 13	Enzyme
PEX	MMP2	P08263	CHEMBL333		4 / 2	Metallo Protease
Stromelysin-1 (by homology)	MMP3	P08264	CHEMBL283		4 / 2	Metallo Protease
67 kDa matrix metalloproteinase-8	MMP8	P14780	CHEMBL321		4 / 2	Metallo Protease
Aldose reductase (by homology)	AKR1B1	P15121	CHEMBL1900		19 / 68	Enzyme
Amine oxidase (flavin-containing) A	MAOA	P21387	CHEMBL1981		7 / 31	Enzyme
Amine oxidase (flavin-containing) B (by homology)	MAOB	P27338	CHEMBL2038		7 / 31	Enzyme
ADP-ribosyl cyclase 1	CD38	P28907	CHEMBL4080		1 / 2	Enzyme
Adenosine receptor A1 (by homology)	ADORA1	P30542	CHEMBL228		0 / 23	Membrane receptor
Macrophage metallo elastase	MMP12	P38900	CHEMBL4393		4 / 2	Metallo Protease
Collagenase 3 (by homology)	MMP13	P45452	CHEMBL230		4 / 2	Metallo Protease
Xanthine dehydrogenase/oxidase	XDH	P47989	CHEMBL1929		9 / 14	Enzyme
Lactylglutathione lyase	GLO1	Q04700	CHEMBL2424		3 / 4	Enzyme
Lysine-tRNA ligase	WARS	Q15048	CHEMBL5578		4 / 3	Enzyme

* Probabilities have been computed based on a cross-validation. They may therefore not represent the actual probability of success for any new molecule (see FAQ).

Swiss Institute of Bioinformatics - © 2013

Luteolin

SwissTargetPrediction

Swiss Institute of Bioinformatics

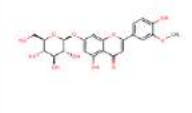
Home FAQ Help Download Contact Disclaimer

List of predicted targets

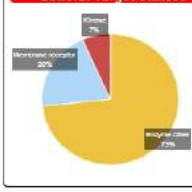
These targets have been predicted using the method described in:


Gleiter D, Michielin O, & Zoete V. Shaping the interaction landscape of bioactive molecules. *Bioinformatics* (2013) 29:3073-3079.






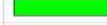









Query Molecule



General Target Classes



Retrieve data: 

Target	Common name	Uniprot ID	ChEMBL ID	Probability*	# sim. empds (3D / 2D)	Target Class
Tyrosyl-DNA phosphodiesterase 1	TDP1	Q9NUW8	CHEMBL1675138		8 / 17	Enzyme
Lysine-specific demethylase 5A	KDM5A	Q78164	CHEMBL5990		1 / 3	Enzyme
Lysine-specific demethylase 4B (by homology)	KDM4B	Q94953			1 / 3	Enzyme
Lysine-specific demethylase 4C (by homology)	KDM4C	Q9H3R0	CHEMBL5176		1 / 3	Enzyme
Aldo-keto reductase family 1 member B10 (by homology)	AKR1B10	Q00218	CHEMBL5983		13 / 07	Enzyme
Aldose reductase	AKR1B1	P15121	CHEMBL1900		15 / 67	Enzyme
Aldo-keto reductase family 1 member B15 (by homology)	AKR1B15	Q5JR26			15 / 67	Enzyme
Adenosine receptor A1 (by homology)	ADORA1	P30542	CHEMBL228		45 / 17	Membrane receptor
Xanthine dehydrogenase/oxidase	XDH	P47989	CHEMBL1929		2 / 13	Enzyme
Aldehyde oxidase (by homology)	AOX1	Q06278	CHEMBL3257		2 / 13	Enzyme
Dual specificity tyrosine-phosphatase-regulated kinase 1A (by homology)	DYRK1A	Q13827	CHEMBL2092		7 / 13	Ser_Thr_Tyr Kinase
Alpha-2A adrenergic receptor	ADRA2A	P08913	CHEMBL1907		2 / 2	Membrane receptor
Alpha-2C adrenergic receptor	ADRA2C	P18820	CHEMBL1916		2 / 2	Membrane receptor
Alcohol dehydrogenase [NADP(+)] (by homology)	AKR1A1	P14550	CHEMBL3246		5 / 9	Enzyme
1,5-anhydro-D-fructose reductase (by homology)	AKR1E2	Q96UD9			5 / 9	Enzyme

* Probabilities have been computed based on a cross-validation. They may therefore not represent the actual probability of success for any new molecule (see FAQ).





Swiss Institute of Bioinformatics - © 2013

Luteolin 7-O-B-glucoside-3-methyl ether

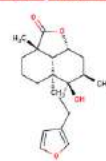
SIB Swiss Institute of Bioinformatics
 Home FAQ Help Download Contact Disclaimer

SwissTargetPrediction

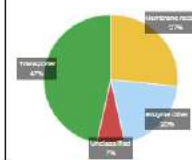
List of predicted targets
 These targets have been predicted using the method described in:
 Cfellier D., Michelin O. & Zoete V. Shaping the interaction landscape of bioactive molecules. *Bioinformatics* 20(12):29-3075-3079.
















Retrieve data:    

Query Molecule



General Target Classes



Target	Common name	Uniprot ID	ChEMBL ID	Probability*	# sim. cmpds (3D / 2D)	Target Class
Mu-type opioid receptor	OPRM1	P35372	CHEMBL233		303 / 190	Membrane receptor
Delta-type opioid receptor (by homology)	OPRD1	P41143	CHEMBL258		365 / 190	Membrane receptor
Kappa-type opioid receptor	OPRK1	P41145	CHEMBL237		310 / 190	Membrane receptor
Nocodolin receptor	OPRL1	P41146	CHEMBL2014		290 / 180	Membrane receptor
Macrophage migration inhibitory factor	MIIF	P14174	CHEMBL2085		1 / 1	Enzyme
Tyrosyl-DNA phosphodiesterase 1	TDP1	Q5N1U8	CHEMBL1075138		40 / 4	Enzyme
Microtubule-associated protein tau	MAPT	P10806	CHEMBL1293224		91 / 1	Unclassified
Sodium-dependent noradrenaline transporter (by homology)	SLOC82	P22975	CHEMBL222		209 / 13	Transporter
Sodium-dependent serotonin transporter (by homology)	SLOC84	P31045	CHEMBL225		278 / 13	Transporter
Sodium-dependent dopamine transporter	SLOC83	Q01909	CHEMBL238		299 / 13	Transporter
Cytochrome P400 19A1	CYP19A1	P11011	CHEMBL1978		45 / 1	Enzyme
Sodium- and chloride-dependent glycine transporter 1 (by homology)	SLOC88	P48007	CHEMBL2337		190 / 13	Transporter
Sodium-dependent protein transporter (by homology)	SLOC87	Q99884			190 / 13	Transporter
Sodium- and chloride-dependent neutral and basic amino acid transporter B(0+)	SLOC814	Q5JN78			190 / 13	Transporter
Sodium- and chloride-dependent glycine transporter 2 (by homology)	SLOC85	Q9Y345	CHEMBL3050		190 / 13	Transporter

* Probabilities have been computed based on a cross-validation. They may therefore not represent the actual probability of success for any new molecule (see FAQ).





Swiss Institute of Bioinformatics - © 2013

Marubiin

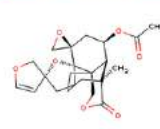
SIB Swiss Institute of Bioinformatics
 Home FAQ Help Download Contact Disclaimer

SwissTargetPrediction

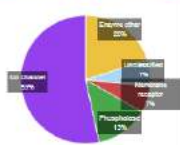
List of predicted targets
 These targets have been predicted using the method described in:
 Cfellier D., Michelin O. & Zoete V. Shaping the interaction landscape of bioactive molecules. *Bioinformatics* 20(12):29-3075-3079.
















Retrieve data:    

Query Molecule



General Target Classes



Target	Common name	Uniprot ID	ChEMBL ID	Probability*	# sim. cmpds (3D / 2D)	Target Class
Tyrosyl-DNA phosphodiesterase 1	TDP1	Q5N1U8	CHEMBL1075138		09 / 1	Enzyme
Microtubule-associated protein tau	MAPT	P10030	CHEMBL1293224		105 / 13	Unclassified
Platelet-activating factor receptor	PTAFR	P20105	CHEMBL250		22 / 7	Membrane receptor
Prostaglandin G/H synthase 2	PTGS2	P25364	CHEMBL230		4 / 8	Enzyme
Prostaglandin G/H synthase 1 (by homology)	PTGS1	P23219	CHEMBL221		4 / 8	Enzyme
M-phase inducer phosphatase 2	CDC25B	P30305	CHEMBL4894		2 / 12	Phosphatase
M-phase inducer phosphatase 1 (by homology)	CDC25A	P30304	CHEMBL5775		2 / 12	Phosphatase
Potassium voltage-gated channel subfamily A member 3	KCNJ3	P22001	CHEMBL4523		5 / 2	Ion channel
Potassium voltage-gated channel subfamily A member 5	KCNJ5	P22480	CHEMBL4508		5 / 2	Ion channel
Potassium voltage-gated channel subfamily A member 2 (by homology)	KCNJ2	P19389	CHEMBL2058		5 / 2	Ion channel
Potassium voltage-gated channel subfamily A member 6 (by homology)	KCNJ6	P17893	CHEMBL2779		5 / 2	Ion channel
Potassium voltage-gated channel subfamily A member 4 (by homology)	KCNJ4	P22459	CHEMBL4205		5 / 2	Ion channel
Potassium voltage-gated channel subfamily A member 1 (by homology)	KCNJ1	Q09470	CHEMBL2309		5 / 2	Ion channel
Potassium voltage-gated channel subfamily A member 10 (by homology)	KCNJ10	Q16322			5 / 2	Ion channel
Potassium voltage-gated channel subfamily A member 7 (by homology)	KCNJ7	Q98RP9	CHEMBL2773		5 / 2	Ion channel





* Probabilities have been computed based on a cross-validation. They may therefore not represent the actual probability of success for any new molecule (see FAQ).

Nepetaefolin

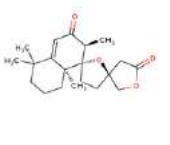
SIB Swiss Institute of Bioinformatics
 Home FAQ Help Download Contact Disclaimer

Swiss targetPrediction


List of predicted targets
 These targets have been predicted using the method described in:
 Gfeller D., Michielin O. & Zoete V. **Shaping the interaction landscape of bioactive molecules**, *Bioinformatics* (2013) 29:3073-3079.

Retrieves data:    

Query Molecule



General Target Classes



Target	Common name	Uniprot ID	CHEMBL ID	Probability*	# sim. omps (3D / 2D)	Target Class
Protein kinase C gamma type (by homology)	PRKCG	P06129	CHEMBL2938	<div style="width: 100%; height: 10px; background-color: green;"></div>	3 / 244	Ser_Thr Kinase
Protein kinase C beta type (by homology)	PRKCB	P05771	CHEMBL3046	<div style="width: 100%; height: 10px; background-color: green;"></div>	3 / 244	Ser_Thr Kinase
Protein kinase C alpha type	PRKCA	P17252	CHEMBL289	<div style="width: 100%; height: 10px; background-color: green;"></div>	3 / 244	Ser_Thr Kinase
Complex	FNTA/FNTB	P49354/P49358	CHEMBL2894108	<div style="width: 100%; height: 10px; background-color: green;"></div>	109 / 7	Enzyme
Complex	PGG1B/FNTA	P2309/P49254	CHEMBL295104	<div style="width: 100%; height: 10px; background-color: green;"></div>	89 / 1	Enzyme
Microtubule-associated protein tau	MAPT	P10636	CHEMBL1292224	<div style="width: 100%; height: 10px; background-color: green;"></div>	170 / 61	Unclassified
Androgen receptor	AR	P10275	CHEMBL1071	<div style="width: 100%; height: 10px; background-color: green;"></div>	9 / 26	Transcription Factor
Mineralocorticoid receptor	NR3C2	P08235	CHEMBL1994	<div style="width: 100%; height: 10px; background-color: green;"></div>	16 / 28	Transcription Factor
Estrogen receptor	ESR1	P03372	CHEMBL206	<div style="width: 100%; height: 10px; background-color: green;"></div>	6 / 4	Transcription Factor
Estrogen receptor beta	ESR2	Q82731	CHEMBL242	<div style="width: 100%; height: 10px; background-color: green;"></div>	6 / 4	Transcription Factor
Prostaglandin G/H synthase 1 (by homology)	PTGS1	P23219	CHEMBL231	<div style="width: 100%; height: 10px; background-color: green;"></div>	30 / 15	Enzyme
Prostaglandin G/H synthase 2	PTGS2	P38354	CHEMBL230	<div style="width: 100%; height: 10px; background-color: green;"></div>	30 / 15	Enzyme
Glucocorticoid receptor	NR3C1	P04150	CHEMBL2034	<div style="width: 100%; height: 10px; background-color: green;"></div>	16 / 24	Transcription Factor
Subkinase-K receptor	TACR2	P21452	CHEMBL2307	<div style="width: 100%; height: 10px; background-color: green;"></div>	3 / 1	Membrane receptor
Sodium-dependent neuronal nitrate transporter	SLC8A2	P23875	CHEMBL222	<div style="width: 100%; height: 10px; background-color: green;"></div>	28 / 4	Transporter

* Probabilities have been computed based on a cross-validation. They may therefore not represent the actual probability of success for any new molecule (see FAQ).





Swiss Institute of Bioinformatics © 2013

Leoleorin G

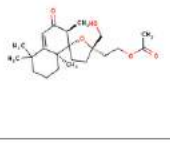
SIB Swiss Institute of Bioinformatics
 Home FAQ Help Download Contact Disclaimer

Swiss targetPrediction


List of predicted targets
 These targets have been predicted using the method described in:
 Gfeller D., Michielin O. & Zoete V. **Shaping the interaction landscape of bioactive molecules**, *Bioinformatics* (2013) 29:3073-3079.

Retrieves data:    

Query Molecule



General Target Classes



Target	Common name	Uniprot ID	CHEMBL ID	Probability*	# sim. omps (3D / 2D)	Target Class
Androgen receptor	AR	P10275	CHEMBL1071	<div style="width: 100%; height: 10px; background-color: green;"></div>	9 / 24	Transcription Factor
Protein kinase C gamma type	PRKCG	P06129	CHEMBL2938	<div style="width: 100%; height: 10px; background-color: green;"></div>	125 / 227	Ser_Thr Kinase
Protein kinase C beta type	PRKCB	P05771	CHEMBL3046	<div style="width: 100%; height: 10px; background-color: green;"></div>	125 / 227	Ser_Thr Kinase
Protein kinase C alpha type	PRKCA	P17252	CHEMBL289	<div style="width: 100%; height: 10px; background-color: green;"></div>	125 / 227	Ser_Thr Kinase
Protein kinase C delta type	PRKCD	Q04759	CHEMBL3929	<div style="width: 100%; height: 10px; background-color: green;"></div>	128 / 230	Ser_Thr Kinase
Protein kinase C delta type regulatory subunit	PRKCD	Q05555	CHEMBL2896	<div style="width: 100%; height: 10px; background-color: green;"></div>	120 / 230	Ser_Thr Kinase
3-hydroxy-3-methylglutaryl-coenzyme A reductase	HMGCR	P04026	CHEMBL402	<div style="width: 100%; height: 10px; background-color: green;"></div>	150 / 94	Enzyme
Mineralocorticoid receptor	NR3C2	P08235	CHEMBL1994	<div style="width: 100%; height: 10px; background-color: green;"></div>	62 / 33	Transcription Factor
Microtubule-associated protein tau	MAPT	P10636	CHEMBL1293224	<div style="width: 100%; height: 10px; background-color: green;"></div>	69 / 45	Unclassified
Quinone oxidoreductase (by homology)	CRYZ	Q08237	CHEMBL1116	<div style="width: 100%; height: 10px; background-color: green;"></div>	2 / 24	Enzyme
Estrogen receptor	ESR1	P03372	CHEMBL206	<div style="width: 100%; height: 10px; background-color: green;"></div>	13 / 7	Transcription Factor
Glucocorticoid receptor	NR3C1	P04150	CHEMBL2034	<div style="width: 100%; height: 10px; background-color: green;"></div>	82 / 31	Transcription Factor
Estrogen receptor beta (by homology)	ESR2	Q82731	CHEMBL242	<div style="width: 100%; height: 10px; background-color: green;"></div>	13 / 7	Transcription Factor
Acylcholine 5-lipoxygenase	ALOX5	P09917	CHEMBL216	<div style="width: 100%; height: 10px; background-color: green;"></div>	29 / 3	Enzyme
Acylcholine 15-lipoxygenase (by homology)	ALOX15	P18060	CHEMBL2903	<div style="width: 100%; height: 10px; background-color: green;"></div>	28 / 3	Enzyme

* Probabilities have been computed based on a cross-validation. They may therefore not represent the actual probability of success for any new molecule (see FAQ).

Swiss Institute of Bioinformatics © 2013

Leoleorin H

Click/Drug About us SwissDock SwissParam SwissSidechain SwissBioStere SwissTargetPrediction SwissKME SwissSimilarity

SIB
Swiss Institute of Bioinformatics

SwissTargetPrediction

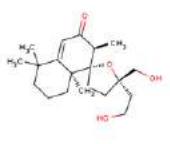
Home FAQ Help Download Contact Disclaimer

List of predicted targets

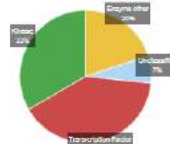
These targets have been predicted using the method described in:


Grefler D., Michielin O. & Zoete V. Shaping the interaction landscape of bioactive molecules. *Bioinformatics* (2014) 29:3673-3679.
















Query Molecule



General Target Classes



Retrieve data: 

Target	Common name	Uniprot ID	ChEMBL ID	Probability*	# sim. ompds (3D / 2D)	Target Class
Quinone oxidoreductase (by homology)	CRYZ	Q09267	CHEMBL16118		8 / 23	Enzyme
Microtubule-associated protein tau	MAPT	P10630	CHEMBL1250224		80 / 40	Unclassified
Mineralocorticoid receptor	NR3C2	P08235	CHEMBL1994		77 / 42	Transcription Factor
Cytochrome P450 19A1	CYP19A1	P11511	CHEMBL1578		17 / 92	Enzyme
Protein kinase C gamma type (by homology)	PRKCG	P05129	CHEMBL2938		47 / 192	Ser_Thr Kinase
Protein kinase C beta type (by homology)	PRKCB	P05771	CHEMBL3045		47 / 192	Ser_Thr Kinase
Protein kinase C alpha type	PRKCA	P17252	CHEMBL299		47 / 192	Ser_Thr Kinase
Protein kinase C theta type (by homology)	PRKCO	Q04750	CHEMBL3520		47 / 195	Ser_Thr Kinase
Protein kinase C delta type regulatory subunit (by homology)	PRKCD	Q05555	CHEMBL2995		47 / 195	Ser_Thr Kinase
S-hydroxy-S-methylglutaryl-coenzyme A reductase	HMGCR	P04935	CHEMBL402		82 / 93	Enzyme
Androgen receptor	AR	P10275	CHEMBL1871		87 / 64	Transcription Factor
Transcription factor AP-1	JUN	P05412	CHEMBL4977		4 / 6	Transcription Factor
Transcription factor Jun-B (by homology)	JUNB	P17275			4 / 6	Transcription Factor
Transcription factor Jun-D (by homology)	JUND	P17535			4 / 6	Transcription Factor
Glucocorticoid receptor	NR3C1	P04150	CHEMBL2034		75 / 35	Transcription Factor

* Probabilities have been computed based on a cross-validation. They may therefore not represent the actual probability of success for any new molecule (see FAQ).

Swiss Institute of Bioinformatics - © 2013

Leoleorin I

SIB
Swiss Institute of Bioinformatics

SwissTargetPrediction

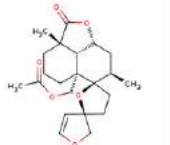
Home FAQ Help Download Contact Disclaimer

List of predicted targets

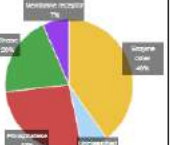
These targets have been predicted using the method described in:


Grefler D., Michielin O. & Zoete V. Shaping the interaction landscape of bioactive molecules. *Bioinformatics* (2014) 29:3673-3679.
















Query Molecule



General Target Classes



Retrieve data: 

Target	Common name	Uniprot ID	ChEMBL ID	Probability*	# sim. ompds (3D / 2D)	Target Class
Complex	FMXAFNTG	P49954/P49366	CHEMBL2094109		78 / 1	Enzyme
Complex	PSST1B/FNTA	P63009/P49354	CHEMBL2095104		59 / 1	Enzyme
Microtubule-associated protein tau	MAPT	P10630	CHEMBL1293224		227 / 12	Unclassified
Tyrosyl-DNA phosphodiesterase 1	TDP1	Q9H4W8	CHEMBL1079139		53 / 1	Enzyme
Mgpiase inducer phosphatase 2	DDC25B	P30305	CHEMBL4804		2 / 15	Ser_Thr_Tyr Phosphatase
Mgpiase inducer phosphatase 1 (by homology)	DDC25A	P30304	CHEMBL3775		2 / 13	Ser_Thr_Tyr Phosphatase
Prostaglandin G/H synthase 1	PTGS1	P23219	CHEMBL321		15 / 9	Enzyme
Prostaglandin G/H synthase 2	PTGS2	P35354	CHEMBL230		15 / 9	Enzyme
Protein kinase C gamma type (by homology)	PRKCG	P05129	CHEMBL2938		1 / 152	Ser_Thr Kinase
Protein kinase C beta type (by homology)	PRKCB	P05771	CHEMBL3045		1 / 152	Ser_Thr Kinase
Protein kinase C alpha type	PRKCA	P17252	CHEMBL299		1 / 152	Ser_Thr Kinase
Tyrosine-protein phosphatase non-receptor type 1	PTPN1	P10001	CHEMBL335		13 / 8	Tyr Phosphatase
Tyrosine-protein phosphatase non-receptor type 2 (by homology)	PTPN2	P17705	CHEMBL3907		12 / 5	Tyr Phosphatase
Fatty-acid amide hydrolase 1 (by homology)	FAAH	Q00919	CHEMBL2243		20 / 2	Enzyme
Platelet-activating factor receptor	PTAFR	P25105	CHEMBL250		17 / 11	Membrane receptor

* Probabilities have been computed based on a cross-validation. They may therefore not represent the actual probability of success for any new molecule (see FAQ).

Swiss Institute of Bioinformatics - © 2013

Leonurun

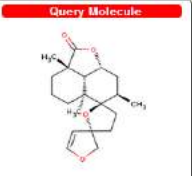
SIB Swiss Institute of Bioinformatics
 Home FAQ Help Download Contact Disclaimer

SwissTargetPrediction


List of predicted targets
 These targets have been predicted using the method described in:
 Gfeller D, Michelin O, & Zoete V. Shaping the interaction landscape of bioactive molecules. *Bioinformatics* (2013) 29:3073-3079.

Retrieve data:

Query Molecule



General Target Classes



Target	Common name	Uniprot ID	ChEMBL ID	Probability*	# sim. ompds (30 / 20)	Target Class
M-phase inducer phosphatase 2	DDC2B	P30300	CHEMBL4894		1 / 13	Sw_Thr_Tyr Phosphatase
M-phase inducer phosphatase 1 (by homology)	DDC25A	P30304	CHEMBL3770		1 / 13	Sw_Thr_Tyr Phosphatase
Complex	FNTA/FNTB	P49356/P49360	CHEMBL2094108		46 / 2	Enzyme
Complex	PGG1B/FNTA	P83608/P49364	CHEMBL2095154		28 / 1	Enzyme
Microtubule-associated protein tau	MAPT	P19035	CHEMBL1293224		30 / 7	Unclassified
Prostaglandin G/H synthase 1 (by homology)	PTGS1	P23218	CHEMBL321		7 / 0	Enzyme
Prostaglandin G/H synthase 2	PTGS2	P95354	CHEMBL230		7 / 5	Enzyme
Tyrosyl-DNA phosphodiesterase 1	TDP1	Q8N1W8	CHEMBL1076138		37 / 1	Enzyme
Cytochrome P450 19A1	CYP19A1	P11811	CHEMBL1373		24 / 4	Enzyme
Potassium voltage-gated channel subfamily A member 3	KCNK3	P22001	CHEMBL4033		24 / 1	Ion channel
Potassium voltage-gated channel subfamily A member 5	KCNK5	P22400	CHEMBL4300		24 / 1	Ion channel
Potassium voltage-gated channel subfamily A member 2 (by homology)	KCNK2	P16388	CHEMBL2055		24 / 1	Ion channel
Potassium voltage-gated channel subfamily A member 6 (by homology)	KCNK6	P17608	CHEMBL5273		24 / 1	Ion channel
Potassium voltage-gated channel subfamily A member 4 (by homology)	KCNK4	P22489	CHEMBL4295		24 / 1	Ion channel
Potassium voltage-gated channel subfamily A member 1 (by homology)	KCNK1	Q09470	CHEMBL2309		24 / 1	Ion channel

* Probabilities have been computed based on a cross-validation. They may therefore not represent the actual probability of success for any new molecule (see FAQ).

Swiss Institute of Bioinformatics - © 2013

13S-Premarrubin


SIB Swiss Institute of Bioinformatics
 Home FAQ Help Download Contact Disclaimer

SwissTargetPrediction


List of predicted targets
 These targets have been predicted using the method described in:
 Gfeller D, Michelin O, & Zoete V. Shaping the interaction landscape of bioactive molecules. *Bioinformatics* (2013) 29:3073-3079.

Retrieve data:

Query Molecule



General Target Classes



Target	Common name	Uniprot ID	ChEMBL ID	Probability*	# sim. ompds (30 / 20)	Target Class
Glucosylceramidase	GBA	P04062	CHEMBL2179		1 / 8	Enzyme
Muscleblind-like protein 1	MBNL1	Q8NR56	CHEMBL1293317		00 / 3	Unclassified
Muscleblind-like protein 2 (by homology)	MBNL2	Q8VZF2			00 / 3	Unclassified
Muscleblind-like protein 3 (by homology)	MBNL3	Q8NFU9			05 / 3	Unclassified
Microtubule-associated protein tau	MAPT	P19035	CHEMBL1293224		46 / 6	Unclassified
Multidrug resistance protein 1	ABCB1	P08183	CHEMBL4302		20 / 21	Transporter
Bile salt export pump (by homology)	ABCB11	Q95342	CHEMBL0020		20 / 21	Unclassified
Multidrug resistance protein 3 (by homology)	ABCB4	P21439	CHEMBL1745125		20 / 21	Enzyme
ATP-binding cassette sub-family B member 5 (by homology)	ABCB5	Q2M300	CHEMBL1772928		20 / 21	Unclassified
Protein kinase C gamma type (by homology)	PRKCG	P05128	CHEMBL2938		27 / 29	Ser_Thr Kinase
Protein kinase C beta type (by homology)	PRKCB	P05771	CHEMBL3045		27 / 29	Ser_Thr Kinase
Protein kinase C alpha type	PRKCA	P17262	CHEMBL288		27 / 28	Ser_Thr Kinase
Protein kinase C theta type (by homology)	PRKCD	Q84788	CHEMBL3820		28 / 28	Ser_Thr Kinase
Protein kinase C delta type regulatory subunit (by homology)	PRKCD	Q00005	CHEMBL2880		28 / 28	Ser_Thr Kinase
DNA polymerase alpha catalytic subunit	POLA1	P09384	CHEMBL1928		11 / 1	Enzyme

* Probabilities have been computed based on a cross-validation. They may therefore not represent the actual probability of success for any new molecule (see FAQ).

Swiss Institute of Bioinformatics - © 2013

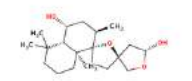
Leoleorin D

SwissTargetPrediction

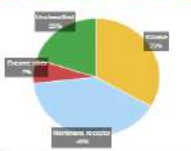
Home FAQ Help Download Contact Disclaimer






List of predicted targets
 These targets have been predicted using the method described in:
 Gfeller D., Michielin O. & Zoete V. Shaping the interaction landscape of bioactive molecules. *Bioinformatics* 2013;29:3673-3679.

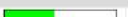
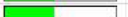
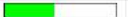
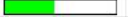
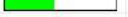










Query Molecule



General Target Classes



Retrieve data:     

Target	Common name	Uniprot ID	ChEMBL ID	Probability*	# sim. compounds (3D / 2D)	Target Class
Cyclin-dependent kinase 1	CDK1	P06493	CHEMBL308		39 / 1	Ser_Thr_Kinase
Cyclin-dependent kinase 4 (by homology)	CDK4	P11802	CHEMBL331		39 / 1	Ser_Thr_Kinase
Cyclin-dependent kinase 2	CDK2	P24941	CHEMBL301		39 / 1	Ser_Thr_Kinase
Cyclin-dependent kinase 3 (by homology)	CDK3	Q09526	CHEMBL4442		39 / 1	Ser_Thr_Kinase
Cyclin-dependent kinase 6 (by homology)	CDK6	Q09534	CHEMBL2008		39 / 1	Ser_Thr_Kinase
Muscarinic acetylcholine receptor M2 (by homology)	CHRM2	P08172	CHEMBL211		19 / 1	Membrane_receptor
Muscarinic acetylcholine receptor M4 (by homology)	CHRM4	P09173	CHEMBL1821		22 / 1	Membrane_receptor
Muscarinic acetylcholine receptor M1	CHRM1	P11229	CHEMBL210		21 / 1	Membrane_receptor
Muscarinic acetylcholine receptor M3 (by homology)	CHRM3	P20309	CHEMBL245		21 / 1	Membrane_receptor
Muscarinic acetylcholine receptor M5 (by homology)	CHRM5	P08912	CHEMBL2035		18 / 1	Membrane_receptor
Tyrosyl-DNA phosphodiesterase 1	TDP1	Q9NJV8	CHEMBL1070138		20 / 2	Enzyme
Muscleblind-like protein 1	MBNL1	Q9NR56	CHEMBL1293317		71 / 3	Unclassified
Muscleblind-like protein 2 (by homology)	MBNL2	Q9VZF2			71 / 3	Unclassified
Muscleblind-like protein 3 (by homology)	MBNL3	Q9NLR0			71 / 3	Unclassified
5-hydroxytryptamine receptor 1B (by homology)	HTR1B	P28222	CHEMBL1885		41 / 1	Membrane_receptor

* Probabilities have been computed based on a cross-validation. They may therefore not represent the actual probability of success for any new molecule (see FAQ).

Swiss Institute of Bioinformatics - © 2013

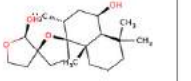
Leoleorin E

SwissTargetPrediction

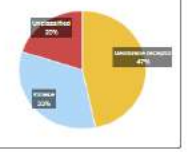
Home FAQ Help Download Contact Disclaimer






List of predicted targets
 These targets have been predicted using the method described in:
 Gfeller D., Michielin O. & Zoete V. Shaping the interaction landscape of bioactive molecules. *Bioinformatics* 2013;29:3673-3679.












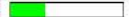



Query Molecule



General Target Classes



Retrieve data:     

Target	Common name	Uniprot ID	ChEMBL ID	Probability*	# sim. compounds (3D / 2D)	Target Class
Muscarinic acetylcholine receptor M2 (by homology)	CHRM2	P08172	CHEMBL211		44 / 1	Membrane_receptor
Muscarinic acetylcholine receptor M4 (by homology)	CHRM4	P09173	CHEMBL1821		44 / 1	Membrane_receptor
Muscarinic acetylcholine receptor M5 (by homology)	CHRM5	P08912	CHEMBL2035		42 / 1	Membrane_receptor
Muscarinic acetylcholine receptor M1	CHRM1	P11229	CHEMBL210		45 / 1	Membrane_receptor
Muscarinic acetylcholine receptor M3 (by homology)	CHRM3	P20309	CHEMBL245		42 / 1	Membrane_receptor
Cyclin-dependent kinase 1	CDK1	P06493	CHEMBL308		18 / 1	Ser_Thr_Kinase
Cyclin-dependent kinase 4 (by homology)	CDK4	P11802	CHEMBL331		18 / 1	Ser_Thr_Kinase
Cyclin-dependent kinase 2	CDK2	P24941	CHEMBL301		18 / 1	Ser_Thr_Kinase
Cyclin-dependent kinase 3 (by homology)	CDK3	Q09526	CHEMBL4442		18 / 1	Ser_Thr_Kinase
Cyclin-dependent kinase 6 (by homology)	CDK6	Q09534	CHEMBL2008		18 / 1	Ser_Thr_Kinase
Alpha-1A adrenergic receptor (by homology)	ADRA1A	P30248	CHEMBL229		20 / 1	Membrane_receptor
Muscleblind-like protein 1	MBNL1	Q9NR56	CHEMBL1293317		69 / 3	Unclassified
Muscleblind-like protein 2 (by homology)	MBNL2	Q9VZF2			69 / 3	Unclassified
Muscleblind-like protein 3 (by homology)	MBNL3	Q9NLR0			69 / 3	Unclassified
D(2) dopamine receptor	DRD2	P14418	CHEMBL217		61 / 1	Membrane_receptor

* Probabilities have been computed based on a cross-validation. They may therefore not represent the actual probability of success for any new molecule (see FAQ).

Swiss Institute of Bioinformatics - © 2013

Leoleorin F






SwissTargetPrediction

Home FAQ Help Download Contact Disclaimer

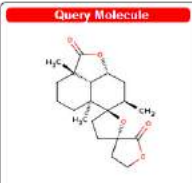
List of predicted targets

These targets have been predicted using the method described in:


Gfeller D, Michelin O, & Zoete V. Shaping the interaction landscape of bioactive molecules. *Bioinformatics* (2015), 29, 3073-3079.
















Retrieve data:     

Query Molecule



General Target Classes



Target	Common name	Uniprot ID	CHEMBL ID	Probability*	# sim. cmpds (3D / 2D)	Target Class
Platelet-activating factor receptor	PTAFR	P25105	CHEMBL200		14 / 47	Membrane receptor
Microtubule-associated protein tau	MAPT	P10636	CHEMBL1293224		189 / 14	Unclassified
Cannabinoid receptor 1	CNR1	P21554	CHEMBL218		22 / 19	Membrane receptor
Cannabinoid receptor 2	CNR2	P34972	CHEMBL263		21 / 13	Membrane receptor
Mu-type opioid receptor	OPRM1	P35372	CHEMBL233		7 / 29	Membrane receptor
Delta-type opioid receptor	OPRD1	P41143	CHEMBL230		7 / 29	Membrane receptor
Kappa-type opioid receptor	OPRK1	P41145	CHEMBL237		7 / 29	Membrane receptor
Nociceptin receptor (by homology)	OPRL1	P41148	CHEMBL2014		8 / 29	Membrane receptor
Multidrug resistance protein 1	ABCB1	P59183	CHEMBL4302		1 / 95	Transporter
Bile salt export pump (by homology)	ABCB11	O86342	CHEMBL0020		1 / 98	Unclassified
Multidrug resistance protein 3 (by homology)	ABCG4	P21439	CHEMBL1743129		1 / 36	Enzyme
ATP-binding cassette sub-family B member 5 (by homology)	ABCB5	Q2M390	CHEMBL1772923		1 / 38	Unclassified
Protein kinase C gamma type (by homology)	PRKCG	P05129	CHEMBL2936		2 / 109	Ser_Thr_Kinase
Protein kinase C beta type (by homology)	PRKCB	P05771	CHEMBL3045		2 / 109	Ser_Thr_Kinase
Protein kinase C alpha type	PRKCA	P17262	CHEMBL299		2 / 109	Ser_Thr_Kinase

* Probabilities have been computed based on a cross-validation. They may therefore not represent the actual probability of success for any new molecule (see FAQ).

Swiss Institute of Bioinformatics - © 2013

EDD






SwissTargetPrediction

Home FAQ Help Download Contact Disclaimer

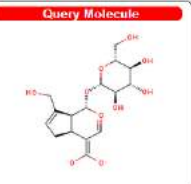
List of predicted targets

These targets have been predicted using the method described in:


Gfeller D, Michelin O, & Zoete V. Shaping the interaction landscape of bioactive molecules. *Bioinformatics* (2015), 29, 3073-3079.
















Retrieve data:     

Query Molecule



General Target Classes



Target	Common name	Uniprot ID	CHEMBL ID	Probability*	# sim. cmpds (3D / 2D)	Target Class
Microtubule-associated protein tau	MAPT	P10636	CHEMBL1293224		189 / 14	Unclassified
Hypoxia-inducible factor 1-alpha	HIF1A	Q15900	CHEMBL4261		2 / 2	Transcription Factor
Endothelial PAS domain-containing protein 1	EPAS1	Q39914	CHEMBL1744622		2 / 2	Unclassified
Tyrosyl-DNA phosphodiesterase 1	TDOP1	Q9R9J8	CHEMBL1025138		46 / 2	Enzyme
Protein kinase C gamma type (by homology)	PRKCG	P05129	CHEMBL2936		1 / 10	Ser_Thr_Kinase
Protein kinase C beta type (by homology)	PRKCB	P05771	CHEMBL3045		1 / 10	Ser_Thr_Kinase
Protein kinase C alpha type	PRKCA	P17262	CHEMBL299		1 / 10	Ser_Thr_Kinase
Protein kinase C theta type (by homology)	PRKCD	Q04709	CHEMBL3920		1 / 10	Ser_Thr_Kinase
Protein kinase C delta type regulatory subunit	PRKCD	Q05855	CHEMBL2596		1 / 10	Ser_Thr_Kinase
Muscarinic acetylcholine receptor M2 (by homology)	CHRM2	P08172	CHEMBL211		9 / 1	Membrane receptor
Muscarinic acetylcholine receptor M1	CHRM1	P11229	CHEMBL216		9 / 1	Membrane receptor
Muscarinic acetylcholine receptor M3	CHRM3	P20309	CHEMBL246		8 / 1	Membrane receptor
Muscarinic acetylcholine receptor M4 (by homology)	CHRM4	P08173	CHEMBL1821		9 / 1	Membrane receptor
Transient receptor potential cation channel subfamily V member 1 (by homology)	TRPV1	Q5NER1	CHEMBL4794		24 / 12	Ion channel
Sodium-dependent noradrenaline transporter	SLC6A2	P23975	CHEMBL222		29 / 1	Transporter

* Probabilities have been computed based on a cross-validation. They may therefore not represent the actual probability of success for any new molecule (see FAQ).

Swiss Institute of Bioinformatics - © 2013

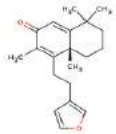
Geniposidic Acid

SIB Swiss Institute of Bioinformatics
 SwissTargetPrediction
 Home FAQ Help Download Contact Disclaimer

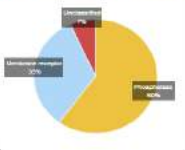
List of predicted targets
 These targets have been predicted using the method described in:
 Cifaller D, Michielin O. & Zoella V. Shaping the interaction landscape of bioactive molecules. *Bioinformatics* 2014;28:3670-3678

Retrieve data:

Query Molecule



General Target Classes



Target	Common name	Uniprot ID	ChEMBL ID	Probability*	# sim. compds (3D / 2D)	Target Class
M-phase inducer phosphatase 1	CDC25A	P30304	CHEMBL3776	<div style="width: 100%; height: 10px; background-color: green;"></div>	3 / 4	Ser_Thr_Tyr Phosphatase
Dual specificity protein phosphatase 9	DUSP9	P01452	CHEMBL2036	<div style="width: 100%; height: 10px; background-color: green;"></div>	3 / 3	Ser_Thr_Tyr Phosphatase
M-phase inducer phosphatase 2 (by homology)	CDC25B	P30305	CHEMBL4804	<div style="width: 100%; height: 10px; background-color: green;"></div>	2 / 4	Ser_Thr_Tyr Phosphatase
Inactive dual specificity phosphatase 27 (by homology)	DUSP27	Q5VZP6		<div style="width: 100%; height: 10px; background-color: green;"></div>	2 / 3	Ser_Thr_Tyr Phosphatase
Dual specificity phosphatase DUSP1 (by homology)	DUSP1	Q8B444		<div style="width: 100%; height: 10px; background-color: green;"></div>	3 / 3	Ser_Thr_Tyr Phosphatase
Dual specificity protein phosphatase 18 isoform NCSP (by homology)	DUSP13	Q5B611		<div style="width: 100%; height: 10px; background-color: green;"></div>	2 / 3	Ser_Thr_Tyr Phosphatase
Dual specificity protein phosphatase 26 (by homology)	DUSP26	Q8BV47		<div style="width: 100%; height: 10px; background-color: green;"></div>	3 / 3	Ser_Thr_Tyr Phosphatase
Cannabinoid receptor 1	CNR1	P21554	CHEMBL218	<div style="width: 100%; height: 10px; background-color: green;"></div>	43 / 3	Membrane receptor
Cannabinoid receptor 2	CNR2	P34972	CHEMBL253	<div style="width: 100%; height: 10px; background-color: green;"></div>	40 / 3	Membrane receptor
Tyrosine-protein phosphatase non-receptor type 1	PTPN1	P18051	CHEMBL335	<div style="width: 100%; height: 10px; background-color: green;"></div>	1 / 1	Tyr Phosphatase
Tyrosine-protein phosphatase non-receptor type 2 (by homology)	PTPN2	P17706	CHEMBL3807	<div style="width: 100%; height: 10px; background-color: green;"></div>	1 / 1	Tyr Phosphatase
Microtubule-associated protein tau	MAPT	P10030	CHEMBL1283224	<div style="width: 100%; height: 10px; background-color: green;"></div>	13 / 3	Unclassified
Mu-type opioid receptor	OPRM1	P35372	CHEMBL233	<div style="width: 100%; height: 10px; background-color: green;"></div>	2 / 1	Membrane receptor
Delta-type opioid receptor	OPRD1	P41143	CHEMBL236	<div style="width: 100%; height: 10px; background-color: green;"></div>	2 / 1	Membrane receptor
Kappa-type opioid receptor	OPRK1	P41145	CHEMBL237	<div style="width: 100%; height: 10px; background-color: green;"></div>	2 / 1	Membrane receptor

* Probabilities have been computed based on a cross-validation. They may therefore not represent the actual probability of success for any new molecule (see FAQ).

Swiss Institute of Bioinformatics - © 2013

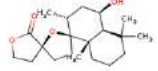
Leoleorin B

SIB Swiss Institute of Bioinformatics
 SwissTargetPrediction
 Home FAQ Help Download Contact Disclaimer

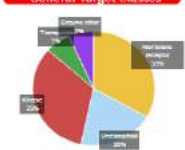
List of predicted targets
 These targets have been predicted using the method described in:
 Cifaller D, Michielin O. & Zoella V. Shaping the interaction landscape of bioactive molecules. *Bioinformatics* 2014;28:3670-3678

Retrieve data:

Query Molecule



General Target Classes



Target	Common name	Uniprot ID	ChEMBL ID	Probability*	# sim. compds (3D / 2D)	Target Class
Platelet-activating factor receptor	PTAFR	P28108	CHEMBL250	<div style="width: 100%; height: 10px; background-color: green;"></div>	18 / 47	Membrane receptor
Microtubule-associated protein tau	MAPT	P10030	CHEMBL1283224	<div style="width: 100%; height: 10px; background-color: green;"></div>	156 / 14	Unclassified
Protein kinase C gamma type (by homology)	PRKCG	P05129	CHEMBL2938	<div style="width: 100%; height: 10px; background-color: green;"></div>	30 / 169	Ser_Thr Kinase
Protein kinase C beta type (by homology)	PRKCB	P06771	CHEMBL3045	<div style="width: 100%; height: 10px; background-color: green;"></div>	30 / 169	Ser_Thr Kinase
Protein kinase C alpha type	PRKCA	P17262	CHEMBL299	<div style="width: 100%; height: 10px; background-color: green;"></div>	30 / 169	Ser_Thr Kinase
Protein kinase C theta type (by homology)	PRKCG	Q04750	CHEMBL3530	<div style="width: 100%; height: 10px; background-color: green;"></div>	29 / 171	Ser_Thr Kinase
Protein kinase C delta type regulatory subunit	PRKCD	Q00050	CHEMBL2990	<div style="width: 100%; height: 10px; background-color: green;"></div>	29 / 171	Ser_Thr Kinase
Multidrug resistance protein 1	ABCB1	P08183	CHEMBL4302	<div style="width: 100%; height: 10px; background-color: green;"></div>	9 / 35	Transporter
Bile salt export pump (by homology)	ABCB11	Q55342	CHEMBL0020	<div style="width: 100%; height: 10px; background-color: green;"></div>	9 / 35	Unclassified
Multidrug resistance protein 3 (by homology)	ABCB4	P21438	CHEMBL1743129	<div style="width: 100%; height: 10px; background-color: green;"></div>	9 / 35	Enzyme
ATP-binding cassette sub-family B member 5 (by homology)	ABCB5	Q5M350	CHEMBL1772925	<div style="width: 100%; height: 10px; background-color: green;"></div>	9 / 35	Unclassified
Mu-type opioid receptor	OPRM1	P35372	CHEMBL233	<div style="width: 100%; height: 10px; background-color: green;"></div>	202 / 29	Membrane receptor
Delta-type opioid receptor	OPRD1	P41143	CHEMBL236	<div style="width: 100%; height: 10px; background-color: green;"></div>	202 / 29	Membrane receptor
Kappa-type opioid receptor	OPRK1	P41145	CHEMBL237	<div style="width: 100%; height: 10px; background-color: green;"></div>	205 / 29	Membrane receptor
Nociceptin receptor (by homology)	OPRL1	P41148	CHEMBL2014	<div style="width: 100%; height: 10px; background-color: green;"></div>	244 / 29	Membrane receptor

* Probabilities have been computed based on a cross-validation. They may therefore not represent the actual probability of success for any new molecule (see FAQ).

Swiss Institute of Bioinformatics - © 2013

Leoleorin C



Click/Dring About us SwissDock SwissPharm SwissDatabase SwissBioinformatics **SwissTargetPrediction** SwissHOME SwissSimilarity

SIB
Swiss Institute of Bioinformatics

SwissTargetPrediction

Home FAQ Help Download Contact Disclaimer

List of predicted targets

These targets have been predicted using the method described in:

Gfeller D., Michielin O. & Zoete V.
Shaping the interaction landscape of bioactive molecules. *Bioinformatics* (2013) 29:3073-3078.

Retrieve data:

Query Molecule

General Target Classes

Target	Common name	Uniprot ID	ChEMBL ID	Probability*	# sim. cmpds (3D / 2D)	Target Class
Mu-type opioid receptor	OPRM1	P35372	CHEMBL133	<div style="width: 100%; height: 10px; background-color: green;"></div>	320 / 67	Membrane receptor
Delta-type opioid receptor	OPRD1	P41143	CHEMBL130	<div style="width: 100%; height: 10px; background-color: green;"></div>	320 / 67	Membrane receptor
Kappa-type opioid receptor	OPRK1	P41145	CHEMBL237	<div style="width: 100%; height: 10px; background-color: green;"></div>	287 / 72	Membrane receptor
Opioid receptor (by homology)	OPRL1	P41148	CHEMBL2014	<div style="width: 100%; height: 10px; background-color: green;"></div>	263 / 68	Membrane receptor
Microtubule-associated protein tau	MAPT	P10536	CHEMBL1293224	<div style="width: 100%; height: 10px; background-color: green;"></div>	99 / 8	Unclassified
Cytochrome P450 19A1	CYP19A1	P11511	CHEMBL1978	<div style="width: 100%; height: 10px; background-color: green;"></div>	42 / 27	Enzyme
Macrophage migration inhibitory factor	MF	P14174	CHEMBL2005	<div style="width: 100%; height: 10px; background-color: green;"></div>	1 / 1	Enzyme
Androgen receptor	AR	P19278	CHEMBL1871	<div style="width: 100%; height: 10px; background-color: green;"></div>	104 / 18	Transcription Factor
Tyrosyl-DNA phosphodiesterase 1	TDP1	Q8N0W8	CHEMBL1075138	<div style="width: 100%; height: 10px; background-color: green;"></div>	50 / 6	Enzyme
Camelinoid receptor 1 (by homology)	CNR1	P21554	CHEMBL128	<div style="width: 100%; height: 10px; background-color: green;"></div>	78 / 3	Membrane receptor
Camelinoid receptor 2	CNR2	P34972	CHEMBL253	<div style="width: 100%; height: 10px; background-color: green;"></div>	51 / 3	Membrane receptor
Glucocorticoid receptor	NR5C1	P04150	CHEMBL2034	<div style="width: 100%; height: 10px; background-color: green;"></div>	70 / 9	Transcription Factor
Mineralocorticoid receptor (by homology)	NR5C2	P08235	CHEMBL1594	<div style="width: 100%; height: 10px; background-color: green;"></div>	71 / 10	Transcription Factor
Tyrosine-protein phosphatase non-receptor type 2 (by homology)	PTPN2	P17700	CHEMBL3807	<div style="width: 100%; height: 10px; background-color: green;"></div>	0 / 3	Tyrosine Phosphatase
Tyrosine-protein phosphatase non-receptor type 1	PTPN1	P16031	CHEMBL330	<div style="width: 100%; height: 10px; background-color: green;"></div>	0 / 3	Tyrosine Phosphatase

* Probabilities have been computed based on a cross-validation. They may therefore not represent the actual probability of success for any new molecule (see FAQ).

Swiss Institute of Bioinformatics - © 2013

Compound Y (Leoleorin A)

Swiss Institute of Bioinformatics

SwissTargetPrediction

Home FAQ Help Download Contact Disclaimer

List of predicted targets

These targets have been predicted using the method described in:

Gfeller D., Michielin O. & Zoete V.
Shaping the interaction landscape of bioactive molecules. *Bioinformatics* (2013) 29:3073-3078.

Retrieve data:

Query Molecule

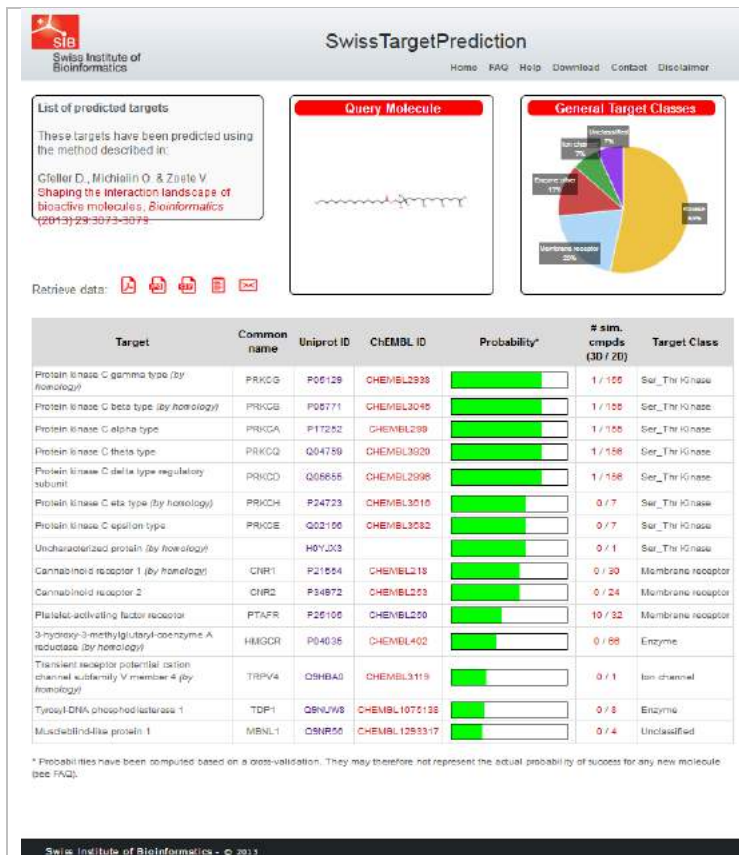
General Target Classes

Target	Common name	Uniprot ID	ChEMBL ID	Probability*	# sim. cmpds (3D / 2D)	Target Class
Tyrosyl-DNA phosphodiesterase 1	TDP1	Q5N0W8	CHEMBL1075138	<div style="width: 100%; height: 10px; background-color: green;"></div>	9 / 17	Enzyme
Lysine-specific demethylase 4A	KDM4A	Q75164	CHEMBL5886	<div style="width: 100%; height: 10px; background-color: green;"></div>	1 / 3	Enzyme
Lysine-specific demethylase 4B (by homology)	KDM4B	Q84853		<div style="width: 100%; height: 10px; background-color: green;"></div>	1 / 3	Enzyme
Lysine-specific demethylase 4C (by homology)	KDM4C	Q84330	CHEMBL0175	<div style="width: 100%; height: 10px; background-color: green;"></div>	1 / 3	Enzyme
Aldo-keto reductase family 1 member B10 (by homology)	AKR1B10	Q60218	CHEMBL5993	<div style="width: 100%; height: 10px; background-color: green;"></div>	9 / 68	Enzyme
Aldose reductase (by homology)	AKR1B1	P15121	CHEMBL1900	<div style="width: 100%; height: 10px; background-color: green;"></div>	9 / 68	Enzyme
Aldo-keto reductase family 1 member B15 (by homology)	AKR1B10	Q8JR28		<div style="width: 100%; height: 10px; background-color: green;"></div>	9 / 68	Enzyme
Xanthine dehydrogenase/dease	XDH	P47868	CHEMBL1929	<div style="width: 100%; height: 10px; background-color: green;"></div>	2 / 13	Enzyme
Aldehyde oxidase (by homology)	ADOX1	Q08278	CHEMBL3257	<div style="width: 100%; height: 10px; background-color: green;"></div>	2 / 13	Enzyme
Adenosine receptor A1 (by homology)	ADORA1	P30542	CHEMBL228	<div style="width: 100%; height: 10px; background-color: green;"></div>	42 / 17	Membrane receptor
Muscleblind-like protein 1	MBNL1	Q9NR05	CHEMBL1283317	<div style="width: 100%; height: 10px; background-color: green;"></div>	5 / 7	Unclassified
Muscleblind-like protein 2 (by homology)	MBNL2	Q9VZF2		<div style="width: 100%; height: 10px; background-color: green;"></div>	5 / 7	Unclassified
Muscleblind-like protein 3 (by homology)	MBNL3	Q9NJK0		<div style="width: 100%; height: 10px; background-color: green;"></div>	5 / 7	Unclassified
Alcohol dehydrogenase [NADPH-] (by homology)	AKR1A1	P14550	CHEMBL2248	<div style="width: 100%; height: 10px; background-color: green;"></div>	5 / 10	Enzyme
1,5-enhydro-D-fructose reductase (by homology)	AKR1E2	Q86JDB		<div style="width: 100%; height: 10px; background-color: green;"></div>	5 / 10	Enzyme

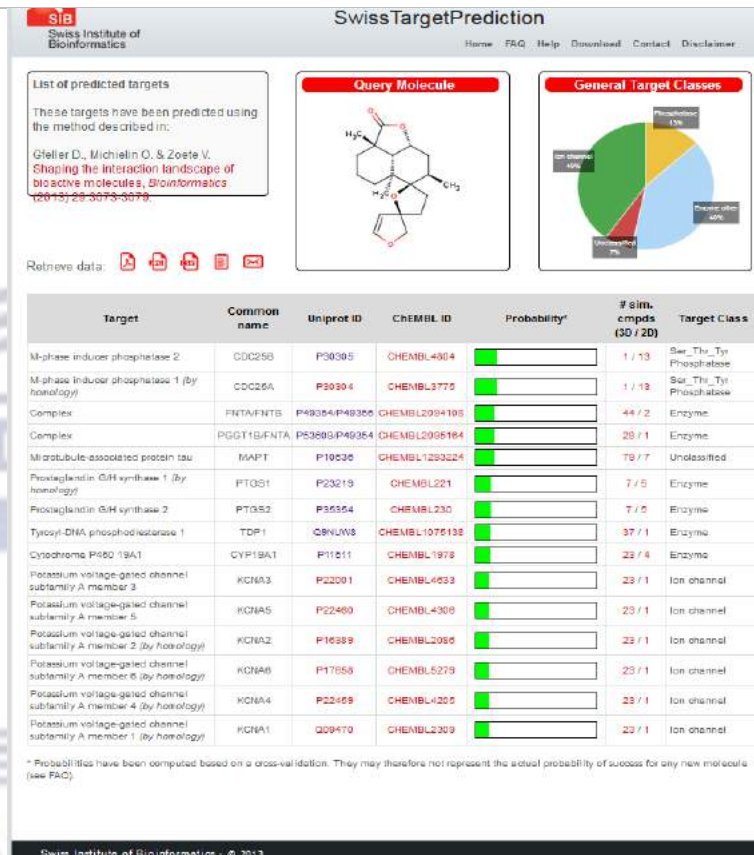
* Probabilities have been computed based on a cross-validation. They may therefore not represent the actual probability of success for any new molecule (see FAQ).

Swiss Institute of Bioinformatics - © 2013

Cynaroside



Dihydroxyphytyl palmitate



13R-Premarrubin

SwissTargetPrediction

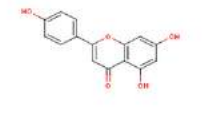
Swiss Institute of Bioinformatics

Home FAQ Help Download Contact Disclaimer


List of predicted targets

These targets have been predicted using the method described in:
 Gfeller D, Michielin O, & Zoete V. Shaping the interaction landscape of bioactive molecules. *Bioinformatics* 2014;28:3073-3078.

Query Molecule



General Target Classes



Retrieve data:

Target	Common name	Uniprot ID	CHEMBL ID	Probability*	# sim. cmpds (3D / 2D)	Target Class
Aldo-keto reductase family 1 member B10 (by homology)	AKR1B10	O60218	CHEMBL5983		21 / 87	Enzyme
Estrogen receptor	ESR1	P03372	CHEMBL200		105 / 60	Transcription Factor
Cytochrome P450 1A2 (by homology)	CYP1A2	P05177	CHEMBL3359		7 / 13	Enzyme
Cyclin-dependent kinase 1 (by homology)	CDK1	P08493	CHEMBL368		13 / 22	Ser_Thr Kinase
Microtubule-associated protein tau	MAPT	P10030	CHEMBL1293224		44 / 88	Unclassified
Cytochrome P450 19A1	CYP19A1	P11011	CHEMBL1978		10 / 19	Enzyme
Cyclin-dependent kinase 4 (by homology)	CDK4	P11802	CHEMBL331		13 / 22	Ser_Thr Kinase
Extradial 17-beta-dehydrogenase 1	HSD17B1	P14081	CHEMBL3181		87 / 4	Enzyme
Aldose reductase (by homology)	AKR1B1	P15121	CHEMBL1900		21 / 67	Enzyme
Casain kinase II subunit alpha' (by homology)	CSNK2A2	P19784	CHEMBL4070		3 / 2	Ser_Thr Kinase
Amine oxidase (flavin-containing) A	MAOA	P21387	CHEMBL1951		8 / 48	Enzyme
Prostaglandin G/H synthase 1 (by homology)	PTGS1	P23219	CHEMBL221		15 / 15	Enzyme
Cyclin-dependent kinase 2 (by homology)	CDK2	P24541	CHEMBL361		13 / 22	Ser_Thr Kinase
Amine oxidase (flavin-containing) B (by homology)	MAOB	P27338	CHEMBL2039		8 / 45	Enzyme
Adenosine receptor A2a (by homology)	AORA2A	P29274	CHEMBL251		5 / 13	Membrane receptor

* Probabilities have been computed based on a cross-validation. They may therefore not represent the actual probability of success for any new molecule (see FAQ).

Swiss Institute of Bioinformatics - © 2013

Apigenin

SwissTargetPrediction

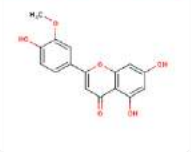
Swiss Institute of Bioinformatics

Home FAQ Help Download Contact Disclaimer


List of predicted targets

These targets have been predicted using the method described in:
 Gfeller D, Michielin O, & Zoete V. Shaping the interaction landscape of bioactive molecules. *Bioinformatics* 2014;28:3073-3078.

Query Molecule



General Target Classes



Retrieve data:

Target	Common name	Uniprot ID	CHEMBL ID	Probability*	# sim. cmpds (3D / 2D)	Target Class
Cytochrome P450 1A2 (by homology)	CYP1A2	P05177	CHEMBL3359		11 / 13	Enzyme
Multi drug resistance-associated protein 1	ABCC1	P33527	CHEMBL3004		3 / 12	Transporter
Cytochrome P450 1B1	CYP1B1	Q10578	CHEMBL4878		11 / 13	Enzyme
Cytochrome P400 1A1 (by homology)	CYP1A1	P04788	CHEMBL2231		11 / 15	Enzyme
Canalicular multispecific organic anion transporter 2 (by homology)	ABCC3	Q15436	CHEMBL5918		3 / 12	Unclassified
Canalicular multispecific organic anion transporter 1 (by homology)	ABCC2	Q82887	CHEMBL5746		3 / 12	Unclassified
Aldose reductase (by homology)	AKR1B1	P15121	CHEMBL1900		23 / 69	Enzyme
Aldo-keto reductase family 1 member B15 (by homology)	AKR1B15	Q8JF28			23 / 69	Enzyme
Aldose reductase family 1 member B10 (by homology)	AKR1B10	Q60218	CHEMBL5883		23 / 69	Enzyme
Fibrinogen chain B	FLG	P00747	CHEMBL1801		2 / 2	Swine Protease
Alloisopterinase (by homology)	LPA	P08519			2 / 2	Serine Protease
Xanthine dehydrogenase/oxidase	XDH	P47889	CHEMBL1829		3 / 14	Enzyme
Aldehyde oxidase (by homology)	XOX1	Q00278	CHEMBL3257		3 / 14	Enzyme
NADPH oxidase 4	NOX4	Q5NPH5	CHEMBL1200375		8 / 8	Enzyme
Estrogen receptor (by homology)	ESR1	P03372	CHEMBL200		85 / 28	Transcription Factor

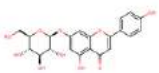
* Probabilities have been computed based on a cross-validation. They may therefore not represent the actual probability of success for any new molecule (see FAQ).

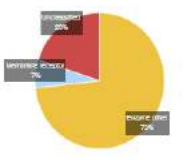
Swiss Institute of Bioinformatics - © 2013


Chrysoeriol
















SwissTargetPrediction
 Swiss Institute of Bioinformatics
 Home FAQ Help Download Contact Disclaimers

List of predicted targets
 These targets have been predicted using the method described in:
 Gfeller D., Michielin O. & Zoete V.
 Shaping the interaction landscape of bioactive molecules. *Bioinformatics* (2013) 29:3673-3679

Query Molecule


General Target Classes


Retrieve data: 

Target	Common name	Uniprot ID	ChEMBL ID	Probability*	# sim. cmpds (3D / 2D)	Target Class
Tyrosyl-DNA phosphodiesterase 1	TDP1	Q2N0V8	CHEMBL1075138		0 / 15	Enzyme
Aldo-keto reductase family 1 member B10 (by homology)	AKR1B10	Q80218	CHEMBL3063		15 / 69	Enzyme
Aldose reductase (by homology)	AKR1B1	P15121	CHEMBL1900		15 / 69	Enzyme
Aldo-keto reductase family 1 member B15 (by homology)	AKR1B15	Q3UR28			15 / 69	Enzyme
Lysine-specific demethylase 5A	KDM5A	Q75154	CHEMBL3595		1 / 3	Enzyme
Lysine-specific demethylase 4D (by homology)	KDM4B	Q84953			1 / 3	Enzyme
Lysine-specific demethylase 4C (by homology)	KDM4C	Q8H930	CHEMBL0175		1 / 3	Enzyme
Adenosine receptor A1 (by homology)	ADORA1	P30542	CHEMBL326		40 / 17	Membrane receptor
Muscleblind-like protein 1	MBNL1	Q9NR55	CHEMBL1293317		4 / 10	Unclassified
Muscleblind-like protein 2 (by homology)	MBNL2	Q5VZF2			4 / 10	Unclassified
Muscleblind-like protein 3 (by homology)	MBNL3	Q9KUK3			4 / 10	Unclassified
Xanthine dehydrogenase/oxidase	XDH	P47959	CHEMBL1929		2 / 13	Enzyme
Aldehyde oxidase (by homology)	AOX1	Q05278	CHEMBL3257		2 / 13	Enzyme
Aldehyde dehydrogenase, mitochondrial	ALDH2	P05091	CHEMBL1935		1 / 40	Enzyme
Unclassified protein (by homology)	FSYP20				1 / 40	Enzyme

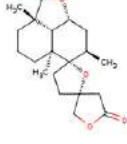
* Probabilities have been computed based on a cross-validation. They may therefore not represent the actual probability of success for any new molecule (see FAQ).

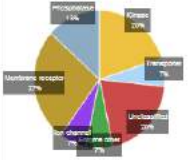
Swiss Institute of Bioinformatics - © 2013


Comosiin





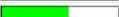

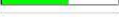








SwissTargetPrediction
 Swiss Institute of Bioinformatics
 Home FAQ Help Download Contact Disclaimers

List of predicted targets
 These targets have been predicted using the method described in:
 Gfeller D., Michielin O. & Zoete V.
 Shaping the interaction landscape of bioactive molecules. *Bioinformatics* (2013) 29:3673-3679

Query Molecule


General Target Classes


Retrieve data: 

Target	Common name	Uniprot ID	ChEMBL ID	Probability*	# sim. cmpds (3D / 2D)	Target Class
Protein kinase C gamma type (by homology)	PRKCG	P95120	CHEMBL2038		1 / 191	Ser_Thr Kinase
Protein kinase C beta type (by homology)	PRKCB	P95771	CHEMBL3045		1 / 191	Ser_Thr Kinase
Protein kinase C alpha type	PRKCA	P17282	CHEMBL2399		1 / 181	Ser_Thr Kinase
Multidrug resistance protein 1	ABCB1	P98183	CHEMBL4302		1 / 35	Transporter
Bile salt export pump (by homology)	ABCB11	Q95242	CHEMBL2020		1 / 35	Unclassified
Multidrug resistance protein 3 (by homology)	ABCB4	P21439	CHEMBL1743129		1 / 35	Enzyme
ATP-binding cassette sub-family B member 5 (by homology)	ABCB5	Q2M390	CHEMBL1772928		1 / 35	Unclassified
Microtubule-associated protein tau	MAPT	P10930	CHEMBL1293224		107 / 15	Unclassified
Transient receptor potential cation channel subfamily V member 4 (by homology)	TRPV4	Q8HBA8	CHEMBL3118		1 / 4	Ion channel
Platelet-activating factor receptor	PTAFR	P25105	CHEMBL250		11 / 42	Membrane receptor
Tyrosine-protein phosphatase non-receptor type 2 (by homology)	PTPN2	P17700	CHEMBL3607		11 / 17	Tyr Phosphatase
Tyrosine-protein phosphatase non-receptor type 1	PTPN1	P18031	CHEMBL335		11 / 17	Tyr Phosphatase
Cannabinoid receptor 1	CNR1	P21964	CHEMBL218		18 / 19	Membrane receptor
Cannabinoid receptor 2	CNR2	P34872	CHEMBL253		17 / 13	Membrane receptor
Mu-type opioid receptor	OPRM1	P95372	CHEMBL233		12 / 18	Membrane receptor

* Probabilities have been computed based on a cross-validation. They may therefore not represent the actual probability of success for any new molecule (see FAQ).

Swiss Institute of Bioinformatics - © 2013





Compound X

SwissTargetPrediction

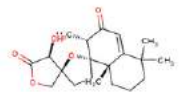
Home | FAQ | Help | Download | Contact | Disclaimer

List of predicted targets

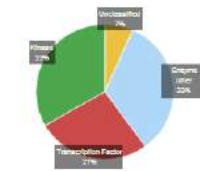
These targets have been predicted using the method described in:
 Gfeller D., Michielin O. & Zoete V. Shaping the interaction landscape of bioactive molecules. *Bioinformatics* (2013) 29:3073-3079.

Retrieve data:    

Query Molecule



General Target Classes



Target	Common name	Uniprot ID	ChEMBL ID	Probability*	# sim. compds (3D / 2D)	Target Class
Microtubule-associated protein tau	MAPT	P10838	CHEMBL1293224	<div style="width: 100%; height: 10px; background-color: green;"></div>	228 / 40	Unclassified
Prostaglandin G/H synthase 1 (by homology)	PTGS1	P23218	CHEMBL221	<div style="width: 100%; height: 10px; background-color: green;"></div>	35 / 15	Enzyme
Prostaglandin G/H synthase 2	PTGS2	P38354	CHEMBL230	<div style="width: 100%; height: 10px; background-color: green;"></div>	33 / 16	Enzyme
Quinone oxidoreductase (by homology)	CRYZ	Q08267	CHEMBL1118	<div style="width: 100%; height: 10px; background-color: green;"></div>	5 / 25	Enzyme
Androgen receptor	AR	P19270	CHEMBL1871	<div style="width: 100%; height: 10px; background-color: green;"></div>	73 / 23	Transcription Factor
3-hydroxy-3-methylglutaryl-coenzyme A reductase	HMGCR	P04035	CHEMBL402	<div style="width: 100%; height: 10px; background-color: green;"></div>	40 / 82	Enzyme
Protein kinase C gamma type (by homology)	PRKCG	P08120	CHEMBL2938	<div style="width: 100%; height: 10px; background-color: green;"></div>	31 / 242	Ser_Thr Kinase
Protein kinase C beta type (by homology)	PRKCB	P05771	CHEMBL5045	<div style="width: 100%; height: 10px; background-color: green;"></div>	31 / 242	Ser_Thr Kinase
Protein kinase C alpha type	PRKCA	P17252	CHEMBL389	<div style="width: 100%; height: 10px; background-color: green;"></div>	31 / 242	Ser_Thr Kinase
Protein kinase C theta type (by homology)	PRKCT	Q04758	CHEMBL3920	<div style="width: 100%; height: 10px; background-color: green;"></div>	30 / 240	Ser_Thr Kinase
Protein kinase C delta type regulatory subunit	PRKCD	Q05555	CHEMBL2896	<div style="width: 100%; height: 10px; background-color: green;"></div>	30 / 240	Ser_Thr Kinase
Mitogen-activated protein kinase receptor	NR3C2	P09236	CHEMBL1994	<div style="width: 100%; height: 10px; background-color: green;"></div>	61 / 26	Transcription Factor
Transcription factor p85	RELA	Q04206	CHEMBL5530	<div style="width: 100%; height: 10px; background-color: green;"></div>	8 / 15	Transcription Factor
Proto-oncogene c-Rel (by homology)	REL	Q04694		<div style="width: 100%; height: 10px; background-color: green;"></div>	8 / 15	Transcription Factor
Estradiol 17-beta-dehydrogenase 2	HSD17B2	P07050	CHEMBL2789	<div style="width: 100%; height: 10px; background-color: green;"></div>	59 / 12	Enzyme

* Probabilities have been computed based on a cross-validation. They may therefore not represent the actual probability of success for any new molecule (see FAQ).

Swiss Institute of Bioinformatics · © 2013





14α-hydroxy-9α-13α-epoxylabd-5(6)-en-7-on-16 15-olide

SwissTargetPrediction

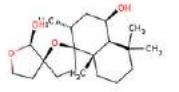
Home | FAQ | Help | Download | Contact | Disclaimer

List of predicted targets

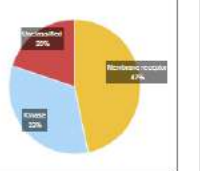
These targets have been predicted using the method described in:
 Gfeller D., Michielin O. & Zoete V. Shaping the interaction landscape of bioactive molecules. *Bioinformatics* (2013) 29:3073-3079.

Retrieve data:    

Query Molecule



General Target Classes



Target	Common name	Uniprot ID	ChEMBL ID	Probability*	# sim. compds (3D / 2D)	Target Class
Muscarinic acetylcholine receptor M2 (by homology)	CHRM2	P08172	CHEMBL211	<div style="width: 100%; height: 10px; background-color: green;"></div>	44 / 1	Membrane receptor
Muscarinic acetylcholine receptor M4 (by homology)	CHRM4	P08173	CHEMBL1921	<div style="width: 100%; height: 10px; background-color: green;"></div>	44 / 1	Membrane receptor
Muscarinic acetylcholine receptor M5 (by homology)	CHRM5	P08912	CHEMBL2036	<div style="width: 100%; height: 10px; background-color: green;"></div>	42 / 1	Membrane receptor
Muscarinic acetylcholine receptor M1	CHRM1	P11225	CHEMBL216	<div style="width: 100%; height: 10px; background-color: green;"></div>	40 / 1	Membrane receptor
Muscarinic acetylcholine receptor M3 (by homology)	CHRM3	P20309	CHEMBL245	<div style="width: 100%; height: 10px; background-color: green;"></div>	42 / 1	Membrane receptor
Cyclin dependent kinase 1	CDK1	P08493	CHEMBL308	<div style="width: 100%; height: 10px; background-color: green;"></div>	18 / 1	Ser_Thr Kinase
Cyclin dependent kinase 4 (by homology)	CDK4	P11602	CHEMBL331	<div style="width: 100%; height: 10px; background-color: green;"></div>	18 / 1	Ser_Thr Kinase
Cyclin dependent kinase 2	CDK2	P24941	CHEMBL381	<div style="width: 100%; height: 10px; background-color: green;"></div>	18 / 1	Ser_Thr Kinase
Cyclin-dependent kinase 3 (by homology)	CDK3	Q00528	CHEMBL4442	<div style="width: 100%; height: 10px; background-color: green;"></div>	18 / 1	Ser_Thr Kinase
Cyclin-dependent kinase 6 (by homology)	CDK6	Q00534	CHEMBL2506	<div style="width: 100%; height: 10px; background-color: green;"></div>	18 / 1	Ser_Thr Kinase
Alpha 1A adrenergic receptor (by homology)	ADRA1A	P08048	CHEMBL229	<div style="width: 100%; height: 10px; background-color: green;"></div>	28 / 1	Membrane receptor
Muscleblind-like protein 1	MBNL1	Q8NR06	CHEMBL1293317	<div style="width: 100%; height: 10px; background-color: green;"></div>	66 / 3	Unclassified
Muscleblind-like protein 2 (by homology)	MBNL2	Q8VZF2		<div style="width: 100%; height: 10px; background-color: green;"></div>	66 / 3	Unclassified
Muscleblind-like protein 3 (by homology)	MBNL3	Q8NUN0		<div style="width: 100%; height: 10px; background-color: green;"></div>	68 / 3	Unclassified
D(2) dopamine receptor	DRD2	P14416	CHEMBL217	<div style="width: 100%; height: 10px; background-color: green;"></div>	61 / 1	Membrane receptor

* Probabilities have been computed based on a cross-validation. They may therefore not represent the actual probability of success for any new molecule (see FAQ).

Swiss Institute of Bioinformatics · © 2013

6epi-Leoleorin F

SwissTargetPrediction

Home | FAQ | Help | Download | Contact | Disclaimer

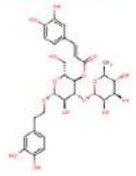
List of predicted targets

These targets have been predicted using the method described in:

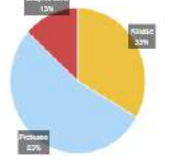
Gfeller D., Michielin O. & Zoete V. Shaping the interaction landscape of bioactive molecules. *Bioinformatics* (2013) 29:3073-3078.

Retrieve data:

Query Molecule



General Target Classes



Target	Common name	Uniprot ID	ChEMBL ID	Probability*	# sim. cmpds (30 / 20)	Target Class
Protein kinase C gamma type (by homology)	PRKCG	P05129	CHEMBL2938		10 / 58	Ser_Thr_Kinase
Protein kinase D beta type (by homology)	PRKCB	P05771	CHEMBL3045		18 / 28	Ser_Thr_Kinase
Protein kinase C alpha type	PRKCA	P17262	CHEMBL299		18 / 28	Ser_Thr_Kinase
Protein kinase C theta type (by homology)	PRKCD	Q04759	CHEMBL3920		18 / 40	Ser_Thr_Kinase
Protein kinase C delta type regulatory subunit (by homology)	PRKCD	Q05655	CHEMBL2990		18 / 40	Ser_Thr_Kinase
22 kDa interstitial collagenase (by homology)	MMP1	P03950	CHEMBL332		1 / 5	Metallo Protease
PEX	MMP2	P08263	CHEMBL233		2 / 5	Metallo Protease
Stromelysin-1 (by homology)	MMP3	P08294	CHEMBL283		1 / 5	Metallo Protease
67 kDa matrix metalloproteinase-9 (by homology)	MMP9	P14780	CHEMBL321		2 / 5	Metallo Protease
Macrophage metalloelastase	MMP12	P35900	CHEMBL4383		1 / 5	Metallo Protease
Collagenase 3 (by homology)	MMP13	P45452	CHEMBL280		1 / 5	Metallo Protease
Stromelysin-2 (by homology)	MMP10	P09238	CHEMBL4270		1 / 5	Metallo Protease
Matrix metalloproteinase-27 (by homology)	MMP27	Q9H305		1 / 5	Metallo Protease	
Aldo-keto reductase family 1 member B10	AKR1B10	Q00216	CHEMBL5983		1 / 23	Enzyme
Aldose reductase	AKR1B1	P15121	CHEMBL1900		1 / 23	Enzyme

* Probabilities have been computed based on a cross-validation. They may therefore not represent the actual probability of success for any new molecule (see FAQ).

Swiss Institute of Bioinformatics - © 2013

Acteoside

SwissTargetPrediction

Home | FAQ | Help | Download | Contact | Disclaimer

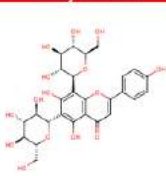
List of predicted targets

These targets have been predicted using the method described in:

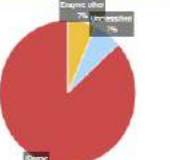
Gfeller D., Michielin O. & Zoete V. Shaping the interaction landscape of bioactive molecules. *Bioinformatics* (2013) 29:3073-3078.

Retrieve data:

Query Molecule



General Target Classes



Target	Common name	Uniprot ID	ChEMBL ID	Probability*	# sim. cmpds (30 / 20)	Target Class
Troponin-C phosphodiesterase 1	TDP1	Q9N1W9	CHEMBL1075138		2 / 10	Enzyme
Microtubule-associated protein tau	MAPT	P10936	CHEMBL1293224		0 / 16	Unclassified
Dual specificity tyrosine phosphorylation-regulated kinase 1A	DYRK1A	Q13027	CHEMBL2252		5 / 11	Ser_Thr_Tyr_Kinase
Protein kinase C gamma type	PRKCG	P05129	CHEMBL2938		2 / 1	Ser_Thr_Kinase
Protein kinase C beta type	PRKCB	P05771	CHEMBL3045		2 / 1	Ser_Thr_Kinase
Protein kinase C alpha type	PRKCA	P17262	CHEMBL299		2 / 1	Ser_Thr_Kinase
Protein kinase C eta type	PRKCH	P24723	CHEMBL2816		1 / 1	Ser_Thr_Kinase
Protein kinase C epsilon type	PRKCE	Q02190	CHEMBL3582		1 / 1	Ser_Thr_Kinase
Protein kinase C theta type	PRKCD	Q04759	CHEMBL3920		2 / 1	Ser_Thr_Kinase
Protein kinase C delta type regulatory subunit	PRKCD	Q05655	CHEMBL2990		2 / 1	Ser_Thr_Kinase
Cyclin-dependent kinase 1	CDK1	P06490	CHEMBL303		1 / 7	Ser_Thr_Kinase
Cyclin-dependent kinase 4	CDK4	P11802	CHEMBL331		1 / 7	Ser_Thr_Kinase
Cyclin-dependent kinase 2	CDK2	P24841	CHEMBL301		1 / 7	Ser_Thr_Kinase
Cyclin-dependent kinase 3	CDK3	Q00520	CHEMBL4442		1 / 7	Ser_Thr_Kinase
Cyclin-dependent kinase 6	CDK6	Q00534	CHEMBL2508		1 / 7	Ser_Thr_Kinase

* Probabilities have been computed based on a cross-validation. They may therefore not represent the actual probability of success for any new molecule (see FAQ).

Swiss Institute of Bioinformatics - © 2013

Apigenin-6-C-alpha-arabinoside-8-C-beta-glucoside

SIB
Swiss Institute of Bioinformatics

SwissTargetPrediction

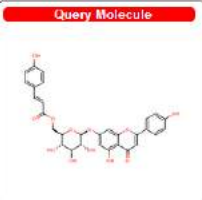
Home FAQ Help Download Contact Disclaimer

List of predicted targets


These targets have been predicted using the method described in:


Gfeller D., Micheli D. & Zoete V. Shaping the interaction landscape of bioactive molecules. *Bioinformatics* (2013) 29:3073-3079.
















Query Molecule



General Target Classes



Retrieve data: 

Target	Common name	Uniprot ID	ChEMBL ID	Probability*	# sim. cmpds (3D / 2D)	Target Class
Adenosine receptor A1 (by homology)	ADORA1	P30042	CHEMBL220		208 / 18	Membrane receptor
Aldose reductase (by homology)	AKR1B1	P15121	CHEMBL1800		6 / 62	Enzyme
Aldo-keto reductase family 1 member B1C (by homology)	AKR1B1C	C6JZ28			6 / 62	Enzyme
Aldo-keto reductase family 1 member B1D (by homology)	AKR1B1D	C6D218	CHEMBL3993		6 / 62	Enzyme
Tyrosyl-DNA phosphodiesterase 1	TDP1	Q8NUW8	CHEMBL1075138		7 / 10	Enzyme
Lysine-specific demethylase 4A	KDM4A	Q75104	CHEMBL2890		1 / 3	Enzyme
Lysine-specific demethylase 4B (by homology)	KDM4B	Q94903			1 / 3	Enzyme
Lysine-specific demethylase 4C (by homology)	KDM4C	Q9H3R0	CHEMBL0178		1 / 3	Enzyme
Xanthine dehydrogenase/oxidase	XDH	P47989	CHEMBL1929		1 / 11	Enzyme
Aldehyde oxidase (by homology)	AOX1	Q00278	CHEMBL3207		1 / 11	Enzyme
cGMP-specific 3',5'-cyclic phosphodiesterase	PDE5A	Q70074	CHEMBL1827		4 / 5	Enzyme
Dual 3',5'-cyclic AMP and -GMP phosphodiesterase 11A (by homology)	PDE11A	Q9HCR9	CHEMBL2711		4 / 5	Enzyme
Prostaglandin G/H synthase 1	PTGS1	P23219	CHEMBL021		2 / 8	Enzyme
Prostaglandin G/H synthase 2	PTGS2	P30364	CHEMBL230		2 / 8	Enzyme
Muscleblind-like protein 1	MBNL1	Q8NR06	CHEMBL129317		0 / 0	Unclassified

* Probabilities have been computed based on a cross-validation. They may therefore not represent the actual probability of success for any new molecule (see FAQ).

Swiss Institute of Bioinformatics - © 2013

Apigenin-7-O-6-O-p-coumaryl-β-glucoside

SIB
Swiss Institute of Bioinformatics

SwissTargetPrediction

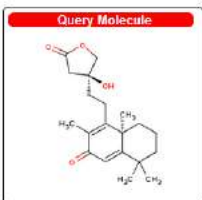
Home FAQ Help Download Contact Disclaimer

List of predicted targets


These targets have been predicted using the method described in:


Gfeller D., Micheli D. & Zoete V. Shaping the interaction landscape of bioactive molecules. *Bioinformatics* (2013) 29:3073-3079.








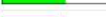







Query Molecule



General Target Classes



Retrieve data: 

Target	Common name	Uniprot ID	ChEMBL ID	Probability*	# sim. cmpds (3D / 2D)	Target Class
Cytochrome P450 19A1	CYP19A1	P11511	CHEMBL1978		81 / 71	Enzyme
Estradiol 17β-dehydrogenase 2	HSD17B2	P37058	CHEMBL2785		67 / 2	Enzyme
Corticosteroid 11β-dehydrogenase isozyme 2	HSD11B2	P90305	CHEMBL2740		67 / 12	Enzyme
Glucocorticoid receptor	NR3C1	P04150	CHEMBL2034		225 / 62	Transcription Factor
Mineralocorticoid receptor	NR3C2	P08235	CHEMBL1984		228 / 84	Transcription Factor
Androgen receptor	AR	P10275	CHEMBL1871		160 / 29	Transcription Factor
S-hydroxy-S-methylglutaryl coenzyme A reductase (by homology)	HMGCR	P04035	CHEMBL492		162 / 80	Enzyme
Corticosteroid 11β-dehydrogenase isozyme 1	HSD11B1	P28645	CHEMBL4295		51 / 17	Enzyme
Hydroxysteroid 11β-dehydrogenase 1-like protein (by homology)	HSD11B1L	Q7Z6J1			49 / 17	Enzyme
Steroid 17α-hydroxylase/17,20 lyase	CYP17A1	P00093	CHEMBL3822		55 / 10	Enzyme
Microtubule-associated protein tsu	MAPT	P10836	CHEMBL1293224		310 / 26	Unclassified
Progesterone receptor	PGR	P08401	CHEMBL200		80 / 15	Transcription Factor
Cannabinoid receptor 1 (by homology)	CNR1	P21554	CHEMBL216		197 / 25	Membrane receptor
Cannabinoid receptor 2	CNR2	P34872	CHEMBL263		140 / 13	Membrane receptor
Estrogen receptor	ESR1	P03372	CHEMBL296		62 / 5	Transcription Factor

* Probabilities have been computed based on a cross-validation. They may therefore not represent the actual probability of success for any new molecule (see FAQ).

Swiss Institute of Bioinformatics - © 2013

13ξ-hydroxyabd-5(6) 8(9)-dien-7-on-16 15-olide

Appendix 9: Target prediction of Compounds using swistargetprediction.ch

Compound Name	Target	Uniprot ID	Gene code	Probability
6-Methoxyluteolin-4-methylether	Aldose reductase	P15121	AKR1B1	0.85
	Aldo-keto reductase family 1 member B15	C9JRZ8	AKR1B15	0.85
	Aldo-keto reductase family 1 member B10	O60218	AKR1B10	0.85
	Microtubule-associated protein tau	P10636	MAPT	0.8
	Xanthine dehydrogenase/oxidase	P47989	XDH	0.78
	Aldehyde oxidase	Q06278	AOX1	0.78
	FAD-linked sulfhydryl oxidase ALR	P55789	GFER	0.78
	Adenosine receptor A1	P30542	ADORA1	0.73
	Dual specificity tyrosine-phosphorylation-regulated kinase 1A	Q13627	DYRK1A	0.73

	Adenosine receptor A2a	P29274	ADORA2A	0.69
	Arachidonate 5-lipoxygenase	P09917	ALOX5	0.67
	Arachidonate 15-lipoxygenase	P16050	ALOX15	0.67
	Arachidonate 12-lipoxygenase 12S-type	P18054	ALOX12	0.67
	Arachidonate 15-lipoxygenase B	O15296	ALOX15B	0.67
	Arachidonate 12-lipoxygenase 12R-type	O75342	ALOX12B	0.67
13-R Premarrubin	M-phase inducer phosphatase 2	P30305	CDC25B	0.14
	M-phase inducer phosphatase 1	P30304	CDC25A	0.14
	Complex	P49354&P49356	FNTA&FNTB	0.14

	Complex	P53609&P49354	PGGT1B&FNTA	0.14
	Cytochrome P450 19A1	P11511	CYP19A1	0.13
	Microtubule-associated protein tau	P10636	MAPT	0.11
	Tyrosyl-DNA phosphodiesterase 1	Q9NUW8	TDP1	0.11
	Prostaglandin G/H synthase 1	P23219	PTGS1	0.1
	Prostaglandin G/H synthase 2	P35354	PTGS2	0.1
	Platelet-activating factor receptor	P25105	PTAFR	0.09
	Potassium voltage-gated channel subfamily A member 3	P22001	KCNA3	0.09
	Potassium voltage-gated channel subfamily A member 5	P22460	KCNA5	0.09
	Potassium voltage-gated channel subfamily A member 2	P16389	KCNA2	0.09
	Potassium voltage-gated channel subfamily A member 6	P17658	KCNA6	0.09

	Potassium voltage-gated channel subfamily A member 4	P22459	KCNA4	0.09
13-S Premarrubin	Prostaglandin G/H synthase 1	P23219	PTGS1	0.18
	Prostaglandin G/H synthase 2	P35354	PTGS2	0.18
	Microtubule-associated protein tau	P10636	MAPT	0.15
	M-phase inducer phosphatase 2	P30305	CDC25B	0.14
	M-phase inducer phosphatase 1	P30304	CDC25A	0.14
	Complex	P49354&P4 9356	FNTA&FNT B	0.12
	Complex	P53609&P4 9354	PGGT1B&F NTA	0.12
	Tyrosyl-DNA phosphodiesterase 1	Q9NUW8	TDP1	0.12
	Cytochrome P450 19A1	P11511	CYP19A1	0.1
	Mu-type opioid receptor	P35372	OPRM1	0.1

	Delta-type opioid receptor	P41143	OPRD1	0.1
	Kappa-type opioid receptor	P41145	OPRK1	0.1
	Nociceptin receptor	P41146	OPRL1	0.1
	Potassium voltage-gated channel subfamily A member 3	P22001	KCNA3	0.09
	Potassium voltage-gated channel subfamily A member 5	P22460	KCNA5	0.09
13 ξ -hydroxylabd-5(6) 8(9)-dien-7-on-16 15-olide	Cytochrome P450 19A1	P11511	CYP19A1	0.83
	Estradiol 17-beta-dehydrogenase 2	P37059	HSD17B2	0.61
	Corticosteroid 11-beta-dehydrogenase isozyme 2	P80365	HSD11B2	0.61
	Glucocorticoid receptor	P04150	NR3C1	0.58
	Mineralocorticoid receptor	P08235	NR3C2	0.58

	Androgen receptor	P10275	AR	0.56
	3-hydroxy-3-methylglutaryl-coenzyme A reductase	P04035	HMGCR	0.56
	Corticosteroid 11-beta-dehydrogenase isozyme 1	P28845	HSD11B1	0.51
	Hydroxysteroid 11-beta-dehydrogenase 1-like protein	Q7Z5J1	HSD11B1L	0.51
	Steroid 17-alpha-hydroxylase/17	20 lyase	P05093	0.49
	Microtubule-associated protein tau	P10636	MAPT	0.49
	Progesterone receptor	P06401	PGR	0.49
	Cannabinoid receptor 1	P21554	CNR1	0.49
	Cannabinoid receptor 2	P34972	CNR2	0.49
	Oestrogen receptor	P03372	ESR1	0.47
	Microtubule-associated protein tau	P10636	MAPT	0.65

14 α -hydroxy-9 α 13 α -epoxylabd-5(6)-en-7-on-16 15-olide	Prostaglandin G/H synthase 1	P23219	PTGS1	0.61
	Prostaglandin G/H synthase 2	P35354	PTGS2	0.61
	Quinone oxidoreductase	Q08257	CRYZ	0.61
	Androgen receptor	P10275	AR	0.56
	3-hydroxy-3-methylglutaryl-coenzyme A reductase	P04035	HMGCR	0.56
	Protein kinase C gamma type	P05129	PRKCG	0.5
	Protein kinase C beta type	P05771	PRKCB	0.5
	Protein kinase C alpha type	P17252	PRKCA	0.5
	Protein kinase C theta type	Q04759	PRKCQ	0.5
	Protein kinase C delta type regulatory subunit	Q05655	PRKCD	0.5
	Mineralocorticoid receptor	P08235	NR3C2	0.5
	Transcription factor p65	Q04206	RELA	0.48

	Proto-oncogene c-Rel	Q04864	REL	0.48
	Estradiol 17-beta-dehydrogenase 2	P37059	HSD17B2	0.48
16epi-Leoleorin F	Muscarinic acetylcholine receptor M2	P08172	CHRM2	0.54
	Muscarinic acetylcholine receptor M4	P08173	CHRM4	0.54
	Muscarinic acetylcholine receptor M5	P08912	CHRM5	0.54
	Muscarinic acetylcholine receptor M1	P11229	CHRM1	0.54
	Muscarinic acetylcholine receptor M3	P20309	CHRM3	0.54
	Cyclin-dependent kinase 1	P06493	CDK1	0.44
	Cyclin-dependent kinase 4	P11802	CDK4	0.44
	Cyclin-dependent kinase 2	P24941	CDK2	0.44

	Cyclin-dependent kinase 3	Q00526	CDK3	0.44
	Cyclin-dependent kinase 6	Q00534	CDK6	0.44
	Cytochrome P450 2D6	P10635	CYP2D6	0.4
	Cytochrome P450 2J2	P51589	CYP2J2	0.4
	D(2) dopamine receptor	P14416	DRD2	0.36
	D(4) dopamine receptor	P21917	DRD4	0.36
	D(3) dopamine receptor	P35462	DRD3	0.36
Acteoside	Protein kinase C gamma type	P05129	PRKCG	0.97
	Protein kinase C beta type	P05771	PRKCB	0.97
	Protein kinase C alpha type	P17252	PRKCA	0.97
	Protein kinase C theta type	Q04759	PRKCQ	0.97
	Protein kinase C delta type regulatory subunit	Q05655	PRKCD	0.97

	22 kDa interstitial collagenase	P03956	MMP1	0.95
	PEX	P08253	MMP2	0.95
	Stromelysin-1	P08254	MMP3	0.95
	67 kDa matrix metalloproteinase-9	P14780	MMP9	0.95
	Macrophage metalloelastase	P39900	MMP12	0.95
	Collagenase 3	P45452	MMP13	0.95
	Stromelysin-2	P09238	MMP10	0.95
	Matrix metalloproteinase-27	Q9H306	MMP27	0.95
	Aldo-keto reductase family 1 member B10	O60218	AKR1B10	0.38
	Aldose reductase	P15121	AKR1B1	0.38
Apigenin	Aldo-keto reductase family 1 member B10	O60218	AKR1B10	0.95

	Oestrogen receptor	P03372	ESR1	0.95
	Cytochrome P450 1A2	P05177	CYP1A2	0.95
	Cyclin-dependent kinase 1	P06493	CDK1	0.95
	Microtubule-associated protein tau	P10636	MAPT	0.95
	Cytochrome P450 19A1	P11511	CYP19A1	0.95
	Cyclin-dependent kinase 4	P11802	CDK4	0.95
	Estradiol 17-beta-dehydrogenase 1	P14061	HSD17B1	0.95
	Aldose reductase	P15121	AKR1B1	0.95
	Casein kinase II subunit alpha'	P19784	CSNK2A2	0.95
	Amine oxidase [flavin-containing] A	P21397	MAOA	0.95
	Prostaglandin G/H synthase 1	P23219	PTGS1	0.95
	Cyclin-dependent kinase 2	P24941	CDK2	0.95

	Amine oxidase [flavin-containing] B	P27338	MAOB	0.95
	Adenosine receptor A2a	P29274	ADORA2A	0.95
Apigenin-6-C- α -arabinoside-8-C- β -glucoside	Tyrosyl-DNA phosphodiesterase 1	Q9NUW8	TDP1	0.53
	Microtubule-associated protein tau	P10636	MAPT	0.45
	Dual specificity tyrosine-phosphorylation-regulated kinase 1A	Q13627	DYRK1A	0.22
	Protein kinase C gamma type	P05129	PRKCG	0.16
	Protein kinase C beta type	P05771	PRKCB	0.16
	Protein kinase C alpha type	P17252	PRKCA	0.16
	Protein kinase C eta type	P24723	PRKCH	0.16
	Protein kinase C epsilon type	Q02156	PRKCE	0.16

	Protein kinase C theta type	Q04759	PRKCQ	0.16
	Protein kinase C delta type regulatory subunit	Q05655	PRKCD	0.16
	Cyclin-dependent kinase 1	P06493	CDK1	0.16
	Cyclin-dependent kinase 4	P11802	CDK4	0.16
	Cyclin-dependent kinase 2	P24941	CDK2	0.16
	Cyclin-dependent kinase 3	Q00526	CDK3	0.16
	Cyclin-dependent kinase 6	Q00534	CDK6	0.16
Apigenin-7-O-(6''-O-p-coumaroyl)- β -glucoside	Adenosine receptor A1	P30542	ADORA1	0.75
	Aldose reductase	P15121	AKR1B1	0.71
	Aldo-keto reductase family 1 member B15	C9JRZ8	AKR1B15	0.71
	Aldo-keto reductase family 1 member B10	O60218	AKR1B10	0.71

	Tyrosyl-DNA phosphodiesterase 1	Q9NUW8	TDP1	0.66
	Lysine-specific demethylase 4A	O75164	KDM4A	0.66
	Lysine-specific demethylase 4B	O94953	KDM4B	0.66
	Lysine-specific demethylase 4C	Q9H3R0	KDM4C	0.66
	Xanthine dehydrogenase/oxidase	P47989	XDH	0.51
	Aldehyde oxidase	Q06278	AOX1	0.51
	cGMP-specific 3' 5'-cyclic phosphodiesterase	O76074	PDE5A	0.41
	Dual 3' 5'-cyclic-AMP and -GMP phosphodiesterase 11A	Q9HCR9	PDE11A	0.41
	Prostaglandin G/H synthase 1	P23219	PTGS1	0.38
	Prostaglandin G/H synthase 2	P35354	PTGS2	0.38
	Muscleblind-like protein 1	Q9NR56	MBNL1	0.34
Chryseriol	Cytochrome P450 1A2	P05177	CYP1A2	1

Multidrug resistance-associated protein 1	P33527	ABCC1	1
Cytochrome P450 1B1	Q16678	CYP1B1	1
Cytochrome P450 1A1	P04798	CYP1A1	1
Canalicular multispecific organic anion transporter 2	O15438	ABCC3	1
Canalicular multispecific organic anion transporter 1	Q92887	ABCC2	1
Aldose reductase	P15121	AKR1B1	0.85
Aldo-keto reductase family 1 member B15	C9JRZ8	AKR1B15	0.85
Aldo-keto reductase family 1 member B10	O60218	AKR1B10	0.85
Plasmin light chain B	P00747	PLG	0.83
Apolipoprotein(a)	P08519	LPA	0.83

	Xanthine dehydrogenase/oxidase	P47989	XDH	0.82
	Aldehyde oxidase	Q06278	AOX1	0.82
	NADPH oxidase 4	Q9NPH5	NOX4	0.79
	Oestrogen receptor	P03372	ESR1	0.76
Compound X	Protein kinase C gamma type	P05129	PRKCG	0.72
	Protein kinase C beta type	P05771	PRKCB	0.72
	Protein kinase C alpha type	P17252	PRKCA	0.72
	Multidrug resistance protein 1	P08183	ABCB1	0.59
	Bile salt export pump	O95342	ABCB11	0.59
	Multidrug resistance protein 3	P21439	ABCB4	0.59
	ATP-binding cassette sub-family B member 5	Q2M3G0	ABCB5	0.59
	Microtubule-associated protein tau	P10636	MAPT	0.56

	Transient receptor potential cation channel subfamily V member 4	Q9HBA0	TRPV4	0.52
	Platelet-activating factor receptor	P25105	PTAFR	0.52
	Tyrosine-protein phosphatase non-receptor type 2	P17706	PTPN2	0.48
	Tyrosine-protein phosphatase non-receptor type 1	P18031	PTPN1	0.48
	Cannabinoid receptor 1	P21554	CNR1	0.48
	Cannabinoid receptor 2	P34972	CNR2	0.48
	Mu-type opioid receptor	P35372	OPRM1	0.41
Leoleorin A	Mu-type opioid receptor	P35372	OPRM1	0.34
	Delta-type opioid receptor	P41143	OPRD1	0.34
	Kappa-type opioid receptor	P41145	OPRK1	0.34
	Nociceptin receptor	P41146	OPRL1	0.34

Microtubule-associated protein tau	P10636	MAPT	0.32
Macrophage migration inhibitory factor	P14174	MIF	0.25
Cytochrome P450 19A1	P11511	CYP19A1	0.23
Androgen receptor	P10275	AR	0.22
Glucocorticoid receptor	P04150	NR3C1	0.21
Mineralocorticoid receptor	P08235	NR3C2	0.21
Tyrosyl-DNA phosphodiesterase 1	Q9NUW8	TDP1	0.19
Cannabinoid receptor 1	P21554	CNR1	0.19
Cannabinoid receptor 2	P34972	CNR2	0.19
Dual specificity protein phosphatase 3	P51452	DUSP3	0.18
Inactive dual specificity phosphatase 27	Q5VZP5	DUSP27	0.18

Comosiin	Tyrosyl-DNA phosphodiesterase 1	Q9NUW8	TDP1	0.93
	Aldo-keto reductase family 1 member B10	O60218	AKR1B10	0.91
	Aldose reductase	P15121	AKR1B1	0.91
	Aldo-keto reductase family 1 member B15	C9JRZ8	AKR1B15	0.91
	Lysine-specific demethylase 4A	O75164	KDM4A	0.87
	Lysine-specific demethylase 4B	O94953	KDM4B	0.87
	Lysine-specific demethylase 4C	Q9H3R0	KDM4C	0.87
	Adenosine receptor A1	P30542	ADORA1	0.83
	Muscleblind-like protein 1	Q9NR56	MBNL1	0.71
	Muscleblind-like protein 2	Q5VZF2	MBNL2	0.71
	Muscleblind-like protein 3	Q9NUK0	MBNL3	0.71
Xanthine dehydrogenase/oxidase	P47989	XDH	0.69	

	Aldehyde oxidase	Q06278	AOX1	0.69
	Aldehyde dehydrogenase mitochondrial	P05091	ALDH2	0.65
	Uncharacterized protein	F8VP50		0.65
Cynaroside	Tyrosyl-DNA phosphodiesterase 1	Q9NUW8	TDP1	0.98
	Lysine-specific demethylase 4A	O75164	KDM4A	0.9
	Lysine-specific demethylase 4B	O94953	KDM4B	0.9
	Lysine-specific demethylase 4C	Q9H3R0	KDM4C	0.9
	Aldo-keto reductase family 1 member B10	O60218	AKR1B10	0.88
	Aldose reductase	P15121	AKR1B1	0.88
	Aldo-keto reductase family 1 member B15	C9JRZ8	AKR1B15	0.88
	Xanthine dehydrogenase/oxidase	P47989	XDH	0.82

	Aldehyde oxidase	Q06278	AOX1	0.82
	Adenosine receptor A1	P30542	ADORA1	0.79
	Muscleblind-like protein 1	Q9NR56	MBNL1	0.69
	Muscleblind-like protein 3	Q9NUK0	MBNL3	0.69
	Alcohol dehydrogenase [NADP(+)]	P14550	AKR1A1	0.69
	1, 5-anhydro-D-fructose reductase	Q96JD6	AKR1E2	0.69
Dihydroxyphytyl Palmitate	Protein kinase C gamma type	P05129	PRKCG	0.82
	Protein kinase C beta type	P05771	PRKCB	0.82
	Protein kinase C alpha type	P17252	PRKCA	0.82
	Protein kinase C theta type	Q04759	PRKCQ	0.82
	Protein kinase C delta type regulatory subunit	Q05655	PRKCD	0.82
	Protein kinase C eta type	P24723	PRKCH	0.64

	Protein kinase C epsilon type	Q02156	PRKCE	0.64
	Uncharacterized protein	H0YJX3		0.64
	Cannabinoid receptor 1	P21554	CNR1	0.6
	Cannabinoid receptor 2	P34972	CNR2	0.6
	Platelet-activating factor receptor	P25105	PTAFR	0.46
	3-hydroxy-3-methylglutaryl-coenzyme A reductase	P04035	HMGCR	0.39
	Transient receptor potential cation channel subfamily V member 4	Q9HBA0	TRPV4	0.31
	Tyrosyl-DNA phosphodiesterase 1	Q9NUW8	TDP1	0.29
	Muscleblind-like protein 1	Q9NR56	MBNL1	0.27
EDD	Platelet-activating factor receptor	P25105	PTAFR	0.79
	Microtubule-associated protein tau	P10636	MAPT	0.74
	Cannabinoid receptor 1	P21554	CNR1	0.54

Cannabinoid receptor 2	P34972	CNR2	0.54
Mu-type opioid receptor	P35372	OPRM1	0.52
Delta-type opioid receptor	P41143	OPRD1	0.52
Kappa-type opioid receptor	P41145	OPRK1	0.52
Nociceptin receptor	P41146	OPRL1	0.52
Multidrug resistance protein 1	P08183	ABCB1	0.5
Bile salt export pump	O95342	ABCB11	0.5
Multidrug resistance protein 3	P21439	ABCB4	0.5
ATP-binding cassette sub-family B member 5	Q2M3G0	ABCB5	0.5
Protein kinase C gamma type	P05129	PRKCG	0.46
Protein kinase C beta type	P05771	PRKCB	0.46
Protein kinase C alpha type	P17252	PRKCA	0.46

Geniposidic acid	Microtubule-associated protein tau	P10636	MAPT	0.74
	Hypoxia-inducible factor 1-alpha	Q16665	HIF1A	0.27
	Endothelial PAS domain-containing protein 1	Q99814	EPAS1	0.27
	Tyrosyl-DNA phosphodiesterase 1	Q9NUW8	TDP1	0.18
	Protein kinase C gamma type	P05129	PRKCG	0.18
	Protein kinase C beta type	P05771	PRKCB	0.18
	Protein kinase C alpha type	P17252	PRKCA	0.18
	Protein kinase C theta type	Q04759	PRKCQ	0.18
	Protein kinase C delta type regulatory subunit	Q05655	PRKCD	0.18
	Muscarinic acetylcholine receptor M2	P08172	CHRM2	0.14

	Muscarinic acetylcholine receptor M1	P11229	CHRM1	0.14
	Muscarinic acetylcholine receptor M3	P20309	CHRM3	0.14
	Muscarinic acetylcholine receptor M4	P08173	CHRM4	0.14
	Transient receptor potential cation channel subfamily V member 1	Q8NER1	TRPV1	0.14
	Sodium-dependent noradrenaline transporter	P23975	SLC6A2	0.14
Leoleorin B	M-phase inducer phosphatase 1	P30304	CDC25A	0.21
	Dual specificity protein phosphatase 3	P51452	DUSP3	0.21
	M-phase inducer phosphatase 2	P30305	CDC25B	0.21
	Inactive dual specificity phosphatase 27	Q5VZP5	DUSP27	0.21

	Dual specificity phosphatase DUPD1	Q68J44	DUPD1	0.21
	Dual specificity protein phosphatase 13 isoform MDSP	Q6B8I1	DUSP13	0.21
	Dual specificity protein phosphatase 26	Q9BV47	DUSP26	0.21
	Cannabinoid receptor 1	P21554	CNR1	0.18
	Cannabinoid receptor 2	P34972	CNR2	0.18
	Tyrosine-protein phosphatase non- receptor type 1	P18031	PTPN1	0.11
	Tyrosine-protein phosphatase non- receptor type 2	P17706	PTPN2	0.11
	Microtubule-associated protein tau	P10636	MAPT	0.11
	Mu-type opioid receptor	P35372	OPRM1	0.1
	Delta-type opioid receptor	P41143	OPRD1	0.1
	Kappa-type opioid receptor	P41145	OPRK1	0.1

Leoleorin C	Platelet-activating factor receptor	P25105	PTAFR	0.85
	Microtubule-associated protein tau	P10636	MAPT	0.71
	Protein kinase C gamma type	P05129	PRKCG	0.67
	Protein kinase C beta type	P05771	PRKCB	0.67
	Protein kinase C alpha type	P17252	PRKCA	0.67
	Protein kinase C theta type	Q04759	PRKCQ	0.67
	Protein kinase C delta type regulatory subunit	Q05655	PRKCD	0.67
	Multidrug resistance protein 1	P08183	ABCB1	0.65
	Bile salt export pump	O95342	ABCB11	0.65
	Multidrug resistance protein 3	P21439	ABCB4	0.65
	ATP-binding cassette sub-family B member 5	Q2M3G0	ABCB5	0.65
	Mu-type opioid receptor	P35372	OPRM1	0.63

	Delta-type opioid receptor	P41143	OPRD1	0.63
	Kappa-type opioid receptor	P41145	OPRK1	0.63
	Nociceptin receptor	P41146	OPRL1	0.63
Leoleorin D	Glucosylceramidase	P04062	GBA	0.56
	Muscleblind-like protein 1	Q9NR56	MBNL1	0.42
	Muscleblind-like protein 2	Q5VZF2	MBNL2	0.42
	Muscleblind-like protein 3	Q9NUK0	MBNL3	0.42
	Microtubule-associated protein tau	P10636	MAPT	0.38
	Multidrug resistance protein 1	P08183	ABCB1	0.31
	Bile salt export pump	O95342	ABCB11	0.31
	Multidrug resistance protein 3	P21439	ABCB4	0.31
	ATP-binding cassette sub-family B member 5	Q2M3G0	ABCB5	0.31

	Protein kinase C gamma type	P05129	PRKCG	0.31
	Protein kinase C beta type	P05771	PRKCB	0.31
	Protein kinase C alpha type	P17252	PRKCA	0.31
	Protein kinase C theta type	Q04759	PRKCQ	0.31
	Protein kinase C delta type regulatory subunit	Q05655	PRKCD	0.31
	DNA polymerase alpha catalytic subunit	P09884	POLA1	0.29
Leoleorin E	Cyclin-dependent kinase 1	P06493	CDK1	0.44
	Cyclin-dependent kinase 4	P11802	CDK4	0.44
	Cyclin-dependent kinase 2	P24941	CDK2	0.44
	Cyclin-dependent kinase 3	Q00526	CDK3	0.44

	Cyclin-dependent kinase 6	Q00534	CDK6	0.44
	Muscarinic acetylcholine receptor M2	P08172	CHRM2	0.42
	Muscarinic acetylcholine receptor M4	P08173	CHRM4	0.42
	Muscarinic acetylcholine receptor M1	P11229	CHRM1	0.42
	Muscarinic acetylcholine receptor M3	P20309	CHRM3	0.42
	Muscarinic acetylcholine receptor M5	P08912	CHRM5	0.42
	Tyrosyl-DNA phosphodiesterase 1	Q9NUW8	TDP1	0.36
	Muscleblind-like protein 1	Q9NR56	MBNL1	0.36
	Muscleblind-like protein 2	Q5VZF2	MBNL2	0.36
	Muscleblind-like protein 3	Q9NUK0	MBNL3	0.36

	5-hydroxytryptamine receptor 1B	P28222	HTR1B	0.31
Leoleorin F	Muscarinic acetylcholine receptor M2	P08172	CHRM2	0.47
	Muscarinic acetylcholine receptor M4	P08173	CHRM4	0.47
	Muscarinic acetylcholine receptor M5	P08912	CHRM5	0.47
	Muscarinic acetylcholine receptor M1	P11229	CHRM1	0.47
	Muscarinic acetylcholine receptor M3	P20309	CHRM3	0.47
	Cyclin-dependent kinase 1	P06493	CDK1	0.38
	Cyclin-dependent kinase 4	P11802	CDK4	0.38
	Cyclin-dependent kinase 2	P24941	CDK2	0.38
	Cyclin-dependent kinase 3	Q00526	CDK3	0.38
	Cyclin-dependent kinase 6	Q00534	CDK6	0.38

	Alpha-1A adrenergic receptor	P35348	ADRA1A	0.31
	Muscleblind-like protein 1	Q9NR56	MBNL1	0.31
	Muscleblind-like protein 2	Q5VZF2	MBNL2	0.31
	Muscleblind-like protein 3	Q9NUK0	MBNL3	0.31
	D(2) dopamine receptor	P14416	DRD2	0.29
Leoleorin G	Muscarinic acetylcholine receptor M2	P08172	CHRM2	0.54
	Muscarinic acetylcholine receptor M4	P08173	CHRM4	0.54
	Muscarinic acetylcholine receptor M5	P08912	CHRM5	0.54
	Muscarinic acetylcholine receptor M1	P11229	CHRM1	0.54
	Muscarinic acetylcholine receptor M3	P20309	CHRM3	0.54
	Cyclin-dependent kinase 1	P06493	CDK1	0.44

	Cyclin-dependent kinase 4	P11802	CDK4	0.44
	Cyclin-dependent kinase 2	P24941	CDK2	0.44
	Cyclin-dependent kinase 3	Q00526	CDK3	0.44
	Cyclin-dependent kinase 6	Q00534	CDK6	0.44
	Cytochrome P450 2D6	P10635	CYP2D6	0.4
	Cytochrome P450 2J2	P51589	CYP2J2	0.4
	D(2) dopamine receptor	P14416	DRD2	0.36
	D(4) dopamine receptor	P21917	DRD4	0.36
	D(3) dopamine receptor	P35462	DRD3	0.36
Leoleorin H	Androgen receptor	P10275	AR	0.66
	Protein kinase C gamma type	P05129	PRKCG	0.64
	Protein kinase C beta type	P05771	PRKCB	0.64

	Protein kinase C alpha type	P17252	PRKCA	0.64
	Protein kinase C theta type	Q04759	PRKCQ	0.64
	Protein kinase C delta type regulatory subunit	Q05655	PRKCD	0.64
	3-hydroxy-3-methylglutaryl-coenzyme A reductase	P04035	HMGCR	0.62
	Mineralocorticoid receptor	P08235	NR3C2	0.57
	Microtubule-associated protein tau	P10636	MAPT	0.55
	Quinone oxidoreductase	Q08257	CRYZ	0.55
	Oestrogen receptor	P03372	ESR1	0.55
	Glucocorticoid receptor	P04150	NR3C1	0.55
	Oestrogen receptor beta	Q92731	ESR2	0.55
	Arachidonate 5-lipoxygenase	P09917	ALOX5	0.46

	Arachidonate 15-lipoxygenase	P16050	ALOX15	0.46
Leoleorin I	Quinone oxidoreductase	Q08257	CRYZ	0.61
	Microtubule-associated protein tau	P10636	MAPT	0.49
	Mineralocorticoid receptor	P08235	NR3C2	0.47
	Cytochrome P450 19A1	P11511	CYP19A1	0.44
	Protein kinase C gamma type	P05129	PRKCG	0.44
	Protein kinase C beta type	P05771	PRKCB	0.44
	Protein kinase C alpha type	P17252	PRKCA	0.44
	Protein kinase C theta type	Q04759	PRKCQ	0.44
	Protein kinase C delta type regulatory subunit	Q05655	PRKCD	0.44
	3-hydroxy-3-methylglutaryl-coenzyme A reductase	P04035	HMGCR	0.4
	Androgen receptor	P10275	AR	0.4

	Transcription factor AP-1	P05412	JUN	0.4
	Transcription factor jun-B	P17275	JUNB	0.4
	Transcription factor jun-D	P17535	JUND	0.4
	Glucocorticoid receptor	P04150	NR3C1	0.36
Leoleorin J	Androgen receptor	P10275	AR	0.56
	Tyrosyl-DNA phosphodiesterase 1	Q9NUW8	TDP1	0.51
	Protein kinase C gamma type	P05129	PRKCG	0.38
	Protein kinase C beta type	P05771	PRKCB	0.38
	Protein kinase C alpha type	P17252	PRKCA	0.38
	Protein kinase C theta type	Q04759	PRKCQ	0.38
	Protein kinase C delta type regulatory subunit	Q05655	PRKCD	0.38

	DNA polymerase alpha catalytic subunit	P09884	POLA1	0.38
	3-hydroxy-3-methylglutaryl-coenzyme A reductase	P04035	HMGCR	0.36
	Quinone oxidoreductase	Q08257	CRYZ	0.36
	Mineralocorticoid receptor	P08235	NR3C2	0.36
	cAMP-specific 3'5'-cyclic phosphodiesterase 4B	Q07343	PDE4B	0.33
	cAMP-specific 3'5'-cyclic phosphodiesterase 4D	Q08499	PDE4D	0.33
	cAMP-specific 3'5'-cyclic phosphodiesterase 4A	P27815	PDE4A	0.33
	cAMP-specific 3'5'-cyclic phosphodiesterase 4C	Q08493	PDE4C	0.33
Leonurun	Microtubule-associated protein tau	P10636	MAPT	0.31
	Carbonic anhydrase 12	O43570	CA12	0.29

	Carbonic anhydrase 1	P00915	CA1	0.29
	Carbonic anhydrase 2	P00918	CA2	0.29
	Carbonic anhydrase 3	P07451	CA3	0.29
	Carbonic anhydrase 5A	P35218	CA5A	0.29
	Carbonic anhydrase 7	P43166	CA7	0.29
	Carbonic anhydrase 9	Q16790	CA9	0.29
	Carbonic anhydrase 14	Q9ULX7	CA14	0.29
	Carbonic anhydrase 5B	Q9Y2D0	CA5B	0.29
	Carbonic anhydrase 13	Q8N1Q1	CA13	0.29
	5-hydroxytryptamine receptor 1A	P08908	HTR1A	0.24
	5-hydroxytryptamine receptor 1B	P28222	HTR1B	0.24
	Muscleblind-like protein 1	Q9NR56	MBNL1	0.23

	Muscleblind-like protein 2	Q5VZF2	MBNL2	0.23
Luteolin	22 kDa interstitial collagenase	P03956	MMP1	0.95
	Cytochrome P450 1A2	P05177	CYP1A2	0.95
	PEX	P08253	MMP2	0.95
	Stromelysin-1	P08254	MMP3	0.95
	67 kDa matrix metalloproteinase-9	P14780	MMP9	0.95
	Aldose reductase	P15121	AKR1B1	0.95
	Amine oxidase [flavin-containing] A	P21397	MAOA	0.95
	Amine oxidase [flavin-containing] B	P27338	MAOB	0.95
	ADP-ribosyl cyclase 1	P28907	CD38	0.95
	Adenosine receptor A1	P30542	ADORA1	0.95

	Macrophage metalloelastase	P39900	MMP12	0.95
	Collagenase 3	P45452	MMP13	0.95
	Xanthine dehydrogenase/oxidase	P47989	XDH	0.95
	Lactoylglutathione lyase	Q04760	GLO1	0.95
	Lysine--tRNA ligase	Q15046	KARS	0.95
Luteolin 7-O- β -glucoside-3-methyl ether	Tyrosyl-DNA phosphodiesterase 1	Q9NUW8	TDP1	0.93
	Lysine-specific demethylase 4A	O75164	KDM4A	0.86
	Lysine-specific demethylase 4B	O94953	KDM4B	0.86
	Lysine-specific demethylase 4C	Q9H3R0	KDM4C	0.86
	Aldo-keto reductase family 1 member B10	O60218	AKR1B10	0.84
	Aldose reductase	P15121	AKR1B1	0.84

	Aldo-keto reductase family 1 member B15	C9JRZ8	AKR1B15	0.84
	Adenosine receptor A1	P30542	ADORA1	0.8
	Xanthine dehydrogenase/oxidase	P47989	XDH	0.77
	Aldehyde oxidase	Q06278	AOX1	0.77
	Dual specificity tyrosine-phosphorylation-regulated kinase 1A	Q13627	DYRK1A	0.63
	Alpha-2A adrenergic receptor	P08913	ADRA2A	0.63
	Alpha-2C adrenergic receptor	P18825	ADRA2C	0.63
	Alcohol dehydrogenase [NADP(+)]	P14550	AKR1A1	0.63
	1,5-anhydro-D-fructose reductase	Q96JD6	AKR1E2	0.63
Marrubin	Mu-type opioid receptor	P35372	OPRM1	0.61
	Delta-type opioid receptor	P41143	OPRD1	0.61

	Kappa-type opioid receptor	P41145	OPRK1	0.61
	Nociceptin receptor	P41146	OPRL1	0.61
	Macrophage migration inhibitory factor	P14174	MIF	0.29
	Tyrosyl-DNA phosphodiesterase 1	Q9NUW8	TDP1	0.29
	Microtubule-associated protein tau	P10636	MAPT	0.27
	Sodium-dependent noradrenaline transporter	P23975	SLC6A2	0.18
	Sodium-dependent serotonin transporter	P31645	SLC6A4	0.18
	Sodium-dependent dopamine transporter	Q01959	SLC6A3	0.18
	Cytochrome P450 19A1	P11511	CYP19A1	0.16
	Sodium- and chloride-dependent glycine transporter 1	P48067	SLC6A9	0.16

	Sodium-dependent proline transporter	Q99884	SLC6A7	0.16
	Sodium- and chloride-dependent neutral and basic amino acid transporter B(0+)	Q9UN76	SLC6A14	0.16
	Sodium- and chloride-dependent glycine transporter 2	Q9Y345	SLC6A5	0.16
Nepetaefolin	Tyrosyl-DNA phosphodiesterase 1	Q9NUW8	TDP1	0.28
	Microtubule-associated protein tau	P10636	MAPT	0.26
	Platelet-activating factor receptor	P25105	PTAFR	0.21
	Prostaglandin G/H synthase 2	P35354	PTGS2	0.19
	Prostaglandin G/H synthase 1	P23219	PTGS1	0.19
	M-phase inducer phosphatase 2	P30305	CDC25B	0.18
	M-phase inducer phosphatase 1	P30304	CDC25A	0.18
	Potassium voltage-gated channel subfamily A member 3	P22001	KCNA3	0.18

	Potassium voltage-gated channel subfamily A member 5	P22460	KCNA5	0.18
	Potassium voltage-gated channel subfamily A member 2	P16389	KCNA2	0.18
	Potassium voltage-gated channel subfamily A member 6	P17658	KCNA6	0.18
	Potassium voltage-gated channel subfamily A member 4	P22459	KCNA4	0.18
	Potassium voltage-gated channel subfamily A member 1	Q09470	KCNA1	0.18
	Potassium voltage-gated channel subfamily A member 10	Q16322	KCNA10	0.18
	Potassium voltage-gated channel subfamily A member 7	Q96RP8	KCNA7	0.18
Stachydrine	Muscleblind-like protein 1	Q9NR56	MBNL1	0.43
	Muscleblind-like protein 2	Q5VZF2	MBNL2	0.43
	Muscleblind-like protein 3	Q9NUK0	MBNL3	0.43

	Tyrosyl-DNA phosphodiesterase 1	Q9NUW8	TDP1	0.42
	Cholinesterase	P06276	BCHE	0.34
	Acetylcholinesterase	P22303	ACHE	0.34
	Renin	P00797	REN	0.27
	Cathepsin D	P07339	CTSD	0.27
	Angiotensin-converting enzyme	P12821	ACE	0.27
	Angiotensin-converting enzyme 2	Q9BYF1	ACE2	0.27
	Napsin-A	O96009	NAPSA	0.27
	Angiotensin-converting enzyme	L7MUH0	ACE	0.27
	Glutamate receptor ionotropic	kainate 1	P39086	0.26
	Excitatory amino acid transporter 2	P43004	SLC1A2	0.26
	Glutamate receptor ionotropic	kainate 2	Q13002	0.26

Succinic Acid	Egl nine homolog 1	Q9GZT9	EGLN1	1
	Egl nine homolog 2	Q96KS0	EGLN2	1
	Tyrosyl-DNA phosphodiesterase 1	Q9NUW8	TDP1	0.45
	Histone deacetylase 3	O15379	HDAC3	0.29
	Histone deacetylase 1	Q13547	HDAC1	0.29
	Histone deacetylase 2	Q92769	HDAC2	0.29
	Microtubule-associated protein tau	P10636	MAPT	0.28
	Lysine-specific demethylase 5C	P41229	KDM5C	0.17
	Histone lysine demethylase PHF8	Q9UPP1	PHF8	0.17
	Lysine-specific demethylase 2A	Q9Y2K7	KDM2A	0.17
	Lysine-specific demethylase 5A	P29375	KDM5A	0.17
	Lysine-specific demethylase 5D	Q9BY66	KDM5D	0.17

	Lysine-specific demethylase 5B	Q9UGL1	KDM5B	0.17
	Lysine-specific demethylase PHF2	O75151	PHF2	0.17
	Lysine-specific demethylase 7	Q6ZMT4	JHDM1D	0.17
Uracil	Microtubule-associated protein tau	P10636	MAPT	0.58
	Thymidylate synthase	P04818	TYMS	0.58
	Thymidine phosphorylase	P19971	TYMP	0.31
	Dihydropyrimidine dehydrogenase [NADP(+)]	Q12882	DPYD	0.28
	Tyrosyl-DNA phosphodiesterase 1	Q9NUW8	TDP1	0.22
	Poly [ADP-ribose] polymerase 1	P09874	PARP1	0.21
	Guanine deaminase	Q9Y2T3	GDA	0.17
	Activation peptide fragment 1	P00734	F2	0.15
	Complex	P07384&P04632	CAPN1&CAPNS1	0.15


	Caspase-3 subunit p12	P42574	CASP3	0.15
	Caspase-2 subunit p18	P42575	CASP2	0.15
	Caspase-7 subunit p20	P55210	CASP7	0.15
	Caspase-6 subunit p18	P55212	CASP6	0.15
	Caspase-8 subunit p18	Q14790	CASP8	0.15
	Ribonuclease H1	O60930	RNASEH1	0.14
Vitexin	Microtubule-associated protein tau	P10636	MAPT	0.84
	Tyrosyl-DNA phosphodiesterase 1	Q9NUW8	TDP1	0.62
	Dual specificity tyrosine-phosphorylation-regulated kinase 1A	Q13627	DYRK1A	0.45
	Aldose reductase	P15121	AKR1B1	0.34
	Aldo-keto reductase family 1 member B15	C9JRZ8	AKR1B15	0.34

	Aldo-keto reductase family 1 member B10	O60218	AKR1B10	0.34
	Sodium/glucose cotransporter 1	P13866	SLC5A1	0.3
	Sodium/glucose cotransporter 2	P31639	SLC5A2	0.3
	Low affinity sodium-glucose cotransporter	Q9NY91	SLC5A4	0.3
	Sodium/glucose cotransporter 5	A0PJK1	SLC5A10	0.3
	Sodium/myo-inositol cotransporter	P53794	SLC5A3	0.3
	Sodium/glucose cotransporter 4	Q2M3M2	SLC5A9	0.3
	Sodium/myo-inositol cotransporter 2	Q8WWX8	SLC5A11	0.3
	Protein kinase C alpha type	P17252	PRKCA	0.26
	Protein kinase C theta type	Q04759	PRKCQ	0.26

Appendix 10: Correlation between Compounds, Protein targets and ethnobotanical uses

Target	Roles	Compounds	Disease Condition	Ethnobotanical Use
AKR1B1 (Aldose Reductase)	Catalyses the NADPH-dependent reduction of a wide variety of carbonyl-containing compounds to their corresponding alcohols with a broad range of catalytic efficiencies.	6-Methoxyluteolin-4-methylether; Apigenin ; Apigenin-7-O-(6''-O-p-coumaroyl)- β -glucoside; Chryseriol; Comosiin; Luteolin; Luteolin 7-O- β -glucoside-3-methyl ether	Diabetic Complications: Neuropathy, Retinopathy, Nephropathy	Skin Diseases: rashes, eczema, itching , boils, haemorrhoids, sores(on the leg and head), wound- healing Piles Spider and Snake Bites, scorpion stings respiratory diseases: cough, asthma. colds, influenza, bronchitis Fever Depression and Anxiety Tuberculosis Leprosy Viral Hepatitis, Jaundice Bladder and Kidney disorder Headache Arthritis Pain above the eye Epilepsy, partial paralysis Cancer cardiovascular disease: Hypertension Diabetes Muscle Cramps Rheumatism Gastrointestinal Conditions: Dysentery, Constipation Delayed Menstruation, Emmenagogue
AKR1B15(Aldo-keto reductase family 1 member B15)	Isoform 1: Mainly acts as a reductive enzyme that catalyses the reduction of androgens and oestrogens with high positional selectivity (shows 17-beta-hydroxysteroid dehydrogenase activity) as well as 3-keto-acyl-CoAs. Has a strong selectivity towards NADP(H)	6-Methoxyluteolin-4-methylether; Apigenin-7-O-(6''-O-p-coumaroyl)- β -glucoside; Chryseriol		

<p>AKR1B10 (Aldo-keto reductase family 1 member B10)</p>	<p>Acts as all-trans-retinaldehyde reductase. Can efficiently reduce aliphatic and aromatic aldehydes and is less active on hexoses (in vitro). May be responsible for detoxification of reactive aldehydes in the digested food before the nutrients are passed on to other organs.</p>	<p>6-Methoxyluteolin-4-methylether; Apigenin ; Apigenin-7-O-(6"-O-p-coumaroyl)-β-glucoside; Chryseriol; Comosiin</p>	<p>Lung and Hepatic Carcinomas; Colorectal and Uterine Cancers; Resistance to anticancer drugs</p>	<p>Anthelmintic, Vermifuge Diuretic Obesity</p>
<p>CYP19A1 (Cytochrome P450 19A1; Aromatase)</p>	<p>Catalyses the formation of aromatic C18 oestrogens from C19 androgens.(responsible for the aromatization of androgens into oestrogens)</p>	<p>13ξ-hydroxylabd-5(6) 8(9)-dien-7-on-16 15-olide; Apigenin(shown to inhibit CYP19A1 leading to hypoestrogenism)</p>	<p>Aromatase excess syndrome (can lead to familial gynecomastia); Aromatase deficiency; Pseudohaermaphroditism</p>	
<p>PRKCG(Protein kinase C gamma type</p>	<p>Calcium-activated, phospholipid- and diacylglycerol (DAG)-dependent serine/threonine-protein kinase that plays diverse roles in neuronal cells and eye</p>	<p>Acteoside / Verbascoside; Compound X; Dihydroxyphytyl Palmitate</p>	<p>Spinocerebellar ataxia; Neurodegeneration; Neuropathic pain</p>	

	<p>tissues, such as regulation of the neuronal receptors GRIA4/GLUR4 and GRIN1/NMDAR1, modulation of receptors and neuronal functions related to sensitivity to opiates, pain and alcohol, mediation of synaptic function and cell survival after ischemia, and inhibition of gap junction activity after oxidative stress. Plays a role in neuropathic pain mechanisms and contributes to the maintenance of the allodynia pain produced by peripheral inflammation. Plays an important role in initial sensitivity and tolerance to ethanol, by mediating the behavioural effects of ethanol as well as the effects of this drug on the GABA(A) receptors. During and after cerebral ischemia modulate</p>			
--	--	--	--	--

	<p>neurotransmission and cell survival in synaptic membranes and is involved in insulin-induced inhibition of necrosis, an important mechanism for minimizing ischemic injury.</p>			
<p>PRKCB(Protein kinase C beta type)</p>	<p>Calcium-activated, phospholipid- and diacylglycerol (DAG)-dependent serine/threonine-protein kinase involved in various cellular processes such as regulation of the B-cell receptor (BCR) signalosome, oxidative stress-induced apoptosis, androgen receptor-dependent transcription regulation, insulin signalling and endothelial cells proliferation. May participate in the regulation of glucose transport in adipocytes by negatively modulating the insulin-stimulated</p>	<p>Acteoside / Verbascoside; Compound X; Dihydroxyphytyl Palmitate</p>	<p>Diabetic Macular Oedema; Glioblastoma</p>	

	<p>translocation of the glucose transporter SLC2A4/GLUT4. Under high glucose in pancreatic beta-cells, is probably involved in the inhibition of the insulin gene transcription, via regulation of MYC expression. In endothelial cells, activation of PRKCB induces increased phosphorylation of RB1, increased VEGFA-induced cell proliferation, and inhibits PI3K/AKT-dependent nitric oxide synthase (NOS3/eNOS) regulation by insulin, which causes endothelial dysfunction.</p>			
<p>PRKCA(Protein kinase C alpha type)</p>	<p>Calcium-activated, phospholipid- and diacylglycerol (DAG)-dependent serine/threonine-protein kinase that is involved in positive and negative regulation of cell proliferation, apoptosis,</p>	<p>Acteoside / Verbascoside; Compound X ; Dihydroxyphytyl Palmitate</p>	<p>Renal Artery Atheroma; Glioma</p>	

	<p>differentiation, migration and adhesion, tumorigenesis, cardiac hypertrophy, angiogenesis, platelet function and inflammation, by directly phosphorylating targets such as RAF1, BCL2, CSPG4, TNNT2/CTNT, or activating signalling cascade involving MAPK1/3 (ERK1/2) and RAP1GAP. Involved in cell proliferation and cell growth arrest by positive and negative regulation of the cell cycle</p>			
<p>PRKCQ(Protein kinase C theta type)</p>	<p>Calcium-independent, phospholipid- and diacylglycerol (DAG)-dependent serine/threonine-protein kinase that mediates non-redundant functions in T-cell receptor (TCR) signalling, including T-cells activation, proliferation,</p>	<p>Acteoside / Verbascoside; Dihydroxyphytyl Palmitate</p>	<p>Gastrointestinal Stromal Tumour; Smallpox</p>	

	<p>differentiation, and survival, by mediating activation of multiple transcription factors such as NF-kappa-B, JUN, NFATC1 and NFATC2</p>			
<p>PRKCD(Protein kinase C delta type regulatory subunit)</p>	<p>Calcium-independent, phospholipid- and diacylglycerol (DAG)-dependent serine/threonine-protein kinase that plays contrasting roles in cell death and cell survival by functioning as a pro-apoptotic protein during DNA damage-induced apoptosis, but acting as an anti-apoptotic protein during cytokine receptor-initiated cell death, is involved in tumour suppression as well as survival of several cancers, is required for oxygen radical production by NADPH oxidase and acts as positive or negative regulator in</p>	<p>Acteoside / Verbascoside; Dihydroxyphytyl Palmitate</p>	<p>Autoimmune Lymphoproliferative syndrome, type Iii; Systemic lupus Erythematosus 16</p>	

	platelet functional responses.			
ESR1 (Oestrogen receptor)	<p>ESR1 has been a focus in breast cancer for quite some time, but is also clinically relevant in endometrial, ovarian, and other cancer types. The identification of ER-positive breast cancers that are resistant to hormone therapy have inspired clinical sequencing efforts to shed light on the mechanisms of this resistance. Several mutations in the ligand binding domain of ESR1 have been implicated in hormone resistance and anti-oestrogen therapies. These observations have spurred efforts to develop therapeutics that stimulate ESR1 protein degradation (e.g., Fulvestrant),</p>	Apigenin	<p>Estrogen resistance; Myocardial infarction; Breast Cancer</p>	

	rather than acting as a small molecule antagonist. These agents are currently in clinical trials and have seen some success.		
CYP1A2 (Cytochrome P450 1A2)	Most active in catalysing 2-hydroxylation. Caffeine is metabolized primarily by cytochrome CYP1A2 in the liver through an initial N3-demethylation. Also acts in the metabolism of aflatoxin B1 and acetaminophen. Participates in the bioactivation of carcinogenic aromatic and heterocyclic amines. Catalyses the N-hydroxylation of heterocyclic amines and the O-deethylation of phenacetin.	Apigenin; Chryseriol; Luteolin	Toxicity or Absent response to Clozapine; Acetaminophen Metabolism
CDK1 (Cyclin-dependent kinase 1)	Plays a key role in the control of the eukaryotic cell cycle by modulating the centrosome cycle as well as mitotic onset;	Apigenin	Breast Cancer; Retinal Cancer

	<p>promotes G2-M transition and regulates G1 progress and G1-S transition via association with multiple interphase cyclins.</p>			
<p>MAPT (Microtubule-associated protein tau)</p>	<p>Promotes microtubule assembly and stability and might be involved in the establishment and maintenance of neuronal polarity. The C-terminus binds axonal microtubules while the N-terminus binds neural plasma membrane components, suggesting that tau functions as a linker protein between both. Axonal polarity is predetermined by TAU/MAPT localization (in the neuronal cell) in the domain of the cell body defined by the centrosome. The short isoforms allow plasticity of the cytoskeleton whereas the longer isoforms may preferentially play a role in its stabilization.</p>	<p>Apigenin ; EDD (9, 13-epoxylabda-6(19),15(14)diol dilactone) ; Geniposidic Acid; Leoleorin C; Vitexin</p>	<p>AD, Pick's disease, frontotemporal dementia, cortico-basal degeneration and progressive supranuclear palsy.</p>	

<p>CDK4 (Cyclin-dependent kinase 4)</p>	<p>CDK4, along with its partner CDK6, are key players in cell cycle progression. The kinase component of cyclin D-CDK4 (DC) complexes that phosphorylate and inhibit members of the retinoblastoma (RB) protein family including RB1 and regulate the cell-cycle during G(1)/S transition. Phosphorylation of RB1 allows dissociation of the transcription factor E2F from the RB/E2F complexes and the subsequent transcription of E2F target genes which are responsible for the progression through the G (1) phase. Hypo phosphorylates RB1 in early G (1) phase. Cyclin D-CDK4 complexes are major integrators of various mitogenic and antimitogenic signals. Also phosphorylates SMAD3 in a cell-cycle-</p>	<p>Apigenin</p>	<p>Melanoma, Cutaneous Malignant 3 and Dedifferentiated Liposarcoma.</p>	
---	--	-----------------	--	--

	<p>dependent manner and represses its transcriptional activity. Component of the ternary complex, cyclin D/CDK4/CDKN1B, required for nuclear translocation and activity of the cyclin D-CDK4 complex.</p>			
HSD17B1 (Estradiol 17-beta-dehydrogenase 1)	<p>Favours the reduction of oestrogens and androgens. Also has 20-alpha-HSD activity. Uses preferentially NADH.</p>	Apigenin	Acute T Cell Leukaemia and Endometriosis.	
CSNK2A2 (Casein kinase II subunit alpha')	<p>Catalytic subunit of a constitutively active serine/threonine-protein kinase complex that phosphorylates many substrates containing acidic residues C-terminal to the phosphorylated serine or threonine. Regulates numerous cellular processes, such as cell cycle progression, apoptosis, and transcription, as well as viral infection.</p>	Apigenin	Theileriasis and Spermatogenic Failure 6.	

<p>MAOA(Amine oxidase [flavin-containing] A)</p>	<p>Catalyses the oxidative deamination of biogenic and xenobiotic amines and has important functions in the metabolism of neuroactive and vasoactive amines in the central nervous system and peripheral tissues. MAOA preferentially oxidizes biogenic amines such as 5-hydroxytryptamine (5-HT), norepinephrine and epinephrine.</p>	<p>Apigenin; Luteolin</p>	<p>Brunner Syndrome (Monoamine oxidase A deficiency) ; antisocial personality disorder.; Depression.</p>	
<p>PTGS1 (Prostaglandin G/H synthase 1)</p>	<p>Converts arachidonate to prostaglandin H2 (PGH2), a committed step in prostanoid synthesis. Involved in the constitutive production of prostanoids in the stomach and platelets. In gastric epithelial cells, it is a key step in the generation of prostaglandins, such as prostaglandin E2 (PGE2), which plays an important role in cytoprotection. In</p>	<p>Apigenin</p>	<p>Aspirin Resistance ; Chronic Cystitis; Pain</p>	

	<p>platelets, it is involved in the generation of thromboxane A2 (TXA2), which promotes platelet activation and aggregation, vasoconstriction, and proliferation of vascular smooth muscle cells. Cyclooxygenase (also known as COX, Prostaglandin-endoperoxide synthase, Prostaglandin G/H synthase) is expressed in cells in three isoforms. COX-1 (constitutive) and COX-2 (inducible) isoforms catalyse the rate-limiting step of prostaglandin production.</p>			
<p>CDK2 (Cyclin-dependent kinase 2)</p>	<p>Serine/threonine-protein kinase involved in the control of the cell cycle, essential for meiosis, but dispensable for mitosis. Phosphorylates CTNNB1, USP37, p53/TP53, NPM1, CDK7, RB1, BRCA2, MYC,</p>	<p>Apigenin</p>	<p>Glioblastoma Multiforme and Glioblastoma.</p>	

	<p>NPAT, EZH2. Triggers duplication of centrosomes and DNA. Acts at the G1-S transition to promote the E2F transcriptional program and the initiation of DNA synthesis and modulates G2 progression; controls the timing of entry into mitosis/meiosis by controlling the subsequent activation of cyclin B/CDK1 by phosphorylation and coordinates the activation of cyclin B/CDK1 at the centrosome and in the nucleus. Crucial role in orchestrating a fine balance between cellular proliferation, cell death, and DNA repair in human embryonic stem cells (hESCs). Activity of CDK2 is maximal during S phase and G2; activated by interaction with cyclin E during the early stages of DNA</p>			
--	---	--	--	--

synthesis to permit G1-S transition, and subsequently activated by cyclin A2 (cyclin A1 in germ cells) during the late stages of DNA replication to drive the transition from S phase to mitosis, the G2 phase. EZH2 phosphorylation promotes H3K27me3 maintenance and epigenetic gene silencing. Phosphorylates CABLES1 (By similarity). Cyclin E/CDK2 prevents oxidative stress-mediated Ras-induced senescence by phosphorylating MYC. Involved in G1-S phase DNA damage checkpoint that prevents cells with damaged DNA from initiating mitosis; regulates homologous recombination-dependent repair by phosphorylating BRCA2, this phosphorylation is low in S phase when



	recombination is active but increases as cells progress towards mitosis.		
MAOB(Amine oxidase [flavin-containing] B)	Catalyses the oxidative deamination of biogenic and xenobiotic amines and has important functions in the metabolism of neuroactive and vasoactive amines in the central nervous system and peripheral tissues. MAOB preferentially degrades benzyl amine and phenyl ethylamine; and metabolises Dopamine	Apigenin; Luteolin	Norrie Disease and Post encephalitic Parkinson Disease; AD.
ADORA2A (Adenosine receptor A2a)	Receptor for adenosine. The activity of this receptor is mediated by G proteins which activate adenylyl cyclase	Apigenin	Acute Encephalopathy with Biphasic Seizures and Late Reduced Diffusion; Panic Disorder; Parkinson's disease.

ADORA1(Adenosine receptor A1)	Receptor for adenosine. The activity of this receptor is mediated by G proteins which inhibit adenylyl cyclase.	Apigenin-7-O-(6''-O-p-coumaroyl)- β -glucoside; Luteolin	Brain Ischemia and Rasmussen Encephalitis.
ABCC1 (Multidrug resistance-associated protein 1)	Mediates export of organic anions and drugs from the cytoplasm. Mediates ATP-dependent transport of glutathione and glutathione conjugates, leukotriene C4, estradiol-17-beta-glucuronide, methotrexate, antiviral drugs, and other xenobiotics. Confers resistance to anticancer drugs. Hydrolyses ATP with low efficiency.	Chryseriol	Dubin-Johnson Syndrome and Microsporidiosis.
CYP1B1 (Cytochrome P450 1B)	Cytochromes P450 are a group of heme-thiolate monooxygenases. In liver microsomes, this enzyme is involved in an NADPH-dependent	Chryseriol	Glaucoma 3, Primary Congenital, A and Anterior Segment Dysgenesis 6

	<p>electron transport pathway. It oxidizes a variety of structurally unrelated compounds, including steroids, fatty acids, retinoid, and xenobiotics</p>		
<p>CYP1A1 (Cytochrome P450 1A1)</p>	<p>Cytochromes P450 are a group of heme-thiolate monooxygenases. In liver microsomes, this enzyme is involved in an NADPH-dependent electron transport pathway. It oxidizes a variety of structurally unrelated compounds, including steroids, fatty acids, and xenobiotics.</p>	<p>Chryseriol</p>	<p>Aryl Hydrocarbon Hydroxylase Inducibility (related to aging and lung cancer) and Ehrlich Tumour Carcinoma</p>
<p>ABCC3 (Canalicular multispecific organic anion transporter 2)</p>	<p>May act as an inducible transporter in the biliary and intestinal excretion of organic anions. Acts as an alternative route for the export of bile acids and glucuronides from</p>	<p>Chryseriol</p>	<p>Dubin-Johnson Syndrome and Extrahepatic Cholestasis.</p>

	cholestatic hepatocytes (By similarity).		
ABCC2 (Canalicular multispecific organic anion transporter 1)	Mediates hepatobiliary excretion of numerous organic anions. May function as a cellular cisplatin transporter.	Chryseriol	Dubin-Johnson Syndrome and Bilirubin Metabolic Disorder.
TDP1 (Tyrosyl-DNA phosphodiesterase 1)	DNA repair enzyme that can remove a variety of covalent adducts from DNA through hydrolysis of a 3-phosphodiester bond, giving rise to DNA with a free 3 phosphates.	Comosiin; Cynaroside ; Luteolin 7-O- β -glucoside-3-methyl ether;	Spinocerebellar Ataxia, Autosomal Recessive, With Axonal Neuropathy and Spinocerebellar Ataxia Type 1 With Axonal Neuropathy.
KDM4A (Lysine-specific demethylase 4A)	Histone demethylase that specifically demethylates Lys-9 and Lys-36 residues of histone H3, thereby playing a central role in histone code	Cynaroside; Luteolin 7-O- β -glucoside-3-methyl ether;	DNA Double-Strand Break Repair and DNA Double Strand Break Response.

	<p>(PubMed:26741168). Does not demethylate histone H3 Lys-4, H3 Lys-27 nor H4 Lys-20.</p> <p>Demethylates trimethylated H3 Lys-9 and H3 Lys-36 residue, while it has no activity on mono- and dimethylated residues. Demethylation of Lys residue generates formaldehyde and succinate. Participates in transcriptional repression of ASCL2 and E2F-responsive promoters via the recruitment of histone deacetylases and NCOR1, respectively.</p> <p>Isoform 2: Crucial for muscle differentiation, promotes transcriptional activation of the Myog gene by directing the removal of repressive chromatin marks at its promoter. Lacks the N-terminal demethylase domain.</p>			
--	---	--	--	--

<p>KDM4B (Lysine-specific demethylase 4B)</p>	<p>Histone demethylase that specifically demethylates Lys-9 of histone H3, thereby playing a role in histone code. Does not demethylate histone H3 Lys-4, H3 Lys-27, H3 Lys-36 nor H4 Lys-20. Only able to demethylate trimethylated H3 Lys-9, with a weaker activity than KDM4A, KDM4C and KDM4D. Demethylation of Lys residue generates formaldehyde and succinate.</p>	<p>Cynaroside; Luteolin 7-O-β-glucoside-3-methyl ether;</p>	<p>DNA Double-Strand Break Repair and DNA Double Strand Break Response.</p>	
<p>KDM4C (Lysine-specific demethylase 4C)</p>	<p>Histone demethylase that specifically demethylates Lys-9 and Lys-36 residues of histone H3, thereby playing a central role in histone code. Does not demethylate histone H3 Lys-4, H3 Lys-27 nor H4 Lys-20. Demethylates trimethylated H3 Lys-9 and H3 Lys-36 residue,</p>	<p>Cynaroside ; Luteolin 7-O-β-glucoside-3-methyl ether</p>	<p>Squamous Cell Carcinoma</p>	

	<p>while it has no activity on mono- and dimethylated residues. Demethylation of Lys residue generates formaldehyde and succinate.</p>			
<p>PTAFR (Platelet-activating factor receptor)</p>	<p>Receptor for platelet activating factor, a chemotactic phospholipid mediator that possesses potent inflammatory, smooth-muscle contractile and hypotensive activity. Seems to mediate its action via a G protein that activates a phosphatidylinositol-calcium second messenger system.</p> <p>Platelet-activating factor receptor (PAF-R) is a Gq/G11-coupled-protein receptor that has a role in a wide range of biological processes such as vasodilation, superoxide formation, cell proliferation, angiogenesis, and</p>	<p>EDD ; Leoleorin C</p>	<p>Melanoma Metastasis.</p>	

	regulation of the inflammatory response.		
EGLN1 (Egl nine homolog 1)	Cellular oxygen sensor that catalyses, under normoxic conditions, the post-translational formation of 4-hydroxyproline in hypoxia-inducible factor (HIF) alpha proteins. Hydroxylates a specific proline found in each of the oxygen-dependent degradation (ODD) domains (N-terminal, NODD, and C-terminal, CODD) of HIF1A. Also hydroxylates HIF2A. Prefers the CODD site for both HIF1A and HIF1B.	Succinic Acid	Erythrocytosis, Familial, 3 and Haemoglobin, High Altitude Adaptation.
EGLN2 (Egl nine homolog 2)	Cellular oxygen sensor that catalyses, under normoxic conditions, the post-translational formation of 4-hydroxyproline in hypoxia-inducible factor	Succinic Acid	Hypoxia.

	<p>(HIF) alpha proteins. Hydroxylates a specific proline found in each of the oxygen-dependent degradation (ODD) domains (N-terminal, NODD, and C-terminal, CODD) of HIF1A. Also hydroxylates HIF2A. Prefers the CODD site for both HIF1A and HIF2A.</p>			
<p>MMP1 (Matrix Metalloproteinase 1)</p>	<p>Cleaves collagens of types I, II, and III at one site in the helical domain. Also cleaves collagens of types VII and X. In case of HIV infection, interacts and cleaves the secreted viral Tat protein, leading to a decrease in neuronal TATS mediated neurotoxicity</p>	<p>Luteolin</p>	<p>Epidermolysis Bullosa Dystrophica, Autosomal Recessive and Recessive Dystrophic Epidermolysis Bullosa.</p>	
<p>MMP2 (Matrix Metalloproteinase 2)</p>	<p>Ubiquitous metalloproteinase that is involved in diverse functions such as remodelling of the vasculature, angiogenesis, tissue repair, tumour invasion,</p>	<p>Luteolin</p>	<p>Multicentric Osteolysis, Nodulosis, And Arthropathy and Arthropathy.</p>	

	<p>inflammation, and atherosclerotic plaque rupture. As well as degrading extracellular matrix proteins, can also act on several nonmatrix proteins such as big endothelial 1 and beta-type CGRP promoting vasoconstriction. Also cleaves KISS at a Gly - Leu bond. Appears to have a role in myocardial cell death pathways. Contributes to myocardial oxidative stress by regulating the activity of GSK3beta. Cleaves GSK3beta in vitro. Involved in the formation of the fibrovascular tissues in association with MMP14.</p>			
<p>MMP3 (Matrix Metallopeptidase 3)</p>	<p>Can degrade fibronectin, laminin, gelatines of type I, III, IV, and V; collagens III, IV, X, and IX, and cartilage proteoglycans. Activates procollagenase.</p>	<p>Luteolin</p>	<p>Coronary Heart Disease 6 and Arthritis.</p>	

<p>MMP9 (Matrix Metalloproteinase 9)</p>	<p>May play an essential role in local proteolysis of the extracellular matrix and in leukocyte migration. Could play a role in bone osteoclastic resorption. Cleaves KiSS1 at a Gly-Leu bond. Cleaves type IV and type V collagen into large C-terminal three quarter fragments and shorter N-terminal one quarter fragments. Degrades fibronectin but not laminin or Pz-peptide.</p>	<p>Luteolin</p>	<p>Metaphyseal Anadysplasia 2 and Metaphyseal Anadysplasia.</p>	
<p>CD38 (CD38 Molecule)</p>	<p>Synthesizes the second messengers cyclic ADP-ribose and nicotinate-adenine dinucleotide phosphate, the former a second messenger for glucose-induced insulin secretion. Also has cADPr hydrolase activity. Also moonlights as a receptor in cells of the immune system.</p>	<p>Luteolin</p>	<p>Richter's Syndrome and Leukaemia, Chronic Lymphocytic.</p>	

<p>MMP12 (Matrix Metalloproteinase 12)</p>	<p>May be involved in tissue injury and remodelling. Has significant elastolytic activity. Can accept large and small amino acids at the P1 site but prefers leucine. Aromatic or hydrophobic residues are preferred at the P1 site, with small hydrophobic residues (preferably alanine) occupying P3.</p>	<p>Luteolin</p>	<p>Mid-Dermal Elastolysis and Pulmonary Emphysema.</p>	
<p>MMP13 (Matrix Metalloproteinase 13)</p>	<p>Plays a role in the degradation of extracellular matrix proteins including fibrillar collagen, fibronectin, TNC and ACAN. Cleaves triple helical collagens, including type I, type II, and type III collagen, but has the highest activity with soluble type II collagen. Can also degrade collagen type IV, type XIV and type X. May also function by activating or degrading key</p>	<p>Luteolin</p>	<p>Spondyloepimetaphyseal Dysplasia, Missouri Type and Metaphyseal Dysplasia, Spahr Type.</p>	

	<p>regulatory proteins, such as TGFB1 and CTGF. Plays a role in wound healing, tissue remodelling, cartilage degradation, bone development, bone mineralization and ossification.</p>			
<p>XDH (Xanthine Dehydrogenase)</p>	<p>Key enzyme in purine degradation. Catalyses the oxidation of hypoxanthine to xanthine. Catalyses the oxidation of xanthine to uric acid. Contributes to the generation of reactive oxygen species. Has also low oxidase activity towards aldehydes (in vitro).</p>	<p>Luteolin</p>	<p>Xanthinuria, Type I and Xanthinuria.</p>	
<p>GLO1 (Glyoxalase I)</p>	<p>Catalyses the conversion of hemimercaptal, formed from methylglyoxal and glutathione to S-lactoylglutathione. Involved in the regulation of TNF-induced transcriptional activity of NF-kappa-B.</p>	<p>Luteolin</p>	<p>Triosephosphate Isomerase Deficiency and Diabetic Encephalopathy.</p>	

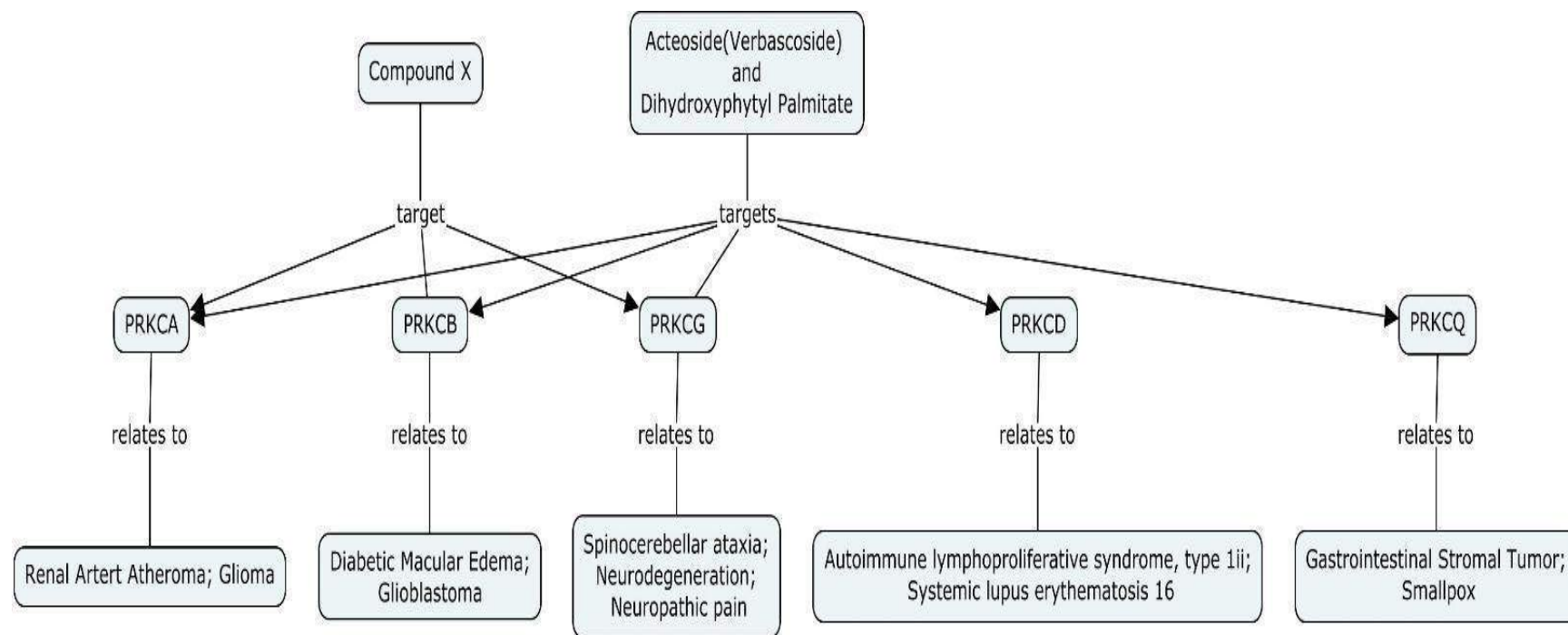
	Required for normal osteoclastogenesis.		
KARS (Lysyl-TRNA Synthetase)	<p>Catalyses the specific attachment of an amino acid to its cognate tRNA in a 2 step reaction: the amino acid (AA) is first activated by ATP to form AA-AMP and then transferred to the acceptor end of the tRNA (PubMed:9278442, PubMed:18029264, PubMed:18272479). When secreted, acts as a signalling molecule that induces immune response through the activation of monocyte/macrophages (PubMed:15851690). Catalyses the synthesis of the signalling molecule diadenosine tetraphosphate (Ap₄A), and thereby mediates</p>	Luteolin	Charcot-Marie-Tooth Disease, Recessive Intermediate B and Deafness, Autosomal Recessive 89.

	<p>disruption of the complex between HINT1 and MITF and the concomitant activation of MITF transcriptional activity (PubMed:5338216, PubMed:14975237, PubMed:19524539, PubMed:23159739).</p> <p>(Microbial infection) Interacts with HIV-1 virus GAG protein, facilitating the selective packaging of tRNA(3)(Lys), the primer for reverse transcription initiation.</p>			
--	--	--	--	--



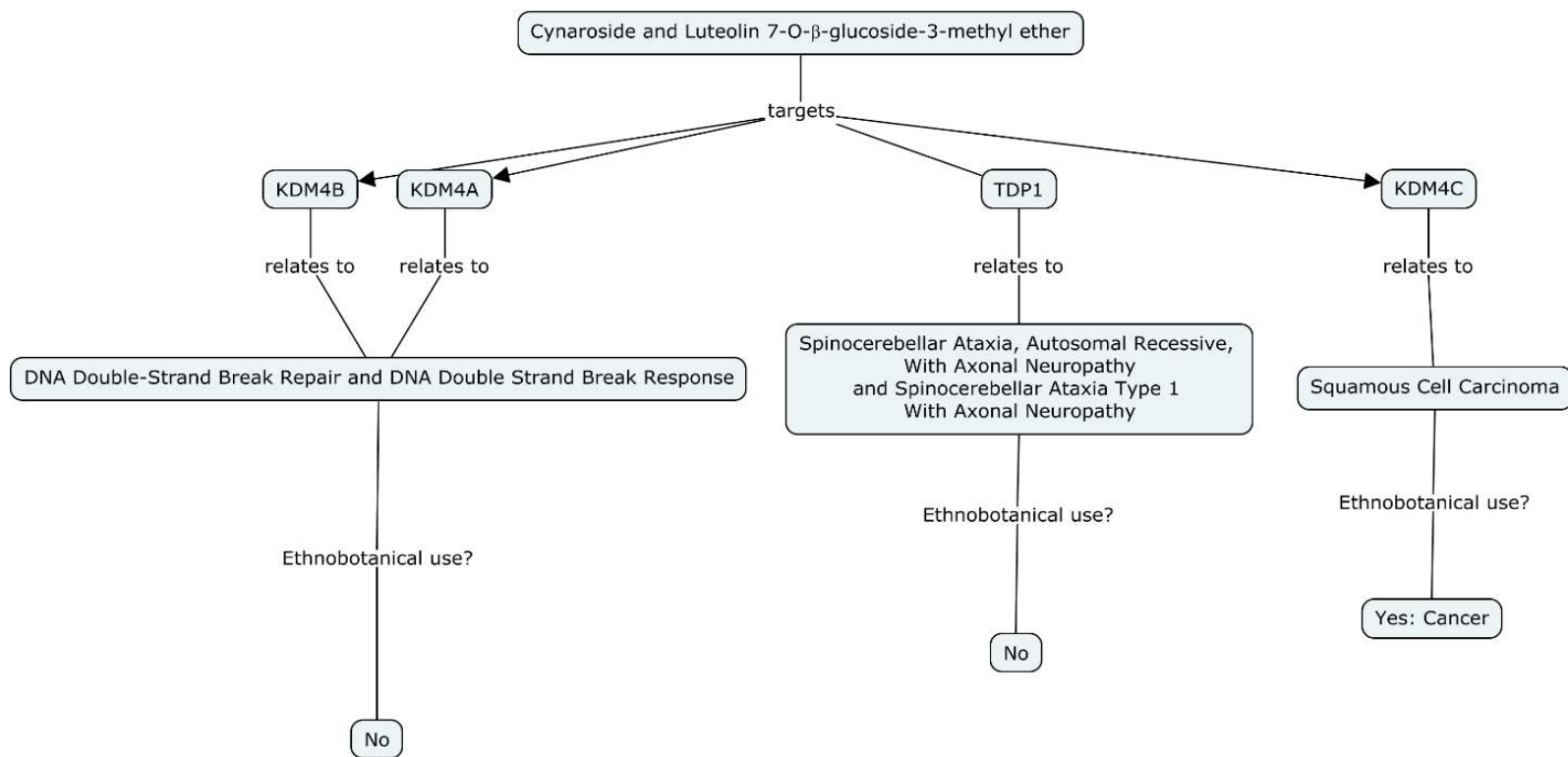
UNIVERSITY *of the*
WESTERN CAPE

Appendix 11: C-Map networking of phytochemicals with correlated ethnobotanical uses and point of actions



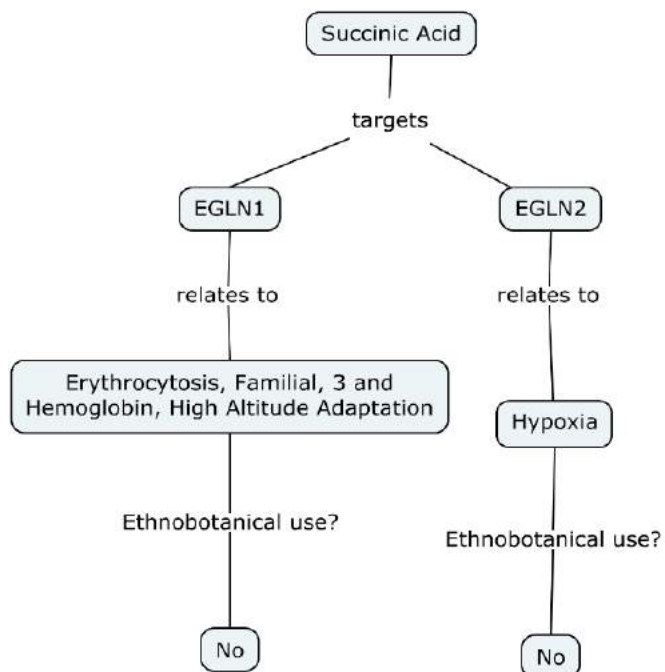
C-map networking of Compound X, Acteoside and Dihydroxyphytyl Palmitate

UNIVERSITY of the
WESTERN CAPE

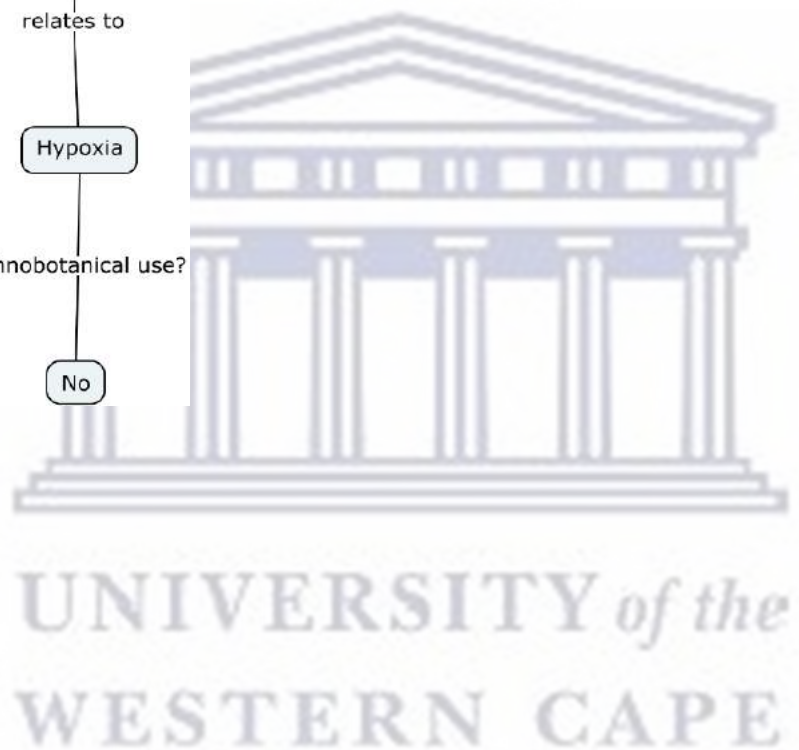


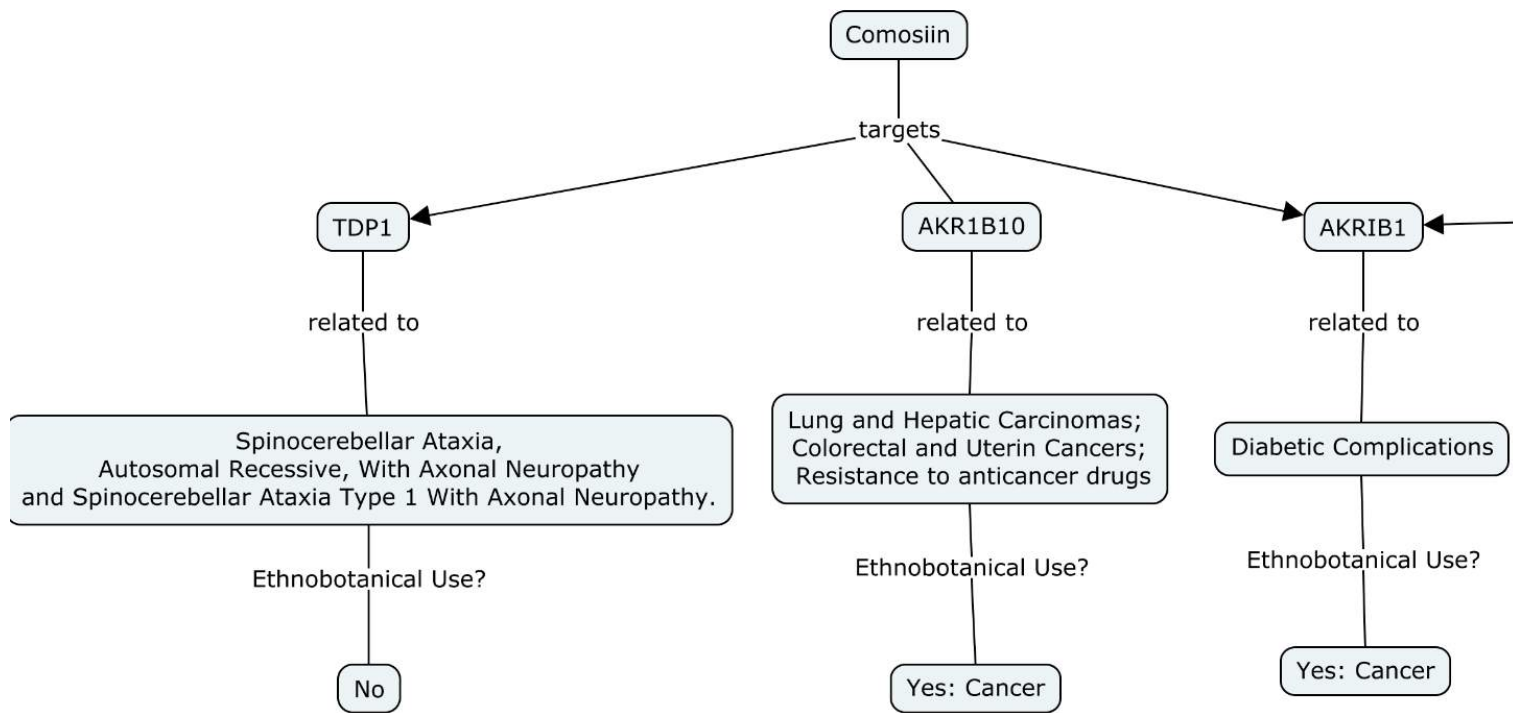
C-map networking of Cynaroside and Luteolin 7-O-β-glucoside-3-methyl ether

UNIVERSITY of the
WESTERN CAPE



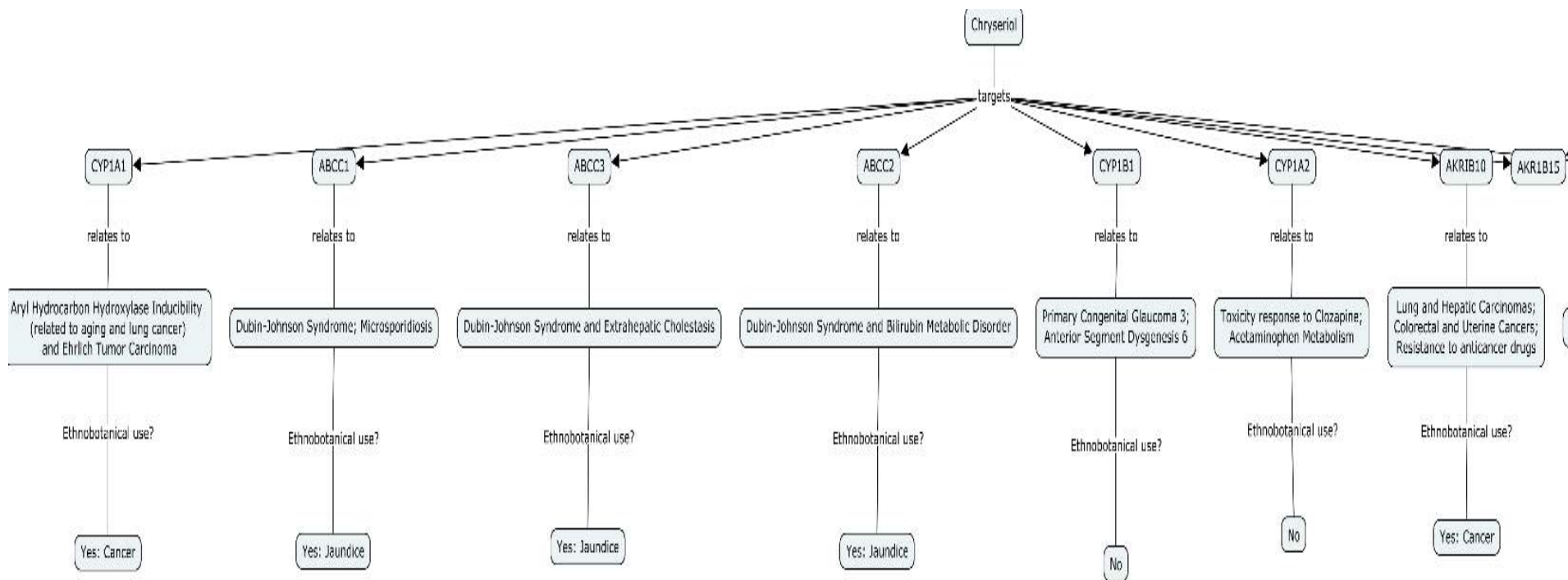
C-map networking of Succinic Acid





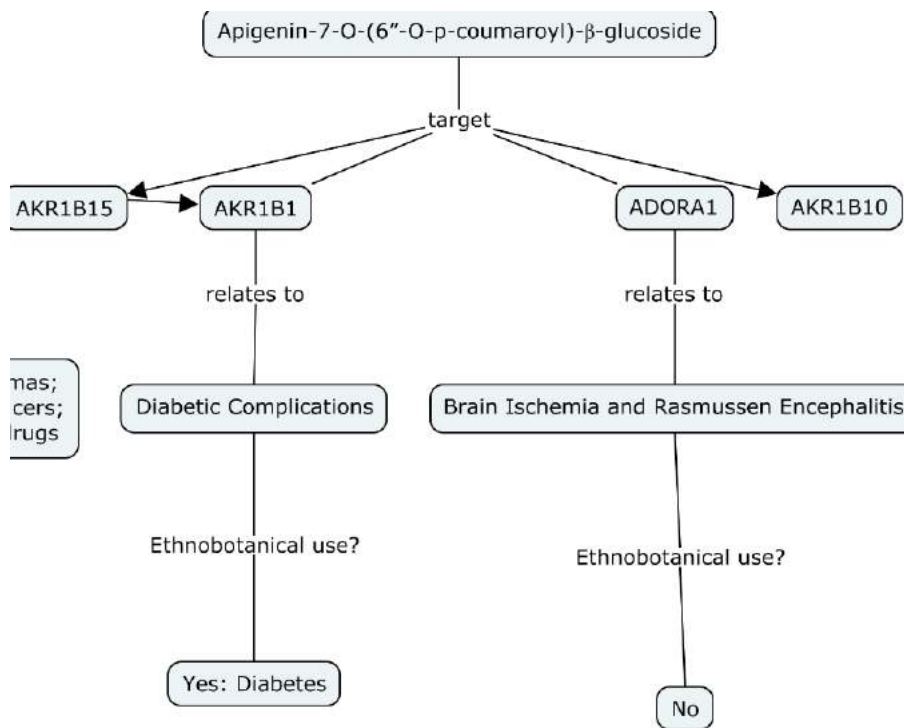
C-map networking of Comosiin

UNIVERSITY of the
WESTERN CAPE



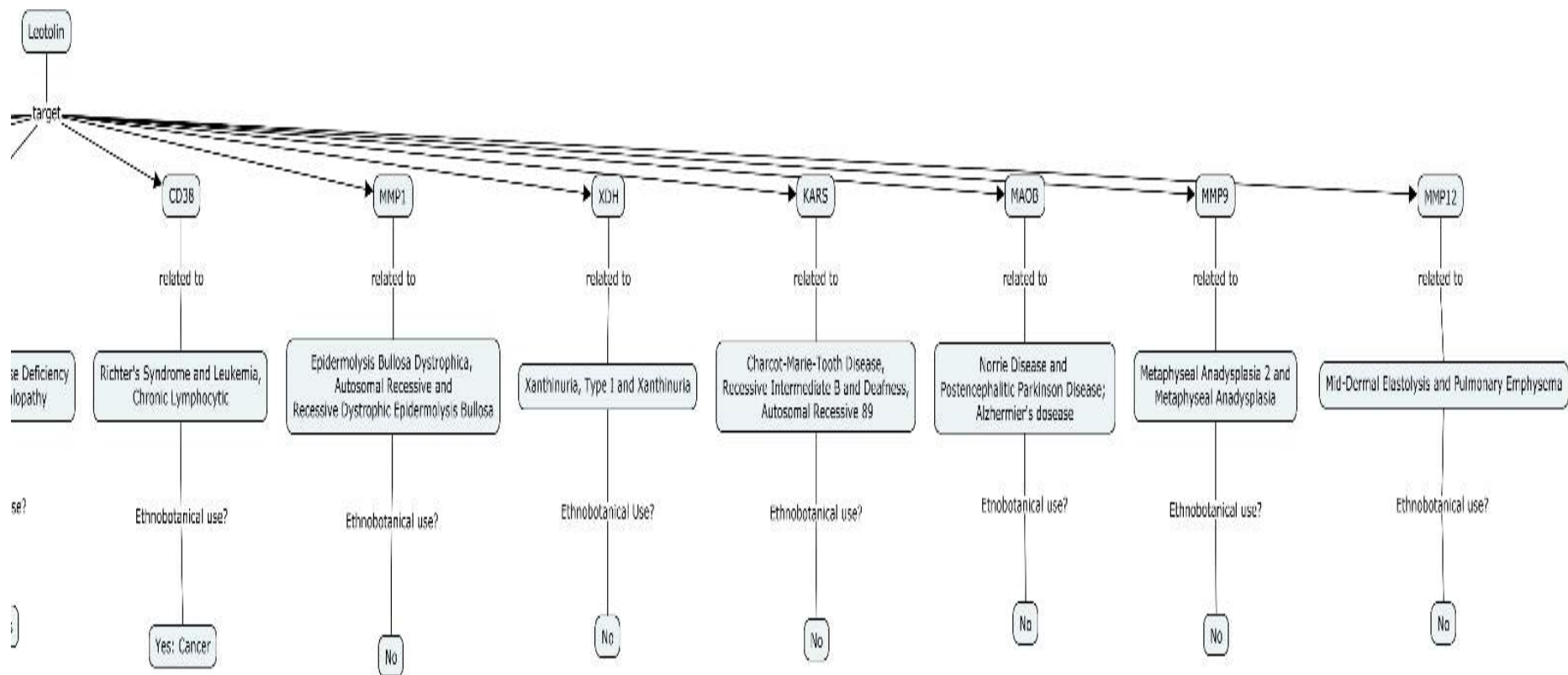
C-map networking of Chryseriol





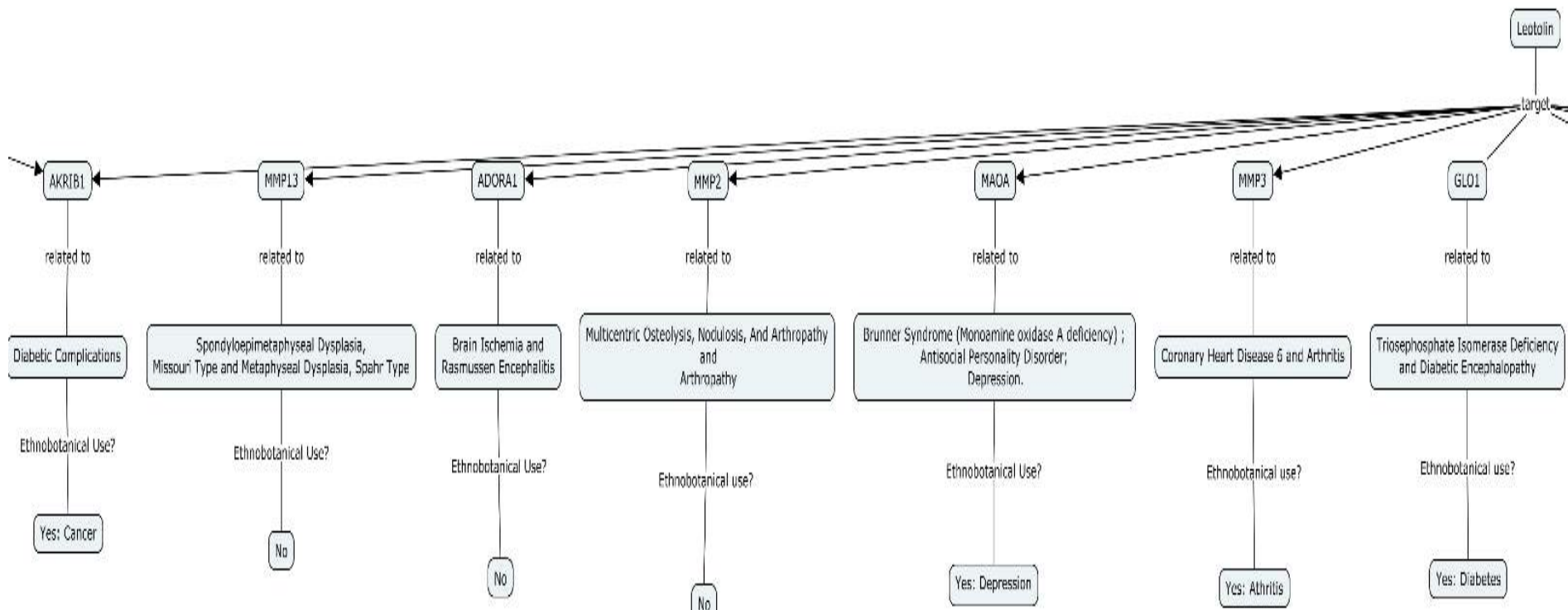
C-map networking of Apigenin-7-O-(6''-O-p-coumaroyl)-β-glucoside

UNIVERSITY of the
WESTERN CAPE



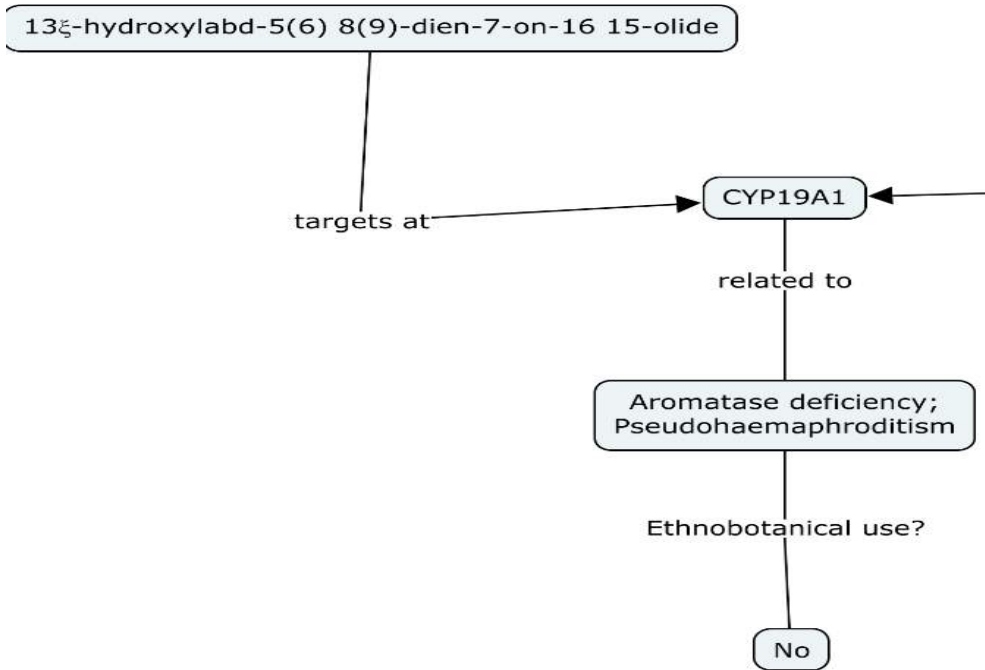
C-map networking of Luteolin

UNIVERSITY of the
WESTERN CAPE



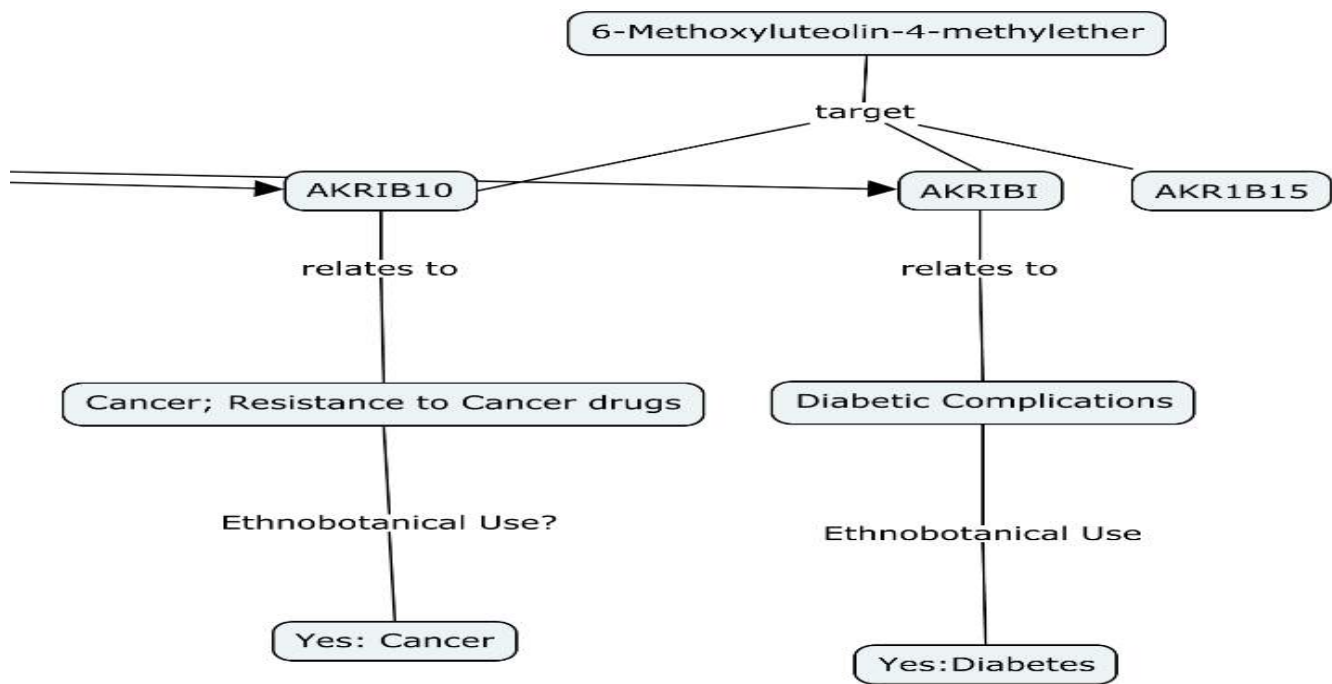
C-map networking of Luteolin

UNIVERSITY of the
WESTERN CAPE

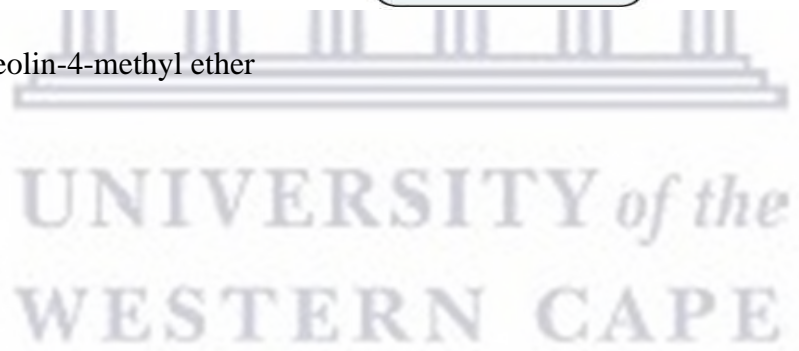


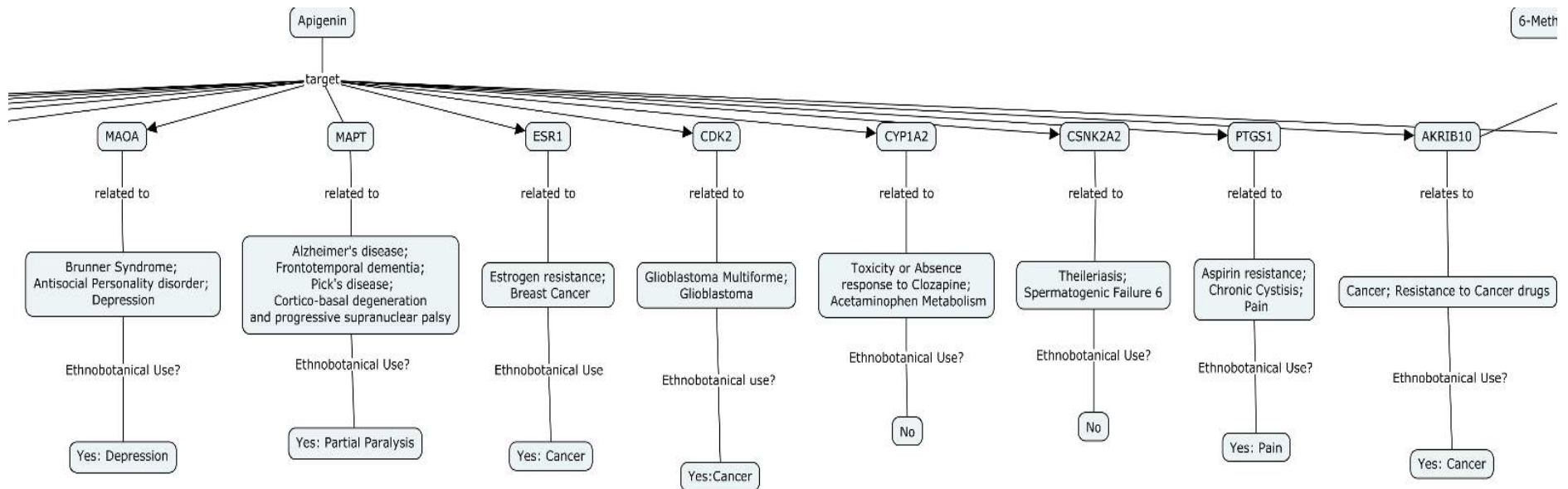
C-map networking of 13ξ-hydroxylabd-5(6) 8(9)-dien-7-on-16 15-olide

UNIVERSITY of the
WESTERN CAPE



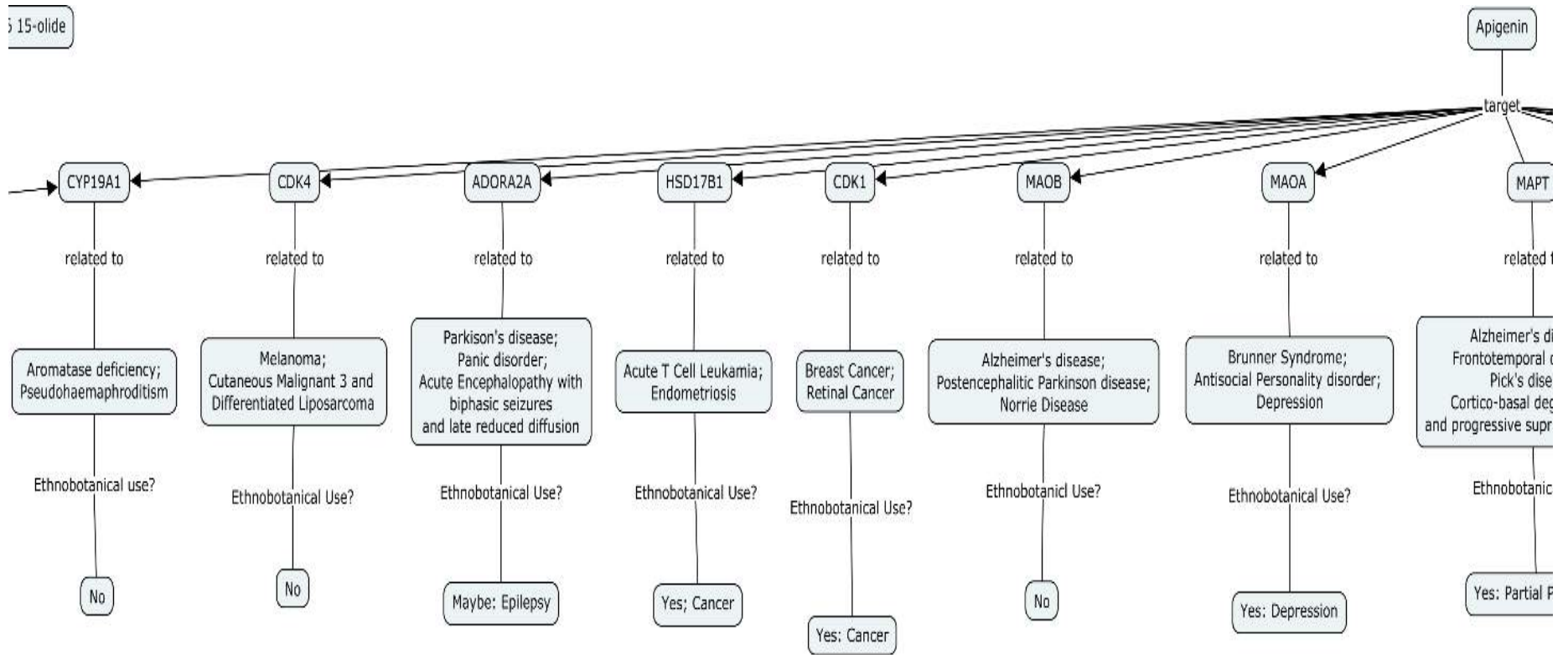
C-map networking of 6-Methoxyluteolin-4-methyl ether





C-map networking of Apigenin





C-map networking of Apigenin

UNIVERSITY of the
WESTERN CAPE

Appendix 12: Molecular docking results on MAO-B in MOE

Compound Name	mol	rseq	S	rmsd_refine	FP:PLIF	PLIF_ligidx	E_conf	E_place	E_score1	E_refine	E_score2	
Apigenin	O=C1c2c(O)cc2O C(c2c(O)cc2)=C1	1	1	-7.588614	0.86687058	1 2 3 4 5	[[3,14,12,9,7,4,2,29,16,15,14,3],[2,29,16,15,14,3],[2,29,16,15,14,3],10,10]	-28.00022	-77.32503	-15.55408	-33.89839	-7.588614
		1	1	-7.511904	2.4948967	2	[[2,29,16,15,14,3]]	-29.56498	-76.22829	-15.67587	-33.08029	-7.511904
		1	1	-7.107574	1.2409133		[]	-27.31957	-60.86884	-15.92585	-25.33449	-7.107574
		1	1	-6.617709	1.5822833		[]	-9.115896	-57.50435	-15.70724	-17.02566	-6.617709
		1	1	-6.425472	1.1211357	6 7 8 2 9	[10,10,1,[17,27,25,22,20,18],[27,27,27,27,27,27]]	-23.61112	-72.68971	-15.59145	-19.87655	-6.425472
		1	1	-4.654346	1.0283343	6 7	[10,10]	-15.19759	-57.47507	-15.86987	6.319545 7	-4.654346
(13S)-9α, 13α-epoxylabda-6β(19),15(14)diol dilactone (EDD)	O=C1[C@]2(C)[C@H]3[C@@](C)([C@]4([C@H](C)C[C@H]3O)O[C@	1	2	-2.024107	1.3903345	10	22	290.4001 2	3.587334 9	-5.28142	62.99102 4	-2.024107
		1	2	-0.430187	1.3106827		[]	264.1877 7	-32.85044	-5.567342	85.94245 9	-0.430187
		1	2	-0.268302	1.2304968		[]	289.8928 2	-17.43631	-5.114517	85.66293 3	-0.268302
		1	2	-0.210977	1.1251408		[]	240.7223 4	-28.40281	-8.729047	85.19559 5	-0.210977
		1	2	0.706479 2	1.2423959	11	[[5,5,5,5,5]]	249.4864 5	-36.3034	-5.552984	96.34785 5	0.706479 2

	@]1(C(=O)OCC1)CC4)CCC2	1	2	0.724472 2	1.1238568		[]	258.9307 6	-31.35452	-5.914775	96.83954 6	0.724472 2
		1	2	1.886058 1	1.3696846	10	25	228.3901 4	-5.620063	-6.165979	109.3877 2	1.886058 1
		1	2	1.943652 7	1.4295039	12	52	328.0174 6	-16.28505	-7.677257	110.1396 6	1.943652 7
		1	2	2.478165 4	1.5521097	12	52	311.9585 6	-22.06457	-8.380101	117.0824 4	2.478165 4
		1	2	2.553482 1	1.164915	13	30	269.7021 2	-9.38831	-5.444992	119.8797 6	2.553482 1
Genoposidic Acid		1	3	-7.882424	1.8663751	10 14 15	[29,29,33]	74.83647 9	-84.29823	-14.85622	-14.52632	-7.882424
		1	3	-7.585336	1.1176922	10 14	[29,29]	74.50247 2	-76.00711	-14.59253	-10.40553	-7.585336
		1	3	-7.514169	1.0751494	16 13 10 14	[1,1,29,29]	75.05616 8	-81.70257	-15.04146	-9.344098	-7.514169
		1	3	-7.132235	1.7824141	10 14 17	[29,29,29]	71.53565 2	-58.06459	-15.06041	-5.5653	-7.132235
		1	3	-7.128611	1.845946	10 14 18	[29,29,33]	85.67542 3	-104.9012	-19.03145	-7.337678	-7.128611
		1	3	-6.840269	1.9834245	10 14	[29,29]	81.13985 4	-90.92059	-17.47163	-3.447568	-6.840269
		1	3	-6.774015	1.8306615	10 14 18	[29,29,33]	85.37750 2	-98.01716	-17.90541	-3.193459	-6.774015
		1	3	-6.56041	1.2463698	11	[[39,39,39,39, 39,39]]	80.29400 6	-83.57967	-14.4736	4.110531 8	-6.56041
		1	3	-6.325914	1.7580287		[]	74.40712	-55.63883	-16.91571	0.760080 8	-6.325914
		1	3	-6.243169	1.4115881	10 14 19	[29,29,1]	255.8334 4	-95.07101	-15.40179	10.58282 3	-6.243169

Leoleorin C	O=C1 [C@ @]2(OC3(C@H] (C)C] C@@ H](O) C4C(C)(C) CCC] C@]3 4C)C C2)C CO1	1	4	-0.480631	1.4120238	20 21 22	[31,[24,24,24, 24,24,24],36]	201.8333	-19.75327	-6.145174	86.30210 9	-0.480631
		1	4	-0.456069	2.2599785		[]	197.4213 6	-15.93506	-4.306464	84.20797	-0.456069
		1	4	-0.207505	1.6307652		[]	338.005	-24.62628	-4.760032	86.19821 2	-0.207505
		1	4	0.238013 1	1.7397155	6 23	[9,37]	291.8468	-7.033928	-5.771152	94.44340 5	0.238013 1
		1	4	0.425358 9	1.6761671	8	9	255.1553	-16.29745	-4.17866	89.68901 8	0.425358 9
		1	4	1.327136 6	1.1366036	11	[[28,28,28,28, 28,28]]	235.6475 2	-24.54419	-4.541804	103.1701 8	1.327136 6
		1	4	1.855998 5	2.0233426	23 15	[37,9]	326.2315 7	-6.445248	-4.505807	109.6164 1	1.855998 5
		1	4	2.011392 8	1.3277135		[]	244.5377 7	-17.94835	-4.896194	107.5835 6	2.011392 8
		1	4	2.216205 6	1.2194319	8	36	280.7092 9	-8.925567	-4.350346	107.1048 8	2.216205 6
1	4	2.575892 7	1.6922306	9 21	[[40,40,40,40, 40,40],[24,24, 24,24,24,24]]	244.7988	-16.25355	-6.348026	116.1376 8	2.575892 7		
Luteolin	O=C1 c2c(O)cc(O) cc2O C(c2c c(O)c(O)cc2)=C1	1	5	-7.554545	1.4598866		[]	-27.16456	-90.71747	-18.76036	-32.96239	-7.554545
		1	5	-7.463802	2.0933297		[]	-30.69261	-87.93931	-20.45863	-31.75004	-7.463802
		1	5	-7.462486	1.2160655		[]	-24.76167	-69.67638	-18.77861	-28.88723	-7.462486
		1	5	-7.433538	1.6958153	24 25 2	[19,19,[12,21, 18,17,15,13]]	-24.85289	-75.63822	-18.91536	-25.65099	-7.433538
		1	5	-7.428017	0.77611721	24 25 2	[19,19,[12,21, 18,17,15,13]]	-24.85239	-83.59824	-18.17476	-25.65444	-7.428017

		1	5	-7.33081	1.2487369	9	[[13,13,13,13,13,13]]	-27.34207	-79.63154	-17.56797	-26.67927	-7.33081
		1	5	-7.323781	0.70323014	24 25 9	[19,19,[13,13,13,13,13]]	-24.53906	-77.49037	-18.92805	-25.879	-7.323781
		1	5	-6.533191	0.79360616	8 24 25 2	[26,19,19,[12,21,18,17,15,13]]	-21.09032	-81.69917	-17.57965	-17.56142	-6.533191
		1	5	-6.380572	1.4425765	8 24 25 9 18	[26,19,19,[13,13,13,13,13],1]	-22.81586	-74.95569	-17.72676	-16.71567	-6.380572
		1	5	-4.872286	1.2897946	17	26	-4.097786	-74.80816	-19.58193	9.121799 5	-4.872286
Vitexin	O=C1c2c(O)cc(O)c(C3[C@H](O)[C@@H](O)[C@H](O)[C@@H](CO)O3)c2OC(c2ccc(O)cc2)=C1	1	6	-3.088221	2.7947295	1 2	[[19,20,21,24,26,29],[6,16,14,11,9,7]]	191.6485 4	-27.4584	-11.46357	50.81094 4	-3.088221
		1	6	-2.29836	1.1294361	26 2	[24,[2,20,19,18,5,3,6,16,14,11,9,7]]	164.8449 1	-12.58802	-12.3555	63.39434 1	-2.29836
		1	6	-1.842185	1.4176173	2	[[6,16,14,11,9,7]]	161.0979	-23.12319	-10.92298	66.50119 8	-1.842185
		1	6	-1.446587	1.9923716	2	[[6,16,14,11,9,7]]	157.8072 1	-35.13589	-11.25179	72.05377 2	-1.446587
		1	6	-1.346564	1.9135053	2	[[6,16,14,11,9,7]]	165.7112 9	-41.09209	-11.30721	73.00463 9	-1.346564
		1	6	-1.12758	1.409484	2	[[6,16,14,11,9,7]]	175.1321 4	-37.60116	-11.08979	73.17269 1	-1.12758
		1	6	-1.099739	1.3245331		[]	181.0455 3	-22.90454	-10.3796	74.86729 4	-1.099739
		1	6	-1.01618	1.7775029	2	[[6,16,14,11,9,7]]	162.7402 6	-61.69795	-12.47291	74.96114 3	-1.01618

		1	6	-0.646614	1.4419589	2 27	[[6,16,14,11,9,7],43]	176.8874 2	-61.21451	-13.10264	80.48647 3	-0.646614
		1	6	-0.537405	2.1644812	2	[[2,20,19,18,5,3,6,16,14,11,9,7]]	178.9854 7	-23.44988	-12.05043	84.02615 4	-0.537405
Selegiline	N(C(Cc1ccc1)C)C#C C	1	7	-7.155185	1.2220657	9	[[26,26,26,26,26,26]]	14.37518 1	-44.42958	-8.909648	-24.88973	-7.155185
		1	7	-7.132165	1.0543808	2 9	[[10,19,17,15,13,11],[19,19,19,19,19]]	18.31419 9	-53.451	-8.675139	-20.91476	-7.132165
		1	7	-6.926451	1.0485711	11	[[26,26,26,26,26,26]]	12.52917 4	-37.12991	-8.946196	-21.89549	-6.926451
		1	7	-6.92055	1.1335802		[]	18.80790 3	-61.26356	-8.966617	-21.80888	-6.92055
		1	7	-6.794433	1.0030442		[]	17.63734 1	-68.33258	-8.846211	-16.09028	-6.794433
		1	7	-6.792941	0.71042424		[]	20.07198	-54.72675	-8.676271	-17.36121	-6.792941
		1	7	-6.759056	2.0752904		[]	12.06552 2	-44.20252	-9.120728	-18.33935	-6.759056
		1	7	-6.758199	1.2251914		[]	14.36631	-46.9489	-8.969446	-19.27607	-6.758199
		1	7	-6.754631	1.8464601		[]	13.16977 8	-50.87315	-8.965952	-19.38282	-6.754631
		1	7	-6.710722	0.91461462	2	[[10,19,17,15,13,11]]	14.44777	-50.31645	-9.013326	-17.24699	-6.710722
Rasagiline	N(CC#C)C1c2c(cccc2)CC1	1	8	-6.628878	1.2335044		[]	-0.430946	-49.36586	-9.796294	-24.80656	-6.628878
		1	8	-6.611316	1.5475247		[]	1.867122 2	-54.64164	-9.93568	-24.36106	-6.611316
		1	8	-6.549404	0.85473794		[]	1.135198 8	-61.91368	-10.12157	-23.7997	-6.549404

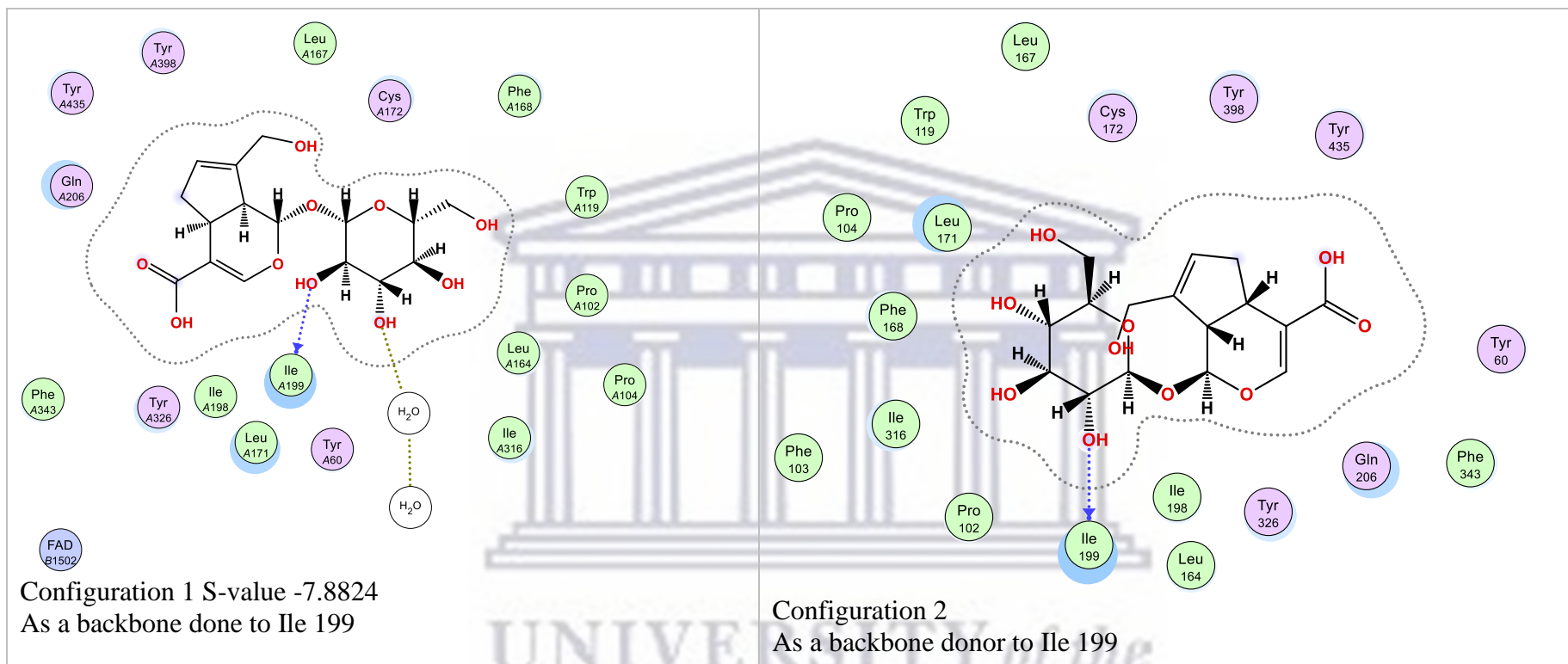
		1	8	-6.456193	0.94186717	20	7	-0.117483	-42.68174	-9.79041	-21.34306	-6.456193
		1	8	-6.441924	1.1194167	1	[[17,26,24,22,20,18]]	4.567894	-36.6296	-10.39553	-23.44466	-6.441924
		1	8	-6.437723	1.8442491		[]	0.979073 8	-41.8744	-10.10182	-22.55197	-6.437723
		1	8	-6.375642	0.62028474	20	7	2.458091	-62.44644	-9.896625	-18.6457	-6.375642
		1	8	-6.363934	1.1801261		[]	2.506461 1	-50.50396	-9.893075	-18.15011	-6.363934
		1	8	-6.152665	1.2406263		[]	2.269842 4	-62.54257	-10.15234	-15.61774	-6.152665
		1	8	-6.141831	1.425056		[]	3.654277 3	-37.31351	-10.21039	-16.58793	-6.141831
Clorgiline	Clc1c(OCCN(C)C#C)ccc(Cl)c1	1	9	-8.234683	0.79440778		[]	24.97761 2	-53.86945	-10.6868	-32.5784	-8.234683
		1	9	-7.895653	1.6154799		[]	20.61165 8	-45.00584	-10.48752	-31.00859	-7.895653
		1	9	-7.843823	0.84657091		[]	27.07616 6	-66.09789	-9.97742	-28.53829	-7.843823
		1	9	-7.794863	0.83308709		[]	24.46287	-48.86266	-10.11759	-27.16232	-7.794863
		1	9	-7.680814	1.0489235	24	26	16.95954 1	-64.09607	-10.0542	-33.69465	-7.680814
		1	9	-7.67149	0.88238519		[]	28.80427	-75.19648	-10.01605	-26.52153	-7.67149
		1	9	-7.569433	1.1724617	2	[[16,23,21,20,18,17]]	25.78155 1	-46.5329	-10.46413	-23.73109	-7.569433
		1	9	-7.555091	0.89715016		[]	21.53667 1	-69.91324	-10.27405	-27.40103	-7.555091

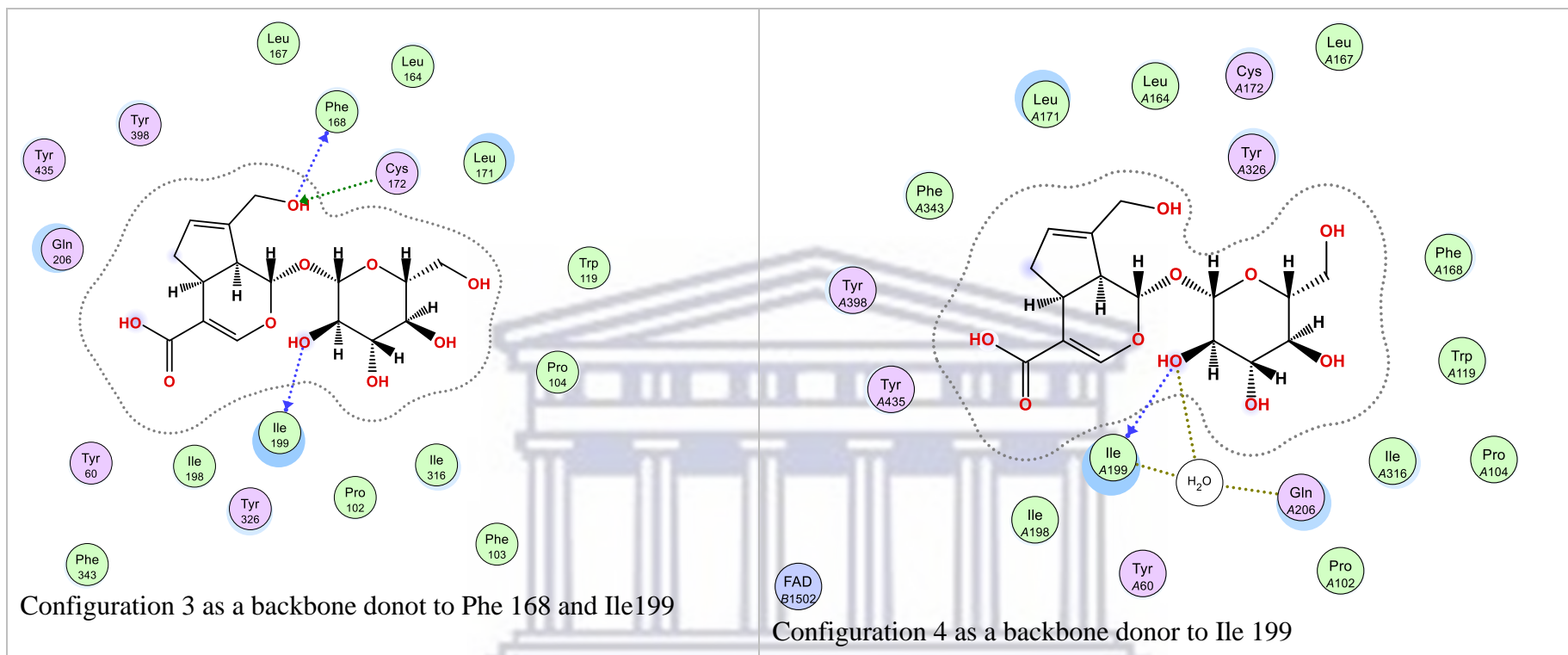
	1	9	-7.551897	0.99442488		□	24.13789 4	-56.96573	-10.02572	-24.52935	-7.551897
	1	9	-7.548344	1.7415954	24	26	17.52348 5	-62.59378	-10.14121	-35.62263	-7.548344



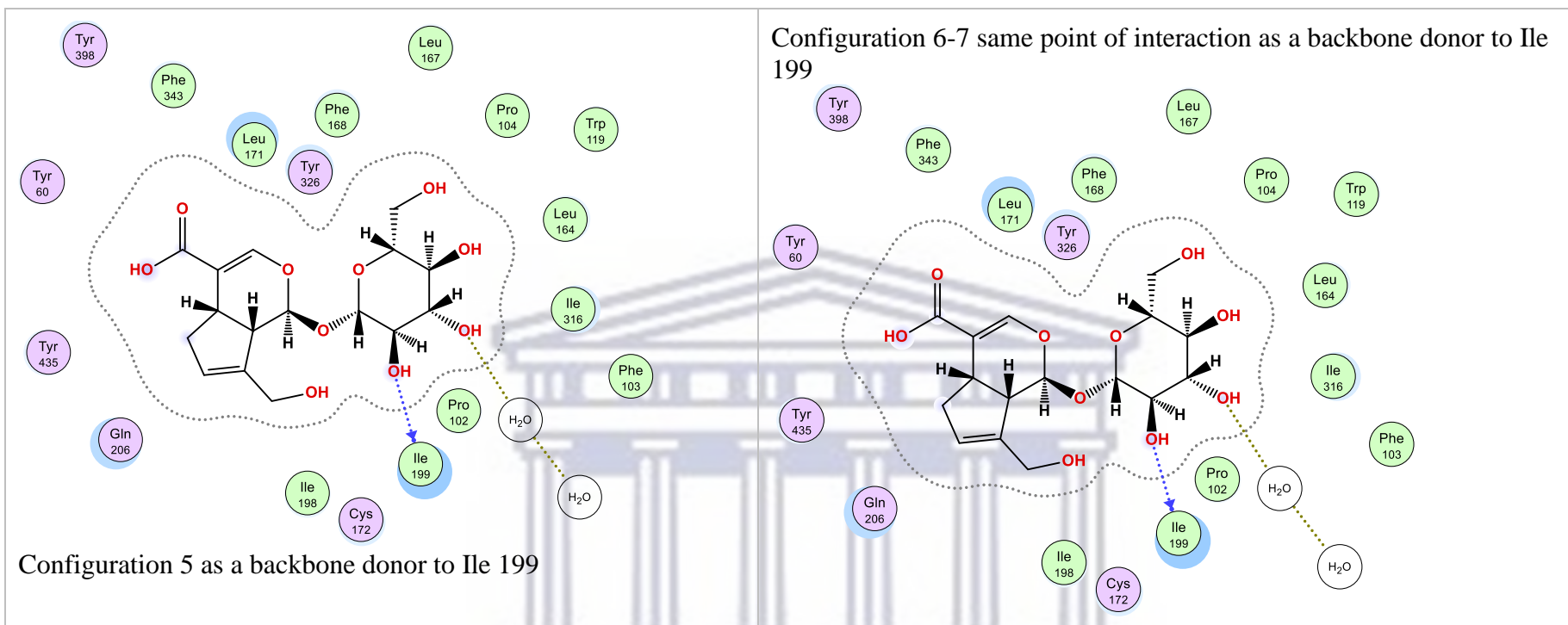
Appendix 13: Ligand interaction diagrams of Molecular docking results

Geniposidic Acid

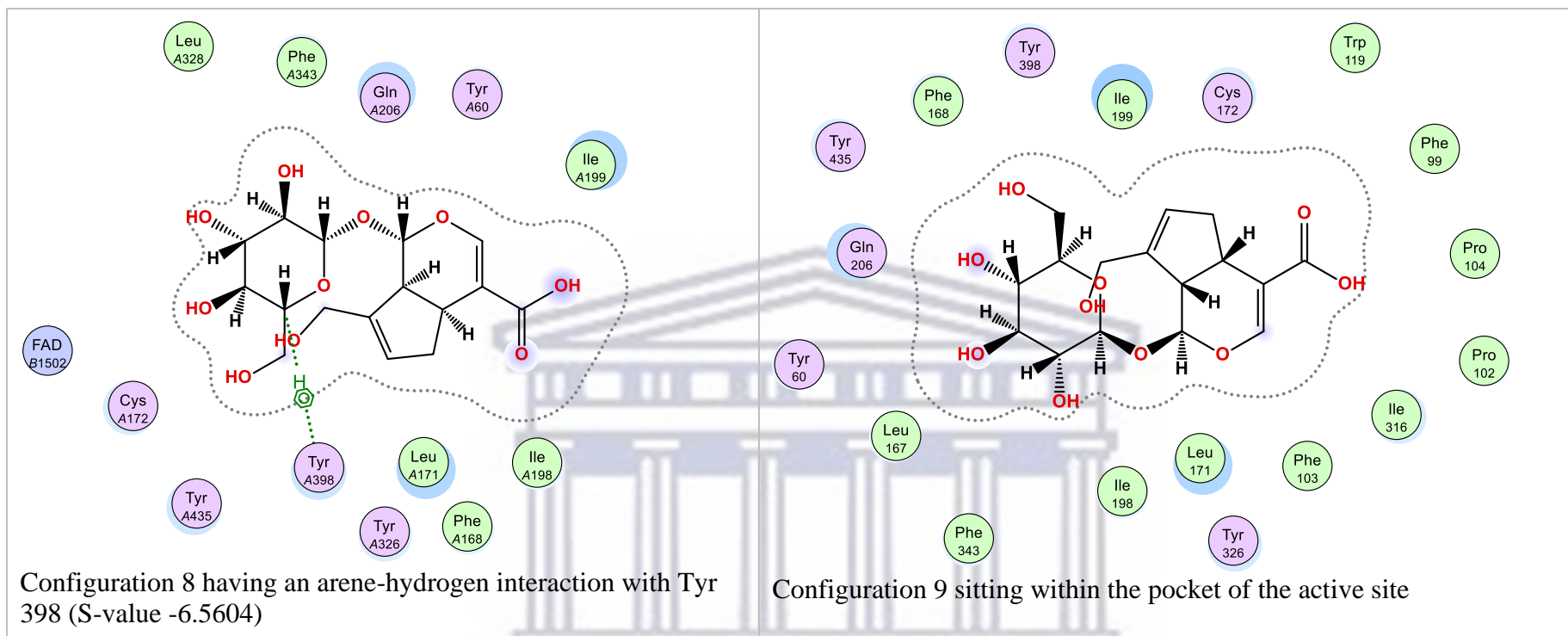




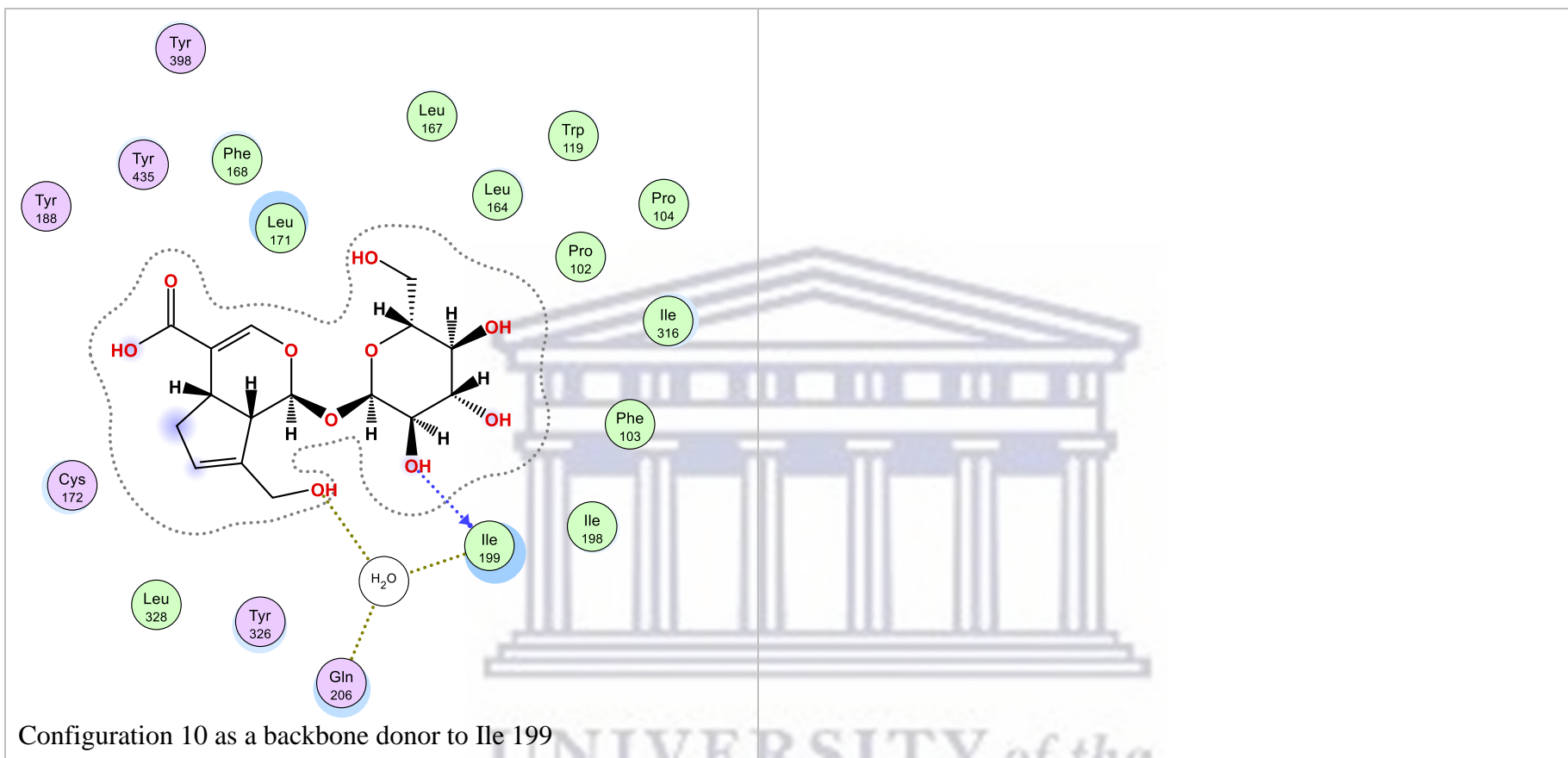
UNIVERSITY of the
WESTERN CAPE



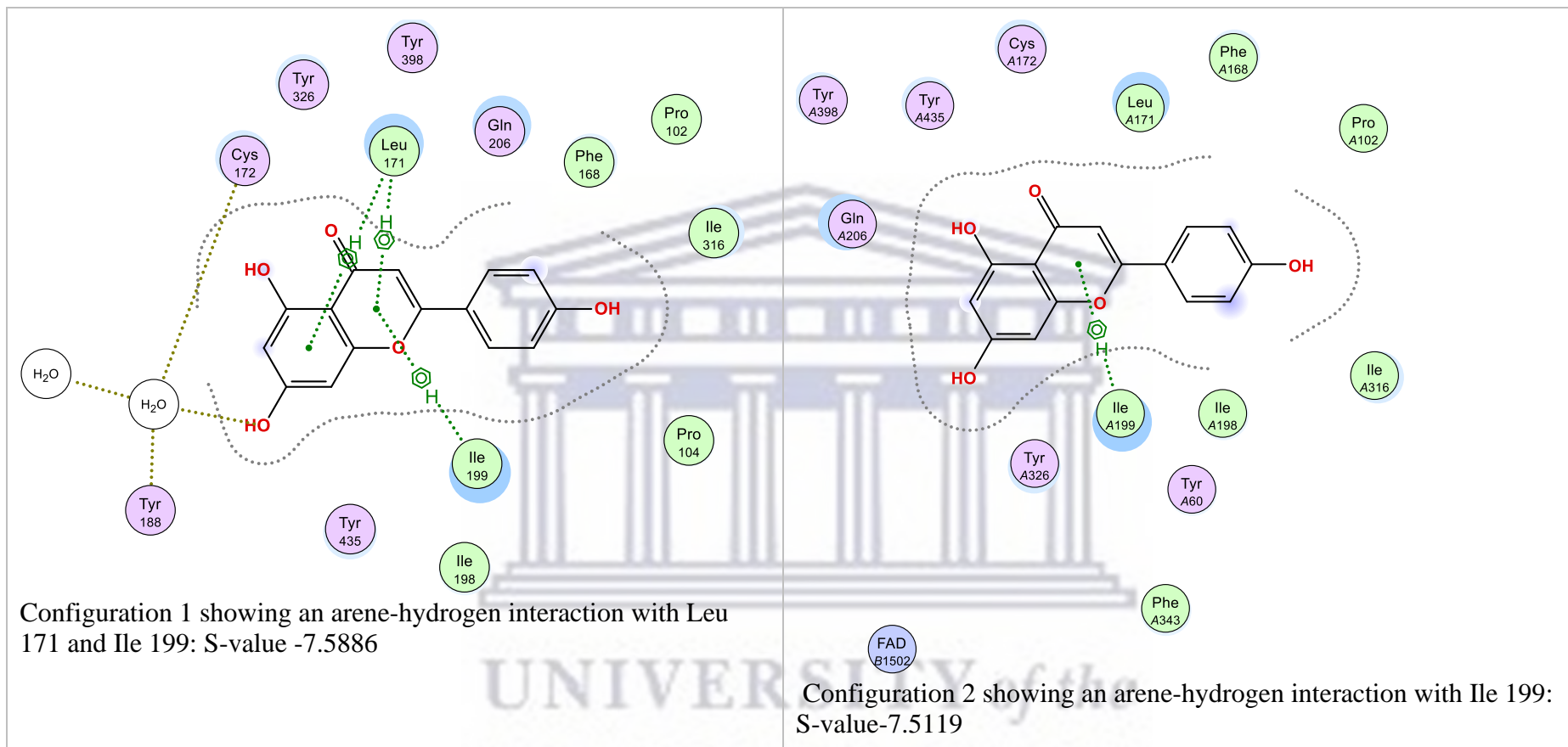
UNIVERSITY of the
WESTERN CAPE



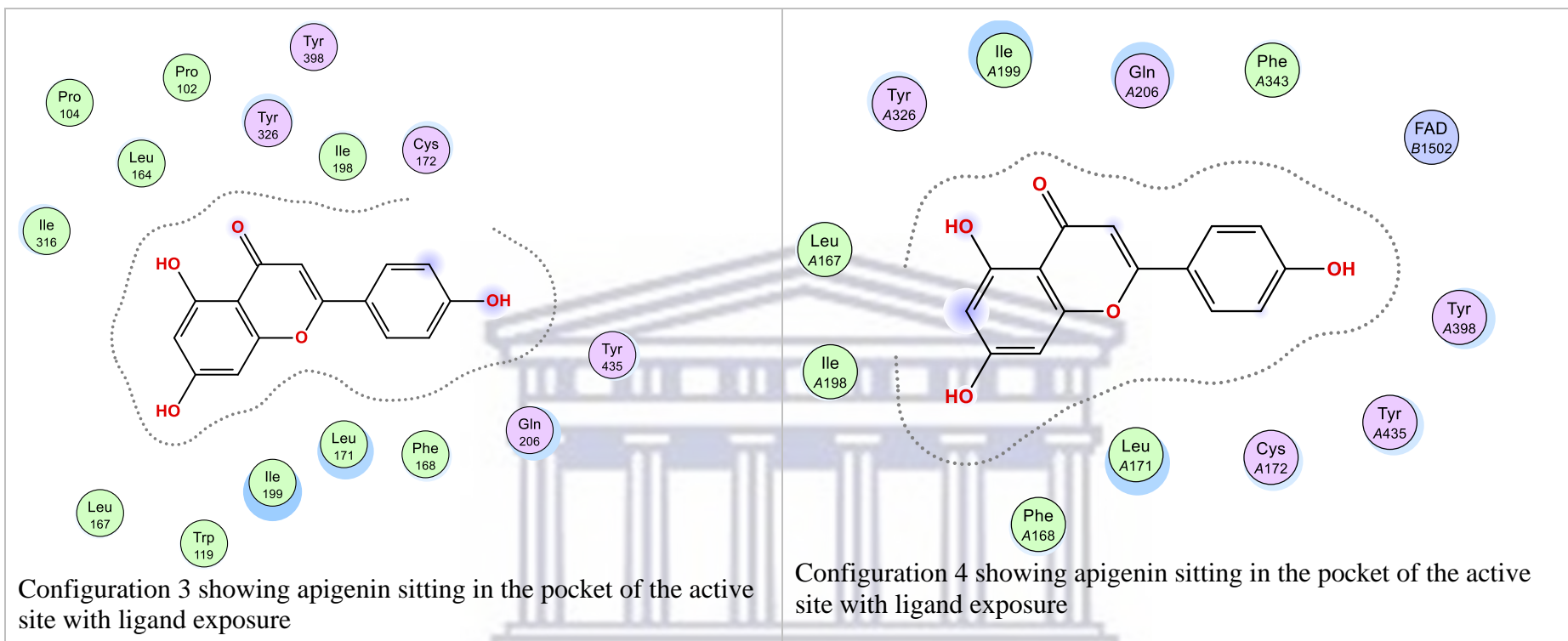
UNIVERSITY of the
WESTERN CAPE



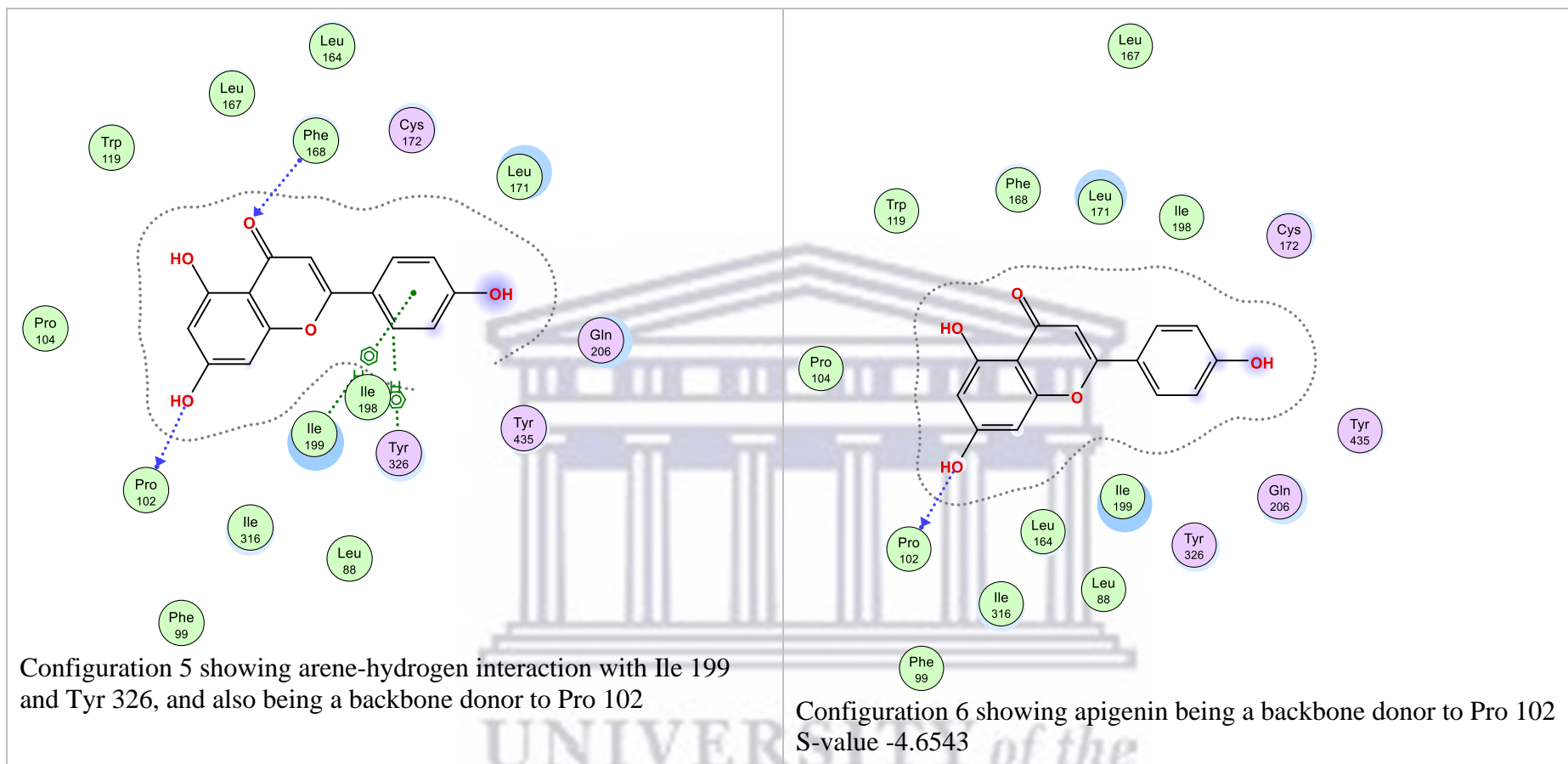
Apigenin



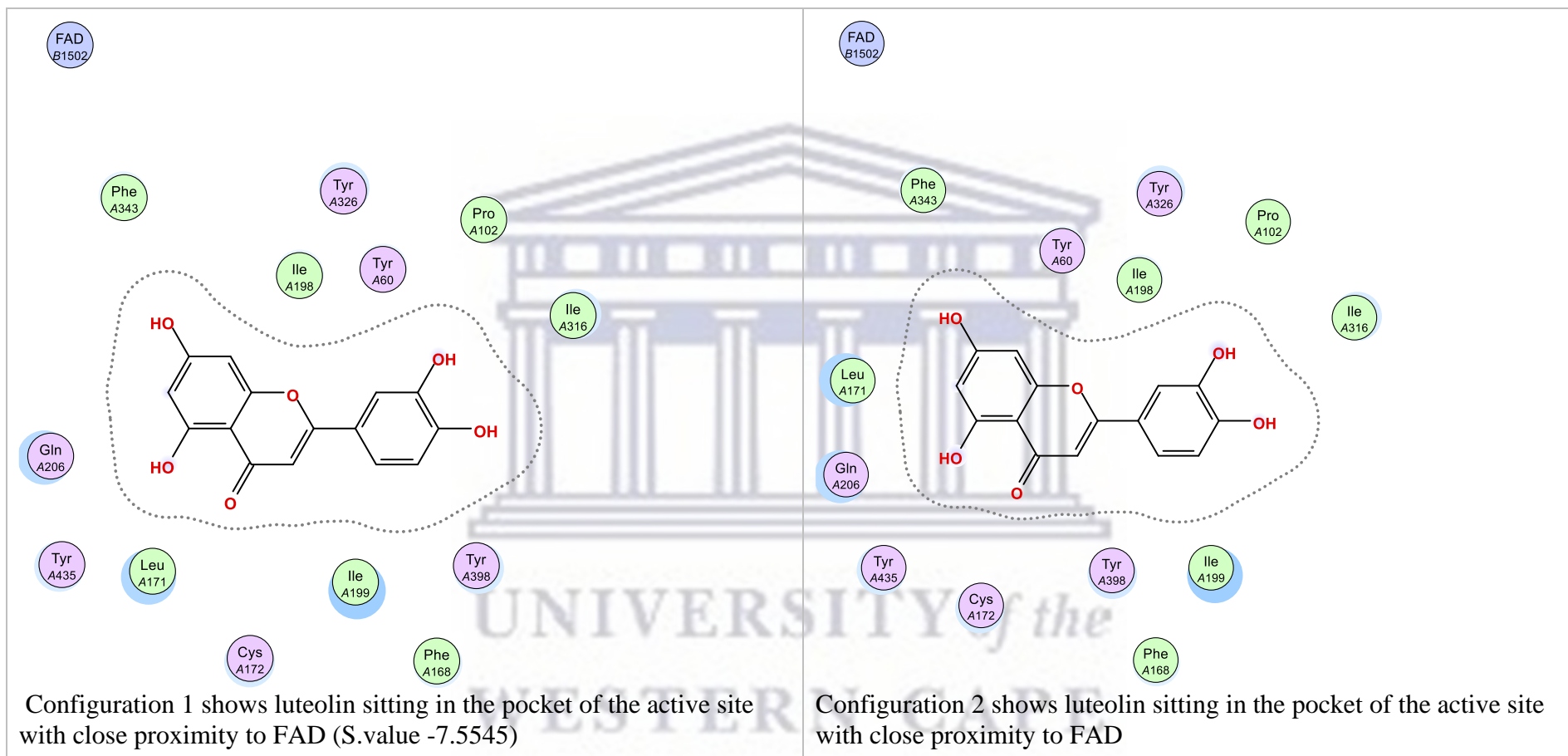
UNIVERSITY of the
WESTERN CAPE

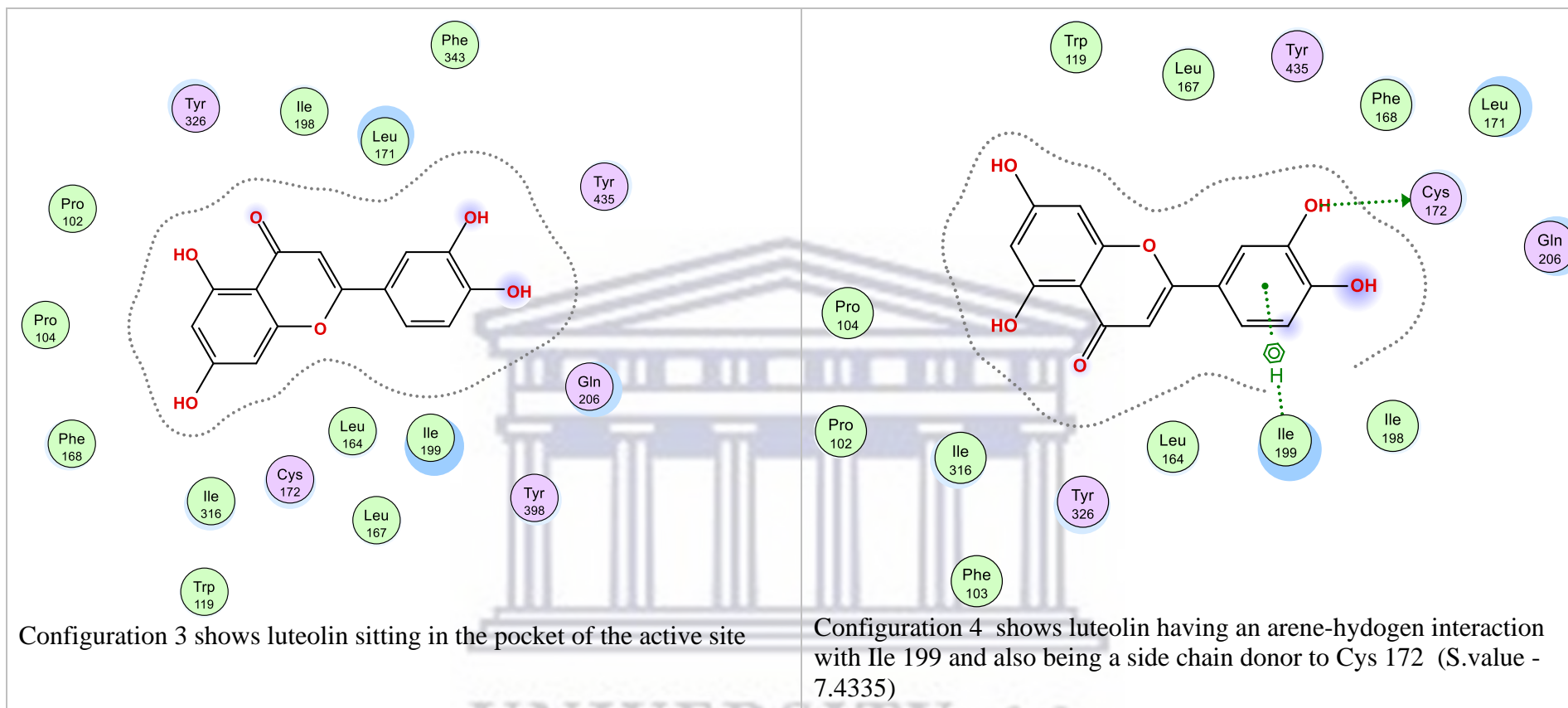


UNIVERSITY of the
WESTERN CAPE

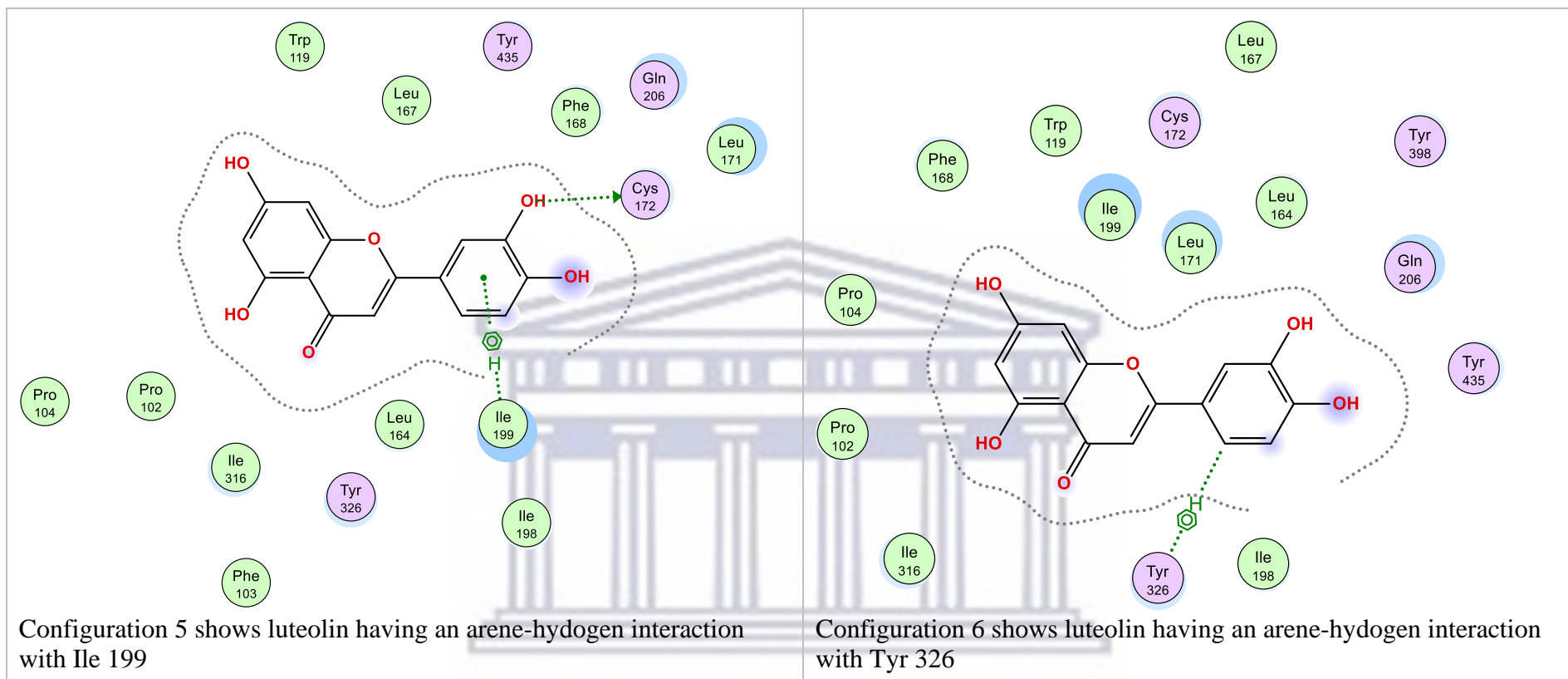


Luteolin

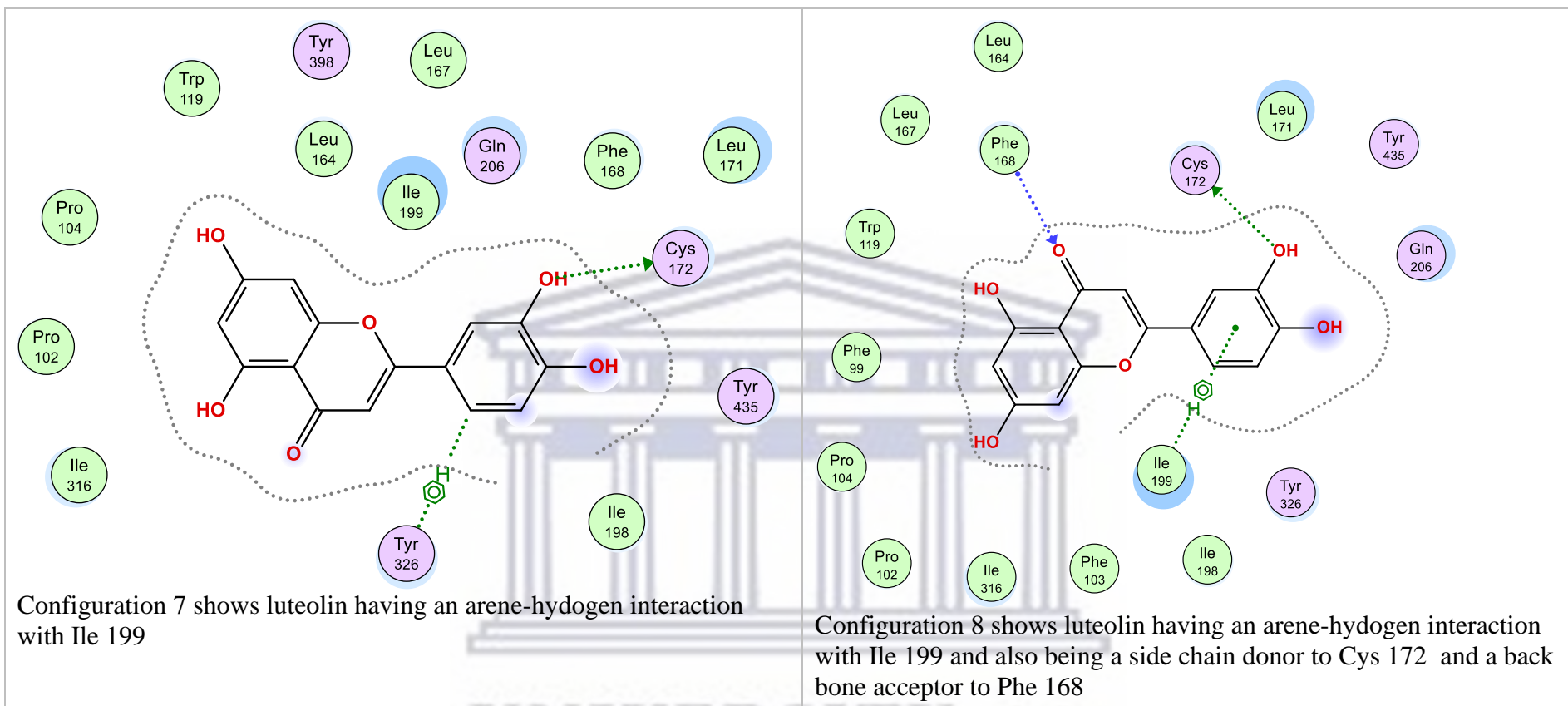




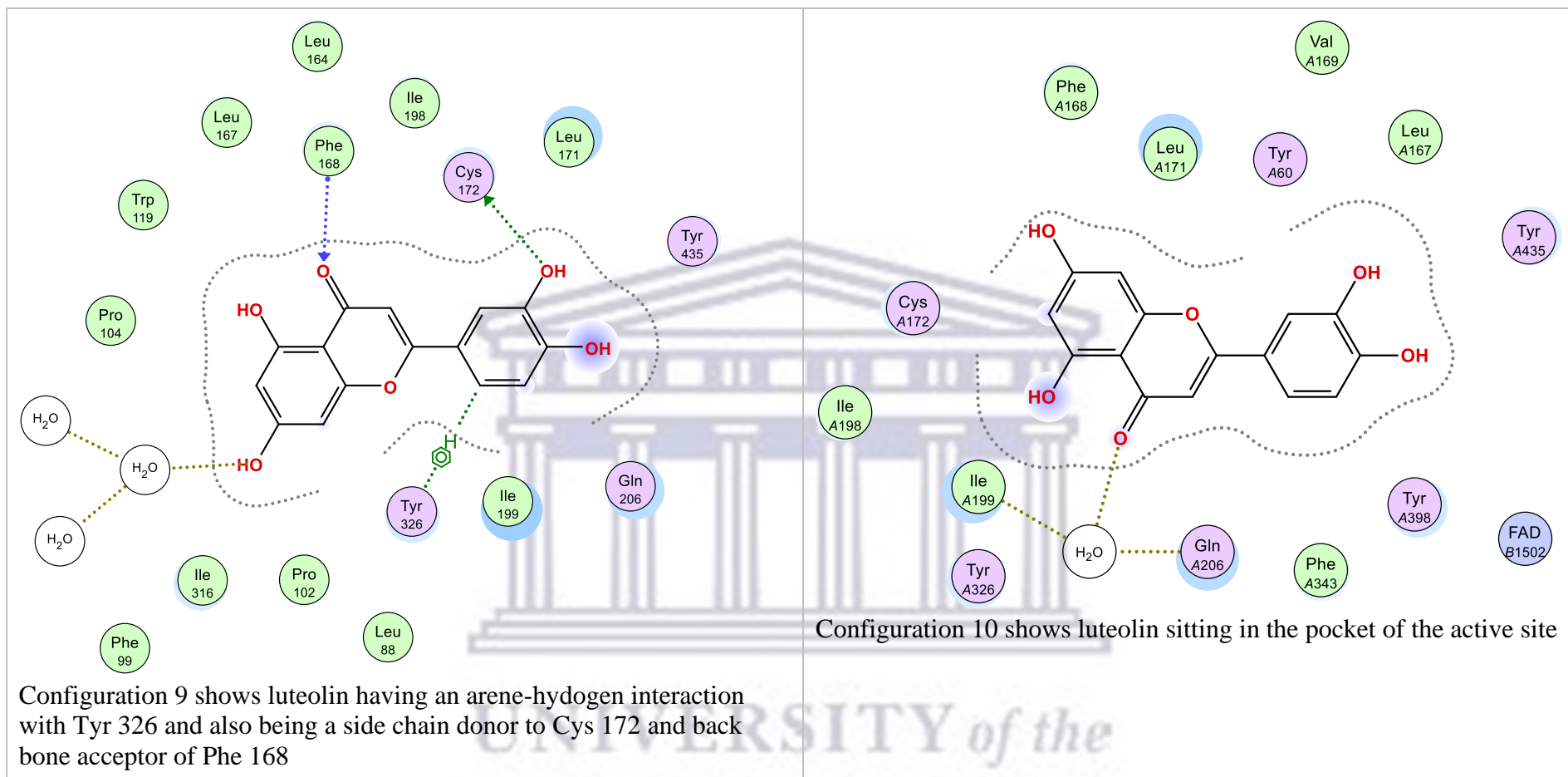
UNIVERSITY of the
WESTERN CAPE



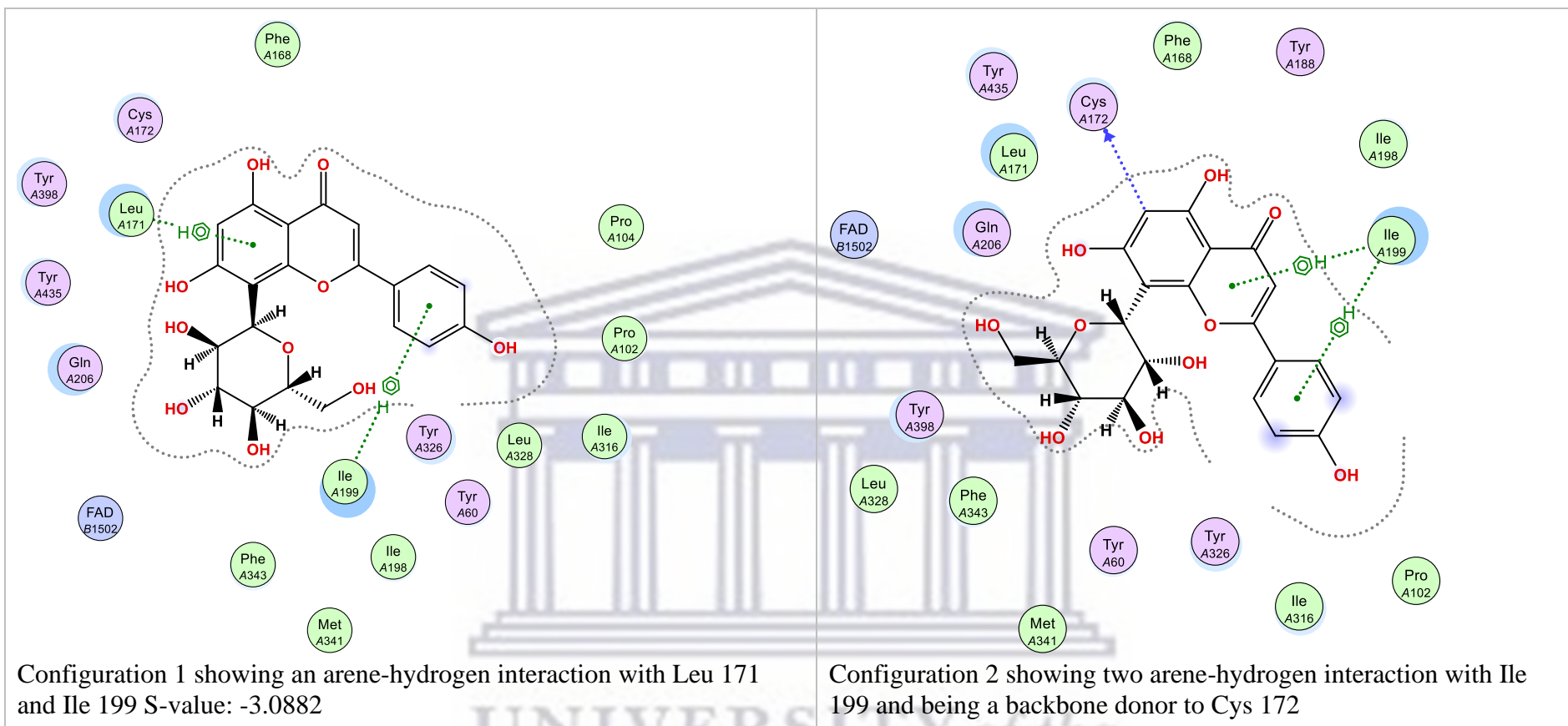
UNIVERSITY of the
WESTERN CAPE



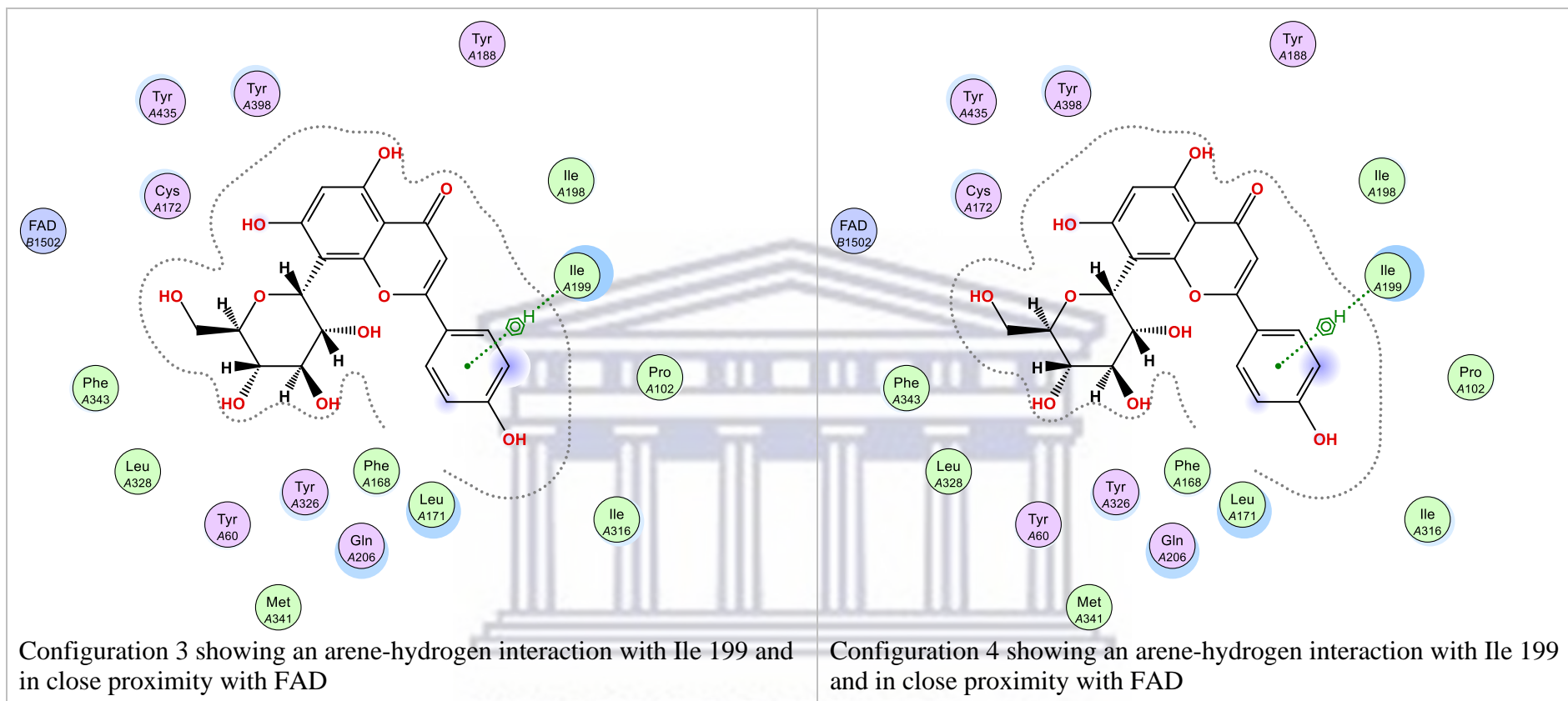
UNIVERSITY of the
WESTERN CAPE



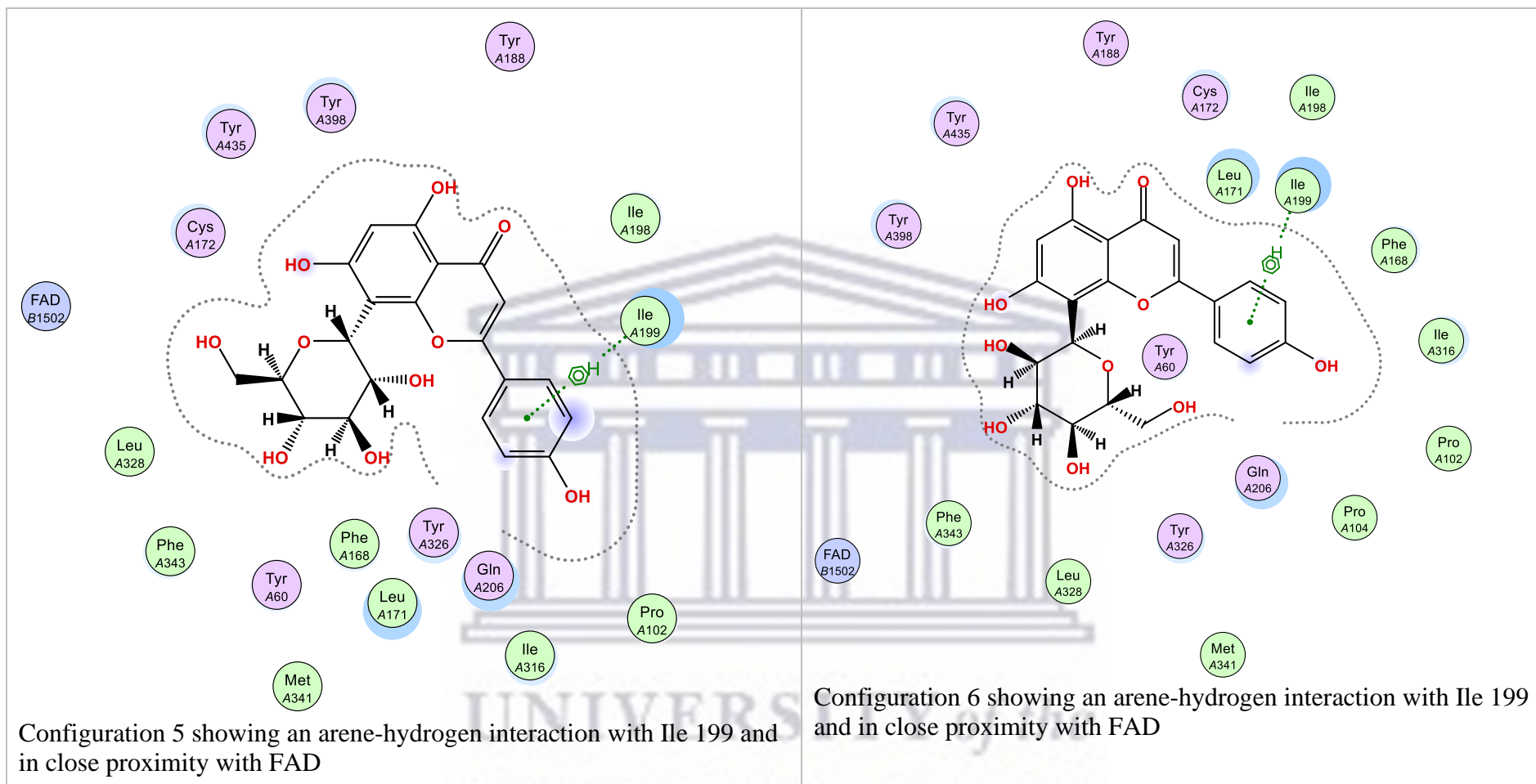
Vitexin



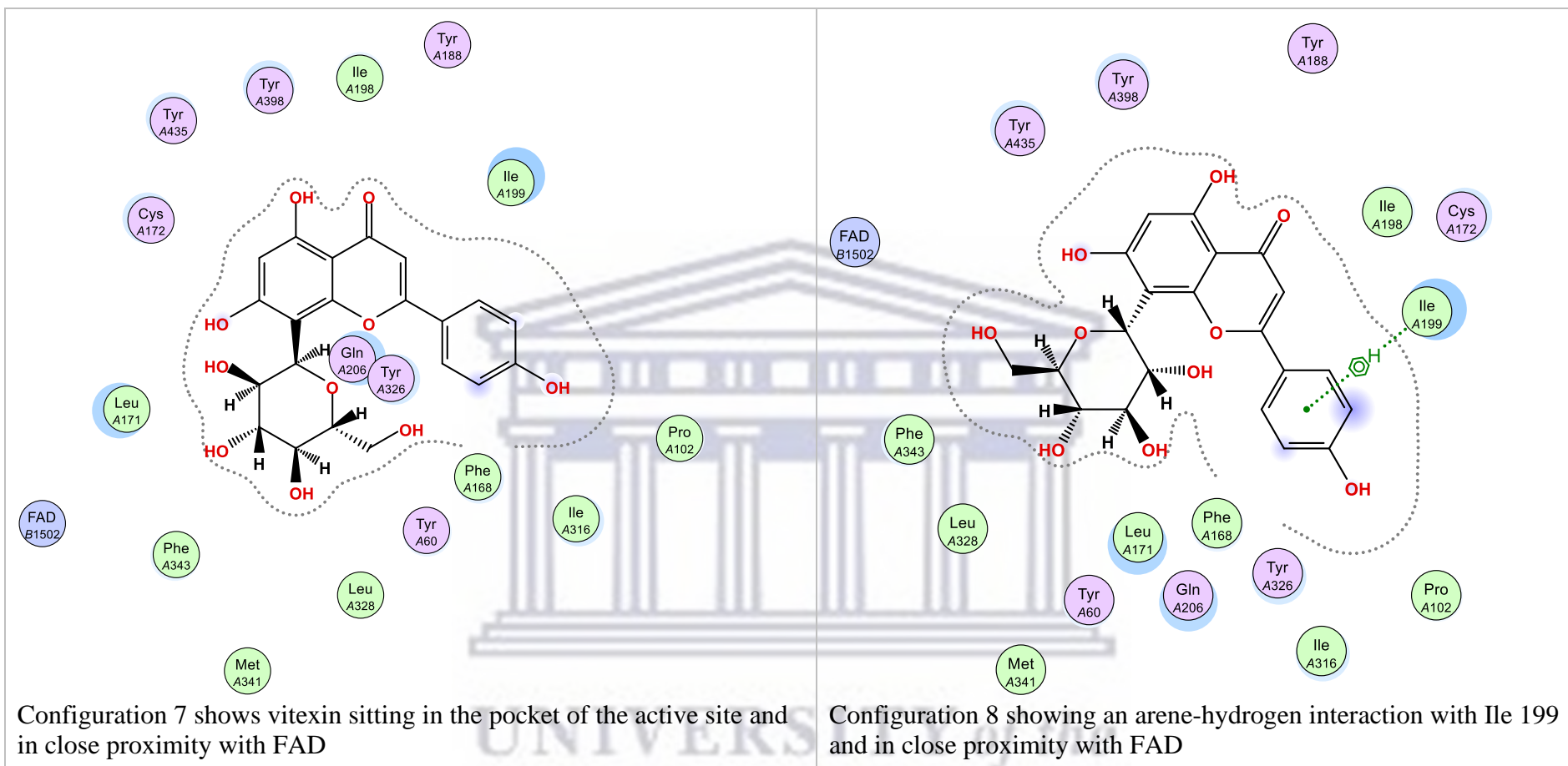
UNIVERSITY of the
WESTERN CAPE



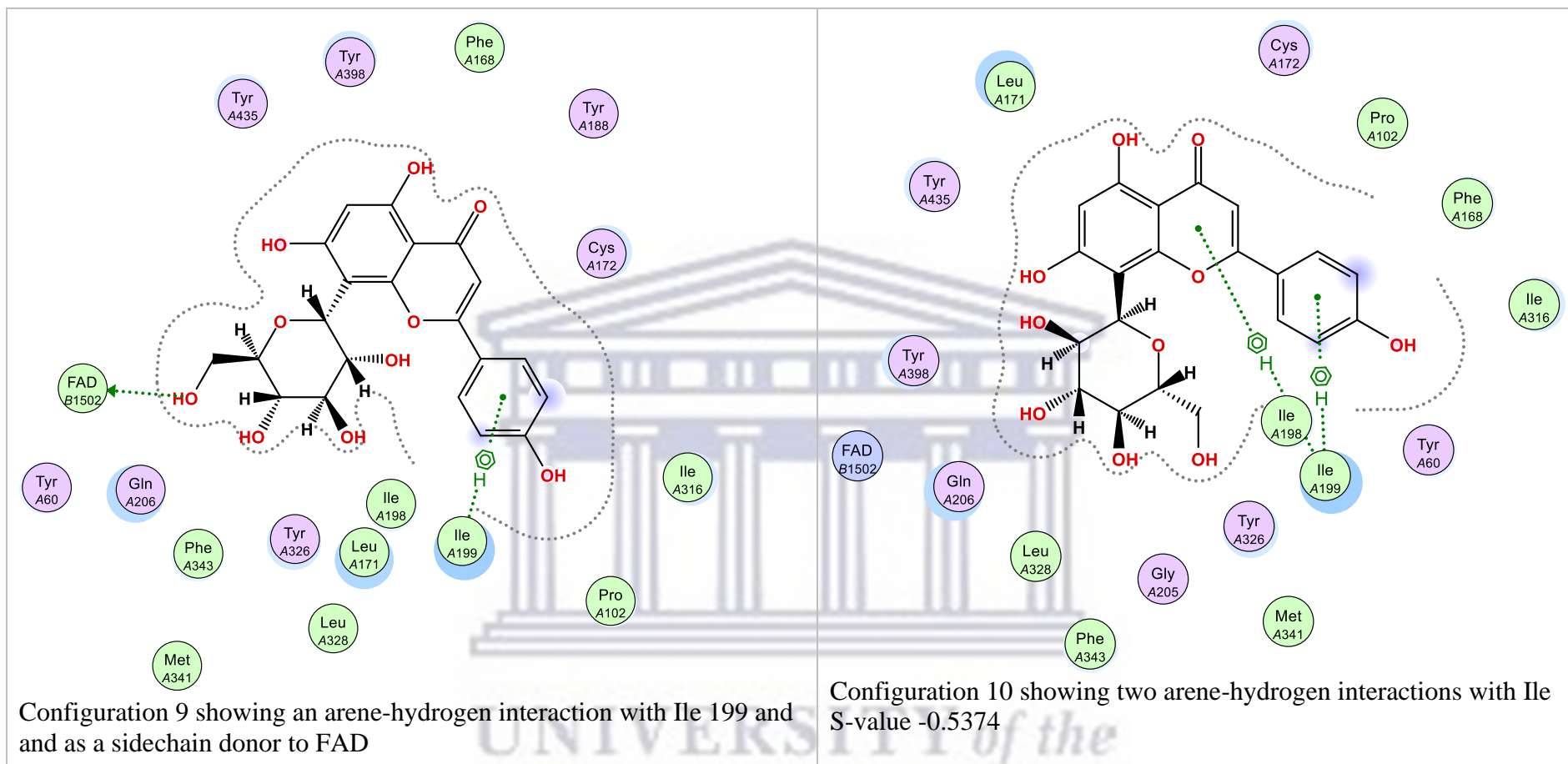
UNIVERSITY of the
WESTERN CAPE



UNIVERSITY OF
WESTERN CAPE

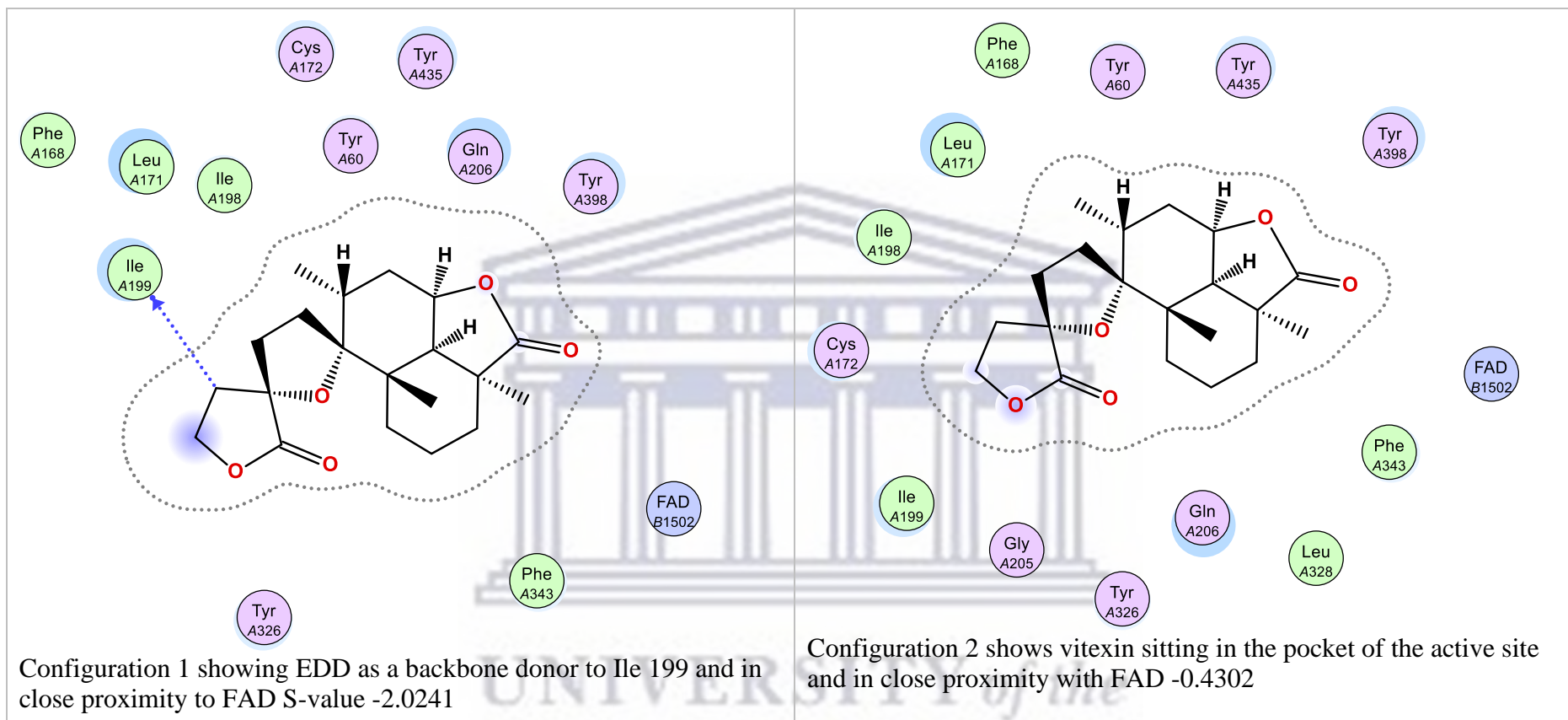


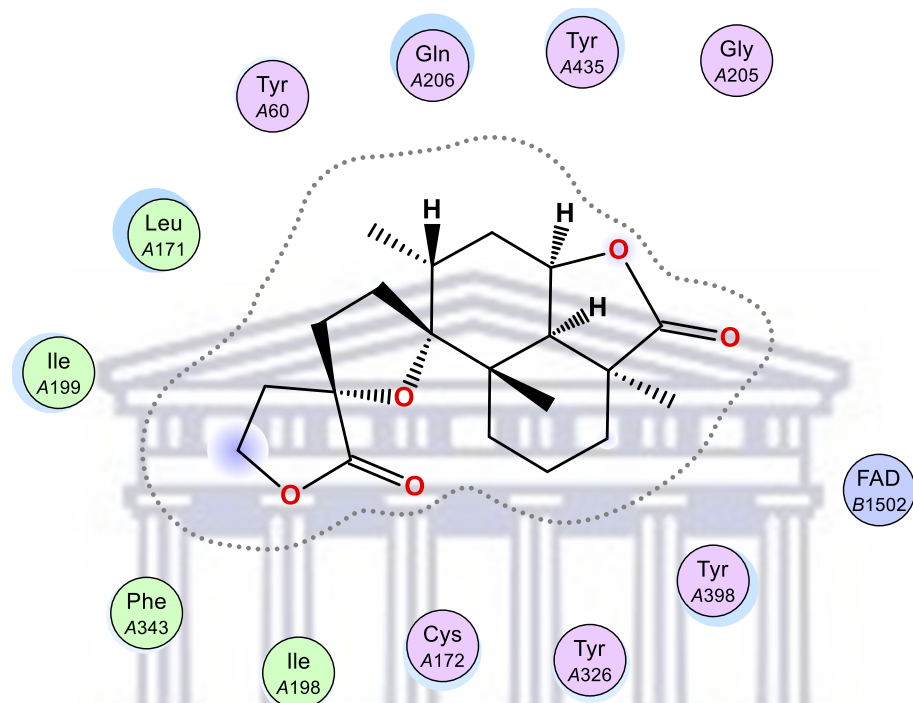
UNIVERSITY OF
WESTERN CAPE



UNIVERSITY of the
WESTERN CAPE

EDD

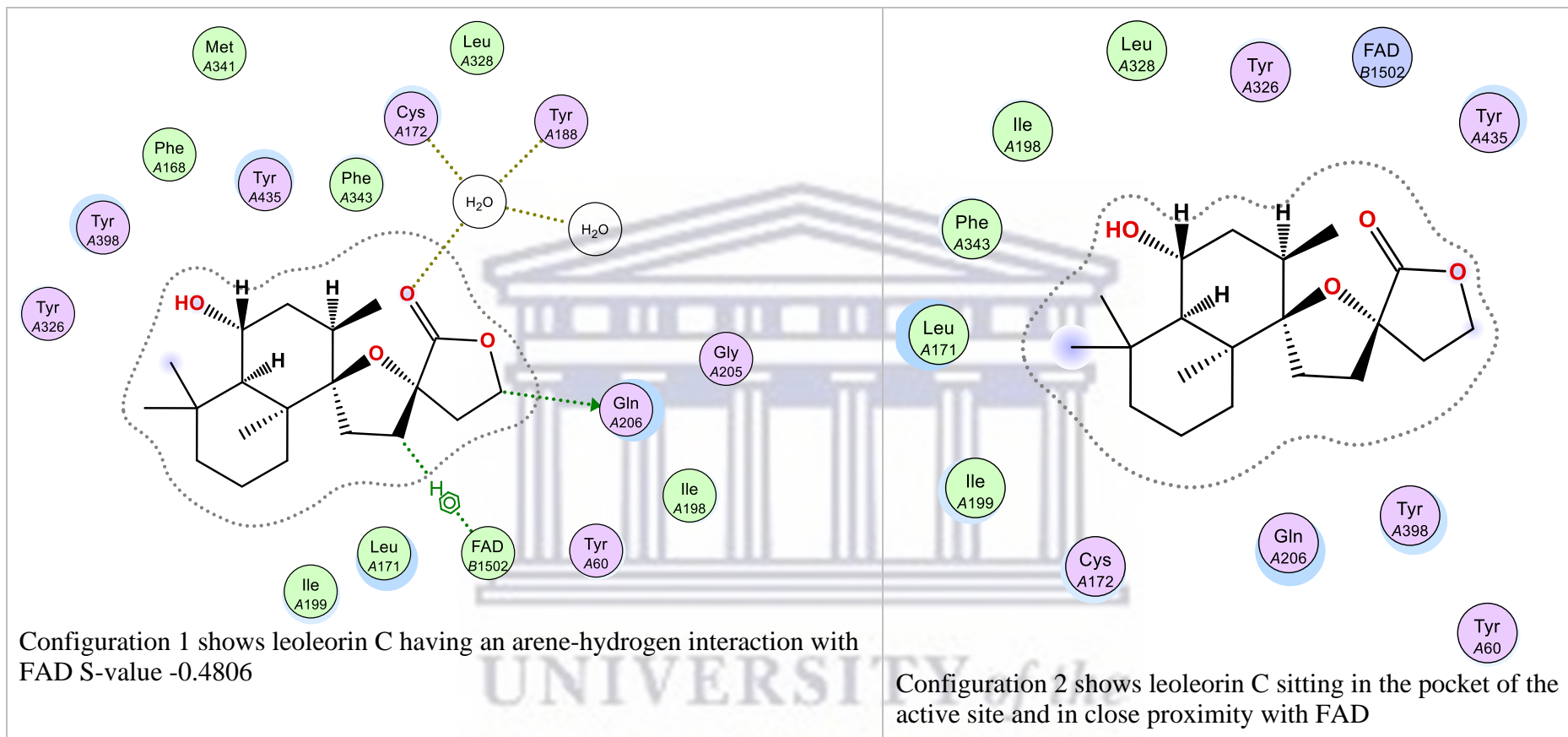


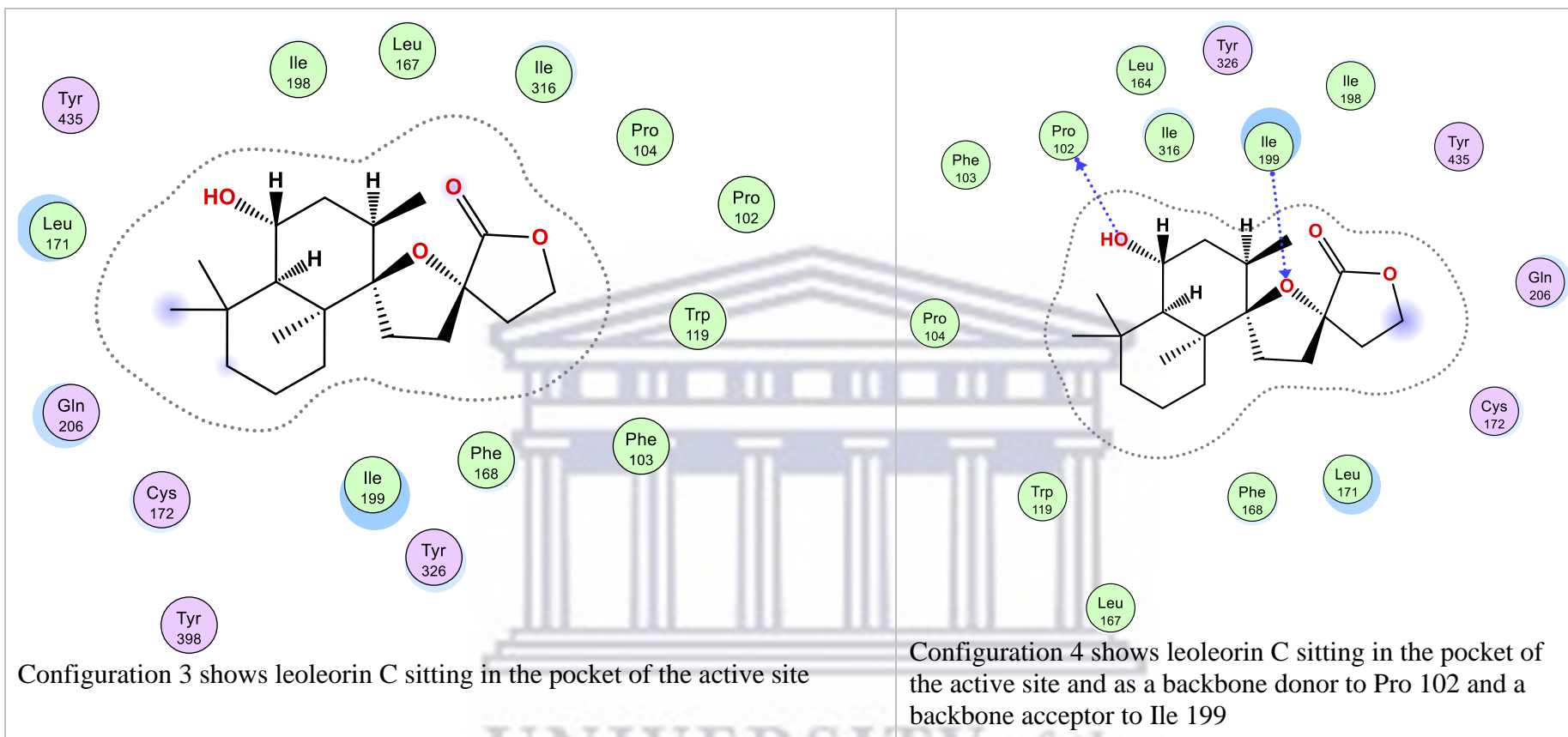


Configuration 3 shows vitexin sitting in the pocket of the active site and in close proximity with FAD S-value-0.2683

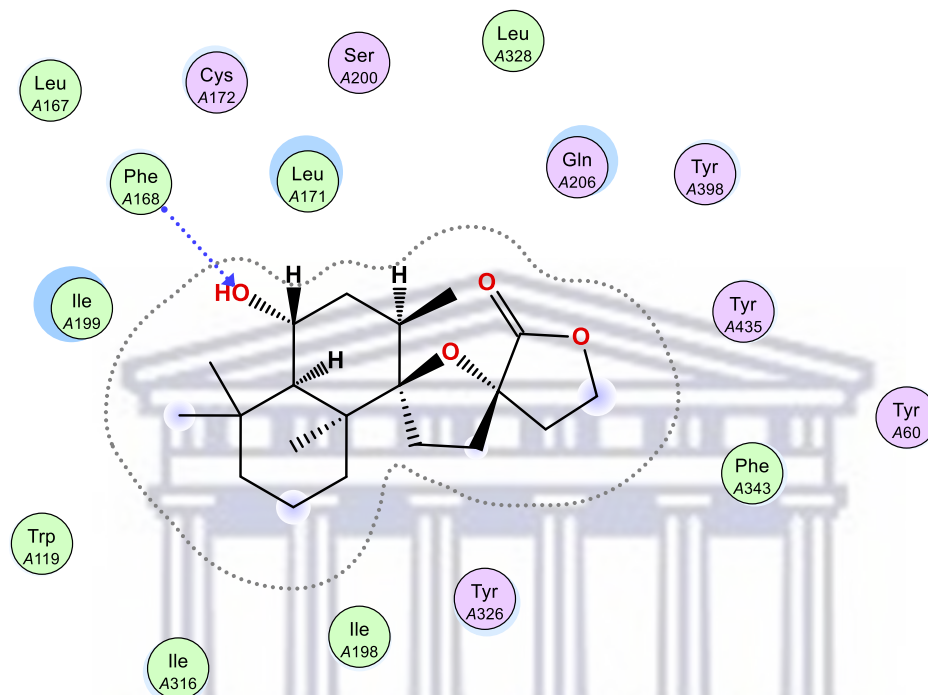
UNIVERSITY of the
WESTERN CAPE

Leoleorin C





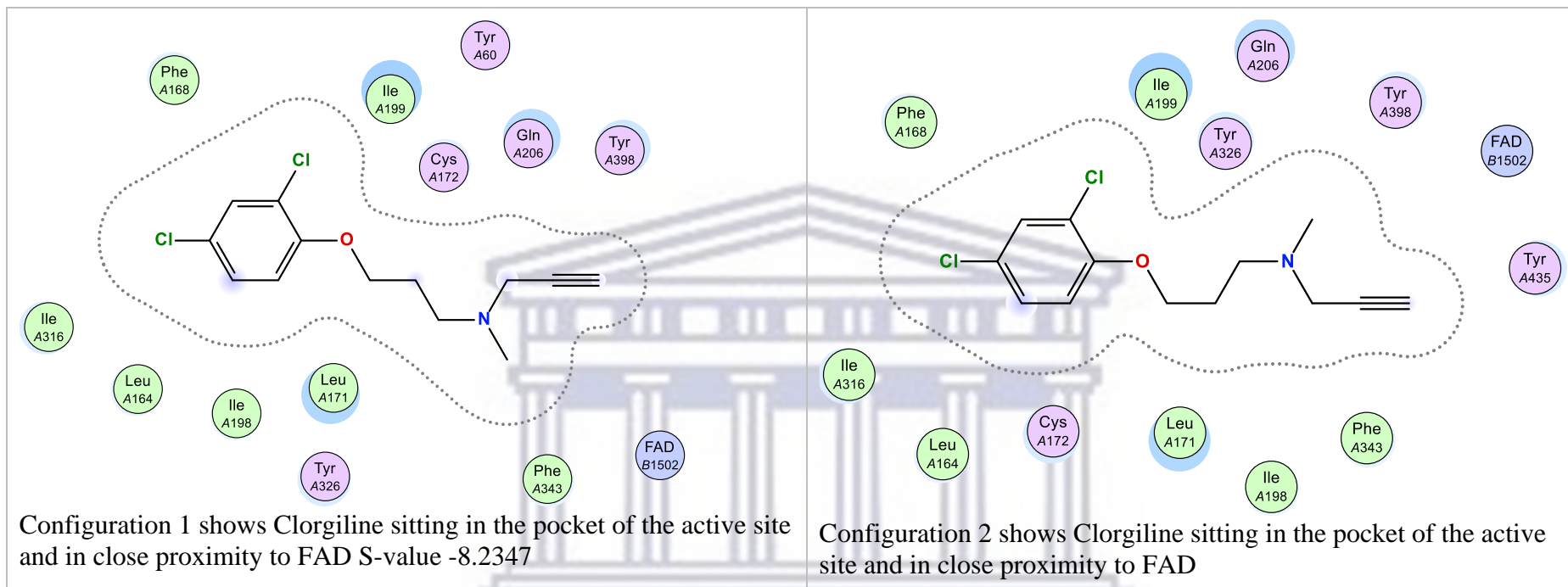
UNIVERSITY of the
WESTERN CAPE



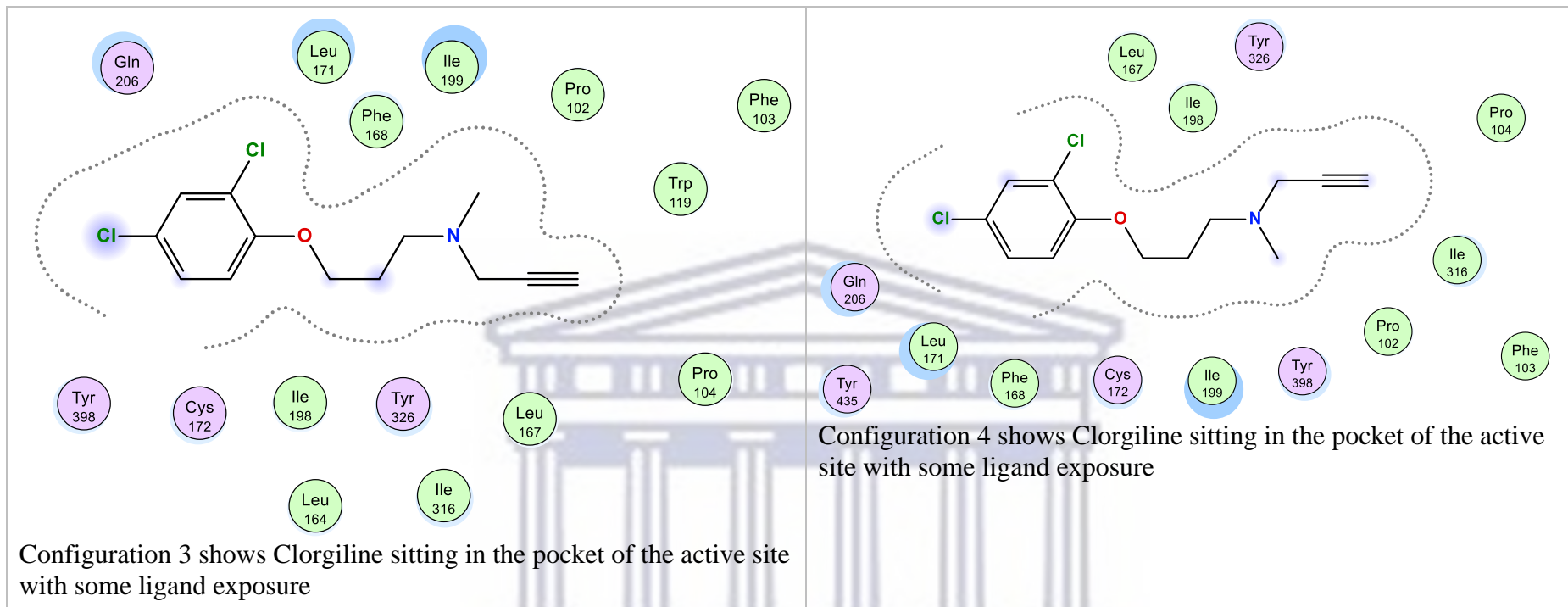
Configuration 5 shows leoleorin C sitting in the pocket of the active site and as a backbone acceptor to Phe 168

UNIVERSITY of the
WESTERN CAPE

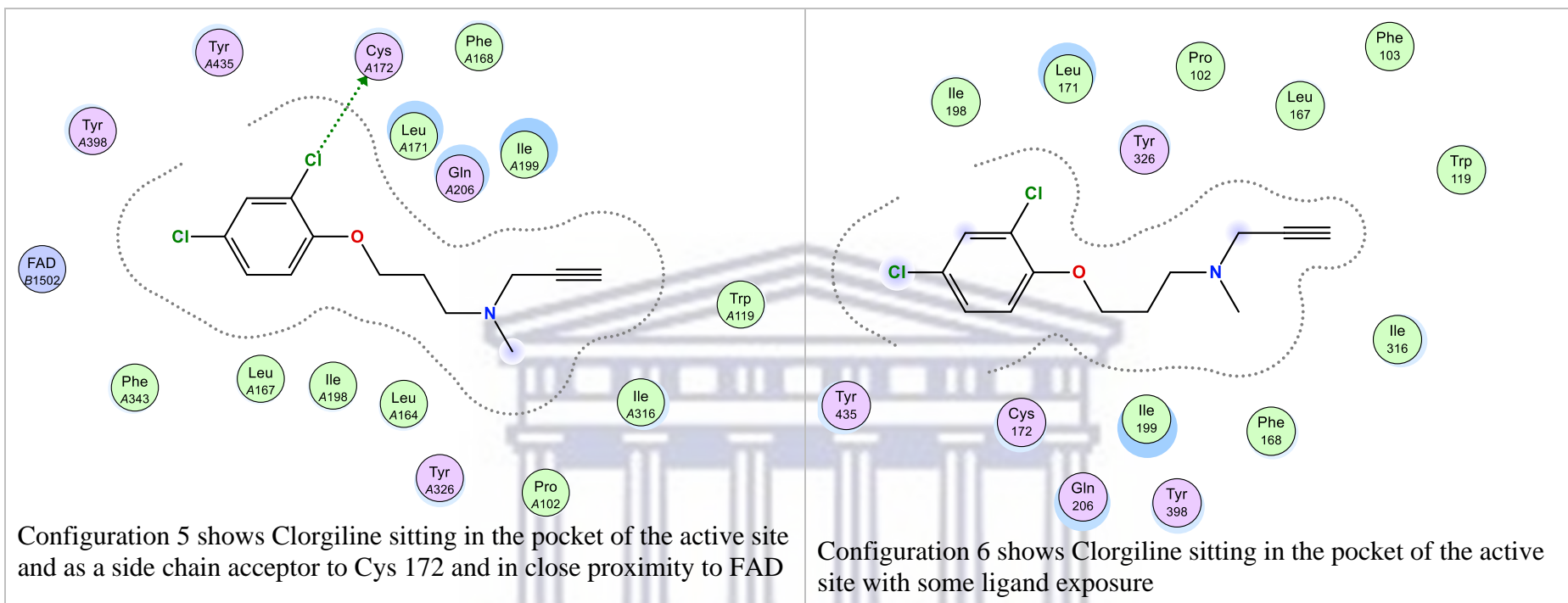
Clorgiline



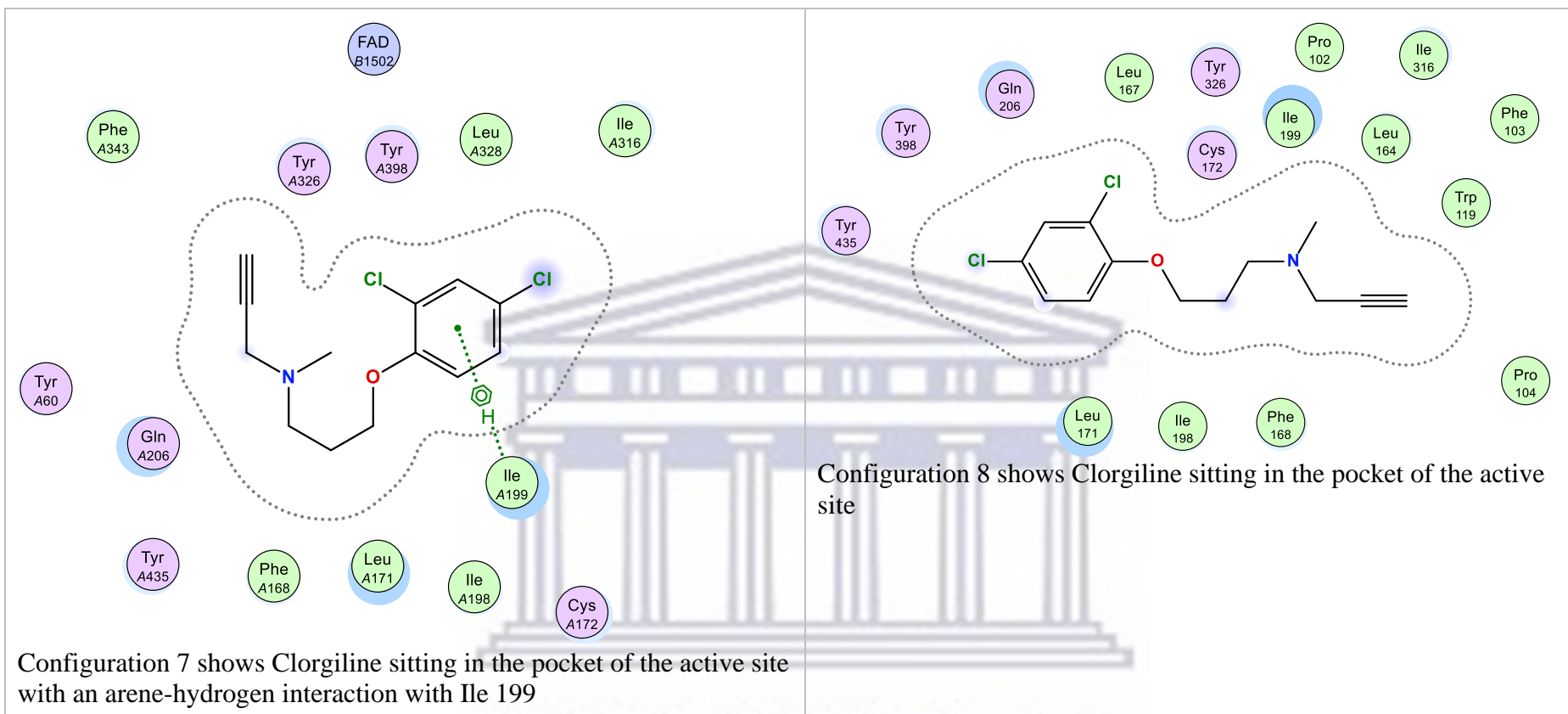
UNIVERSITY of the
WESTERN CAPE



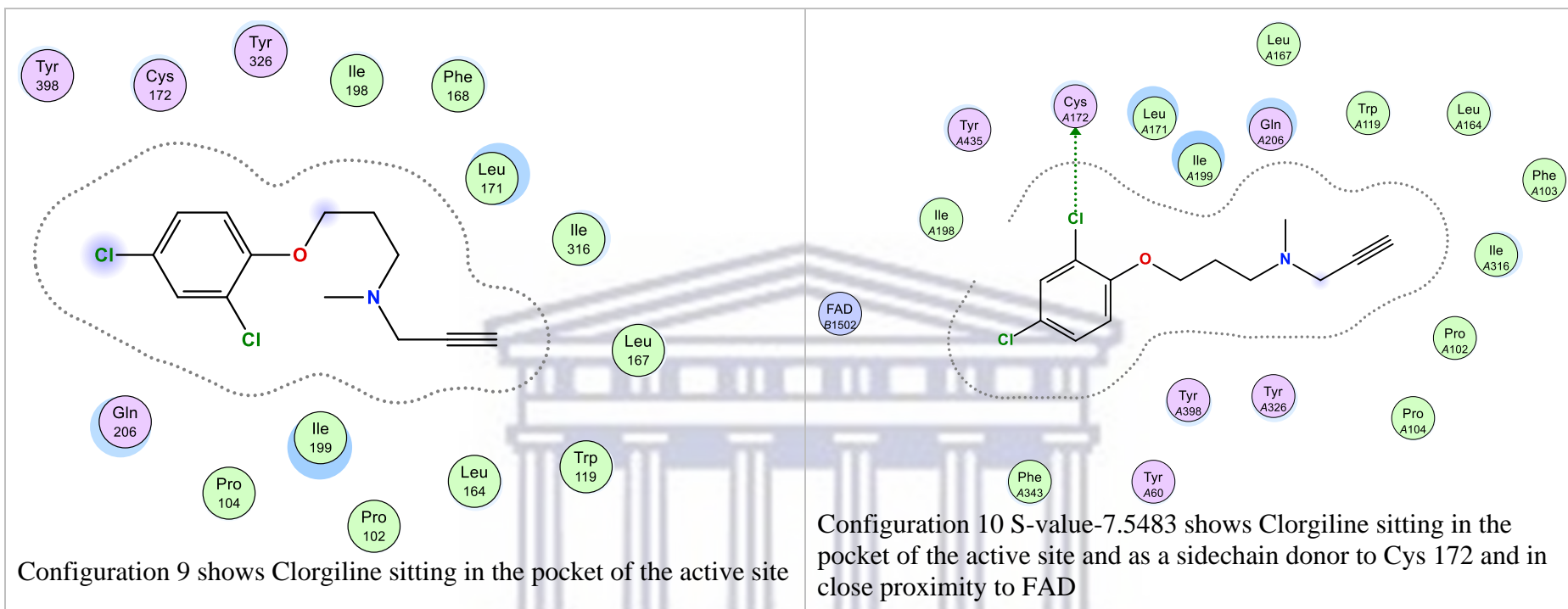
UNIVERSITY of the
WESTERN CAPE



UNIVERSITY of the
WESTERN CAPE

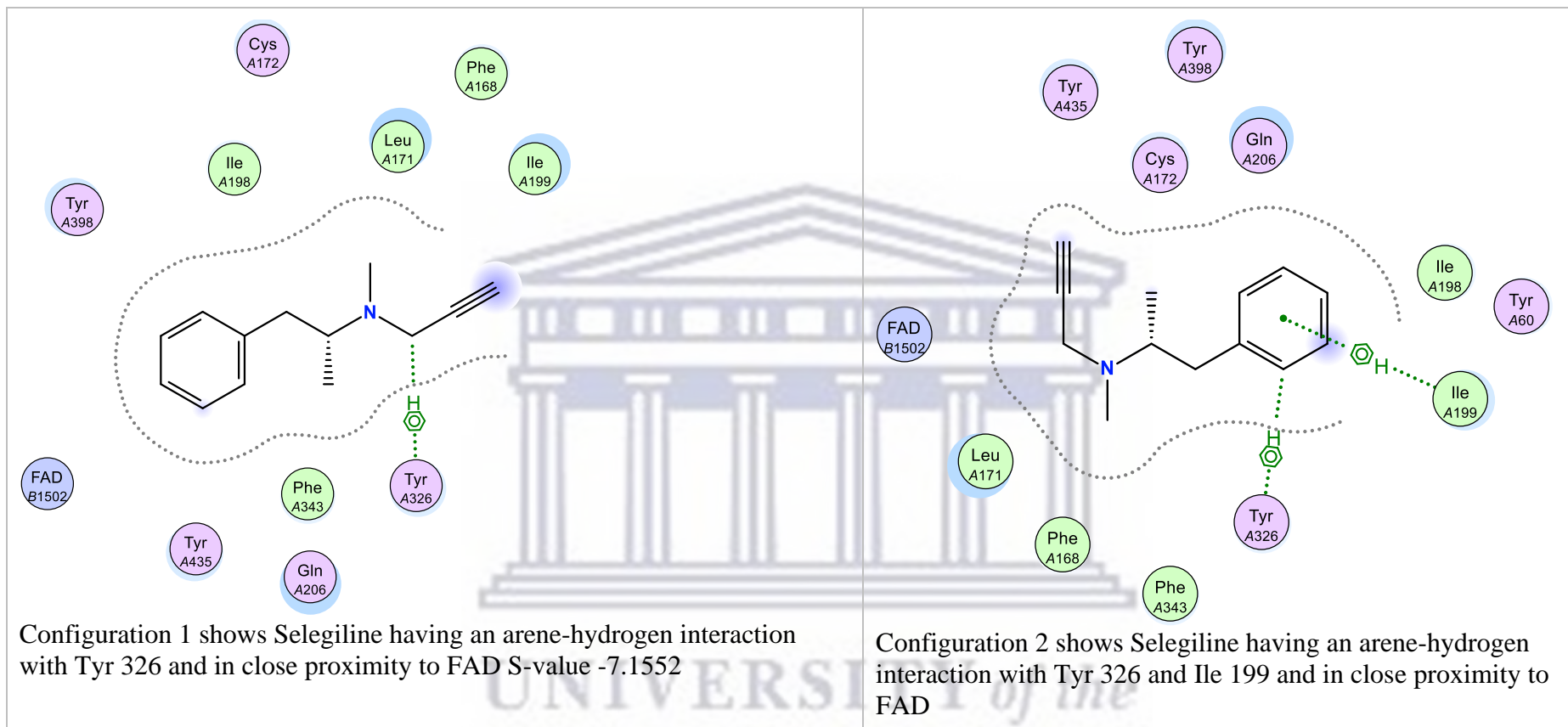


UNIVERSITY of the
WESTERN CAPE

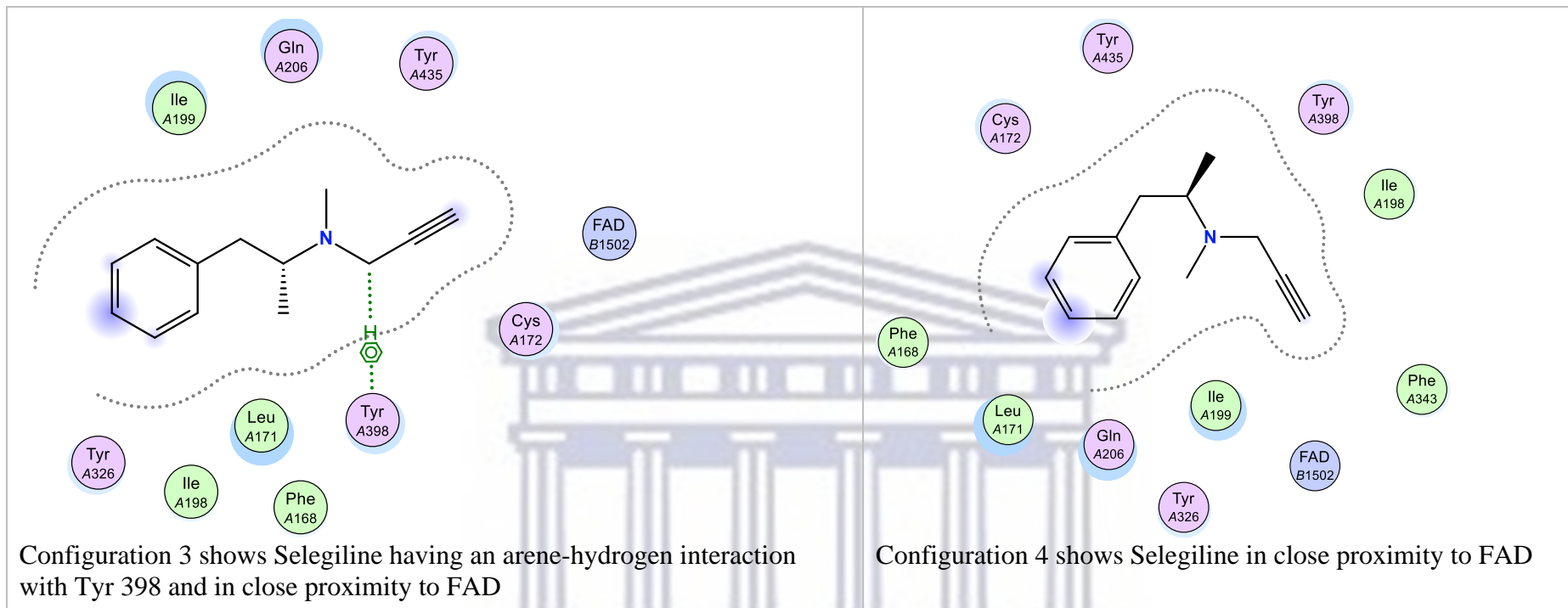


UNIVERSITY of the
WESTERN CAPE

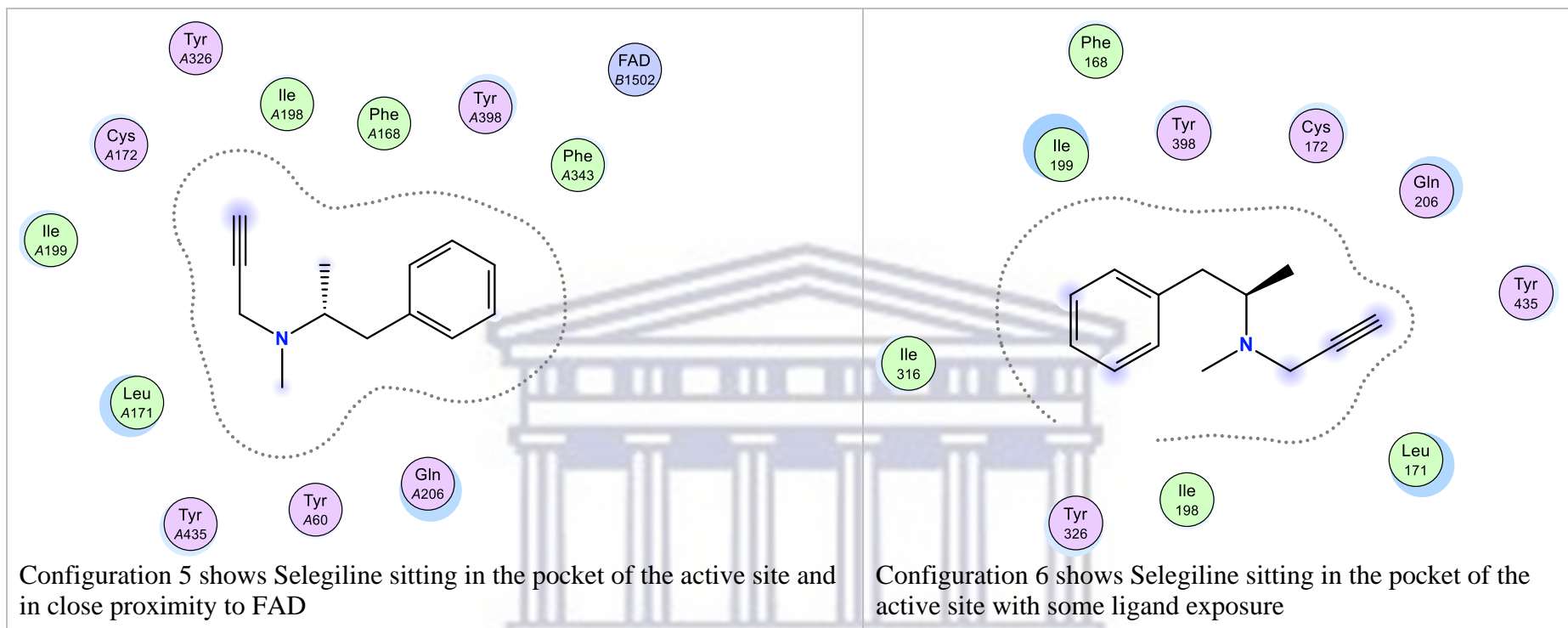
Selegiline

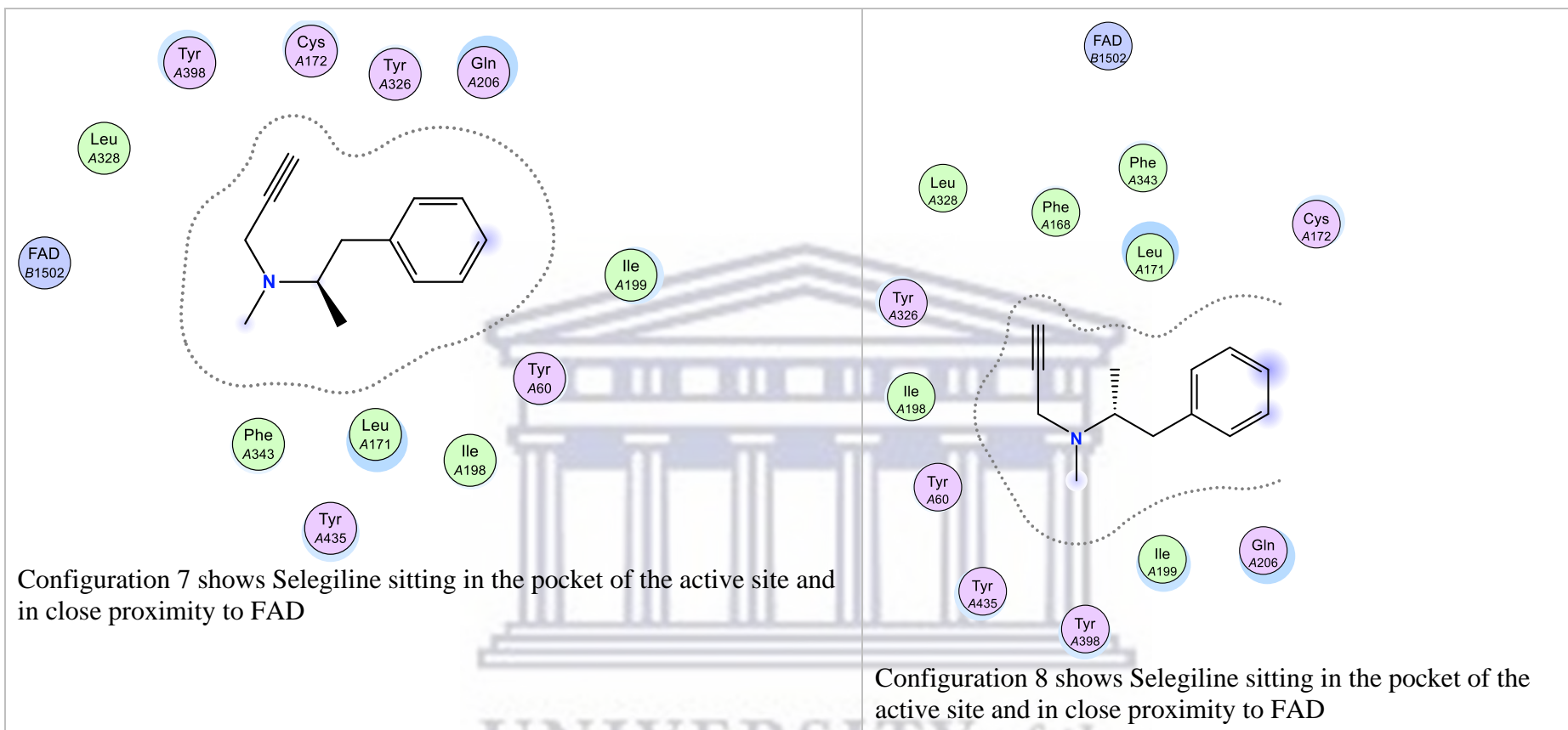


UNIVERSITY of the
WESTERN CAPE

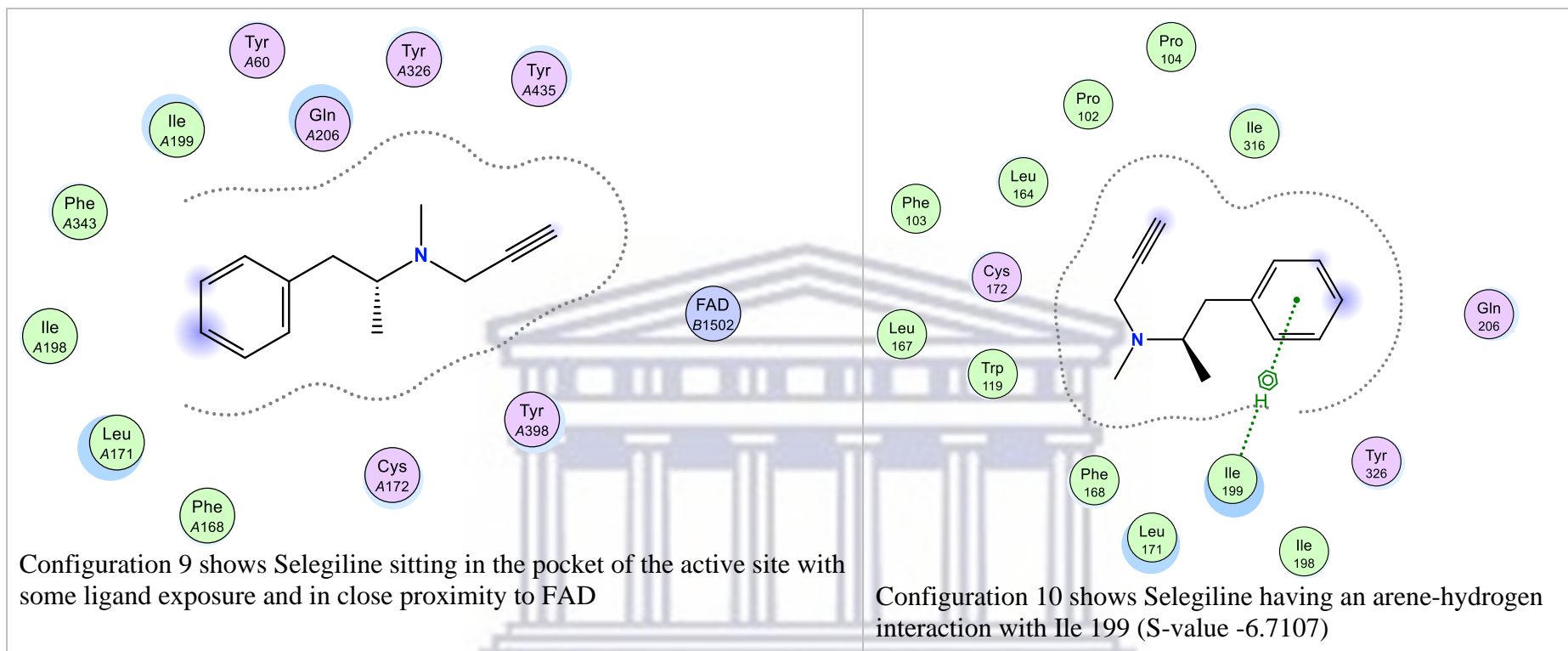


UNIVERSITY of the
WESTERN CAPE



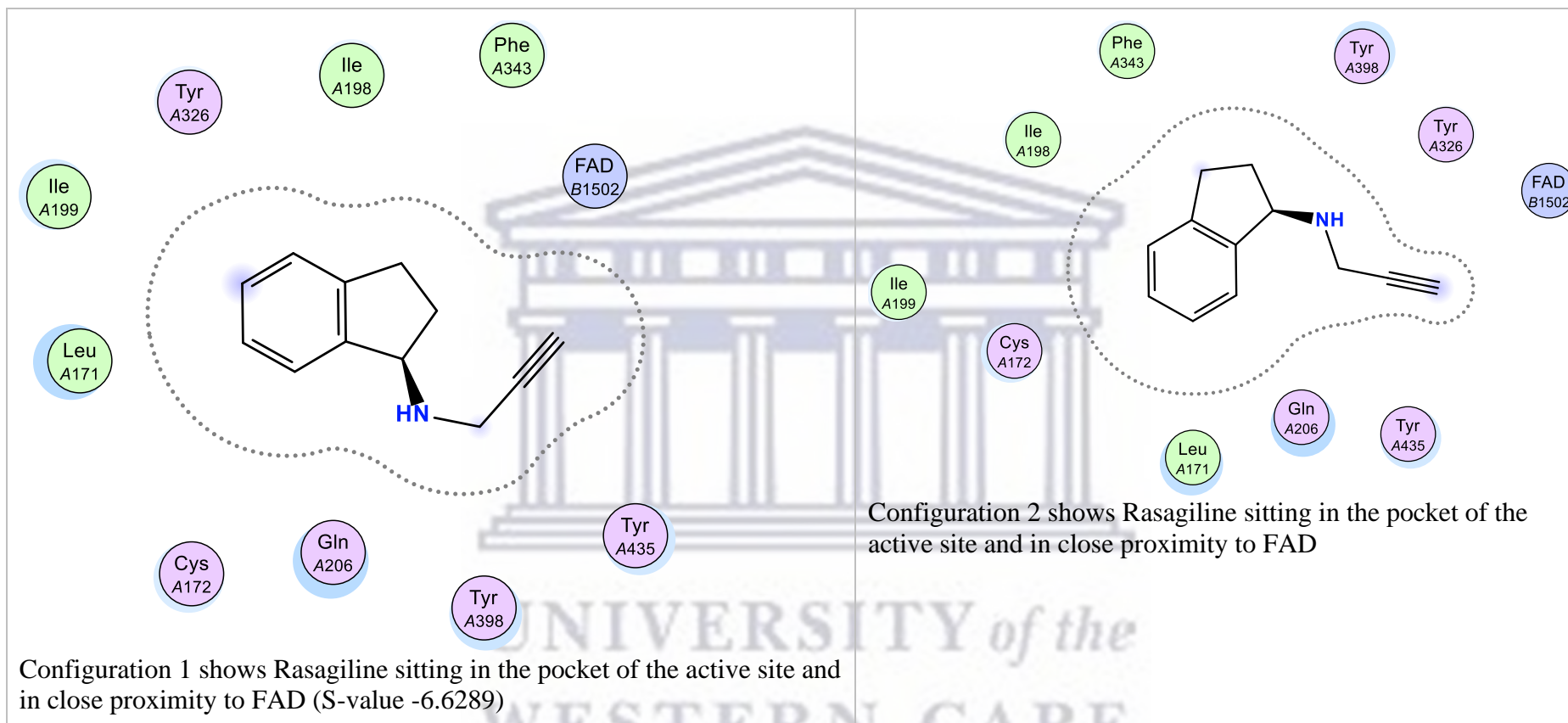


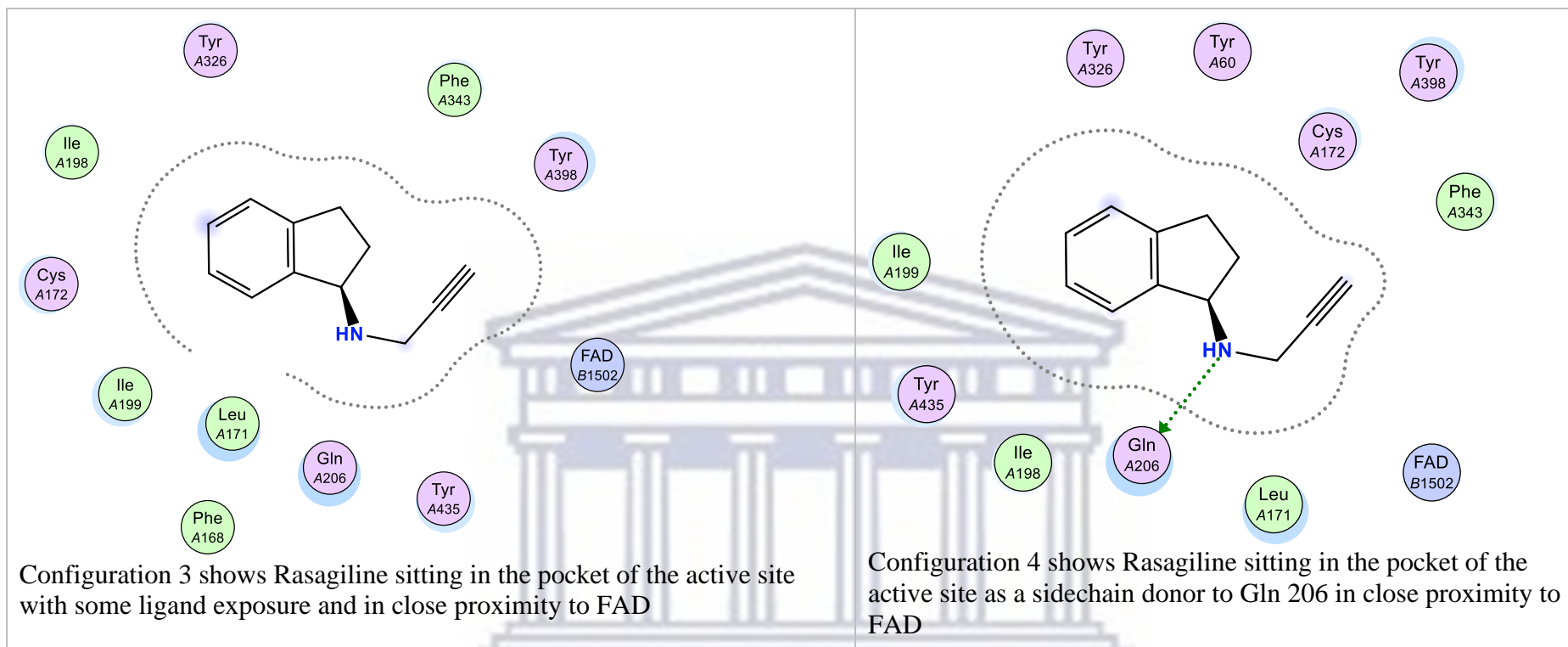
UNIVERSITY of the
WESTERN CAPE



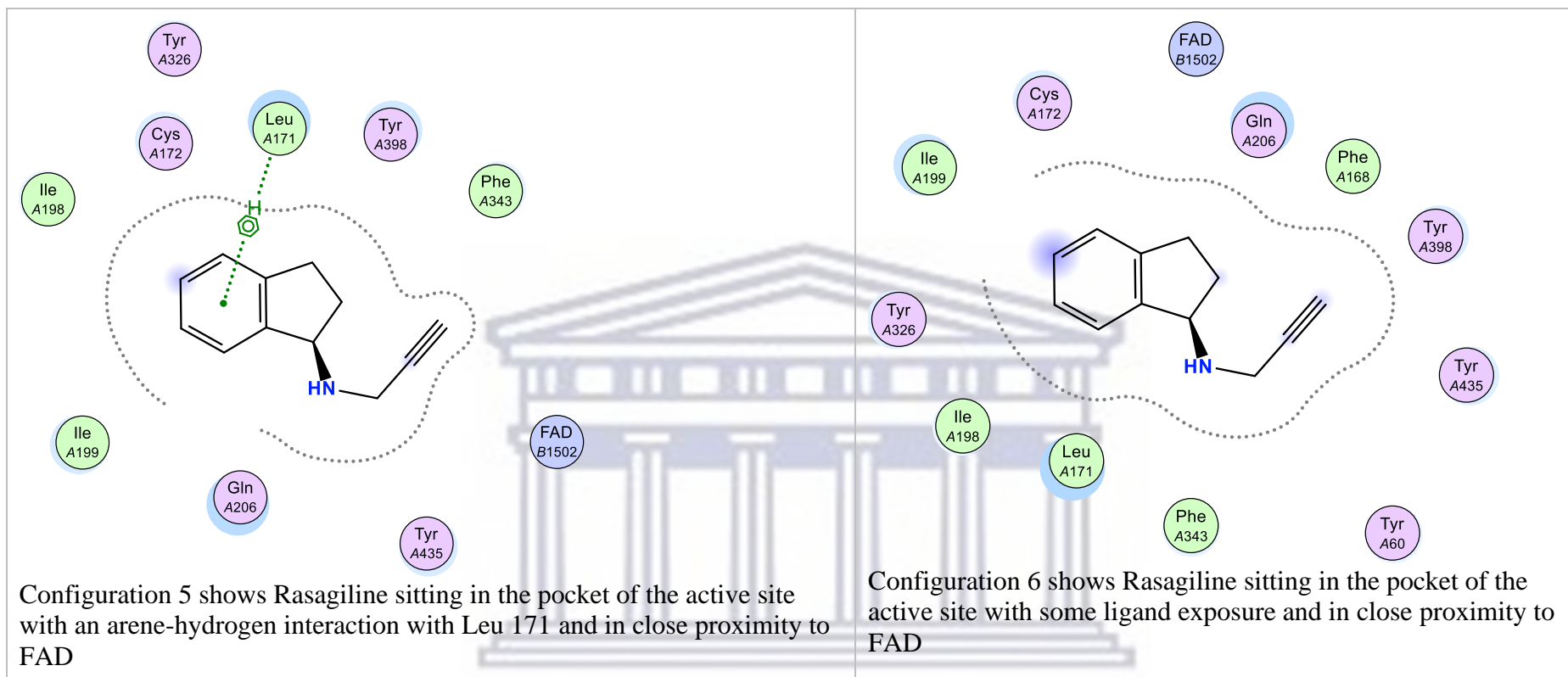
UNIVERSITY of the
WESTERN CAPE

Rasagiline

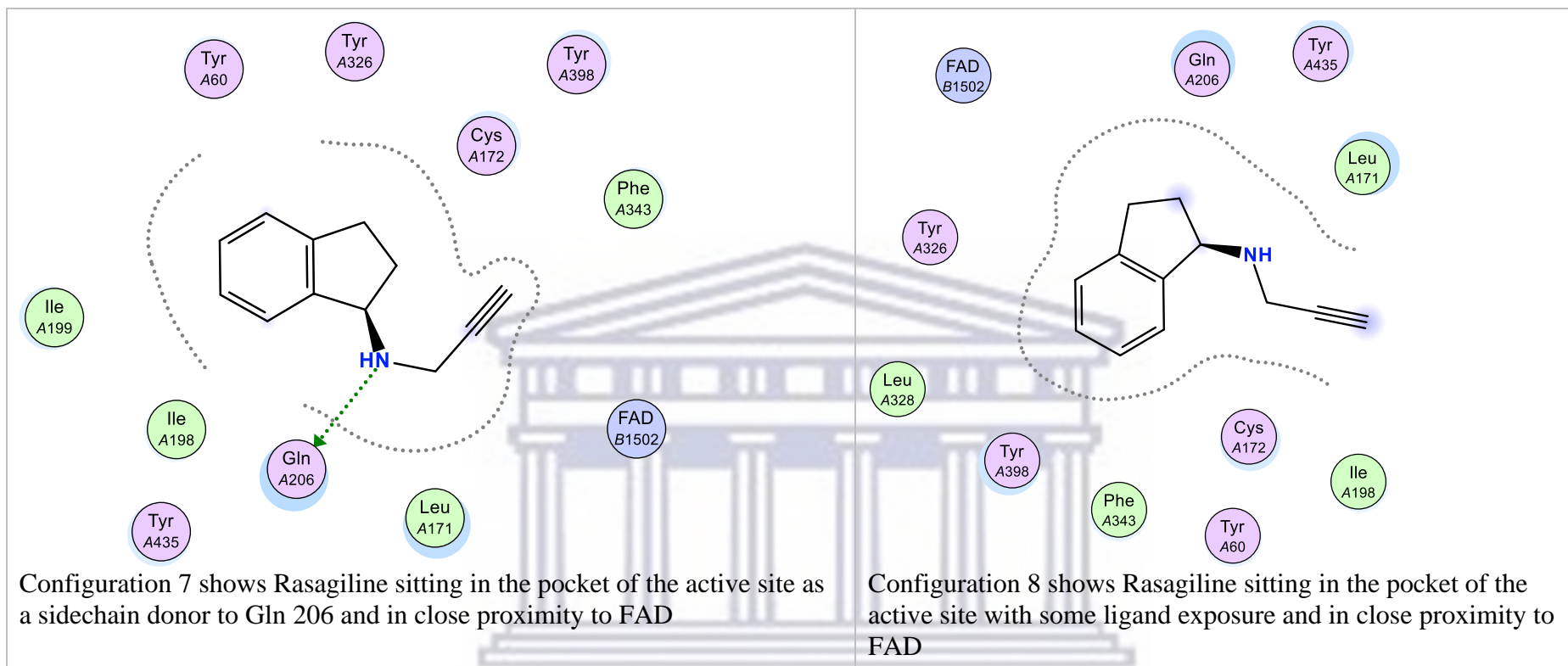




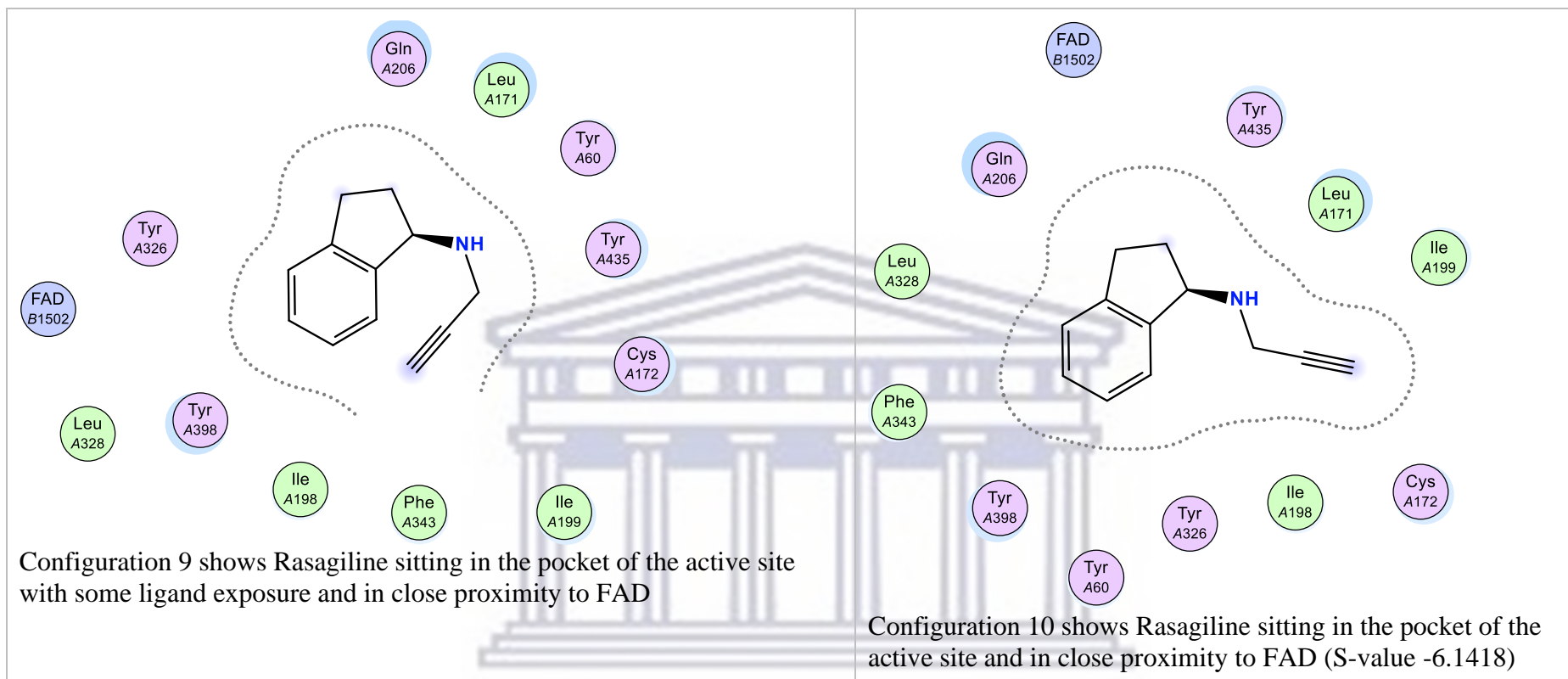
UNIVERSITY of the
WESTERN CAPE



UNIVERSITY of the
WESTERN CAPE



UNIVERSITY of the
WESTERN CAPE



UNIVERSITY of the
WESTERN CAPE



UNIVERSITY *of the*
WESTERN CAPE